MicroRNA and the innate immune response toinfluenza A virus infection in pigs

Brogaard, Louise

Publication date:
2017

Document Version
Publisher's PDF, also known as Version of record

microRNA and the innate immune response to influenza A virus infection in pigs

PhD thesis

Louise Brogaard

October 2017

Division of Immunology and Vaccinology – Innate Immunology
National Veterinary Institute
Technical University of Denmark

Supervisors
Senior researcher Kerstin Skovgaard (main supervisor)
Division of Immunology and Vaccinology – Innate Immunology
National Veterinary Institute, Technical University of Denmark

Professor Lars E. Larsen
Division of Diagnostics and Scientific Advice – Virology
National Veterinary Institute, Technical University of Denmark

Assessment committee
Niels Lorenzen (Chairperson)
Professor
Division of Immunology and Vaccinology
National Veterinary Institute, Technical University of Denmark
Denmark

Elma Tchilian
Group leader
Swine Influenza Immunology Group
The Pirbright Institute
England

Susanna Cirera
Associate Professor
Animal Genetics, Bioinformatics and Breeding
Faculty of Health and Medical Sciences
Copenhagen University
Denmark

Cover artwork
Photo obtained from Colourbox under DTU license

Table of contents

Preface and acknowledgements 5
List of abbreviations 7
List of artwork attributions 9
Summary 10
Resumé (Summary in Danish) 12
1 Introduction 13
2 Background 15
2.1 Influenza A virus 15
2.1.1 Taxonomy and structure 15
2.1.2 IAV replication 16
2.1.3 Antigenic diversity 18
2.1.4 Epidemics and pandemics 18
2.1.5 IAV host range 19
2.1.6 IAV in pigs 20
2.2 Influenza A virus infection 22
2.2.1 Intrinsic barriers for IAV infection 22
2.2.2 Clinical manifestations and host innate immune response to IAV infection 23
2.3 microRNA 25
2.3.1 Canonical miRNA biogenesis 25
2.3.2 miRNA nomenclature 26
2.3.3 miRNA function 27
2.3.4 Clinical applications of miRNAs 28
2.3.5 miRNA and influenza 30
2.4 Methods for transcriptional analysis 31
2.4.1 Reverse transcription quantitative real-time PCR (RT-qPCR) 31
2.4.2 Small RNA sequencing 38
3 Experimental framework and supplementary results 44
3.1 Animal experiments 44
3.1.1 Sampling 45
3.1.2 Clinical signs 45
3.2 Explant culture pilot study 46
3.2.1 Results from explant pilot study 47

3.2.2 Discussion and future work 51
4 Concluding remarks and future perspectives 53
5 References 55
Paper 1: Animal models for host defense against influenza A virus infection: profound translational value of the porcine model 63
Paper 2: Late regulation of immune genes and microRNAs in circulating leukocytes in a pig model of influenza A (H1N2) infection 91
Paper 3: IFN-λ and microRNAs are important modulators of the pulmonary innate immune response against influenza A (H1N2) infection in pigs 117
Paper 4: Clinical outcome after influenza A virus challenge affects the pulmonary microRNA response in vaccinated and unvaccinated pigs 155

Preface and acknowledgements

I have often come across the expression that it takes 10,000 hours to become an expert on something. So let's do the math. 37 hour work week, 52 weeks in a year. Subtract six weeks a year for vacation, roughly one and a half week for national holidays. Three years in the PhD programme. That is a total of about 5,000 hours, so I suppose I should be halfway there. But it still feels like I have only just scratched the surface of this very intriguing topic which I have had the privilege of diving into for the past few years, and I am even more motivated now to continue the research than I was when I began my PhD study. But my thesis deadline is drawing close and I have to somehow summarize the last three years of my working life in the form of a thesis.

The work presented in this thesis was carried out as part of my PhD study at the National Veterinary Institute (DTU Vet), Technical University of Denmark, in the Division for Immunology and Vaccinology – Innate Immunology, from July 2013 to October 2017 (interspersed with ~13 months maternity leave). The study was financed by internal funding.

This thesis comprises three major background chapters as well as manuscripts for three research papers and one review:

- Chapter 1 serves as a brief introduction to the field and the hypotheses investigated during my PhD project.
- Chapter 2 provides background and context regarding influenza A virus infection and the host response, as well as theoretical background for the methods applied for transcriptional analysis.
- Chapter 3 gives an overview of the experimental setup from which I have derived all my results.
- Paper 1 is a review draft entitled *Animal models for host defense against influenza A virus infection: profound translational value of the porcine model* (second author), which is being prepared for submission to the ILAR Journal. This review ties in well with the background presented in Chapter 2 and is therefore the first manuscript presented in this thesis.
- Paper 2 is a research article entitled *Late regulation of immune genes and microRNAs in circulating leukocytes in a pig model of influenza A (H1N2) infection* (first author), published in Scientific Reports (2016).
- Paper 3 is a research article entitled *IFN-λ and microRNAs are important modulators of the pulmonary innate immune response against influenza A (H1N2) infection in pigs* (first author), which is submitted for publication in PLOS ONE, currently under review at the time of thesis submission.
- Paper 4 is a research article draft tentatively entitled *Clinical outcome after influenza A virus challenge affects the pulmonary microRNA response in vaccinated and unvaccinated pigs* (first author), which is being prepared for submission to a peer reviewed scientific journal. The choice of journal has not yet been made at the time of thesis submission as the manuscript is still a work in progress.

It takes a village to produce a PhD thesis, and I would definitely not have been able to do this without the invaluable contributions from a lot of different people. Above all, I owe the

greatest of thank yous to my main supervisor Kerstin Skovgaard for her trust in me since I showed up as a Master student in her office almost six years ago, asking her to please teach me something about innate immunology and gene expression. Her unfailing optimism and solution-oriented and very attentive nature makes her the best supervisor a student could ask for. I have been fortunate enough to also benefit from the experience, knowledge, and network of my co-supervisor Lars E. Larsen. I really believe that I have had a supervisor team that was optimally suited for my temperament and work process. Thank you, Kerstin and Lars.

The kindness and technical assistance of Karin Tarp has been indispensable for my work for as long as I have been here, and I am sure it will continue to be so in the future. DTU Vet is full of amazing people who directly or indirectly have contributed to my experiences as a PhD student. It is a pleasure to go to work every day when you have such inspiring colleagues to collaborate with, and I would especially like to thank Peter M. H. Heegaard and Sofie M. R. Starbæk for their contributions to my PhD work. Massive changes have been taking place at DTU Vet during the years I have been here, and it has been a fascinating evolution to witness – I am eager to find out what the future has in store for us.

It is always fun to throw yourself into doing something no one else at your workplace knows how to do. I am therefore very grateful to Christian Anthon and Jan Gorodkin at RTH for taking the time to introduce me to RNA sequencing data analysis. Along those lines, a massive thank you also goes to Caroline Bonckaert at the Laboratory of Virology at the Faculty of Veterinary Medicine, Ghent University. Had it not been for her, then I fear that my stay at the lab would have been rather fruitless. Hans Nauwynck is thanked for agreeing to host me in his lab, my stay there was a very educational experience. Kristien van Reeth is thanked for helpful input and discussions, and practical assistance with animal handling and cell culture from Loes Geypen and Nele Dennequin was a great help during my stay in Ghent.

Finally, my wonderful boys at home who have been so infinitely patient and horribly neglected over the past few months. Theo, you are the single greatest source of motivation I could ever have asked for. Per, this thesis would simply not be in existence if it had not been for you.

Thank you.

DTU Vet, October 2017
Louise Brogaard

List of abbreviations

Ab	Antibody
Ago	Argonaute protein
AP-1	Activator protein 1
CCL	C-C motif chemokine ligand
cDNA	Complementary DNA
cRNA	Complementary RNA
C_q	Quantification cycle
CXCL	C-X-C motif chemokine ligand
DNA	Deoxyribonucleic acid
dsDNA	Double-stranded DNA
ECDC	European Centre for Disease Prevention and Control
gDNA	Genomic DNA
gRNA	Genomic RNA
HA	Hemagglutinin
HCV	Hepatitis C virus
HPAI	Highly pathogenic avian influenza
hpi	Hours post inoculation
IAV	Influenza A virus
IBV	Influenza B virus
IFC	Integrated fluidic circuit
IFN	Interferon
IgA	Immunoglobulin A
IgG	Immunoglobulin G
IL	Interleukin
IRF	Interferon regulatory factor
ISG	Interferon stimulated gene
LNA	Locked nucleic acid
LPAI	Low pathogenic avian influenza
miRNA	microRNA
mRNA	messenger RNA
NA	Neuraminidase
ncRNA	non-coding RNA
NF-κB	Nuclear factor kappa-light-chain-enhancer of activated B cell
NGS	Next-generation sequencing
NK	Natural killer (cells)
nt	Nucleotides
NTC	Non-template control
MCA	Melting curve analysis
MDCK	Madin-Darby canine kidney (cells)
PAMP	Pathogen-associated molecular pattern
PCR	Polymerase chain reaction
Pre-miRNA	Precursor miRNA

Pri-miRNA	Primary miRNA
PRR	Pathogen recognition receptors
qPCR	Quantitative real-time PCR
RBC	Red blood cell
RdRp	RNA-dependent RNA polymerase
RISC	RNA-induced silencing complex
RLR	Rig-I-like receptor
RNA	Ribonucleic acid
(-)ssRNA	Negative-sense single-stranded RNA
-RT control	Minus reverse transcriptase control
RT-qPCR	Reverse transcription quantitative real-time PCR
SA	Sialic acid
SD	Standard deviation
ssDNA	Single-stranded DNA
ssRNA	Single-stranded RNA
$TCID_{50}$	50 % tissue culture infective dose
TLR	Toll-like receptor
T_m	Melting temperature
TUNEL	Terminal deoxynucleotidyl transferase dUTP nick end labeling

List of artwork attributions

The following figures were obtained from external sources attributed below. All other figures included in this thesis were produced by the author.

Figure 1	Figure is adapted from *At the centre: influenza A virus nucleoproteins*, A. J. Eisfeld *et al.*, Nature Reviews Microbiology **13**, 28-41 (2015), doi:10.1038/nrmicro3367
Figure 2	Figure is adapted from *Influenza virus RNA polymerase: insights into the mechanisms of viral RNA synthesis*, A. J. W. te Velthuis *et al.*, Nature Reviews Microbiology **14**, 479-493 (2016), doi:10.1038/nrmicro.2016.87
Figure 3	Figure is adapted from *Viral determinants of influenza A host range*, A. V. Cauldwell *et al.*, Journal of General Virology **95**, 1193-1210 (2014), doi:10.1099/vir.0.062836-0
Figure 6	Figure is adapted from *Biogenesis and Function of Ago-Associated RNAs*, I. Daugaard *et al.*, Trends in Genetics **33**, 208-219 (2017), doi:10.1016/j.tig.2017.01.003
Figure 7	Figure is copied from *The translational potential of microRNAs as biofluid markers of urological tumours*, A. Fendler *et al*., Nature Reviews Urology **13**, 734-752 (2016), doi:10.1038/nrurol.2016.193
Figure 8	Modified version of original by Enzoklop (Own work) [CC BY-SA 3.0 (http://creativecommons.org/licenses/by-sa/3.0)], via Wikimedia Commons
Figure 11	Picture from the Fluidigm website, https://www.fluidigm.com/reagents/genomics/bmk-m-96.96-96-96-dynamic-array-ifc-for-gene-expression, obtained September 7th 2017
Figure 13	Figure is adapted from original by Kelvinsong (Own work) [CC BY 3.0 (http://creativecommons.org/licenses/by/3.0)], via Wikimedia Commons
Figure 17	Figure is adapted from the online product description of the NEBNext® Multiplex Small RNA Library Prep Set for Illumina® (New England Biolabs), https://www.neb.com/products/e7300-nebnext-multiplex-small-rna-library-prep-set-for-illumina-set-1#pd-description, obtained September 7th 2017
Figure 18	See Figure 17
Figure 19	Figure adapted from *Next-Generation DNA Sequencing Methods*, E. Mardis, Annual Review of Genomics and Human Genetics **9**, 387-402 (2008), doi:10.1146/annurev.genom.9.081307.164359

Summary

Influenza A virus infections are a major public health concern. Many million cases of disease associated with influenza A virus occur every year during seasonal epidemics, and especially vulnerable populations such as the elderly, pregnant women, young children, and individuals with underlying conditions such as diabetes and patients of autoimmune diseases are at higher risk of severe complications from influenza A virus infection. However, in otherwise healthy individuals, influenza A virus infection is relatively short-lived, commonly being cleared within one to two weeks. Influenza A virus causes respiratory infection, primarily infecting the respiratory epithelial cells. In the time span from influenza A virus infects until specific antibodies and cytotoxic T lymphocytes arrive at the site of infection, innate immunity is highly important for restricting viral spread and facilitating development of a tailored adaptive immune response.

Upon infection, the influenza A virus is recognized by innate viral pathogen sensors which initiate the induction of a balanced pro- and anti-inflammatory cytokine response as well as the hallmark interferon response, inducing an 'antiviral state' in the infected cell as well as neighboring cells. As with numerous other cellular processes, the innate host response is modulated by microRNAs, a class of short non-coding RNAs important for the regulation of translation of protein-coding gene transcripts. Comprehensive assessment of the transcriptional host response to influenza A virus infection requires the joint expression profiling of protein-coding gene and microRNA expression.

Paper 1 is a review which emphasizes the importance of the pig in the study of influenza A virus infections. Pigs are themselves natural hosts for influenza A virus, and our close relationship with this species poses an ever present risk of emergence of zoonotic influenza A virus strains. The porcine response to influenza A virus infection greatly mirrors human conditions, and the pig thus represents an important animal model with great translational value for the study of human influenza A virus infection. **Paper 2** presents results demonstrating the temporal dynamics of microRNA expression in circulating leukocytes from pigs after influenza A virus challenge, and emphasizes the need for control of the time parameter in suitable animal models for the evaluation of the biomarker potential of circulating microRNAs. Differential microRNA expression in circulating leukocytes peaks two weeks after challenge, suggesting that microRNAs may influence susceptibility to secondary infections. The study likewise shows that the expression profile of protein-coding genes in porcine circulating leukocytes mirrors what is seen in humans after natural or experimental influenza A virus infection. **Paper 3** examines the local innate immune and microRNA response in the lungs of pigs after influenza A virus challenge. In contrast to observations in circulating leukocytes, differential microRNA expression peaks three day after challenge, suggesting that pulmonary microRNA expression may be aimed at modulating the rapid transcriptional pro-inflammatory response which peaks already one day after challenge. **Paper 4** compares the local lung microRNA expression in vaccinated and unvaccinated pigs after influenza A virus challenge. Vaccinated and unvaccinated pigs displayed significantly different clinical signs, with a more severe course of disease observed in unvaccinated pigs presenting. This difference in disease severity was reflected in the pulmonary transcriptional innate host response of protein-coding genes and microRNA during

infection. Target analysis of the differentially expressed microRNA between the two groups of pigs indicated the involvement of microRNAs in host innate and adaptive immune responses, apoptosis, and lung regeneration.

Resumé (Summary in Danish)

Influenza A virusinfektioner er en stor byrde for verdenssamfundet. Mange millioner tilfælde af sygdom associeret med influenza A virus forekommer årligt i forbindelse med sæsonbetonede epidemier, og særligt sårbare grupper såsom ældre, børn i alderen seks måneder til fem år, gravide og individer med underliggende lidelser som diabetes og autoimmune sygdomme er i særlig risiko for alvorlige komplikationer. I ellers raske individer er influenza A virusinfektion en relativt kortvarig sygdom, som typisk er overstået på en til to uger. Det innate immunforsvar er derfor vigtigt for bekæmpelsen af denne infektion. Influenza A virus forårsager respiratorisk infektion, idet den primært inficerer epitelceller i respirationssystemet. Når influenza A virus inficerer en værtscelle bliver den detekteret af immun sensorer som er specifikke for virale patogener. Dette igangsætter produktionen af pro- og antiinflammatoriske cytokiner og et karakteristik interferonrespons som etablerer en 'antiviral tilstand' i den inficerede celle samt i naboceller. MicroRNA som er en klasse af korte ikke-kodende RNA-molekyler der er vigtige regulatorer af translation af protein-kodende gener. Udførlig karakterisering af det transkriptionelle værtsrespons efter influenza A virusinfektion må nødvendigvis inkludere både proteinkodende gener og microRNA. **Paper 1** er et review som understreger vigtigheden af grisen som en stordyrsmodel i studier af influenza A virus infektioner. Grisen er selv en naturlig vært for influenza A virus og udgør en konstant risiko for fremkomsten af nye zoonotiske influenza A virusstammer. Grisens værtsrespons mod influenza A virusinfektion er meget lig det der ses i mennesker, og grisen udgør dermed en vigtig dyremodel for studiet af humane influenza A virusinfektioner. **Paper 2** præsenterer resultater der demonstrerer den tidsmæssige variation af microRNA-ekspression i cirkulerende leukocytter fra grise efter influenza A virusinfektion, og understreger vigtigheden af prøveudtagningstidspunktet for evaluering af biomarkørpotentialet for cirkulerende microRNA. Differentiel microRNA-ekspression i cirkulerende leukocytter er mest udtalt to uger efter infektion, hvilket indikerer at microRNA kan påvirke modtageligheden for sekundære infektioner. Studiet viser ligeledes at ekspressionsprofilen for proteinkodende gener i cirkulerende leukocytter fra grise er i overensstemmelse med observationer i mennesker efter naturlig eller eksperimentel influenza A virusinfektion. I **Paper 3** undersøges det lokale innate immunforsvar og microRNA-respons i griselunger efter influenza A virus infektion. I modsætning til cirkulerende leukocytter, så er den differentielle ekspression af microRNA mest udpræget tre dage efter infektion, hvilket indikerer at det lokale microRNA-respons i lungen i højere grad er rettet mod regulering af det hurtige transkriptionelle proinflammatoriske respons som er på sit højeste allerede på dag et efter infektion. I **Paper 4** sammenlignes det lokale microRNA-respons i lungerne fra vaccinerede og ikkevaccinerede grise efter de er blevet inficeret med influenza A virus. Vaccinerede og ikkevaccinerede udviste signifikant forskellig klinisk, hvor de ikkevaccinerede grise udviste de mest alvorlige sygdomstegn. Denne forskel var reflekteret i den forskellige ekspression i lungen af innate immungener, samt forskelle i microRNA-responset både under og efter infektion.

1 Introduction

Few infectious diseases are as ubiquitous as influenza. Its victims are everywhere – aquatic, terrestrial, and aerial species are all among the broad range of hosts for influenza. The European Centre for Disease Prevention and Control (ECDC) reports 4-50 million cases of disease and 15,000-70,000 deaths annually in European citizens[1], which are associated with seasonal influenza. The burden of controlling influenza is not made lighter by its zoonotic potential, nor by the fact that important livestock such as pigs and poultry are natural hosts for influenza as well. So not only is influenza a heavy burden on our public health system, it likewise threatens our food production system.

An ounce of prevention is worth a pound of cure[2]. This holds true for influenza, as our most effective method of lowering the impact of influenza is by vaccination. Antivirals are likewise an option, but we are struggling to keep up with the viruses that cause influenza, as they acquire resistance to our treatments and escape the immunity induced by our vaccines, leaving us chasing a moving target. We need to do better, but there are still many unresolved questions regarding influenza A virus infection. Expanding the knowledge of the intricate interplay of host and virus during infection may provide us with much needed ammunition to expand our arsenal for the fight against influenza. Elucidating the changes occurring in the host at the host-virus interface during infection is an important step towards achieving this goal. For this, we need suitable animal models for human influenza, and the pig excels in this regard. Porcine models allow us to perform highly controlled challenge experiments, monitor disease development, and investigate the transcriptional changes in the respiratory system and other relevant organs in an organism which closely mirrors humans with regards to respiratory morphology, clinical manifestations, and antiviral innate immune response.

The hypotheses for this PhD study can be summarized as follows:

I. Experimental infection of pigs with swine origin influenza A virus will induce changes in the transcriptome locally in the lung as well as in circulation. Assessing the transcriptional changes to the antiviral response will demonstrate the importance of the innate immune system in the rapid control of influenza A infection. The temporal changes in microRNA (miRNA) expression in the lung and in circulating leukocytes will reflect the progression of disease.

II. Vaccination against influenza A virus will trigger a distinct miRNA response in porcine lung tissue upon influenza A virus infection compared to unvaccinated pigs, which relates to the protection induced by the vaccination. Vaccination will likewise impact the host innate immune response during the acute phase of disease, demonstrating a molecular causality of the clinical signs observed in vaccinated and unvaccinated pigs after influenza A challenge.

III. *Ex vivo* cultured explants from the porcine nasal mucosa can be established as a viable, stable, 3R compliant tool for transcriptional analysis of the antiviral host response after influenza A infection. This system can provide information of the early

[1] https://ecdc.europa.eu/en/seasonal-influenza/facts/factsheet, accessed September 20th 2017

[2] Benjamin Franklin

host response in the epithelium of the upper respiratory tract, elucidating the mechanisms employed by the host to restrict viral spread and host tissue damage during the very first cycles of viral replication.

The aim was thus to apply the pig as a large animal model to characterize transcriptional changes of the pulmonary innate immune response during and after influenza A virus infection in both vaccinated and unvaccinated animals. The pig model was likewise applied to elucidate the role of locally expressed miRNAs in the modulation of the immune response to influenza A virus infection. It was likewise aimed to assess the temporal dynamics of the systemic expression of antiviral immune genes and miRNAs by means of transcriptional profiling of circulating leukocytes from pig after influenza A virus challenge. Finally, an *ex vivo* explant system from porcine nasal mucosa was set up and tested for its applicability for the study of transcriptional changes in the host after influenza A infection.

2 Background

2.1 Influenza A virus

2.1.1 Taxonomy and structure

The genus *Influenza virus A* belongs to the family of *Orthomyxoviridae* which also includes the genera *Influenza virus B*, *Influenza virus C*, and the very recently described *Influenza virus D*, as well as *Isavirus*, *Thogotovirus*, and *Quaranjavirus* [1–3]. Influenza A virus (IAV) virions are commonly spherical, measuring 80-120 nm in diameter. The viral envelope consists of a host cell-derived lipid bilayer and three different viral proteins: the two antigenic surface proteins hemagglutinin (HA) and neuraminidase (NA), and the transmembrane ion channel M2. Anchored on the inside of the viral envelope is the matrix protein M1. The IAV genome consists of eight protein-coding[3] segments of negative-sense single-stranded RNA ((-)ssRNA), totaling at ~13.5 kb with each segment spanning ~850-2350 nt (**Figure 1, A**). Segments 1, 4, 5, and 6 all encode a single protein (PB2, HA, NP, and NA, respectively) whereas the remaining four segments yield two or three different proteins [4]. Segment 2 encodes the RNA-dependent RNA polymerase (RdRp) subunit PB1, but also PB1-F2 via translational frameshift and PB1-N40 as a truncated version of PB1. Segment 3 encodes another RdRp subunit, PA, as well as PA-X, also via frameshifting during translation. Segments 7 and 8 each produce two proteins due to differential splicing of their mRNA, namely M1 and M2 and NS1 and NEP (NS2), respectively. In addition to the protein coding sequences of the genomic RNA (gRNA) segments each strand also contain 'packaging signals', i.e. specific sequences at their 5' and 3' ends which ensures that just one copy of each segment is packaged into newly formed virions during the viral replication cycle. Inside the virion, each genomic segment is tightly packed into a viral nucleoprotein (vRNP) complex (**Figure 1, B**). In this complex, the strand of gRNA is bound to the NP protein which is folded back on itself to form a coiled structure. The ends of the gRNA/NP strand are bound to the viral RdRp, a trimeric complex consisting of the PB1, PB2, and PA proteins required for virus genome replication in the nucleus of the host cell.

IAVs are subtyped according to their expression of two surface proteins: the glycoproteins hemagglutinin (HA) and neuraminidase (NA). HA is a trimeric protein of which 16 subtypes (H1-H16) have been described to date, whereas NA is a tetramer with nine (N1-N9) known subtypes. H1N1, H1N2, H3N2, and H5N1 are thus all examples of IAV subtype names. Full IAV strain nomenclature includes information on which species it was isolated from, geographic location, and year of isolation. A/swine/Denmark/12687/2003(H1N2) is thus an influenza **A** virus of the **H1N2** subtype isolated from a pig (**swine**) in **Denmark** in **2003**.

[3] Viral proteins: HA – hemagglutinin; NA – neuraminidase; M1 – matrix protein 1; M2 – matrix protein 2; PB1 – polymerase basic protein 1; PB1-F2 – polymerase basic protein 1 F2; PB1-N40 - polymerase basic protein 1 N40; PB2 – polymerase basic protein 2; PA – polymerase acidic protein; PA-X – polymerase acidic protein X; NS1 – non-structural protein 1; NS2/NEP – non-structural protein 2/nuclear export protein; NP – nucleoprotein.

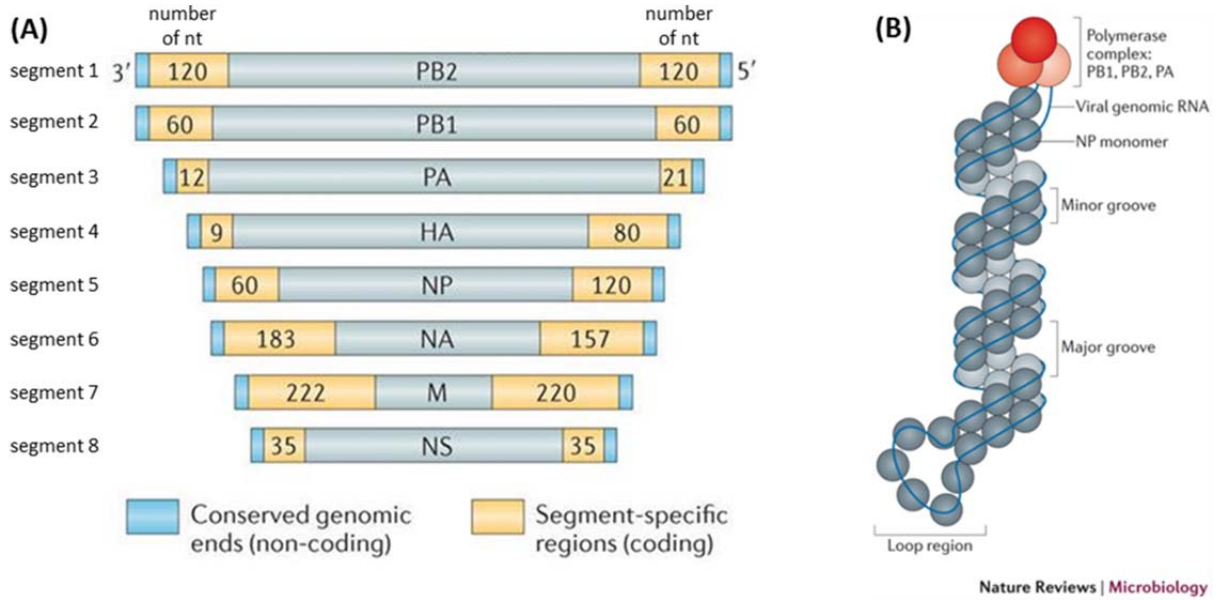

Figure 1. (A) schematic representation of IAV gRNA segments. Highlighted at each end of the segments are the packaging signal sequences. The encoded protein is noted in the middle of each segment. (B) model structure of the vRNP complex, showing the gRNA-NP coil bound to the viral RNA-dependent RNA polymerase complex. Figure is modified from Eisfeld *et al.* 2015 [5].

2.1.2 IAV replication

The IAV replication cycle is summarized in **Figure 2**. Upon host cell attachment by HA to sialic acid residues on host cell surface, IAV is taken up by receptor-mediated endocytosis [6]. Once internalized into an (early) endosome (pH ~5.9-6.8), endosomal trafficking directs the maturation into a late endosome with a lowered pH (~4.8-6.0) [7]. The more acidic environment facilitates the fusion of the viral and endosomal membranes, which releases the viral ribonucleoproteins (vRNPs) into the cytosol of the host cell. Nuclear localization signals in the vRNPs ensure their import into the host cell nucleus where IAV translation and genome replication takes place. Here, the viral RdRp converts the negative-sense viral genome RNA into complementary positive-sense RNA to serve as template for production of new viral genome segments, and mRNA from which viral proteins will be translated.

Transcription and translation

Although IAV utilizes its rather limited coding capabilities well by encoding more than one protein in several of its genomic segments, it must still rely heavily on the exploitation of host factors for its replication. Within the nucleus, RdRp transcribes viral gRNA into mRNA, which is initiated by an event termed ‘cap snatching’. The PB2 subunit of the RdRp cleaves the capped 5’ end of host pre-mRNA to yield a 10-13 nt long primer for viral transcription. By elongation of the host-derived capped primer, viral gRNA is transcribed from the 3’ to 5’ end. Due to a short poly(U) sequence in the viral gRNA, this yields a viral mRNA that is polyadenylated in its 3’ end. Viral mRNA can then be exported from the nucleus to the cytosol and be translated by exploitation of the host translational machinery (**Figure 2**).

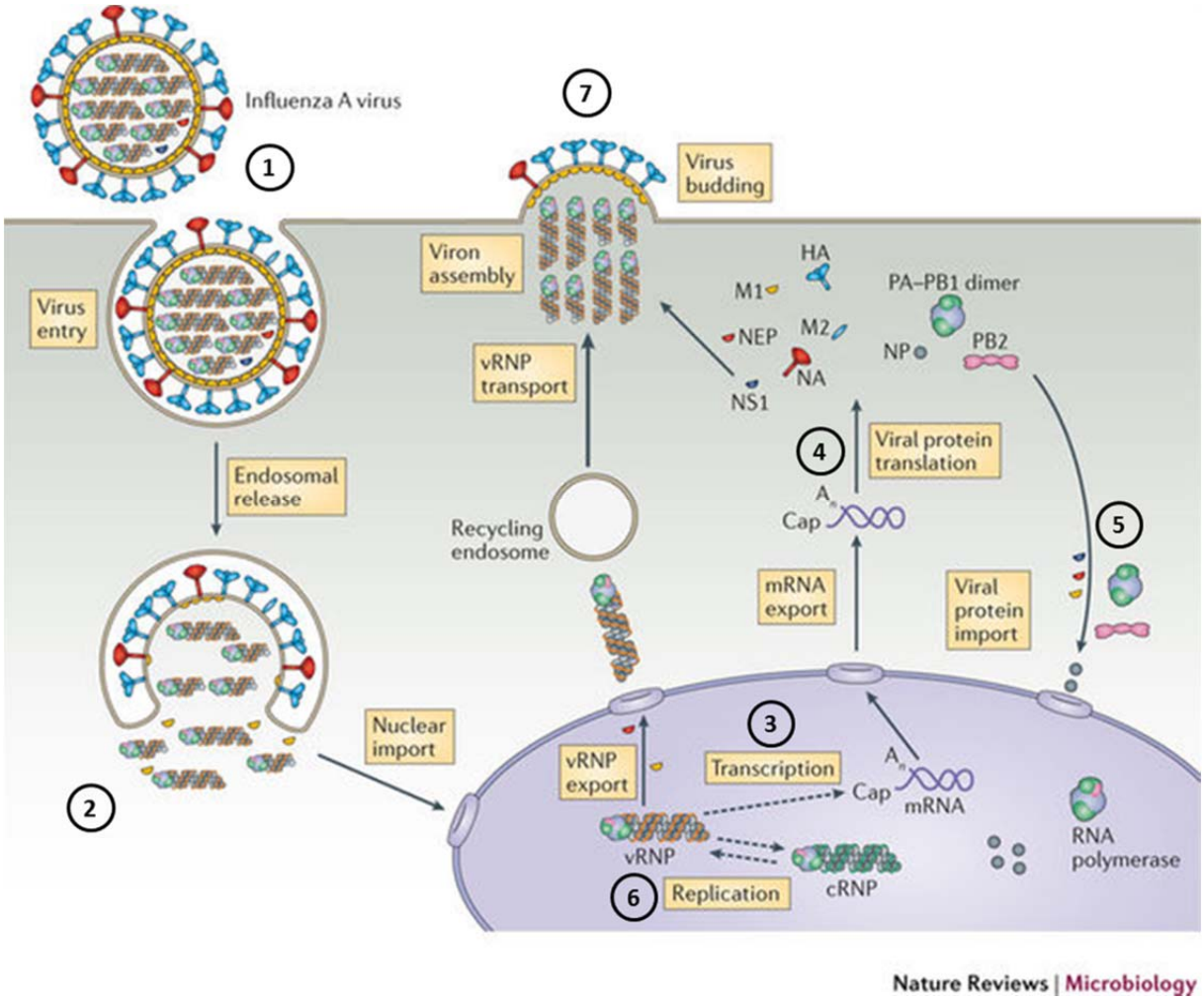

Figure 2. Schematic representation of the IAV replication cycle. 1) the virus attaches to sialic acid residues on the host cell surface and enters the cell by receptor-mediated endocytosis. 2) increasing acidification of the endosome leads to the fusion of host and viral membranes, releasing the viral genome in the form of vRNPs which are imported into the host cell nucleus. 3) transcription of viral gRNA into mRNA is carried out by the viral RdRp complex; this process is primed by 'cap snatching' the 5' capped end of a host pre-mRNA. 4) viral mRNA is exported to the cytosol and translated into proteins by the host translational machinery. 5) several newly synthesized viral proteins enters the nucleus to be included in new vRNPs. 6) the viral genome (vRNPs) is replicated via a cRNA intermediate. 7) newly formed vRNPs are exported from the nucleus and transported to the host cell membrane where new virions are packaged and released. Figure is adapted from te Velthuis *et al*. 2016 [8].

Genome replication

Import of several of the newly synthesized viral proteins into the nucleus is necessary for the formation of new vRNPs (**Figure 2**), including the RdRp subunits and NP [5]. Unlike the transcription of gRNA into viral mRNA by RdRp, the replication process is primer-independent. First, the RdRp synthesizes a full-length complementary RNA (cRNA) copy of the gRNA. The cRNA then serves as a template for new gRNA synthesis. It is proposed that NP associates with the new gRNA as synthesis is ongoing, providing stability and protection to the viral RNA strands [9]. Ultimately, replication results in the formation of new vRNPs which are exported from the nucleus.

Viral release
Newly synthesized vRNPs are released into the cytosol and transported towards the cell membrane (**Figure 2**). The nuclear release process is proposed to be aided by the viral proteins M1 and NEP, as well as the host protein CRM1 (Exportin-1, *XPO1*), a nuclear export receptor [5]. Transport across the cytosol takes place via the cytoskeleton in endosomes in association with the host protein RAB11 [10]. Viral proteins are transported to the cell membrane via the host cell secretory pathway. New IAV virions are formed by budding from the host cell surface (**Figure 2**). This requires the membrane-bound proteins HA and NA to be inserted into the host cell membrane, which initiates budding [11]. vRNPs and other viral proteins are recruited to the budding site, and the new IAV virion can complete the budding process and be released from the host cell.

2.1.3 Antigenic diversity
Enormous genetic diversity is found among IAVs. This can be attributed to two major sources: 1) the lack of proofreading capabilities of the viral RdRp causing many errors in new viral genomes during replication, and 2) the segmented nature of the IAV genome, enabling the mixing of segments from different strains upon viral release from the same host cell. The two processes have been termed 'antigenic drift' and 'antigenic shift', respectively [12].
The mutations that arise during viral replication may be detrimental to the virus, in which case it will never be able to be sustained in the viral quasispecies, or the mutation may be silent (i.e. a synonymous mutation), meaning that it does not lead to an amino acid substitution in the viral protein which can affect the antigenicity. It might however also be a mutation that sustains replication and transmission, leading to antigenic drift which is of great benefit to the virus [12]. HA and NA are the two main IAV antigen targets of antibodies (Abs) due to their virion surface exposure. Previous IAV infections and IAV vaccination ensures a continued level of anti-IAV Abs in the population. These Abs will however only confer protection against IAV if they match the IAV antigens they were raised against. Due to antigenic drift, the existing immunity from previous seasonal IAV infection or vaccination is often not sufficient to provide protection against IAV strains that circulate in the following season [13].
It is possible for a host cell to be simultaneously infected by more than one IAV strain. In such a case, the vRNPs from the different strains may be shuffled during the packaging of new virions [14]. Such genetic reassortment may yield a virus with a genetic composition which is entirely unknown in the population, e.g. if a virus acquires a new gene that affect its host range. Such a distinct antigenic shift can result in viruses for which there is no existing immunity in the population, and it may thus be the cause of a new IAV pandemic.

2.1.4 Epidemics and pandemics
Human influenza epidemics occur annually in the winter months with the currently circulating IAV strains (see **section 2.1.5**) alongside influenza B virus (IBV). In pigs, swine adapted stains of the H1 and H3 subtypes circulate throughout the year, but occasionally new strains and subtypes emerge which are antigenically distinct from those that have been circulating the recent years [15]. When entirely new strains emerge there will often be little to none existing immunity in the population to dampen its impact, and it might evolve into an actual global

pandemic as most recently seen during the 2009 pandemic H1N1 outbreak. Within the last century, humans have experienced four IAV pandemics: H1N1 in 1918, H2N2 in 1957, H3N2 in 1968, and H1N1 in 2009 [16]. IAV pandemics are often characterized by a disproportionately high morbidity and mortality compared to seasonal epidemics, especially in younger individuals as this segment of the population is least likely to harbor any remnants of cross-protection from previous infections against the pandemic virus.
In humans it has been observed that the introduction of pandemic IAV strains into the population often causes the extinction of previously circulating seasonal strains, which was also seen after the H1N1 pandemic of 2009. It has been proposed that this may be attributed by boosting of Abs targeting conserved regions of the IAV antigens by the new pandemic strain; these Abs would thus be able to target the same conserved epitopes on the seasonal strain, causing it to die out [17].

2.1.5 IAV host range

IAV has a wide host range which includes humans, pigs, seals, horses, dogs, bats, and avian species. Currently, only the IAV subtypes H1N1 and H3N2 are circulating in humans as well as in pigs. Additionally, H1N2 is also found in circulation in pigs but not in humans, but strains of this subtype (however distinct from porcine H1N2) have previously been circulating in humans as well [18]. In contrast, all known HA and NA subtypes can be found in avian species, and wild aquatic birds are considered the natural reservoir for IAV [12,19]. Avian IAVs are designated as being of 'high pathogenicity' (HPAI, highly pathogenic avian influenza) or 'low pathogenicity' (LPAI). As the name indicates, HPAI can cause severe disease in avian species with high mortality rates. Pathogenicity is associated with the acquisition of a polybasic cleavage site in the immature form of HA (HA_0). This alteration expands the range of host proteases that are able to process HA_0 into its mature form, which is accompanied by an expansion in host cell tropism from respiratory epithelial cells to include endothelial cells, thus facilitating systemic spread of the virus [20]. To date, only HA of the H5 and H7 subtypes have been found to be of the HPAI pathotype.
HA is indeed a major determinant of IAV host range, and it is this protein which initiates host cell contact and entry by binding to the host cell surface oligosaccharides with a terminal sialic acid moiety. Human and swine IAVs both preferentially bind to α-2,6-linked sialic acid receptors, whereas avian IAVs prefer α-2,3-linked sialic acid receptors. As these receptors are differentially distributed throughout the respiratory system of different IAV hosts (as described in more detail in **Paper 1**), sialic acid binding preference of viral HA is an important factor restricting host range [21]. For an IAV strain to be able to cross the species barrier and become established in a new host it must first adapt to it, i.e. acquire mutations that support its entire life cycle in that new host, as exemplified in **Figure 3**. For example, humans predominantly express the α-2,3-linked sialic acid receptors in the lower, less accessible parts of the respiratory tract [22,23]; in order for an avian IAV to infect a human host it must therefore either penetrate deep into the lung to find the appropriate host cell receptor, or it must adapt to the human host by acquiring mutations that alter the receptor binding preferences of HA.

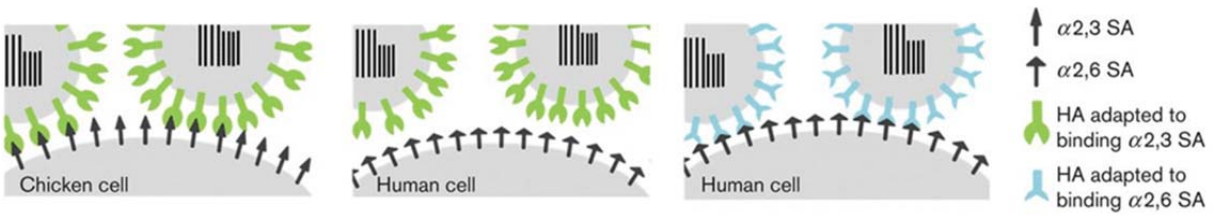

Figure 3. (A) avian host adapted IAV binding to a chicken host cell; avian host adapted IAV unable to bind to human host cell due to receptor mismatch; (C) human host adapted IAV binding to human host cell. SA – sialic acid. Figure is adapted from Cauldwell *et al*. 2014 [24].

It is predominantly observed that avian IAV does not transmit (at least efficiently) between humans, which is attributed to their inaccessible site of replication in the lower airways; human infection with avian IAV requires direct contact with birds shedding the virus. It is a theoretical possibility that avian IAV can acquire the mutations necessary for efficient human-to-human transmission, and such mammalian adaptation was demonstrated in the ferret model using a HPAI H5N1 strain [25]. The authors of this study showed that serial passage of the virus in ferrets (10 passages) – in combination with three site-directed mutations for α-2,6-linked sialic acid receptor adaptation – was sufficient for the virus to acquire the mutations needed for efficient ferret-to-ferret airborne transmission (i.e. via droplets, no direct contact between animals). Of the mutations consistently detected in the airborne viruses, four out of five resided in the HA gene, highlighting the importance of this protein in host range determination [25]. However, though such a study does provide proof-of-concept to some degree, it does not provide evidence that similar adaptation of HPAI H5N1 is likely to occur in humans. Whereas it is important to note that airborne transmission was achieved in the ferret model without the need for reassortment, the resulting H5N1 strain had lost its pathogenicity in ferrets. As described above, HA is an important determinant of viral tropism. Likewise, NA and the RdRp complex also contribute to the restriction of IAV host and tissue range. Just as the sialic acid binding HA protein must be a match for the sialic acid residues on the host cell surface, so must the NA. The function of the enzyme NA is to cleave host sialic acid residues on host cell surface receptors and soluble decoy receptors of the respiratory mucus layer (see **Paper 1** for more details). It is therefore important for the NA to be compatible with the sialic acid residues expressed by the host as well; inability of NA to cleave sialic acid residues would render the virus immobile and hinder its transmissibility [24].

Another commonly described decisive factor of host range is amino acid residue 627 in the RdRp subunit PB2. IAVs adapted to avian hosts almost exclusively contain a glutamic acid (E) residue at this position, whereas mammalian IAVs contain a lysine (K) [26]. Other sites in the vicinity of residue 627 have likewise been found to be very avian- or mammalian-specific. Mammalian adaptation of avian IAV strains by acquiring the E627K mutation has been documented in several fatal cases of human infection with both HPAI and LPAI viruses, thus exemplifying the alteration of host range by viral adaptation [27].

2.1.6 IAV in pigs

IAV in pigs and the use of pigs as large animal models for human IAV infection is described and discussed in detail in **Paper 1**.

Pigs are natural hosts for IAV and overlap with humans with regards to which IAV subtypes that circulate in the pig population. IAV is endemic in pigs worldwide, and considering the close relationship of humans and pigs as a production animal, pigs are considered to play an important role in global IAV ecology. A recent report summarized the results of (primarily) passive IAV surveillance in pig herds in 14 European countries and found that 31 % of all tested herds proved positive for IAV [28]. In Denmark alone, the surveillance report for 2015 summarizing the results of the passive IAV surveillance in pig herds showed that 52 % of the tested herds (256 out of 488) had tested positive for IAV [29]. IAV is thus widespread in pigs, and given the zoonotic potential of IAVs, influenza in pigs is an area that warrants much attention.

Swine IAVs show a binding preference for α-2,6-linked sialic acid residues on the host cell surface. Studies have demonstrated widespread presence of this receptor throughout the respiratory system of pigs [30–32], which is very similar to the receptor distribution found in humans (see **Paper 1** for more details). As is described in more detail in other sections of this thesis, pigs display clinical signs and disease progression as well as innate and adaptive immune responses to IAV infection which closely resembles that which is observed in humans.

From a One Health point of view, more focus should be on the study on IAV infection in a variety of animals. The human population increase and the accompanying increase in demand of animal protein for consumption facilitates enhanced contact and possibility of transmission of IAV between key IAV hosts – humans, pigs, poultry and wild birds. Modern travel habits have made every corner of the world so interconnected and accelerated the pace at which IAV can spread, so that management of human and animal IAV must be considered a global responsibility. The emergence of a new IAV strain with altered virulence in a distinct geographical location could potentially achieve worldwide spread in a matter of weeks. As was observed during the most recent IAV pandemic in 2009 (H1N1), it took only five weeks from it was initially discovered in Mexico until it had been detected on every other continent, a feat which previous pandemics had required many months to accomplish [33].

To control and lower the burden of IAV in humans and other species, continued focus on research in viral evolution and transmission as well as pathogenesis and the host immune response is paramount. Being itself a host for IAV and also an excellent model for the study of human IAV infection, the pig is key in an efficient approach to IAV management.

2.2 Influenza A virus infection

The porcine innate immune response to IAV infection is reviewed in **Paper 1**. This section will thus be a brief summarization of those topics included in **Paper 1**, with some additional relevant details.

2.2.1 Intrinsic barriers for IAV infection

The presence of α-2,6-linked sialic acid receptors in the upper respiratory tract of humans and pigs (**Figure 4**) facilitates IAV binding and infection. However, in order for the IAV to infect and replicate in the host cells, it must first be successful in penetrating the intrinsic immune barriers which continuously guard the host from invading pathogens.

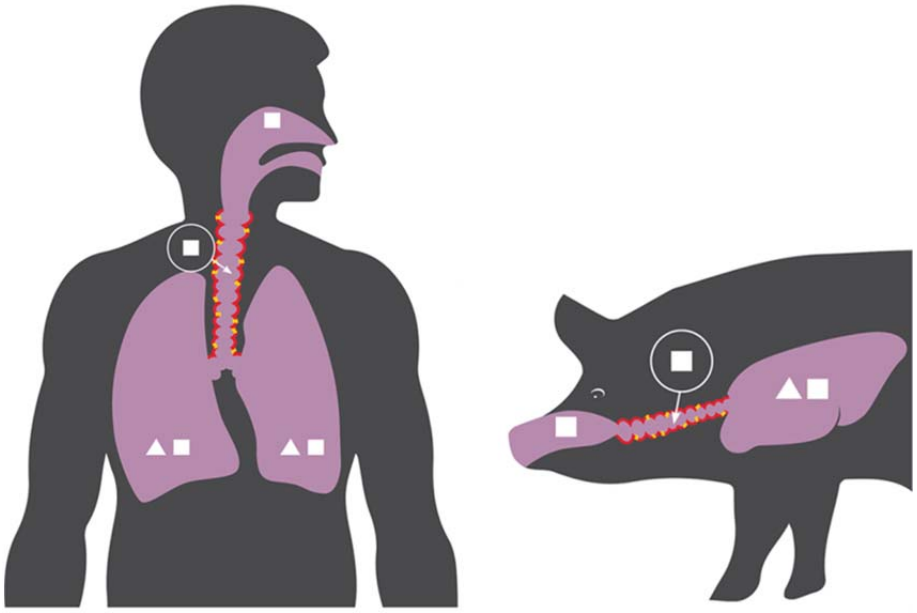

Figure 4. Schematic representation of the high similarity of the human and porcine respiratory systems with regards to important features for IAV infection. The major sialic acid receptor type (squares – α-2,6; triangles – α-2,3) of the nasal cavity, trachea, and lung is shown. The presence of ciliated respiratory epithelial cells is shown in red; the presence of mucus-secreting Goblet cells is shown in yellow. The figure is modified from the version that appears in **Paper 1**.

A clear definition of intrinsic immunity is hard to come by in available literature, but most descriptions agree that intrinsic immune factors are constitutively present at their site of action and exert their antiviral function by direct interaction with the pathogen, without the need for induction of other effector molecules, as is indicated in **Figure 5**. However, upon viral infection, the expression of some intrinsic immune factors may increase, in order to further augment their effect. The mucus layer which lines the respiratory tract constitutes an important barrier which contributes to intrinsic immunity (described in more detail in **Paper 1**). It is composed of a viscous fluid secreted from Goblet cells and submucosal glands which in itself may pose a physical barrier for the IAV in reaching the host epithelial cells [34]. In addition, several soluble factors in the mucus, e.g. mucins and pulmonary surfactants, have antiviral effects. Glycoproteins in the respiratory mucus may contain terminal sialic acid moieties as part of their glycosylation which can act as 'decoy receptors' by binding to the IAV HA surface molecules [35,36]. The virus is thus hindered in its ability to bind host cell surface bound sialic acids, thereby inhibiting IAV cell entry. Invading pathogens and other

inhaled insults which are trapped in the respiratory mucus are continuously cleared and swallowed due to mucociliary clearance by ciliated epithelial cells. As indicated in **Figure 4**, highly similar distribution of ciliated epithelial cells is found in the trachea of humans and pigs [37,38].

2.2.2 Clinical manifestations and host innate immune response to IAV infection

When the IAV does manage to breach the respiratory intrinsic defenses and infect the host, a multifaceted response is induced to restrict viral replication and clear the infection. In humans, seasonal IAV infection typically manifests with symptoms such as fever, nasal discharge, coughing, muscle aches, and general malaise [39]. These symptoms will commonly appear after an incubation period of one to two days and can persist for one to two weeks. Experimental infection of pigs with IAV gives rise to clinical signs which mirror those observed in humans, usually with an early onset within a day after infection [40–44]. However, subclinical IAV infections in pigs are also common [15]. Respiratory epithelial cells are the main site of IAV replication [45–47]. The viral entry and replication process described in **section 2.1.2** initiates host defense processes which include a potent pro-inflammatory and apoptotic response as well as recruitment of immune cells to the site of infection, resulting in gross pathological manifestations such as demarcated areas of hemorrhagic lung lesions [48–50].

The innate immune response against IAV infection is initiated by viral recognition by cellular pathogen recognition receptors (PRRs). Viral RNA constitutes pathogen-associated molecular patterns (PAMPs) which are recognized by the endosomal Toll-like receptors (TLRs) TLR3 and TLR7 (*TLR3*, *TLR7*) and the cytoplasmic RIG-I-like receptors (RLRs) RIG-I and MDA5 (*DDX58*, *IFIH1*). Upon cell entry, IAV PAMPs are detected by these PRRs thus activating signaling cascades which leads to the induction of gene expression, mediated by transcription factors such as nuclear factor kappa-light-chain-enhancer of activated B cells (NF-κB), activator protein 1 (AP-1), and interferon regulatory factors 3 and 7 (IRF3 (*IRF3*), IRF7 (*IRF7*)) [51]. The genes transcribed via these transcription factors mediate a rapid and transient response characterized by transcriptional regulation of pro- and anti-inflammatory cytokines, e.g. the interleukins IL-1β (*IL1B*), IL-6 (*IL6*), IL-10 (*IL10*), and IL-18 (*IL18*), the chemokines CXCL10 (*CXCL10*) and CCL2 (*CCL2*), and the type I and III interferons IFN-β (*IFNB1*) and IFN-λ (*IFNL1*, *IFNL2*, *IFNL3* in humans; *IL29*, *IL28A*, *IL28B* in pigs) (**Figure 5**) [42,52–55]. This induction of interferons induce the expression of a multitude of genes termed interferon stimulated genes (ISGs). The interferon and subsequent ISG response is a hallmark of the antiviral innate host response, and their induced expression upon IAV infection establishes an 'antiviral state' in the infected cell as well as neighboring cells. Interferons are secreted and are thus able to act on other cells which express the appropriate cell surface receptor; type I interferon receptors are found on a wide variety of cells in the respiratory system whereas type III interferon receptor expression is somewhat restricted to epithelial cells [56,57], i.e. the cells which are the primary site of IAV replication.

Although not strictly a part of the innate immune system, microRNAs (miRNAs) (see **section 2.3**) should be considered when assessing the transcriptional host response to infection, both during the innate and adaptive responses (**Figure 5**). As key endogenous modulators of gene

expression, a marked pulmonary miRNA response appears slightly delayed compared to the initial induction of pro-inflammatory and interferon gene expression. This post-transcriptional modulation likely contributes to fine-tuning and balancing the host innate immune response in order to avoid excessive inflammation and tissue damage.

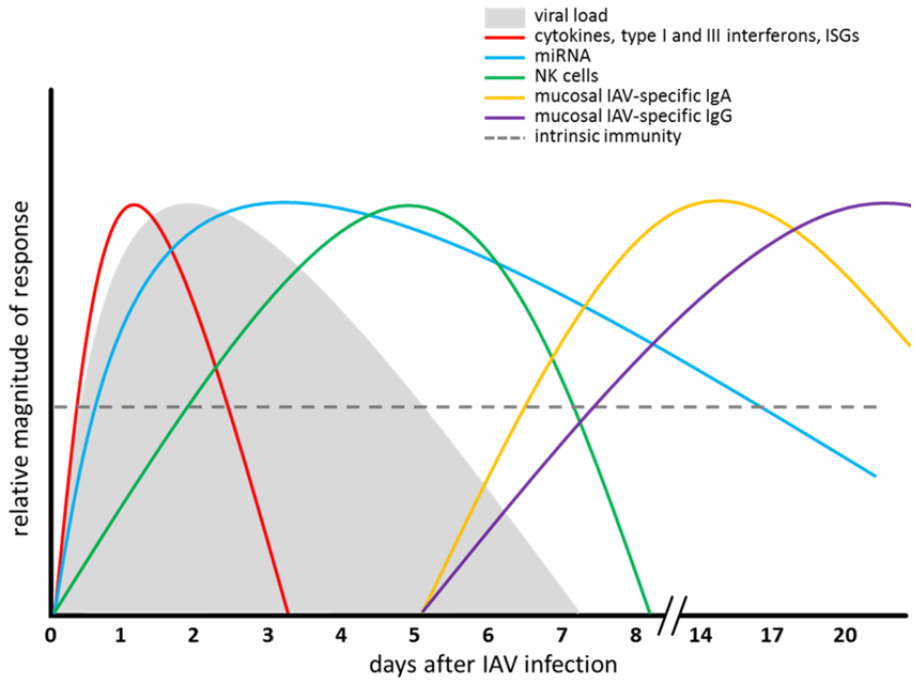

Figure 5. Schematic representation of different components of the pulmonary antiviral host response as well as viral load after IAV infection, demonstrating the general duration and peak time point of each response. The figure is copied from **Paper 1**.

IAV-specific mucosal antibodies appears approx. one week after infection, but by that time the innate antiviral response will have contained and cleared the IAV infection in cases of uncomplicated disease [58] (**Figure 5**).

Different cell types are involved in inducing the innate host response and restricting viral replication and spread after IAV infection. In addition to the respiratory epithelial cells, alveolar macrophages likewise contribute to the cytokine production [59,60]. Additionally, they may have a role in inhibiting IAV infection of type 1 alveolar epithelial cells [61].

Natural killer (NK) cells are cytotoxic lymphocytes of the innate immune system. During IAV infection, they also contribute to cytokine production, and they perform an important task by recognizing and killing virus infected cells [62–64]. As shown in **Figure 5**, NK cells increase from the start of infection, peaking somewhat after the viral load in the lung has started to decrease, which is in accordance with their importance in restricting viral spread.

Apoptosis is often the fate of IAV infected cells, e.g. mediated by NK cells or directly induced by viral proteins. Apoptosis has been described both as a host defense mechanism aimed at limiting viral spread, but also to be induced 'purposely' by IAV to enhance its propagation [65]. Several of the IAV encoded proteins have been shown to interact with host apoptotic pathways resulting in induction of apoptosis, including NP, NS1, PB1-F2, and M2 [66–69].

2.3 microRNA

One outcome of the Human Genome Project was the realization that protein-coding genes accounted for only ~1.2 % of the human genome [70]. The non-protein-coding sequences of the genome cover a variety of functional or non-functional elements, including telomeres, pseudogenes, introns, and non-coding RNAs (ncRNAs). ncRNA is an umbrella term covering transcribed RNA which is not translated into protein, but fulfil some other cellular function, e.g. ribosomal RNA (rRNA), transfer RNA (tRNA), and a multitude of different types of short ncRNAs, including microRNAs (miRNAs). miRNAs are approx. 22 nt in length and function as regulators of protein translation by interacting with messenger RNA (mRNA), thereby interfering with its translation commonly by destabilizing the mRNA leading to its degradation [71]. miRNAs were first identified in the early 1990ies by the parallel efforts of two different research groups who described the involvement of the miRNA lin-4 in larval development of *Caenorhabditis elegans* [72,73]. miRNAs have since been found in a multitude of animal and plant species as well as in viruses, and miRNAs have been found to be remarkably well conserved across animal species [74,75].

miRBase[4] is a central repository for miRNA sequences from all species as well as associated metadata [76]. The current curation of miRBase includes annotated miRNAs for >200 species of animals, plants, and viruses. There are large inter-species variations in the number of 'known' miRNAs deposited in miRBase; the current curation includes e.g. 2,588 mature human miRNAs but only 411 for pig. These are by no means finite numbers nor an accurate representation of significant differences in the number of miRNAs encoded by different species, but merely demonstrate that miRNA discovery is still somewhat in its infancy and that some genomes receive more attention than others.

2.3.1 Canonical miRNA biogenesis

miRNA biogenesis is summarized in **Figure 6**. In animals, mature miRNAs are encoded in the genome as long primary miRNAs (pri-miRNAs) of over 1 kb which are transcribed by RNA polymerase II, either from specific miRNA genes or from within introns or even exons of protein coding genes [77,78]. Pri-miRNAs form an imperfect double-stranded structure which is processed into approx. 70 nt stem-loop structures termed precursor miRNA (pre-miRNA), or simply miRNA hairpins [79]. This is carried out within the nucleus by the trimeric microprocessor complex composed of two DGCR8 subunits, an RNA binding protein, and one Drosha subunit, an RNase III enzyme [80]. The pre-miRNA is exported from the nucleus to the cytosol by Exportin-5 [81], where the endonuclease Dicer is responsible for cleaving the loop of the pre-miRNA stem-loop structure, yielding a miRNA duplex. This duplex is bound by one of four Argonaute proteins (Ago1-4), and the duplex structure separates leaving only the mature 'leading' strand bound to Ago; the other strand, the 'passenger' strand, is degraded. Strand selection – the process of determining which duplex strand is leader and which is passenger – is a complex process dependent on several associated proteins and the thermodynamic stability of the duplex itself [82]. Both strands have the potential to form a mature functional miRNA; often one strand will be more abundant in the cell, but it is possible for both strands to be present and differentially

[4] http://www.mirbase.org/, currently version 21

expressed in response to inflammation or infection. The Ago-bound miRNA exerts its function as the core component of the RNA-induced silencing complex (RISC), a multimeric complex for which there has not yet been elucidated a clear structure [83]. When bound to a miRNA, the RISC is also termed miRISC. It is in the context of the miRISC that the mature miRNA is able to exert its repressive effect on translation.

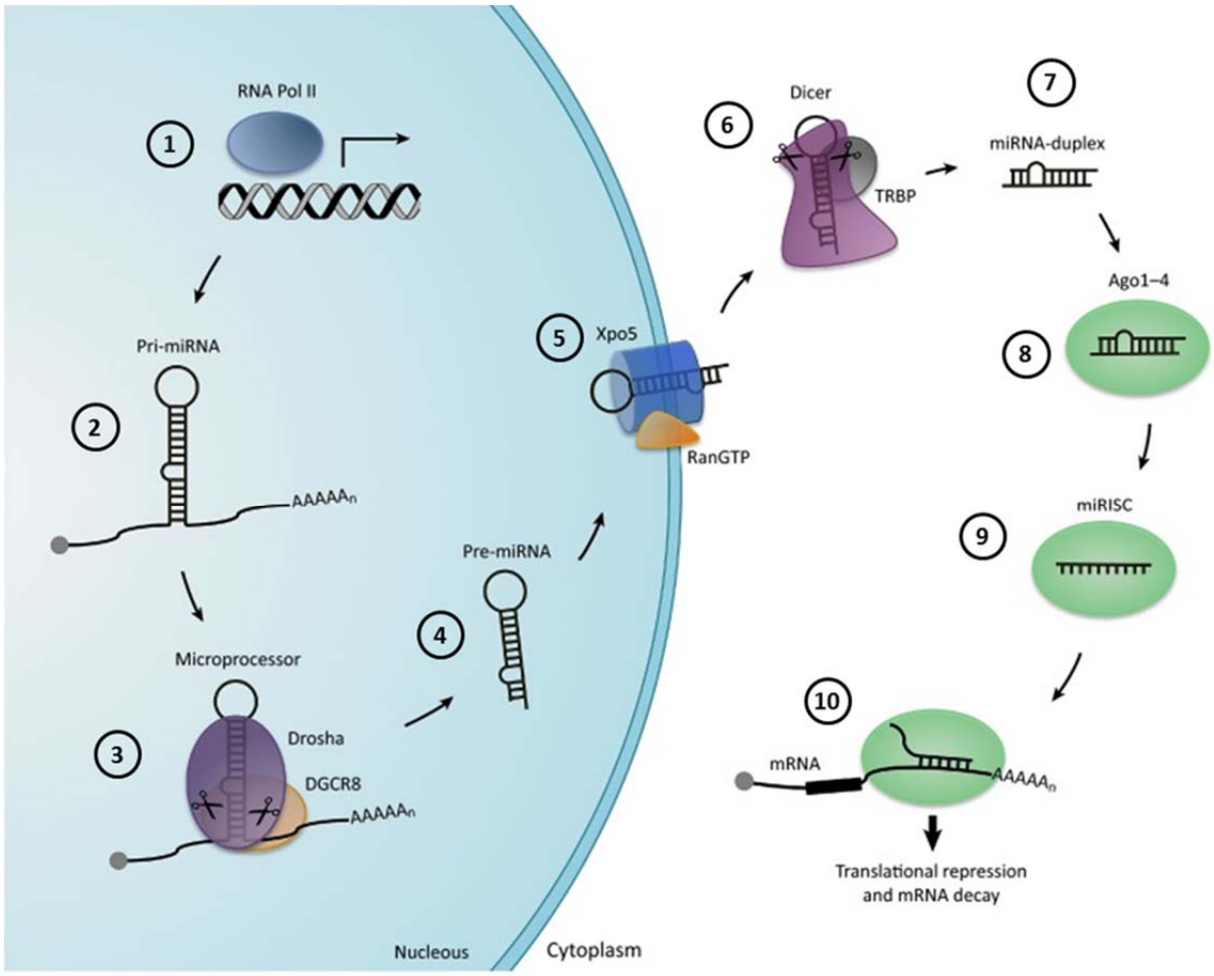

Figure 6. Schematic representation of canonical miRNA biogenesis. The miRNA gene is transcribed by RNA polymerase II (1) to yield pri-miRNAs containing a secondary stem-loop structure (2). The pri-miRNA is processed by the microprocessor complex (3), giving rise to a hairpin pre-miRNA (4) which is exported from the nucleus to the cytosol (5). Here, the pre-miRNA is further processed by Dicer (6) into a miRNA duplex structure (7) which becomes bound by an Ago protein (8). The miRNA duplex separates, leaving only one of the strands bound to Ago (9) forming the miRISC in association with other proteins, which can hinder translation (10). Figure is adapted from Daugaard *et al*. 2017 [78].

2.3.2 miRNA nomenclature

The rapid progression in miRNA research since their discovery has previously caused some confusion in their nomenclature, and even though a systematic approach was suggested already in 2003 [84], novel as well as known miRNAs are still sometimes inconsistently named in the literature [85]. In order to keep track of changes to miRNA names, the online database miRBase Tracker[5] contains all historical and current miRNA annotations [86].

[5] http://www.mirbasetracker.org/

Animal miRNA nomenclature is most easily explained with an example. mi**r**-205 (lower case r) is the name of a pre-miRNA (hairpin). This pre-miRNA yields a duplex with two distinct mature miRNAs, one from each of its 'arms'; the mature miRNA originating from the 5' arm is termed mi**R**-205-**5**p (upper case R), and the one from the 3' arm mi**R**-205-**3**p (upper case R). These designations are species-unspecific; the addition of a three letter species-specific prefix remedies this: hsa-miR-205-5p is thus the human (***H****omo* ***sa****piens*) mature miRNA originating from the 5' arm of the pre-miRNA hsa-mir-205. The gene coding for hsa-mir-205 should be designated *hsa-mir-205*.
The consistent use of the -5p and -3p designations should replace the outdated * (star, asterisk suffix) designation. In the early days of miRNA research it was believed that only one of the duplex strands were biologically functional, and the other – the passenger, denoted with an * – was always degraded. As such, miRBase states 'hsa-miR-205' and 'hsa-miR-205*' as previous names for hsa-miR-205-5p and hsa-miR-205-3p, respectively. The realization that the * strand was sometimes the leading strand prompted the -5p and -3p designation, acknowledging that the two strands may be equally functional and important [85]. In some species, only one mature miRNA has yet been annotated from the pre-miRNA mir-205 and deposited in miRBase. In such a case, the 5p/3p designations are omitted. Thus, the porcine ssc-mir-205 (***S****us* ***sc****rofa*) pre-miRNA is yet only annotated to produce one mature miRNA: ssc-miR-205. It is however known that ssc-miR-205 stems from the 5' arm of ssc-mir-205, and is an exact sequence match to hsa-miR-205-5p.
The numerical part of miRNA names are assigned sequentially as they are discovered. However, if a novel miRNA is discovered in one genome which is a sequence match to a known miRNA from another genome, the numerical name from the known miRNA will be assigned to the novel miRNA. For instance, the miRNA hsa-miR-223-3p is annotated in the human genome but a porcine homolog is not included in the current curation of miRBase (v. 21). The porcine genome does however encode miR-223-3p, so once it is included in miRBase it should be given the name ssc-miR-223-3p, even though many already annotated porcine miRNAs have higher numbers.
In the case of mature miRNAs with highly similar sequences, they will typically have the same numerical name followed by a single letter suffix, e.g. ssc-miR-29a, ssc-miR-29b, and ssc-miR-29c. For historical reasons, a small subset of miRNAs does not adhere to the mir/miR naming convention. For mammals, this pertains to the let-7 family of miRNAs. For these miRNAs it is not possible to distinguish between pre-miRNAs and mature miRNAs based on capitalization of the name, only by the possible use of the -5p and -3p suffixes. If the -5p and -3p mature miRNAs are not both annotated in a given species, the pre-miRNA and mature miRNA names will be identical, as is for example the case for ssc-let-7c.

2.3.3 miRNA function

Sequence complementarity between miRNAs and their mRNA targets is the key to miRNA mediated fine-tuning of translation. miRNAs are short, but the sequences needed for target recognition are even shorter. In fact, only nucleotides 2-7 (approx.) in the 5' end of the miRNA, termed the 'seed' sequence, are required to perfectly pair with the target mRNA sequence in order for the miRISC to exert its effect [87]. The complimentary sequence to the

miRNA seed is most commonly found in the mRNA 3' untranslated region (UTR). Perfect complementarity of animal miRNAs to their mRNA targets is very rare, but commonly observed in plants. When it occurs in animals, full-length complementarity leads to the cleavage of the mRNA target [88]. In humans, only Ago2 has been found to possess the needed endonuclease activity for this mechanism, the remaining three members of the Ago family are not able to cleave mRNA targets [89,90]. Instead, the effect of animal miRNAs on translation is a result of translational repression and mRNA destabilization via deadenylation, leading to mRNA decay [91].
miRNA-mRNA interaction networks can be very complex. Most miRNAs display targeting promiscuity in that they potentially target several hundred different mRNA transcripts, and in addition, one mRNA transcript may be the target of many different miRNAs [92,93]. Predicting the effects of changes in miRNA expression thus quickly becomes a complicated task.
Thousands of miRNA-mRNA interactions have been experimentally validated in mammalian *in vitro* systems, and manually curated online databases collect these information and make them easily accessible for researchers. The most comprehensive of these databases are TarBase[6] [94] and miRTarBase[7] [95]. Experimental approaches for validation of miRNA-mRNA interaction include immunoprecipitation, where the interaction is shown by the co-precipitation of the miRISC and mRNA, or luciferase reporter assays, where the 3' UTR of the mRNA of interest is coupled to the luciferase gene, and the effect of a given miRNA on the luciferase activity is detected. The use of synthetic miRNA mimics or inhibitors are also commonly applied to document a specific effect of a miRNA of interest [96]. *In silico* tools for prediction of miRNA-mRNA interactions provide researchers with a method of identifying which miRNAs could potentially contribute to some observed mRNA regulation – or vice versa, which mRNA transcripts may be influenced by the up- or down-regulation of specific miRNAs. The application of these tools may markedly reduce the number of miRNA-mRNA interactions that are relevant to investigate experimentally, saving valuable resources. Such prediction algorithms take into account e.g. the need for the miRNA seed sequence to match the mRNA transcript (usually in the 3' UTR), the commonly observed conservation of miRNA-mRNA interactions across species, and the thermodynamic stability of the miRISC-mRNA complex [97].

2.3.4 Clinical applications of miRNAs

Since their discovery, miRNAs have been found to be involved in the regulation of countless cellular functions. Thus, the factors which affect miRNA expression are likewise numerous, and comprise e.g. viral and bacterial infections [98,99], aging [100], circadian rhythm [101], cancer [102], autoimmune diseases [103,104], pregnancy [105,106], nutrition and obesity [107,108] – the list goes on. Their ubiquitous impact on health and disease has prompted research into the potential therapeutic applications of miRNAs [109,110]. For example, the host miRNA hsa-miR-122-5p is needed for replication of hepatitis C virus (HCV) in the liver [111]. This has been exploited in the design of a novel anti-HCV drug named Miravirsen, a

[6] http://diana.imis.athena-innovation.gr/DianaTools/index.php?r=tarbase/index, currently version 7.0
[7] http://mirtarbase.mbc.nctu.edu.tw/index.php, currently version 6.0

locked nucleic acid (LNA) molecule with antisense complementarity to hsa-miR-122-5p which has been shown in clinical trials to reduce the viral load in chronically infected HCV patients [112]. Miravirsen is currently the miRNA-targeting drug candidate which has advanced the furthest in clinical trials, but other miRNA based drugs are in the pipeline. These include miRNA inhibitors similar to Miravirsen which are aimed at inhibiting the function of a cellular miRNA, as well as miRNA mimics aimed at augmenting the function of a cellular miRNA [110].

miRNAs have also been heralded great potential as circulating biomarkers for various conditions, assigning them diagnostic as well as prognostic value. One feature of miRNAs supporting their use as biomarkers is the fact that they have been reported to be fairly stable and easily assessable in blood and other body fluids [113–116]. However, our own studies show that different miRNAs exhibit varying ability to withstand heat (80 °C for 120 minutes) and enzymatic (RNase A digestion for 5 minutes) treatment; our results showed that the most stable miRNAs were characterized by a high GC content and a high degree of predicted secondary structure (Lopez *et al*., manuscript in preparation). Although these harsh experimental treatments do not quite mirror the conditions which a patient sample may accidentally be exposed to, the results do serve to remind researchers to consider intrinsic features of individual miRNAs when validating their potential as biomarkers.

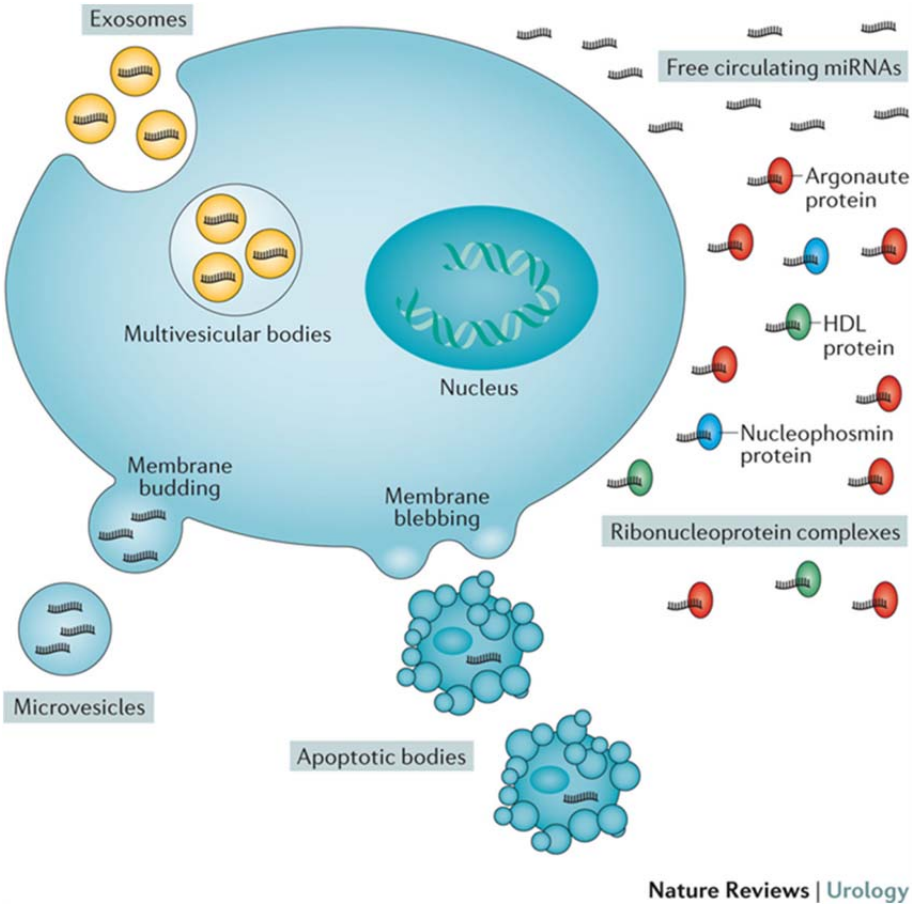

Figure 7. Overview of extracellular miRNAs in body fluids. Extracellular miRNAs appear in many forms; they may me contained in exosomes or other vesicles, bound to lipoprotein, Ago, or other protein complexes. The many different forms of extracellular miRNA warrant caution when evaluating biomarker potential of miRNAs. Figure copied from Fendler *et al*. 2016 [117].

The field of miRNAs as biomarkers also currently needs to address another issue: in body fluids miRNAs can be both intracellular and extracellular, and extracellular miRNAs may again be either contained in exosomes, apoptotic bodies, or other vesicles, they can be associated with lipoproteins, or bound to Ago or other protein complexes [113] (**Figure 7**). As the mechanisms responsible for the different forms of miRNA secretion are not yet fully understood, care should be taken to determine the most optimal sample type and selection of miRNAs for biomarker suitability in a given context. Likewise, strict standardization of sample processing is necessary in order to obtain reproducible results [118].

2.3.5 miRNA and influenza

miRNAs have been found to be important during IAV infection, both by being involved in the regulation of the antiviral host response [119–121], but also by targeting viral RNA directly thus affecting viral translation and replication. The earliest study to demonstrate viral targeting by host miRNAs was performed in Madin-Darby canine kidney (MDCK) cells infected with human H1N1, and showed that miR-323, -491, and -654 could bind to viral PB1 mRNA causing its degradation; these miRNAs were found to bind to a region in PB1 which was conserved in many other IAV subtypes [122].In human lung epithelial cells (A549 cells), PB1 from human 2009 pandemic H1N1 was found to be targeted by hsa-miR-3145 [123], and M1 mRNA from human H1N1 to be the target of hsa-let-7c [124]. Similarly, ssc-miR-204 and -4331 was shown to inhibit replication of a porcine H1N1 strain in newborn pig trachea cells by targeting the HA and NS genomic segments, respectively [125].
As discussed in more detail in **Paper 2**, miRNA expression in circulation of patients with confirmed IAV infection have been shown to be altered relative to healthy subjects, prompting the suggestion of miRNAs as biomarkers in IAV infection [126–128]. One study has also identified miRNAs with biomarker potential for diagnosis of IAV and IBV infection in throat swabs [129].

2.4 Methods for transcriptional analysis

The central dogma of molecular biology in its simplest form tells us that information flows from DNA through RNA into proteins, thus highlighting the intermediary, RNA, that bridges the gap between the schematics of the cell, the DNA, and the machinery, the proteins. In this context RNA can be termed the transcriptome; it is a reflection of the state, the stress, the needs of the cell, and in contrast to the somewhat constant genome, it is ever-changing and provides us with a snapshot of what is happening in the cell at this very moment. In the study of biological processes such as host responses during infectious diseases, the transcriptome is therefore a highly relevant target of research.

2.4.1 Reverse transcription quantitative real-time PCR (RT-qPCR)

The fundamentals of the polymerase chain reaction (PCR) as it is used today have remained the same since its conception in the 1980ies [130]. PCR employs the thermostable *Taq* DNA polymerase to amplify a defined DNA template by the use of a pair of synthetic oligonucleotide primers (termed forward and reverse) that are complementary to the DNA template and define the region of DNA to be amplified. The DNA which is being amplified in RT-qPCR stems from reverse transcription of RNA and is thus termed complementary DNA (cDNA) (more detail in the sections **qPCR quality control** and **mRNA**). During a number (commonly 35-40) of thermal cycles, the amount of cDNA template increase exponentially. Cycling parameters for a qPCR experiment may look like the following (**Figure 8**): double-stranded (ds) cDNA template is denatured at ~95 °C for 15 seconds and PCR primers are annealed to the single-stranded (ss) cDNA template at ~60 °C for 30 seconds after which the *Taq* polymerase synthesizes a new complementary cDNA strand by the addition of nucleotides at ~72 °C for 30 seconds. However, it is also common for annealing and elongation to be carried out at the same thermal step, e.g. at ~60 °C. This yields a new dsDNA product which enters into a new cycle of denaturation, annealing, and elongation.

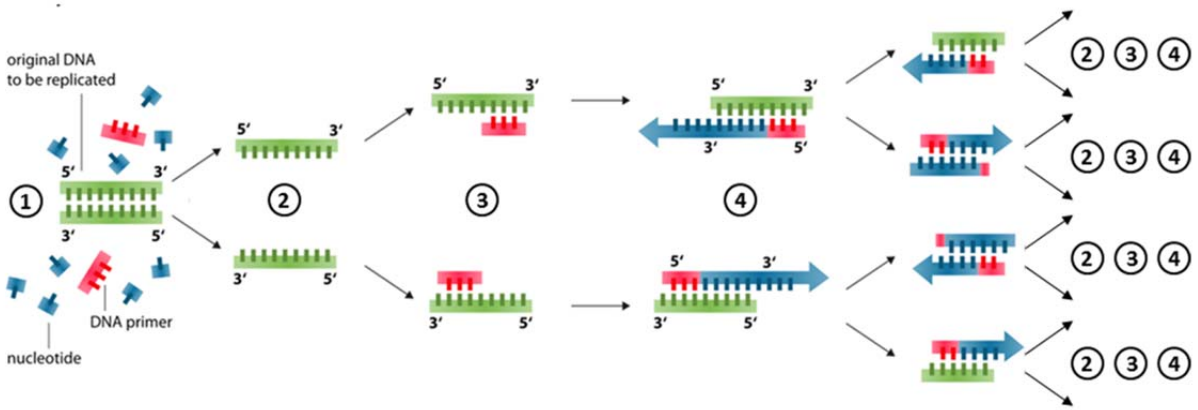

Figure 8. Schematic overview of polymerase chain reaction (PCR). Green – DNA template, red – DNA PCR primer, blue – nucleotides/newly synthesized DNA. Double-stranded DNA template (1) is denatured (2), PCR primers are annealed to the single-stranded DNA template (3), and the thermostable *Taq* DNA polymerase elongates the PCR primers by addition of nucleotides (4), yielding a new double-stranded product complementary to the target sequence. Figure is modified from original by Enzoklop [CC BY-SA 3.0 (http://creativecommons.org/licenses/by-sa/3.0)], via Wikimedia Commons.

These stated time and temperature parameters will often vary between protocols, and it is common for annealing and elongation to be carried out at the same temperature.

PCR becomes ‘real-time’ by the addition of a fluorescent DNA-intercalating dye, such as EvaGreen® or SYBR® Green I, or by using a fluorogenic probe in a probe-based assay. These dyes bind to dsDNA and emit a fluorescent signal which is recorded at the end of each PCR cycle. The intensity of the fluorescent signal directly correlates with the amount of dsDNA product, which is doubled every cycle, which again directly correlates with the initial sample amount of cDNA. The progression of the qPCR is visualized as amplification curves as shown in **Figure 9, left**, thus making it possible to monitor the increase of qPCR product in real-time.

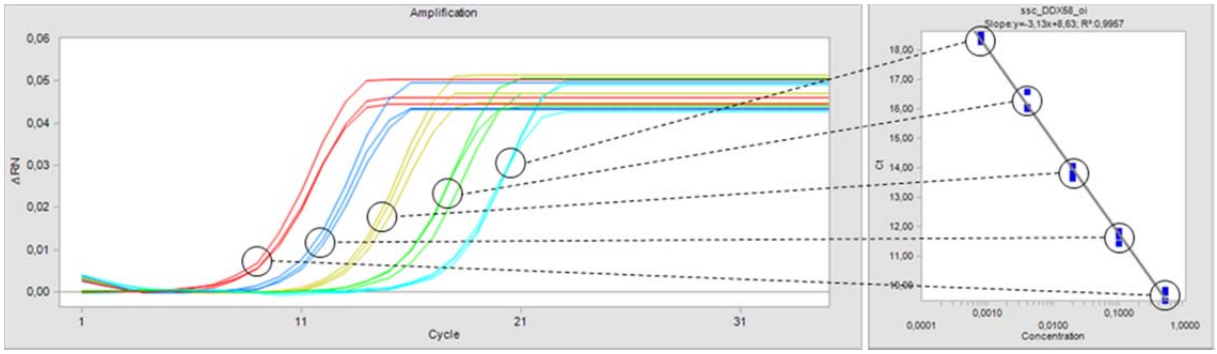

Figure 9. Left – amplification curves obtained from a triplicate 5-step standard of 5-fold dilution series of cDNA of the mRNA coding for the gene *DDX58* from porcine lung tissue. The magnitude of the fluorescent signal is shown on the y-axis, and qPCR cycle number is shown on the x-axis. Right – the C_q values from the dilution series (y-axis) plotted against $\log_{10}$ of their relative concentrations (x-axis). In this instance, linear regression yields a slope of -3.13, which gives a qPCR efficiency of 109 % (efficiency = $-1 + 10^{(-1/\text{slope})}$). Illustration obtained from the Fluidigm Real-Time PCR Analysis software.

Comparability between samples is achieved by measuring the quantification cycle (C_q) for each reaction. The C_q value for a given sample is the cycle number at which the amplification curve crosses a defined threshold. C_q values are thus inversely correlated with the initial concentration of cDNA template; low C_q indicates high template concentration, high C_q indicates low template concentration. The amplification curves in **Figure 9, left** stem from a dilution series which is prepared in order to estimate the dynamic range and efficiency of the assayed qPCR primers. The relative cDNA concentrations of these samples are thus known and utilized to calculate the efficiency of the qPCR reaction. Linear regression is carried out on the dilution series’ C_q values plotted against the $\log_{10}$ of the relative cDNA concentration (**Figure 9, right**): efficiency = $-1 + 10^{(-1/\text{slope})}$. Theoretically, the amount of qPCR product should be doubled after each cycle, which yields an efficiency of 100 %, but it is possible to obtain efficiencies both higher and lower. Low efficiencies occur e.g. when the qPCR primers are not optimally designed for the applied thermal protocol or they form secondary structures. High efficiency based on a dilution series may be the result of inhibitors of the qPCR being present in the reaction mixture, such as carryover from upstream processes (e.g. chloroform, proteins, guanidine). The presence of inhibitors will have a greater impact (inhibitory effect) on the least diluted samples. The C_q value obtained for less diluted samples will therefore be too high, resulting in a linear regression of the standard curve with a lowered (numerical value) slope, which in the end yields a qPCR efficiency >100 %. As such, if inhibition is observed in the most concentrated samples of the dilution series it should not be included in the calculation of efficiency, as this high efficiency would likely not reflect the efficiency

obtained in properly diluted samples. qPCR efficiency is measured for each qPCR assay, and used to efficiency correct the C_q values for all samples analyzed with the given assay.
Given the broad application of qPCR in research, the MIQE guidelines (Minimum Information for publication of Quantitative real-time PCR Experiments) have been set forth to ensure that qPCR data are reported with sufficient thoroughness [131]. Adherence to these guidelines ensures experimental transparency and enables independent validation of results.

qPCR quality control

To ensure that only amplification of desired target is taking place during the qPCR, it is important to include controls which facilitate such assessment of the procedure. A non-template control (NTC), where no template cDNA is added to the reaction, should be included in a qPCR run. No fluorescent signal should be emitted from this reaction unless the reagents are contaminated with DNA that can be amplified, or the qPCR primer pair is able to create double-stranded primer-dimers due to sequence complementarity. When qPCR is applied to assess gene expression (RT-qPCR), the DNA template which is being amplified stems from reverse transcription of mRNA into cDNA. It is important only to quantify cDNA and not genomic DNA (gDNA), and as such, a minus reverse transcriptase control (-RT control) sample is made during the cDNA synthesis, where reverse transcriptase is excluded from the reaction. The -RT control should not emit any fluorescence, as it should not contain any (c)DNA.
The presence of a single, specific qPCR product is commonly assessed by melting curve analysis (MCA). After the last qPCR cycle is completed, the qPCR product will be subjected to a gradual increase in temperature, e.g. raising it from 60 °C to 95 °C at a rate of 1 °C every 3 seconds. This will eventually denature the double-stranded qPCR product, causing the fluorescent signal to cease. The melting temperature (T_m) of the product is defined as the temperature at which half the dsDNA has denatured. The accompanying decrease in fluorescence yields melting curves as those depicted in **Figure 10**, when the derivative of fluorescence with respect to temperature is plotted against the temperature. The T_m of a qPCR product is determined by its length and nucleotide composition.

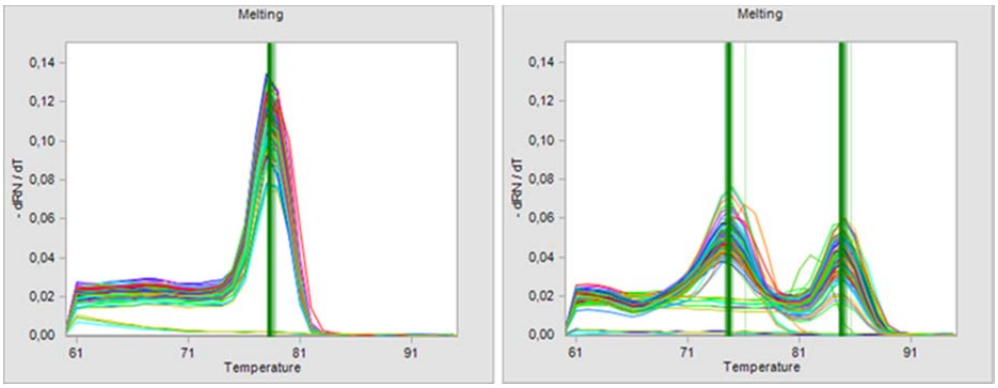

Figure 10. Left: example of a good MCA, the amplification of the gene *DDX58* has yielded one specific product. Right: example of a poor MCA, the amplification of the gene *CASP9* has yielded an unspecific product, likely a primer-dimer. Illustration obtained from the Fluidigm Real-Time PCR Analysis software.

Each dsDNA qPCR product is therefore likely to have its own unique T_m, and so, single peak is indicative of only one specific product having been amplified in the reaction, e.g. **Figure**

10, left. A MCA as the one in **Figure 10, right**, shows that more than one dsDNA product is emitting a fluorescent signal, indicating unspecific, unwanted amplification. Such an error is commonly caused by the presence of primer-dimers.

High-throughput RT-qPCR on the BioMark™ HD platform (Fluidigm)

qPCR can be performed in a relatively high-throughput manner by employing platforms such as the BioMark™ HD from Fluidigm. The reactions are carried out in specially designed Dynamic Array Integrated Fluidic Circuit (IFC) chips like the one depicted in **Figure 11**. Chip formats for gene expression analysis allow for either 96 samples analyzed in 96 assays (96.96), 48 samples analyzed in 48 assays (48.48), or 192 samples assayed in 24 assays (192.24), thus facilitating 9,216, 2,304, or 4,608 parallel reactions in a single run, respectively. qPCR reagents and samples are deposited into the appertaining inlets in excess of what is necessary to carry out the reactions, and distributed in the reaction chambers in microfluidic channels by applying automated air pressure prior to qPCR. The human error of pipetting differences between reaction tubes is thus eliminated.

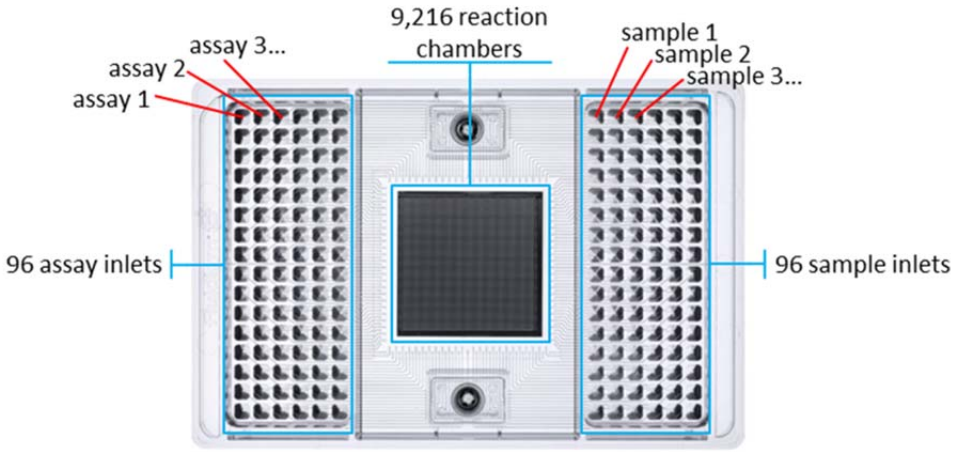

Figure 11. 96.96 Dynamic Array IFC chip. Picture obtained from the Fluidigm website.

The thermal protocol for qPCR in a 96.96 Dynamic Array IFC chip (Fluidigm) is slightly extended compared to that described in **section 2.4.1**. As shown in **Figure 12**, the thermal protocol is initiated by a Thermal Mix phase, which ensures that the reagents are sufficiently mixed inside the small reaction chambers which accommodate only a few nanoliters. If uracil-DNA glycosylase is employed to eliminate potential carryover PCR products, this is carried out in the UNG phase; however, this step is not used in the qPCR described in **Papers 2-4**. During the Hot Start phase the DNA polymerase is activated. Until this time point it has been in an inactivated state, and blocked from synthesizing DNA. The actual qPCR consists of 35 cycles of denaturation and combined annealing and elongation followed by MCA. In total, it takes around two hours to complete 9,216 reactions.

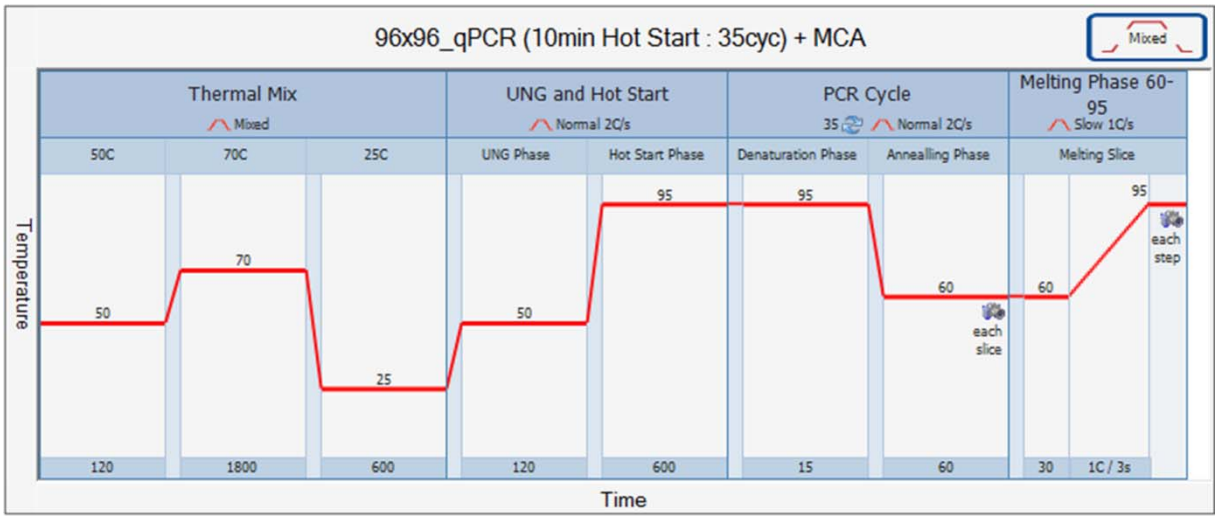

Figure 12. Thermal protocol for qPCR carried out in 96.96 Dynamic Array IFC chips (Fluidigm). The Thermal Mix phase is comprised of 2 minutes at 50 °C, 30 minutes at 70, and 10 minutes at 25 °C. UNG and Hot Start is carried out at 50 °C for 2 minutes and 95 °C for 10 minutes. The qPCR comprises 35 cycles of denaturation for 15 seconds at 95 °C and annealing and elongation for 1 minute at 60 °C. Finally, MCA is carried out by increasing the temperature 1 °C every 3 seconds. Illustration obtained from the Fluidigm Real-Time PCR Analysis software.

Upstream processes – reverse transcription, primer design, and pre-amplification

RT-qPCR has long been considered the 'gold standard' for quantitative gene expression analysis. Reverse transcription of mRNA into cDNA facilitates quantification of the transcriptome by use of methods developed for the quantification of DNA, such as qPCR and sequencing. The enzyme reverse transcriptase is used to synthesize cDNA from a template of extracted RNA, by employing a relevant priming strategy. It is the cDNA copy of the RNA that is subsequently quantified during the qPCR. Reverse transcription and design of qPCR primers is carried out differently for different types of RNA, as will be described in the following for mRNA and miRNA.

mRNA

The transcription of protein-coding genes yields mRNA which is subsequently translated into protein. To quantify mRNA it is necessary first reverse transcribe it into cDNA by the use of reverse transcriptase. Reverse transcription is a process that needs priming, and for mRNA it is possible to use 'universal' reverse transcription primers such as oligo(dT) primers, which anneal to the polyadenylated 3' end of the mature mRNA, or so-called random primers, usually hexamers of randomly generated nucleotide sequences that could potentially anneal anywhere in the transcript. Mature mRNAs are often the product of two or more protein-coding exons being spliced together (**Figure 13**). The initial RNA transcript is composed of alternating exons and non-protein-coding introns. These introns need to be removed from the transcript to achieve a mature, protein-coding mRNA.

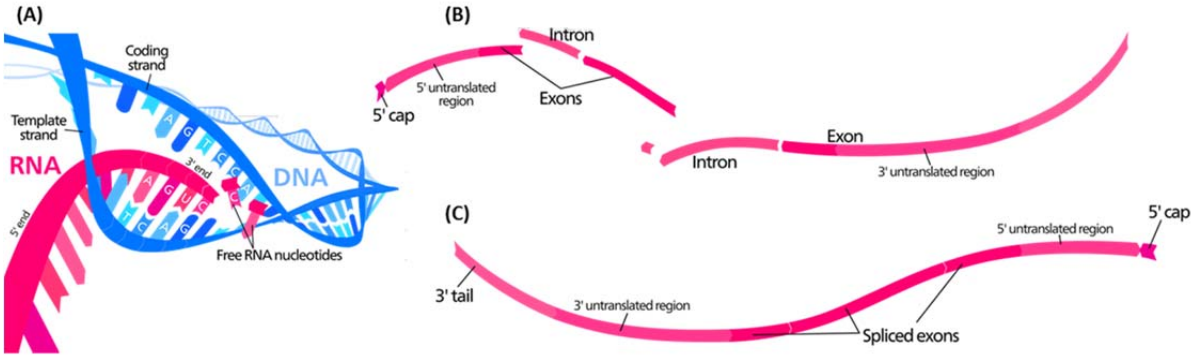

Figure 13. Simplified overview of eukaryotic transcription. RNA is transcribed from the genome (A), and introns are excised form the RNA strand (B). The remaining exons are spliced together to form a mature mRNA that is polyadenylated in the 3' end (3' tail). Figure is modified from original by Kelvinsong [CC BY 3.0 (http://creativecommons.org/licenses/by/3.0)], via Wikimedia Commons

This feature allows for qPCR primer design strategies that can differentiate between cDNA from mRNA and unwanted gDNA in the qPCR. One strategy is to design primers that anneal on either side of an intron, as exemplified by the blue primer pair in **Figure 12**. Theoretically, this primer pair would be able to amplify gDNA if it is present, but the resulting product would be much longer and most likely amplified with a lower efficiency than the desired product. If a sample should be contaminated with gDNA it would be easily identified by MCA. Another strategy is to design one of the primers to anneal to a sequence that overlaps a splice site, as demonstrated by the forward red primer in **Figure 12**. This primer will only be able to anneal to cDNA from a mature, spliced mRNA. Therefore, this primer pair will not be able to amplify gDNA.

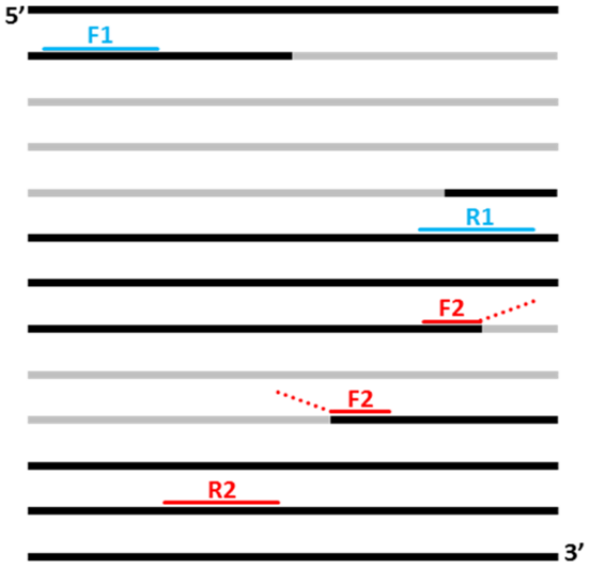

Figure 14. qPCR primer design strategies for protein coding genes (mRNA). Black – exons, grey – introns. The blue qPCR primer pair (forward F1, reverse R1) anneal to regions of two different exons that both flank the same intron. The forward primer F2 of the red qPCR primer pair is designed so that its 3' end anneals to the 3' end of one exon, and its 5' end anneals to the 5' end of the next exon. Thus, F2 will only be able to anneal to cDNA generated from mature, spliced mRNA, and not to gDNA. The matching reverse primer R2 anneals downstream. Note that the forward and reverse primers do not anneal to the same strand, but to complementary strands. They are shown here to anneal to the same schematic representation of ds cDNA for simplicity's sake.

miRNA

miRNAs are not transcribed from the genome in their mature form, but are rather the product of processing of a much longer pri-miRNA (see **section 2.3.1**). As mature miRNAs are structurally very different from mRNA, the same reverse transcription and qPCR design strategies cannot be applied. Different strategies for RT-qPCR of miRNAs exist. The major difference between these methods is essentially how the primers for reverse transcription and qPCR are designed. The method described and used in the work presented in the present thesis was first described by Balcells, Cirera, and Busk [132,133]. This method employs a universal reverse transcription primer and qPCR primer pairs which are both miRNA-specific. Other approaches described in the literature include miRNA-specific reverse transcription primers, a cumbersome method that requires separate reverse transcription reaction for each miRNA of interest, and qPCR primer pairs where only one primer is miRNA-specific and the other universal. In the method described here, the mature miRNA is polyadenylated in its 3' end to provide an annealing site for the reverse transcription primer (**Figure 15**). A reverse transcription primer containing a poly(T) sequence will anneal to the synthetic poly(A) tail and prime the reverse transcription. The reverse transcription primer includes a tag sequence (5'-CAGGTCCAG-3') in its 5' end which is important for primer design and annealing in the subsequent qPCR [132]. Reverse transcription of mature miRNAs thus yield a cDNA product which comprises the miRNA sequence, a poly(T) stretch, and a tag sequence with a combined length of ~48 nucleotides (nt).

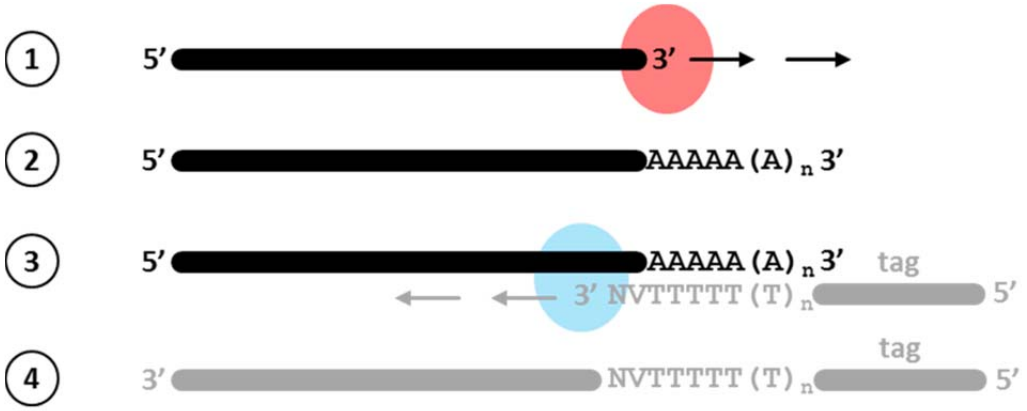

Figure 15. Schematic overview of reverse transcription of miRNA. The mature miRNA (black) is subjected to polyadenylation by poly(A) polymerase (red) (1) to yield a miRNA with a poly(A) tail (2). This allows the annealing of the reverse transcription primer (grey) which primes the cDNA synthesis by reverse transcriptase (blue) (3) to produce a cDNA copy of the miRNA which also contains a tag sequence that will be utilized in the qPCR. Nucleotides: A – adenine; T – thymine; V – guanine (G), cytosine (C), or A; N – A, T, G, or C.

The primer design approach is summarized in **Figure 16**. The majority of the forward primer is complementary to the cDNA sequence corresponding to the original miRNA, making it highly miRNA-specific. Its 5' end comprises a tag sequence which lends length and stability and increases the T_m of the primer. The reverse primer is complementary to the tag sequence originating from the reverse transcription primer, the poly(T) stretch, and the first 4-8 nt of the original miRNA sequence, thus making is semi miRNA-specific.

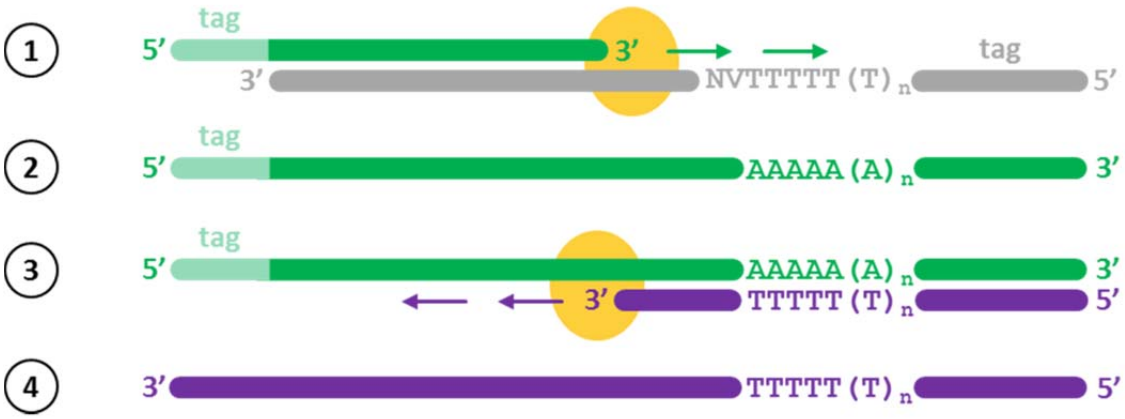

Figure 16. Schematic overview of the qPCR primer design strategy for qPCR analysis of miRNA. The forward primer anneals to the cDNA sequence that corresponds to the majority of the original miRNA sequence, and is thus highly miRNA-specific (1). The 5' end of the forward primer comprises a tag sequence which is not complementary to the cDNA. The *Taq* polymerase (orange) synthesizes a DNA coy of the cDNA template (2). The reverse qPCR primer (purple) is complementary to the tag sequence from the reverse transcription primer, the poly(T) stretch, and a few nt of the original 5' end of the miRNA sequence (3), and will in the qPCR yield a DNA strand (4) that is complementary to the strand in (2). Nucleotides: A – adenine; T – thymine; V – guanine (G), cytosine (C), or A; N – A, T, G, or C.

Pre-amplification

Due to the very small reaction volumes on the Fluidigm Dynamic Array IFC chips, it is necessary to pre-amplify the cDNA targets prior to qPCR in order to ensure detection. The pre-amplification reaction is in essence a highly multiplex PCR. The reaction is carried out with a mix of all qPCR primers to be applied in the subsequent qPCR, but at a lower concentration than it would be in the qPCR. The number of thermal cycles is also lower than it would typically be in a qPCR, The appropriate number of cycles will depend on initial RNA amount for the cDNA synthesis, expression levels of the genes of interest, and the type of protocol (amount of pre-amplification reagents) used during the pre-amplification reaction. Determining the optimal number of cycles, which yields a broad dynamic range and low technical variation, will usually require some optimization.

2.4.2 Small RNA sequencing

Technological advancements in DNA sequencing have led this method to be increasingly common for transcriptional analysis. Next-generation sequencing (NGS, also referred to as second-generation sequencing or massively parallel sequencing) builds on the original Sanger sequencing approach in that specially modified nucleotides are used in a DNA elongation process to detect which nucleotides are present at each position of a DNA template sequence of interest [134]. Sanger sequencing employed labeled nucleotides with the ability to terminate primer-dependent elongation followed by high resolution gel separation of the fragments to determine the sequence of the template (based on the labeling of the modified nucleotides) [135]. In a primer-based sequencing-by-synthesis approach, modern NGS also employs labeled nucleotides to detect the sequence of a DNA template; however, rather than terminating the elongation every time a labeled nucleotide is incorporated, the nucleotides are reversibly blocked [134].

The major strength of small RNA sequencing in comparison with RT-qPCR is the fact that it is a 'hypothesis-free' approach, in that no primers specific for the sequences of interest need to be applied. It is a global approach where the only restricting factor defined by the user is the size selection of the sequenced products, which corresponds to the size range of the type of small RNA of interest. Thus, small RNA sequencing is the primary method for the discovery of new miRNAs. This can be done by applying relevant algorithms in the small RNA sequencing data analysis and/or by alignment analysis (BLASTing) against already known miRNAs from other (related) genomes.

Library preparation

The initial steps NGS for transcriptional analysis are similar to those for RT-qPCR, as the extracted RNA must first be reverse transcribed into cDNA and amplified by PCR. The term 'library preparation' is used to describe the process of preparing an RNA sample for sequencing, summarized in **Figure 17**. These illustrations are taken from the manufacturer protocol (New England Biolabs reagents for sequencing on Illumina platforms) for the library preparation kit applied for small RNA sequencing described in **Paper 3**. The procedure is however very representative for library preparation for small RNA sequencing as it would be carried out using reagents from other manufacturers.

Total RNA is extracted from a biological sample, and the first library preparation step is to ligate adaptors to the 5' and 3' ends of the RNA to serve as annealing site for the reverse transcription primer (the 3' adaptor) and PCR primer (the 5' adaptor) in subsequent procedures. It is advantageous to first ligate the 3' adaptor, and then anneal the reverse transcription primer to the 3' adaptor before the 5' adaptor is ligated. This prevents this prevents the 5' adaptor from ligating to any residual free 3' adaptors, as these will be sequestered by the reverse transcription primer (**Figure 17, 2-4**). It would be wasteful to have such an unwanted adaptor-adaptor product present during sequencing, as it would take up space and reagents. After ligation of the 5' adaptor, reverse transcription of the adaptor-RNA-adaptor construct is carried out.

Once the RNA is copied into cDNA, it needs to be amplified by PCR which is combined with the introduction of barcode sequences which will facilitate the differentiation of samples during the actual sequencing, as this is carried out as a multiplex reaction on a pool of cDNA libraries. The PCR is summarized in **Figure 18**. Both the forward and reverse PCR primers are made up in part of adaptor sequences (NB – different from those described for reverse transcription) which will be used during the sequencing process. Thus, only the 3' ends of the PCR primers anneal to the cDNA, as these are complementary to the adaptor sequences introduced during reverse transcription. In addition to the sequencing adaptor, the reverse primer likewise contains hexameric barcode sequences which will be unique for individual samples. After PCR, the amplified cDNA will thus include sequencing adaptors and sample-specific barcodes. At this point, the cDNA may originate from any RNA that was present in the original sample. To investigate a specific subset of small RNAs, e.g. miRNAs, the amplified cDNA is size fractioned by gel electrophoresis and the band corresponding to the size of the RNA of interest plus the introduced adaptors and barcode is excised. This product is purified, pooled with other samples to be analyzed, and sequenced.

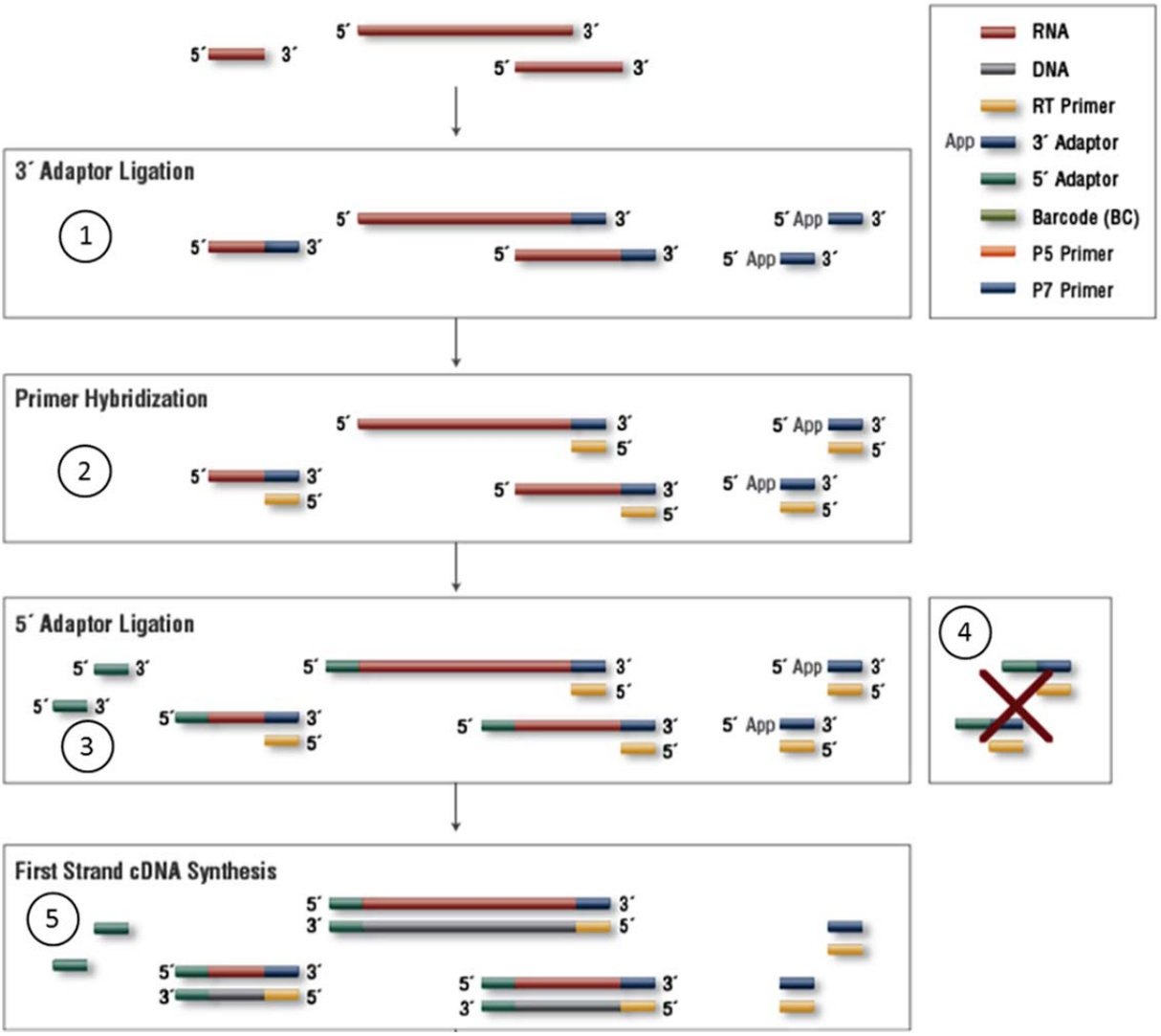

Figure 17. Schematic representation of reverse transcription of RNA to cDNA for small RNA sequencing. 3' adaptors (blue) are ligated to the 3' end of the extracted RNA (red) (1) followed by annealing of the reverse transcription primer (yellow) (2). The 5' adaptor (green) ligates only to the RNA (3), as unligated 3' adaptors are sequestered by the reverse transcription primer (4). cDNA (grey) synthesis proceeds by elongation of the reverse transcription primer (5). Figure is modified from the online product description of the NEBNext® Multiplex Small RNA Library Prep Set for Illumina® (New England Biolabs).

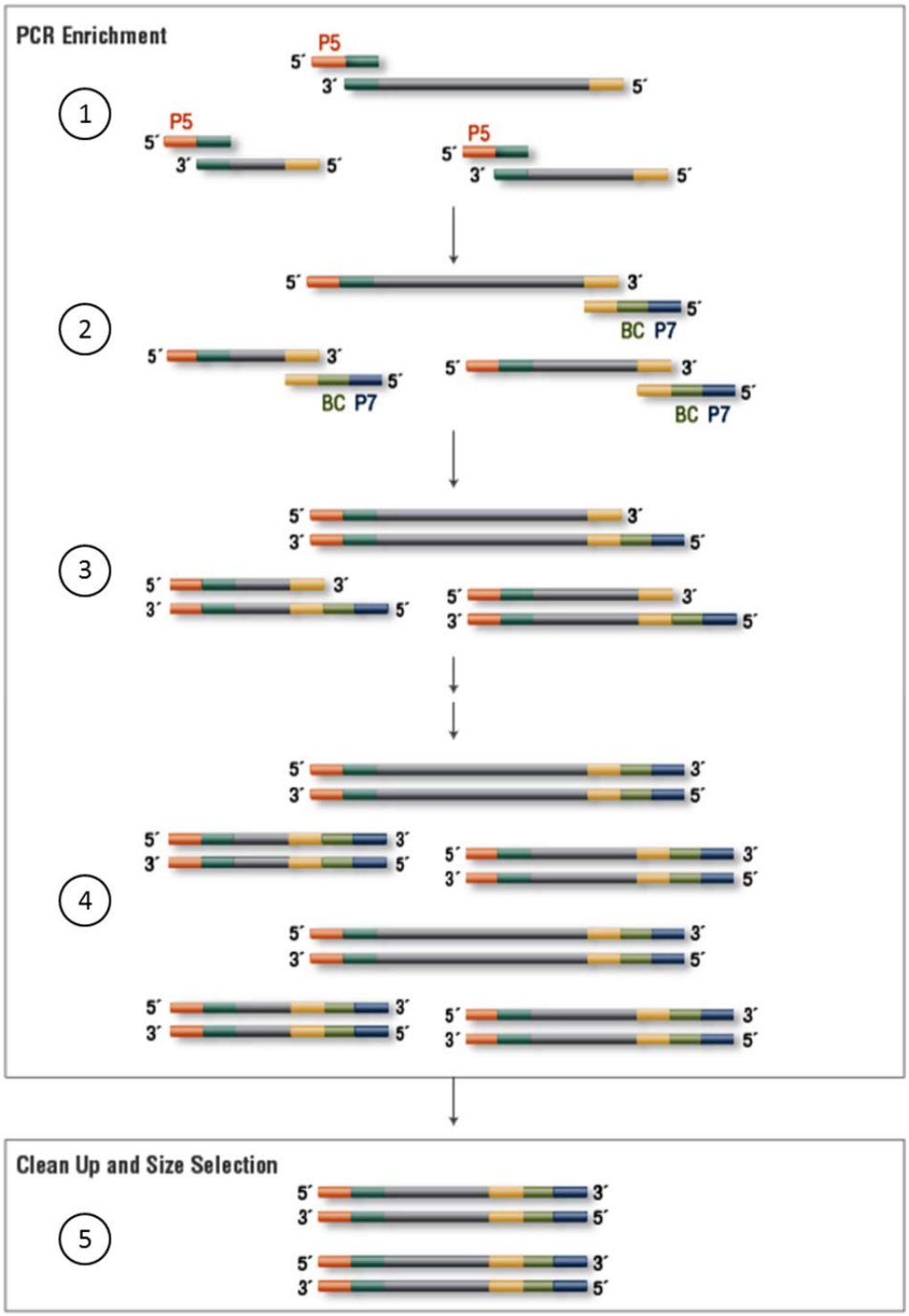

Figure 18. PCR amplification of cDNA for small RNA sequencing. The forward PCR primer (orange/green) anneals to the 5' adaptor sequence from the reverse transcription (1) and the reverse PCR primer (yellow/light green/blue) anneals to the 3' adaptor sequence from the reverse transcription (2). The cDNA (grey) is amplified by PCR (3-4). Amplified cDNA of the desired size is purified for sequencing. The orange part (P5) of the forward primer and the blue part (P7) of the reverse primer are complementary to oligo sequences which are applied in the sequencing process. The green part (BC) of the reverse primer is the barcode sequence. Figure is modified from the online product description of the NEBNext® Multiplex Small RNA Library Prep Set for Illumina® (New England Biolabs).

Cluster generation and sequencing

The purified cDNA pool is added to the surface of a flow cell. Attached to this surface are two different DNA oligos with sequences that are complementary to the two sequencing adaptors introduced during library preparation. The cDNA molecules thus anneal to these oligos, which function as primers for DNA polymerase which copies the cDNA. The original cDNA template is discarded. In a process called bridge amplification, clusters of identical cDNA molecules are generated on the flow cell surface [136] (**Figure 19**). The cDNA bends over and the free end can anneal to a neighboring oligo, forming a bridge. This neighboring oligo thus functions as a primer for the second replication of the cDNA, yielding two complimentary strands of cDNA attached to the flow cell surface. This happens over and over again, creating dense clusters. Ultimately, all cDNA attached to one of the two types of oligos will be cleaved off and discarded, leaving only cDNA stands with the same directionality attached to the flow cell for sequencing.

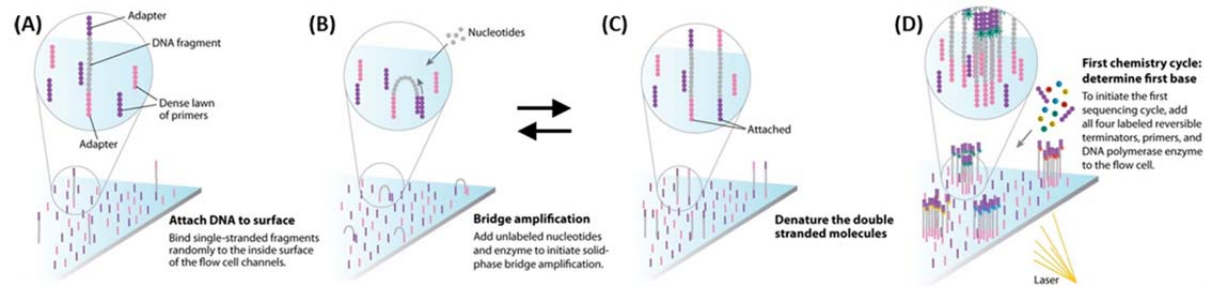

Figure 19. Overview of bridge amplification and sequencing. The cDNA attached to oligos on the flow cell surface (A) form a bridge by annealing to a free flow cell-attached oligo (B). This oligo then acts as a primer for the synthesis of a new cDNA strand (C). This process is repeated until clusters of identical cDNA have been generated which are then sequenced in a primer-dependent manner, using fluorescently labeled nucleotides. Figure is adapted from Mardis 2008 [136].

Sequencing–by-synthesis is carried out by the addition of sequencing primers, polymerase and fluorescently labeled nucleotides in a defined number of cycles (**Figure 19**). The nucleotides are chemically modified to be able to reversibly block the elongation process, ensuring that only one nucleotide is incorporated in each cycle [134]. Each of the four nucleotides are labeled with different dyes, so when laser excitation causes the fluorescent signal to be emitted, each cluster of clonally amplified cDNA fragments should emit the same signal. The signal emitted from each cluster during each cycle is recorded, and can be 'translated' into a nucleotide sequence. This sequence will contain both the barcode sequence identifying which RNA sample the cluster originates from, as well as the sequence of the small RNA of interest.

Small RNA sequencing data analysis

The digital data output from small RNA sequencing is computationally demanding to process. Data is typically supplied as large text files in FASTQ format (.fq). The sequence obtained from a single cluster on the flow cell surface is termed a 'read'. In the FASTQ format, each read is represented by four lines of text, as shown by the example below:

```
@HWI-ST1338:148:H81K3ADXX:1:1101:1502:1998 1:N:0:GAGTGG
GTTTCCGTAGTGTAGTGGTTATCACGTTCGCCTTGGAATTCTCGGGTGCC
+
BBBFFFFFFFFFFIIIIIIFFFFFFBFFFFFBFFIIFFFFFIFFBF'<BB
```

Line 1 is an instrument-specific identifier containing information on the coordinates of the cluster on the flow cell surface; line 2 is the actual read sequence; line 3 is initiated by a + sign and may contain additional identifying information (optional); line 4 contains information on the quality score, Q (Phred quality score), of each base call in the read, and the text strings in line 2 and 4 will always be of equal length as there is one quality score for each position in the read. Q ranges from 0 to 40 and is stored as ASCII characters as follows:

```
!"#$%&'()*+,-./0123456789:;<=>?@ABCDEFGHI
low quality                    high quality
0                                        40
```

Each character translates to a numerical Q value. The probability of an incorrect base call, P, relates to Q by the following: $P = 10^{(-Q/10)}$.
A variety of tools, some with graphical interfaces and some for command line use, are available for small RNA sequencing data analysis, including quantification and prediction of novel small RNAs [137–141], and they all follow similar procedures as outlined in the generic data analysis process in **Figure 20**.

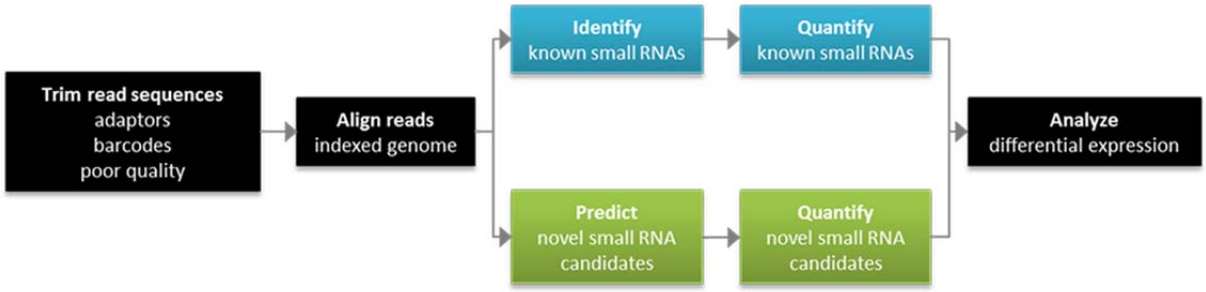

Figure 20. Generic overview of the small RNA sequencing data processing.

The initial step is to trim read sequences for adaptor and barcode sequences as well as bases with poor quality scores. This leaves a high quality read sequence that represents a small RNA that was present in the original biological sample. These trimmed reads are aligned to the relevant (indexed) annotated genome, facilitating identification of those reads representing an already known small RNA. Reads that do not align to a known small RNA may represent a yet undiscovered small RNA. This may be assessed by algorithms that take into account identifying characteristics of the type of small RNA in question. Both known and potentially novel small RNAs are quantified by counting the number of reads that align to the same genome sequence, which is the quantitative output that is used to analyze for differential expression.

3 Experimental framework and supplementary results

As reviewed in **Paper 1**, the pig presents an excellent model for human IAV infection in addition to also being a natural host for IAV itself. As such, the pig model is the experimental backbone of this thesis, applied in *in vivo* as well as *ex vivo* studies of IAV infection. This chapter will provide an overview of the animal experiments (**section 3.1**) which has supplied the material for **Papers 2-4**. Furthermore, a description of and results from a pilot study of the use of *ex vivo* porcine nasal explants for transcriptional analysis of the host response after IAV infection will be presented in **section 3.2**.

3.1 Animal experiments

All data presented in the **Papers 2-4** stem from a large IAV vaccination and challenge study carried out in early 2009 as a collaboration between DTU Vet and IDT Biologika GmbH (Dessau-Rosslau, Germany) at the premises of IDT Biologika. Prior to this PhD project, one study had been published which included transcriptional profiling of mRNA and miRNA from a subset of the animals from this experiment [42]. All procedures and animal care was carried out in accordance with Good Clinical Practice (VICH GL9, CVMP/VICH/595/98), the Directive 2001/82/EC on the Community code relating to veterinary medicinal products, and German Animal Protection Law. The protocol IDT A 03/2004 was approved by the Landesverwaltungsamt Sachsen-Anhalt, Germany (Reference Number: AZ 42502-3-401 IDT). The study included a total of 55 cross-bred Large White x German Landrace pig, who received either no vaccination (n = 20) or a 2-step vaccination (days 0 and 21) against IAV with the RESPIPORC FLU3 vaccine (IDT Biologika) (n = 30), containing inactivated swine IAV of the H1N1, H2N1, and H3N2 subtypes.

Table 1. Overview of animal experiment. 30 pigs received IAV vaccination (days 0 and 21) and IAV challenge (day 28). Vaccinated pigs were slaughtered in groups of ten on days 1, 3, and 14 after IAV challenge. 20 unvaccinated pigs received IAV challenge simultaneously with the vaccinated pigs, and were slaughtered in groups of six, six, and eight on days 1, 3, and 14 after challenge, respectively. Five untreated animals were kept as a control group and slaughtered at the day 14 time point.

	IAV challenge		no challenge
slaughter day (after challenge)	vaccination RESPIPORC FLU3	no vaccination	controls
1	n = 10	n = 6	
3	n = 10	n = 6	
14	n = 10	n = 8	n = 5

Vaccination was given as 2 ml intramuscular injection at the right side of the neck behind the ear. All animals, except five control animals, received IAV challenge on day 28 (relative to first vaccination). The challenge strain (A/swine/Denmark/12687/2003(H1N2) [142]) was given via aerosol exposure to nebulized culture supernatant containing $10^{4.55}$ $TCID_{50}$/ml. The pigs were 12-weeks-old at the time of IAV challenge. A group of unchallenged pigs were kept as controls (n = 5). Treatments, time points, and sample sizes are summarized in **Table 1**.

3.1.1 Sampling

Lung tissue samples were collected at time points 1, 3, and 14 days after IAV challenge. All data from lung tissue presented in this thesis are from samples taken from the left cranial lobe. Nasal swab were collected from pigs after challenge, as indicated in **Table 2**.
Blood samples were collected from all animals throughout the study according to the schedule in **Table 2**.

Table 2. Summarization of blood samples taken during the animal experiment. Yellow background indicates that a nasal swab was also collected at this time point. Time points in black: day after first vaccination; time point in grey: day after challenge.

Sample	Time point	Notes	Sample	Time point	Notes
B0	Day 0	Before any pigs were vaccinated	B11	Day 28 (Day 0)	Seven days after second vaccination; sample taken before challenge
B1	Day 1	Approx. 12 h after first vaccination	B12	Day 29 (Day 1)	Approx. 12 h after challenge
B2	Day 1	Approx. 24 h after first vaccination	B13	Day 29 (Day 1)	Approx. 24 h after challenge
B3	Day 2		B14	Day 30 (Day 2)	
B4	Day 4		B15	Day 31 (Day 3)	
B5	Day 7		B16	Day 32 (Day 4)	
B6	Day 21	Sample taken before second vaccination was administered	B17	Day 33 (Day 5)	
B7	Day 22	Approx. 12 h after second vaccination	B18	Day 34 (Day 6)	
B8	Day 22	Approx. 24 h after second vaccination	B19	Day 35 (Day 7)	
B9	Day 23	Two days after second vaccination	B20	Day 42 (Day 14)	
B10	Day 25	Four days after second vaccination			

3.1.2 Clinical signs

Following IAV challenge, all animals were observed for clinical signs indicative of IAV infection, i.e. increased body temperature and dyspnoea. Body temperature was measured rectally at five time point after challenge as indicated in **Figure 21, left**. Dyspnoea was assessed according to the following scoring scheme: 0 = breathing unaffected; 1 = increased respiratory frequency and moderate flank movement; 2 = marked pumping breathing and severe flank movement; 3 = labored breathing affecting the entire body, pronounced flank

movement and substantial movements of the snout; 4 = severe breathing reflecting substantial lack of oxygen. Dyspnoea of the individual pigs was scored at five time points as indicated in **Figure 21, right**.

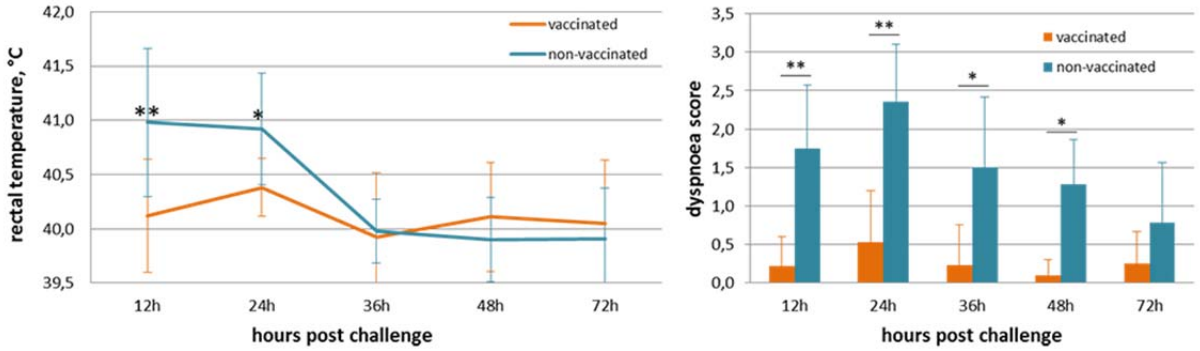

Figure 21. Clinical signs of IAV challenged pigs at 12 (n = 30), 24 (n = 20), 36 (n = 20), 48 (n = 20), and 48 (n = 20) hours after challenge. Left: rectal temperature measured during the first three days after challenge. ** $p < 0.0001$, * $p < 0.01$ (Student's *t*-test). Right: Dyspnoea score monitored during the first three days after challenge. ** $p < 0.0001$, * $p < 0.01$ (Mann-Whitney *U* test). Error bars show SD.

3.2 Explant culture pilot study

Whereas *in vivo* studies in relevant animal models such as the pig are of immense value to IAV research, they are admittedly also a very expensive undertaking. An experimental challenge study as the one just described is arguably not very 3R compliant either. '3R' describes a set of principles to be considered in the context of animal experiments – Replacement, Reduction, and Refinement [143]. Replacement encourages replacing the use of higher animals with non-animal model systems, Reduction calls for the use of a reduced number of animals for an experiment, and Refinement asks for more humane methods to be applied in animal experimentation, ensuring that pain and stress inflicted on the animals are minimized. Even though strict legislation is in place to ensure that animal experimentation is carried out as humanely as possible, it is always desirable from an animal welfare point of view to adopt a more stringent adherence to the 3R principles.

In an effort to implement a 3R compliant *ex vivo* model, a pilot study was set up to test the applicability of porcine nasal mucosal explants as a tool for transcriptional analysis of the host response to IAV infection in the upper respiratory tract. Using this method, one six-week-old pig can typically yield approx. 24 explants, representing the nasal epithelium which is the first host cells that come into contact with IAV during natural infection. This model may thus be suitable for characterization of the very early host response which is taking place during the first few cycles of viral replication in the upper respiratory epithelium.

Explants were obtained by stripping the mucosa from the nasal cavity (septum and conchae) of two six-week-old pigs immediately after euthanization by sodium pentobarbital injection (**Figure 22**).

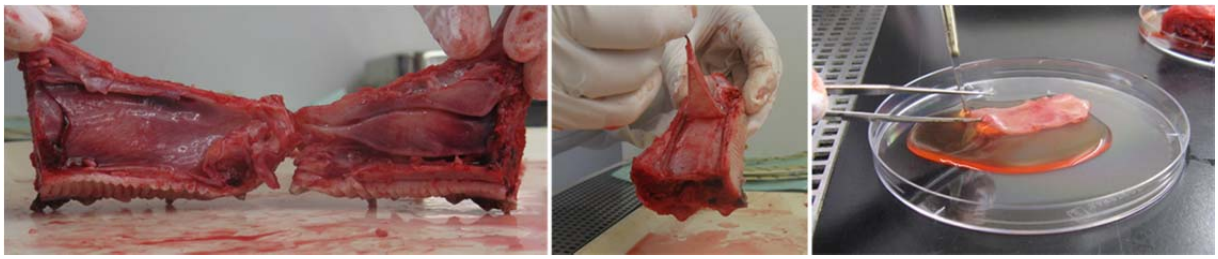

Figure 22. Left – the exposed mucosa of the porcine nasal septum and conchae; middle – carefully peeling the mucosa from the septum keeping ripping and touching of the tissue to an absolute minimum; right – the freed mucosa is kept moistened in medium until it is cut into appropriately sized explants. Own pictures.

The mucosal layer was divided into squares of approx. 0.5 x 0.5 cm and cultivated at the air-liquid interface in growth medium[8], apical side facing up. After harvest, the explants were incubated for 24 h (37 °C, 5 % CO_2) followed by inoculation for 1 h at 37 °C (5 % CO_2) with IAV (0.6 ml virus suspension containing $10^{4.05}$ $TCID_{50}$/ml A/sw/12687/Denmark/2003(H1N2) [142]) or mock treatment (medium). After inoculation, the explants were washed and placed in fresh growth medium and cultured at 37 °C (5 % CO_2). Four virus inoculated explants (two from each pig) and four mock inoculated explants (two from each pig) were harvested at 0, 6, 12, 24, and 48 h post inoculation (hpi) for RNA extraction and transcriptional analysis. At the 0, 12, 24, and 48 hpi time points, 300 µl growth medium was collected from the virus inoculated explants to assess viral replication by titration. Additionally, four virus inoculated explants (two from each pig) and four mock inoculated explants (two from each pig) were harvested at 0, 24, and 48 hpi and placed in Methocel and snap frozen in liquid nitrogen for cryosectioning and TUNEL staining to assess apoptosis. The 0 hpi samples were taken immediately after incubation with virus and washing.

3.2.1 Results from explant pilot study

Viral replication was assessed by determining the 50 % tissue culture infective dose ($TCID_{50}$) of the explant culture supernatant by titration in MDCK cells (**Figure 23**).

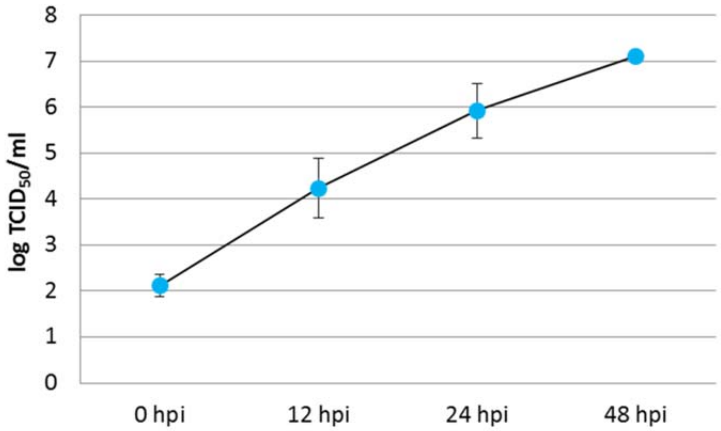

Figure 23. Virus yields as expressed by $TCID_{50}$/ml of the explant culture supernatant. n = 4 at all time points. Error bars depict SD.

[8] 1:1 DMEM and RPMI with penicillin (100 U/ml), streptomycin (0.1 mg/ml), and gentamicin (0.1 mg/ml).

The 0 hpi supernatant sample was collected immediately after the virus inoculated explants had been washed and transferred to fresh growth medium. The virus present in this sample thus likely represents carryover from the inoculation. Assessing the extent of apoptosis in the cultured explants yielded varying results. Using a cryotome, explants were sectioned (6 µm) and mounted on glass slides. Apoptotic cells were detected by terminal deoxynucleotidyl transferase dUTP nick end labeling (TUNEL) assay, enabling the differentiation of normal and apoptotic cells by confocal microscopy. As depicted in **Figure 24**, apoptotic cells varied from being almost undetectable to abundant among different explants (both virus and mock inoculated), and no distinct association between the amount of apoptotic cells, infection status, and duration of explant cultivation was observed.

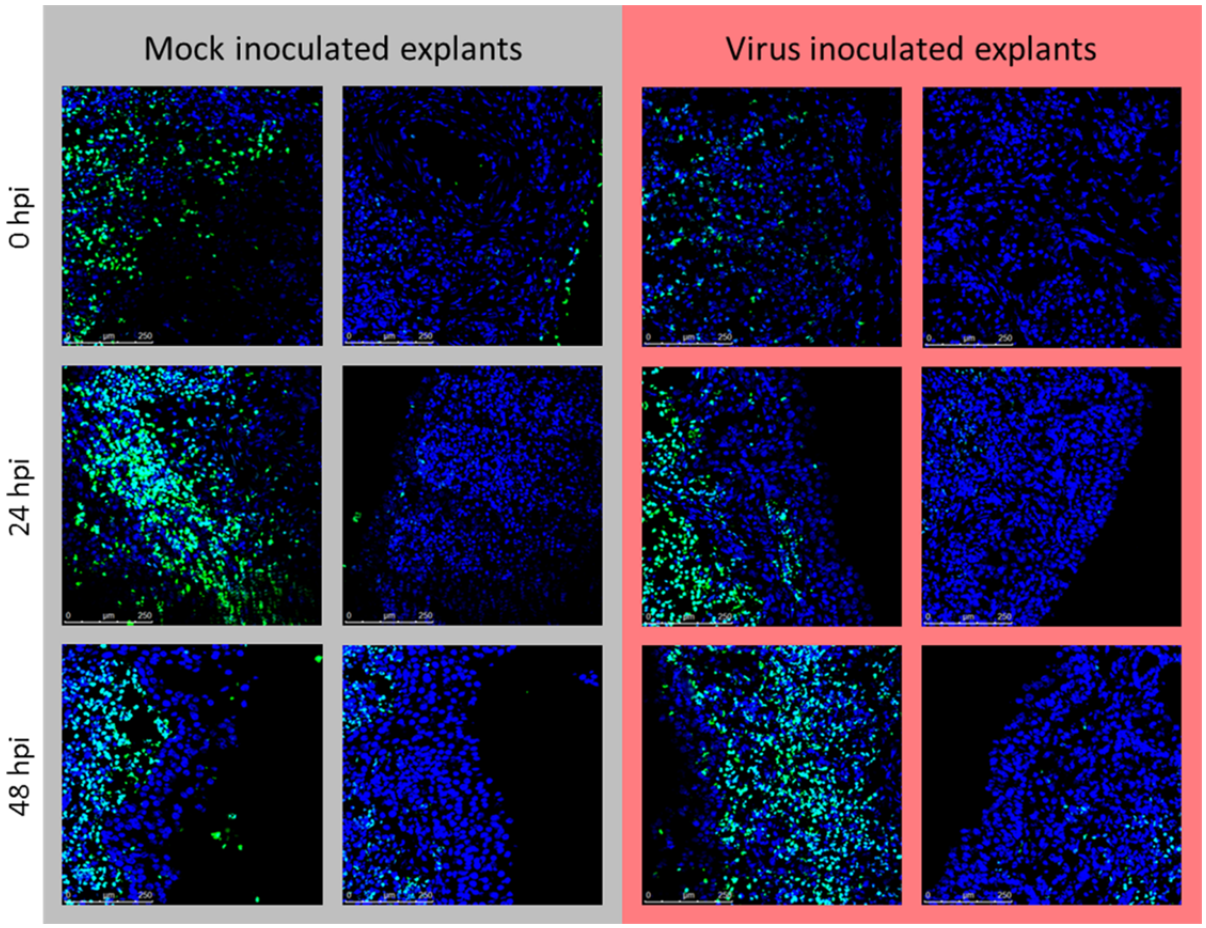

Figure 24. Apoptotic cells in porcine nasal explants detected with TUNEL assay. Blue: nuclei of normal cells (Hoechst stain); green: TUNEL positive cell, i.e. apoptotic (FITC stain). Grey background: mock inoculated explants; red background: virus inoculated cells. The two most extreme examples (lowest and highest amount of apoptotic cells) from each examined time point are shown (0 hpi – left column, 24 hpi – middle column, 48 hpi – right column). Scale bar = 250 µm.

Expression of a panel of 65 miRNAs was assessed in virus and mock inoculated explants at 0, 6, 12, 24, and 48 hpi using high-throughput RT-qPCR. Expression changes of miRNAs at 6, 12, 24, and 48 hpi relative to 0 hpi for virus and mock inoculated explants are shown in **Figure 25**.

Figure 25. Expression levels of 65 miRNAs in mock (grey bars) or virus (red bars) inoculated porcine nasal explants at 6, 12, 24, and 48 hpi. Expression levels are shown relative to the expression level in mock or virus inoculated explants at 0 hpi, respectively. No analysis of the statistical significance of expression changes was made due to the small sample sizes.

There appear to be an overall trend towards expression changes of greater magnitudes at 24 and 48 hpi compared to earlier time point. These preliminary results should be interpreted with caution due to the small sample sizes, but it is noteworthy that miRNA expression is found to be altered in virus as well as mock inoculated explants at all examined time points. For some miRNAs, the mock or virus inoculation seem to result in regulation of expression in opposite directions, e.g. hsa-let-7a, ssc-miR-183, hsa-miR-449a, and ssc-miR-451, whereas others display similar expression patterns in mock and virus inoculated explants, e.g. ssc-miR-29a, ssc-miR-29b, ssc-miR-142-5p, hsa-miR-221, and ssc-miR-222. The expression of a selection of miRNAs in virus inoculated explants relative to mock inoculated explants at 0 hpi

is shown in **Figure 26**; these are some of the most strongly regulated miRNAs in virus inoculated explants and/or have been found to be regulated *in vivo* in the pig lung or circulating leukocytes after challenge with the same swine IAV strain, A/swine/12687/Denmark/2003(H1N2).

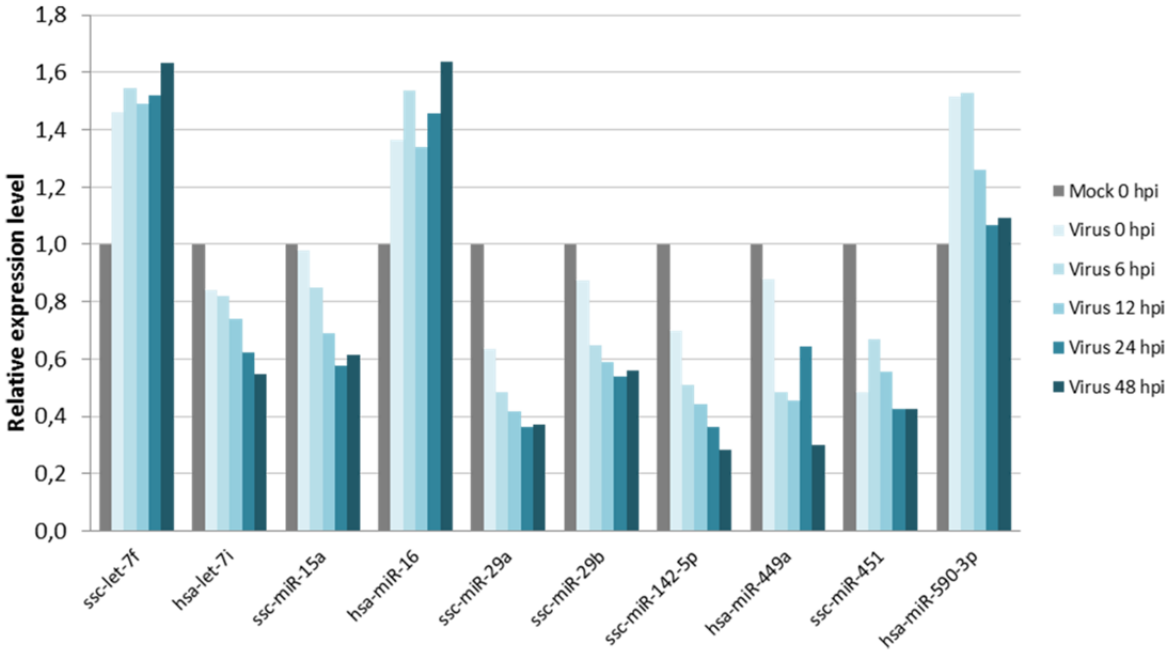

Figure 26. Expression changes of a selected subset of miRNAs in virus inoculated porcine nasal explants at 0, 6, 12, 24, and 48 hpi relative to the expression level in mock inoculated explants at 0 hpi which is scaled to 1. n = 4 for all time points for both mock and virus inoculated explants. No analysis of the statistical significance of expression changes was made due to the small sample sizes.

Quantification of protein-coding gene expression was carried out on a limited number of virus inoculated explants only (**Figure 27**). 32 of the assayed genes were ≥2-fold up- or down-regulated at 6, 12, 24, and/or 48 hpi relative to 0 hpi. The up-regulated genes included viral pathogen recognition receptors (PRRs) and PRR signaling (*DDX58*, *TLR7*, *MYD88*, *IRAK1*), type I interferon (*IFNA1*), and interferon stimulated genes (ISGs) (*MX1*, *OAS1*, *OASL*, *IRF7*). Among the down-regulated genes were also type I and type III interferon (*IFNB1*, *IL28B*), several pro-inflammatory cytokines and chemokines (*IL1B, IL1RN*, *IL6*, *IL8*, *CXCL10*), and the intrinsic host defense factor mucin-1 (*MUC1*). The expression of several genes known to be involved in the pulmonary host innate antiviral defense against IAV was found to be unchanged throughout the experiment, e.g. the PRRs *TLR3* and *MDA5* as well as the ISGs *ISG15*, *SOCS1*, *EIF2AK2*, and *IRF3*. Note however, that only a subset of the virus inoculated explants have been analyzed for differential mRNA expression; the mock inoculated explants were not included, and it is not possible to ascertain that IAV infection alone caused the observed changes in miRNA and protein-coding gene expression. The explants may just as well be responding to the *ex vivo* culturing process itself. All examined virus inoculated explants originated from the same animal.

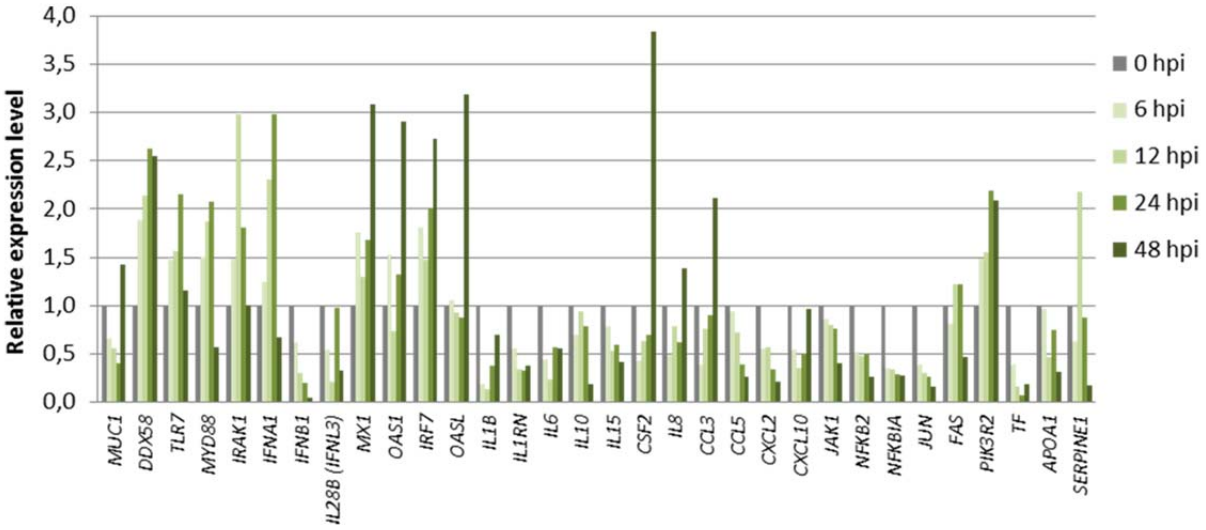

Figure 27. 32 of the assayed protein coding genes displayed ≥2-fold up- or down-regulation at 6, 12, 24, and/or 48 hpi relative to 0 hpi. No test for statistical significance of expression changes was carried out due to the small sample sizes (0 hpi: n = 2; 6 hpi: n = 2; 12 hpi: n = 2; 24 hpi: n = 2; 48 hpi: n = 1).

3.2.2 Discussion and future work

The described method of *ex vivo* culturing of nasal mucosal explants has previously been applied to evaluate IAV replication characteristics and host receptor binding in pigs [144,145]. We wished to assess the applicability of this system for transcriptional analysis of the antiviral host response after IAV infection, and to study how well the 3R compliant explant model mirrored results from previous *in vivo* IAV infection studies in pigs. To this end, a pilot study using explants derived from two six-week-old pigs was set up, and parallel mock and virus infections were carried out.

Encouragingly, the A/swine/12687/Denmark/2003(H1N2) strain replicated well in explants from the porcine nasal mucosa, reaching levels comparable to those previously reported for replication of swine IAV in this explant system [145]. The viability of the explants was evaluated by TUNEL staining, by which apoptotic cells are identified. This resulted in great variability between explants, and no clear picture of apoptosis in response to IAV infection was seen. It is important to gain thorough insight into the inherent degree of apoptosis in the explant system which is independent of virus infection. Apoptosis is induced during IAV infection, both as a host defense tactic to limit viral spread, but also as a mechanism for IAV to ensure efficient viral propagation [49,65]. Caution should be exercised when interpreting gene expression results obtained from the explant system, if the cause of apoptosis cannot be attributed to IAV infection alone.

miRNA expression was found to be affected throughout the experiment in mock and virus inoculated explants. Given the involvement of miRNAs in a wide variety of cellular processes, this is not an unexpected result, and based on these results it is not possible to distinguish regulation which is mediated by virus infection and that which is simply a response of the tissue to being cultured *ex vivo*. Some of the miRNAs found to be differentially expressed in virus inoculated explants relative to mock inoculated explants were also differentially expressed in pig lung after IAV infection (**Paper 3**). Down-regulation of hsa-miR-449a and up-regulating of hsa-miR-590-3p is seen both in lungs and nasal mucosa,

whereas ssc-miR-29b and ssc-miR-15a are up-regulated in the lung and down-regulated in nasal mucosa during the first few days after IAV infection. Whether this is a reflection of an actual difference in the nasal epithelial and lung tissue miRNA responses to IAV infection, or due to the different cell composition of the lung samples 'drowning' out the specific lung epithelial response warrants further investigation. Furthermore, ssc-miR-29b and ssc-miR-15a do both seem to be affected in mock inoculate explants as well.

ssc-miR-451 (-451a in humans) is the most abundant miRNA in red blood cells (RBCs) and has been shown to be highly indicative of hemolysis [146]. We and others have reported the upregulation of this miRNA in lung tissue at various time points after IAV infection [147–149], and according to our own observations there is large variation in lung tissue levels of ssc-miR-451 from animal to animal. This may however simply be a reflection of large variations in the number of RBCs/amount of hemolysis between samples, and be independent of IAV infection. In the porcine nasal explants we found ssc-miR-451 to be significantly down-regulated in virus inoculated explants relative to mock inoculation at 0 hpi which may be a more accurate representation of the IAV-specific ssc-miR-451 response, or a tissue response to *ex vivo* cultivation.

Protein-coding gene expression was quantified in a limited number of virus inoculated explants, and further validation of these results in sufficient numbers of explants determined by statistical power analysis is necessary before any conclusions are drawn. These preliminary results do however suggest potentially interesting findings which contrasted with our previous observations in the pig lung on day 1 after IAV challenge (**Paper 3**). These differences may be a reflection of the tissue responding to being cultured *ex vivo* rather than changes induced by IAV infection.

An aberrant response of pro-inflammatory cytokines and chemokines such as *IL1B*, *IL6*, and *CXCL10* was seen in the explants. This may reflect a tissue response to *ex vivo* culturing, given that up-regulation of two hallmark viral PRRs was seen, namely *DDX58* and *TLR7*. One recent study of IAV infection of human nasal epithelial cells *in vitro* showed results mirroring ours regarding *DDX58*, *TLR7*, *IRF7*, and *IFNA1* expression, but did also demonstrate up-regulation of many of the pro-inflammatory factors which we find down-regulated in the explant pilot study [150]. Importantly, the human nasal epithelial cell study was carried out at an incubation temperature of 35 °C. A lower temperature for explant culturing therefore could be attempted, as 37 °C may not optimally reflect *in vivo* conditions. Future studies of host gene expression in response to IAV infection in porcine nasal mucosal explants should thus address optimization of *ex vivo* conditions including culturing temperature. Little information is available regarding nasal cavity temperatures, but some studies report temperatures of approx. 30 °C and 32-34 °C in young suckling pigs and healthy adult humans, respectively [151,152].

4 Concluding remarks and future perspectives

Pigs are indispensable for a One Health oriented strategy for the management of IAV infection in humans and animals alike. Pigs are important natural hosts for IAV, making the risk of the emergence of novel zoonotic IAV strains ever present. They are also a highly relevant model for the study of human IAV infection as s discussed in **Paper 1**. The pig model demonstrates high face and target validity for the study of human IAV infection. To date, the mouse has been the most widely used animal model for this purpose, and it will surely continue to provide mechanistic insight into key aspects of innate immunology. However, the translational value is much higher for the pig model, and it would be valuable for future IAV research to apply this model as an intermediary between mice and humans for the translation of results from animal models into human application.

The work presented in this thesis serves to demonstrate the applicability of the pig model in the study of the innate immune response to IAV infection. By using the pig model, it was possible to characterize the host response locally at the site of infection in the lung. It is of paramount importance to elucidate the mechanisms by which the host locally responds to infection and how this response contributes to disease development. This knowledge is a prerequisite for future development of IAV vaccines and antiviral therapeutics, which are urgently needed today due to the constantly changing target. However, it is next to impossible to gain knowledge of the pulmonary response from humans, as this type of sample material is extremely rare.

Elucidating the transcriptional host response to infection should preferentially be performed in a holistic manner which includes not only genes coding for relevant innate immune proteins, but also non-coding regulators of gene expression, such as miRNAs. Obtaining a comprehensive picture of the transcriptional landscape could facilitate the identification of new targets for antiviral therapeutics. In the work presented here (**Papers 2-4**), we have shown that the expression of protein-coding genes as well as miRNAs changes according to infection and vaccination status. We have likewise shown that timing of sampling can be critical when assessing miRNA levels in circulation. This serves to further emphasize the need for relevant animal models like the pig which allow control of the time parameter when evaluating miRNA biomarker potential.

Novel results are presented in this thesis regarding the protracted miRNA response locally in the lung as well as in circulation. This delayed response is greatly interesting as it may have implications for lung regeneration and the susceptibility to secondary bacterial or viral infections, and should be a focus point in future IAV research in the porcine model.

The work presented here also includes the first *in vivo* description of local type III interferon expression in the pig lung in response to IAV infection. Type III interferon has tentatively been proposed as a potential anti-IAV therapeutic with limited inflammatory side effects [153,154]. Due to the emergence of viral resistance to available anti-IAV drugs, we are in need of new IAV therapeutics which do not directly target viral components leading to an enhanced selection for resistant strains. However, the temporal dynamics of type III interferon expression and its distinct function compared to type I interferons in the porcine lung after IAV infection is poorly understood. The predictive validity of the porcine model for IAV

infection is in need of assessment, in order to facilitate its use in the evaluation of type III interferons and other compounds for use as anti-IAV therapeutics.
Further efforts should likewise be put into characterizing and establishing porcine nasal mucosal explants as an *ex vivo* tool for examination of the host response to IAV infection. This tissue represents the site of first contact during natural infection, and the host response in these respiratory epithelial cells may be decisive for the entire course of infection and disease. As conventional anti-IAV drugs are most effective when they are given as early as possible or even prophylactically, the nasal explant system may even be suitable for the evaluation of anti-IAV therapeutics delivered at this site.

In general, the results presented in this thesis should be validated in the pig model using other swine IAV strains including the same subtypes as those currently circulating in humans (H1N1, H3N2). The IAV strains which circulate in humans as well as pigs are constantly changing, and the swine H1N2 strain applied for the work presented here is just one of many strains which would be relevant to apply in future challenge studies in pigs. Available literature has described strain-specific miRNA expression profiles in the lungs of non-human primates and mice in relation to differential IAV virulence [155,156]. It is highly relevant to determine if the porcine pulmonary miRNA response is different against other circulating swine IAV strains. This may help define a limited set of miRNAs responsible for modulating an efficient host innate immune response against IAV infection.

5 References

1. Hause B, Collin E, Liu R, Huang B, Sheng Z, Lu W. Characterization of a novel influenza virus strain in cattle and swine: proposal for a new genus in the Orthomyxoviridae family. MBio. 2014;5:1–10.
2. Presti RM, Zhao G, Beatty WL, Mihindukulasuriya KA, Travassos da Rosa APA, Popov VL, et al. Quaranfil, Johnston Atoll, and Lake Chad Viruses Are Novel Members of the Family Orthomyxoviridae. J. Virol. 2009;83:11599–606.
3. MacLachlan NJ, Dubovi EJ, editors. Chapter 21 Orthomyxoviridae. Fenner's Vet. Virol. 4th ed. Elsevier; 2011. p. 353–70.
4. Krug RM, Fodor E. Chapter 4 The virus genome and its replication. In: Webster RG, Monto AS, Braciale TJ, Lamb RA, editors. Textb. Influ. 2nd ed. Wiley Blackwell; 2013. p. 57–66.
5. Eisfeld AJ, Neumann G, Kawaoka Y. At the centre: influenza A virus ribonucleoproteins. Nat. Rev. Microbiol. Nature Publishing Group; 2014;13:28–41.
6. Lakadamyali M, Rust MJ, Zhuang X. Endocytosis of influenza viruses. Microbes Infect. 2004;6:929–36.
7. Edinger TO, Pohl MO, Stertz S. Entry of influenza A virus: Host factors and antiviral targets. J. Gen. Virol. 2014;95:263–77.
8. te Velthuis AJW, Fodor E. Influenza virus RNA polymerase: insights into the mechanisms of viral RNA synthesis. Nat. Rev. Microbiol. 2016;14:479–93.
9. Zheng W, Tao YJ. Structure and assembly of the influenza A virus ribonucleoprotein complex. FEBS Lett. 2013;587:1206–14.
10. Hutchinson EC, Fodor E. Transport of the influenza virus genome from nucleus to nucleus. Viruses. 2013;5:2424–46.
11. Pohl MO, Lanz C, Stertz S. Late stages of the influenza a virus replication cycle—A tight interplay between virus and host. J. Gen. Virol. 2016;97:2058–72.
12. Shao W, Li X, Goraya MU, Wang S, Chen JL. Evolution of influenza a virus by mutation and re-assortment. Int. J. Mol. Sci. Multidisciplinary Digital Publishing Institute (MDPI); 2017.
13. Wiersma L, Rimmelzwaan G, de Vries R. Developing Universal Influenza Vaccines: Hitting the Nail, Not Just on the Head. Vaccines. 2015;3:239–62.
14. McDonald SM, Nelson MI, Turner PE, Patton JT. Reassortment in segmented RNA viruses: mechanisms and outcomes. Nat. Rev. Microbiol. 2016;14:448–60.
15. Van Reeth K. Avian and swine influenza viruses: Our current understanding of the zoonotic risk. Vet. Res. 2007;38:243–60.
16. Taubenberger JK, Kash JC. Influenza Virus Evolution, Host Adaptation, and Pandemic Formation. Cell Host Microbe. 2010;7:440–51.
17. Pica N, Hai R, Krammer F, Wang TT, Maamary J, Eggink D, et al. Hemagglutinin stalk antibodies elicited by the 2009 pandemic influenza virus as a mechanism for the extinction of seasonal H1N1 viruses. Proc. Natl. Acad. Sci. 2012;109:2573–8.
18. Webby R, Richt J. Chapter 12 Influenza in swine. In: Webster RG, Monto AS, Braciale TJ, Lamb RA, editors. Textb. Influ. 2nd ed. Wiley Blackwell; 2013. p. 190–202.
19. Shi Y, Wu Y, Zhang W, Qi J, Gao GF. Enabling the "host jump": structural determinants of receptor-binding specificity in influenza A viruses. Nat. Rev. Microbiol. 2014;12:822–31.
20. Short KR, Veldhuis Kroeze EJB, Reperant LA, Richard M, Kuiken T. Influenza virus and endothelial cells: A species specific relationship. Front. Microbiol. 2014;5:1–11.
21. De Graaf M, Fouchier RAM. Role of receptor binding specificity in influenza A virus transmission and pathogenesis. EMBO J. 2014. p. 823–41.
22. Shinya K, Ebina M, Yamada S, Ono M, Kasai N, Kawaoka Y. Avian flu: Influenza virus receptors in the human airway. Nature. 2006;440:435–6.

23. Ge S, Wang Z. An overview of influenza A virus receptors. Crit. Rev. Microbiol. 2011;37:157–65.
24. Cauldwell A, Long J, Moncorge O, Barclay W. Viral determinants of influenza A virus host range.
25. Herfst S, Schrauwen EJA, Linster M, Chutinimitkul S, de Wit E, Munster VJ, et al. Airborne Transmission of Influenza A/H5N1 Virus Between Ferrets. Science (80-.). 2012;336:1534–41.
26. Nilsson BE, te Velthuis AJ, Fordor E. Role of the PB2 627 Domain in Influenza A Virus Polymerase Function. J. Virol. 2017;91:e02467-16.
27. Rodriguez-Frandsen A, Alfonso R, Nieto A. Influenza virus polymerase: Functions on host range, inhibition of cellular response to infection and pathogenicity. Virus Res. Elsevier B.V.; 2015;209:23–38.
28. Simon G, Larsen LE, Dürrwald R, Foni E, Harder T, Van Reeth K, et al. European Surveillance Network for Influenza in Pigs: Surveillance Programs, Diagnostic Tools and Swine Influenza Virus Subtypes Identified in 14 European Countries from 2010 to 2013. PLoS One. 2014;9:e115815.
29. Krog JS, Hjulsager CK, Larsen LE. Overvågning af influenza A virus i svin - Slutrapport 2015. 2016.
30. Trebbien R, Larsen LE, Viuff BM. Distribution of sialic acid receptors and influenza A virus of avian and swine origin in experimentally infected pigs. Virol. J. BioMed Central Ltd; 2011;8:434.
31. Nelli RK, Kuchipudi S V, White G a, Perez BB, Dunham SP, Chang K-C. Comparative distribution of human and avian type sialic acid influenza receptors in the pig. BMC Vet. Res. 2010;6:4.
32. Iwatsuki-Horimoto K, Nakajima N, Shibate M, Takahashi K, Sato Y, Kiso M, et al. The Microminipig as an Animal Model for Influenza A Virus Infection. J. Virol. 2017;91:e01716-16.
33. Wang TT, Palese P. Chapter 14 Emergence and evolution of the 1918, 1957, 1968, and 2009 pandemic virus strains. In: Webster RG, Monto AS, Braciale TJ, Lamb RA, editors. Textb. Influ. 2nd ed. Wiley Blackwell; 2013. p. 218–28.
34. Jeffery PK. Morphologic Features of Airway Surface Epithelial Cells and Glands. Am. Rev. Respir. Dis. 1983;128:S14–20.
35. Cohen M, Zhang X-Q, Senaati HP, Chen H-W, Varki NM, Schooley RT, et al. Influenza A penetrates host mucus by cleaving sialic acids with neuraminidase. Virol. J. 2013;10:321.
36. Yang X, Steukers L, Forier K, Xiong R, Braeckmans K, Van Reeth K, et al. A beneficiary role for neuraminidase in influenza virus penetration through the respiratory mucus. PLoS One. 2014;9:1–11.
37. Zhang L, Button B, Gabriel SE, Burkett S, Yan Y, Skiadopoulos MH, et al. CFTR delivery to 25% of surface epithelial cells restores normal rates of mucus transport to human cystic fibrosis airway epithelium. PLoS Biol. 2009;7.
38. Wallace P, Kennedy JR, Mendicino J. Transdifferentiation of outgrowth cells and cultured epithelial cells from swine trachea. Vitr. Cell. Dev. Biol. - Anim. 1994;3:168–80.
39. Taubenberger JK, Morens DM. The Pathology of Influenza Virus Infections. Annu. Rev. Pathol. Mech. Dis. 2007;0:71015171337001.
40. Brookes SM, Núñez A, Choudhury B, Matrosovich M, Essen SC, Clifford D, et al. Replication, pathogenesis and transmission of pandemic (H1N1) 2009 virus in non-immune pigs. PLoS One. 2010;5:e9068.
41. Ma W, Belisle SE, Mosier D, Li X, Stigger-Rosser E, Liu Q, et al. 2009 pandemic H1N1 influenza virus causes disease and upregulation of genes related to inflammatory and immune responses, cell death, and lipid metabolism in pigs. J.Virol. 2011. p. 11626–37.

42. Skovgaard K, Cirera S, Vasby D, Podolska A, Breum SO, Durrwald R, et al. Expression of innate immune genes, proteins and microRNAs in lung tissue of pigs infected experimentally with influenza virus (H1N2). Innate Immun. 2013;19:531–44.
43. Jiang P, Zhou N, Chen X, Zhao X, Li D, Wang F, et al. Integrative analysis of differentially expressed microRNAs of pulmonary alveolar macrophages from piglets during H1N1 swine influenza A virus infection. Sci. Rep. 2015;5:8167.
44. Brogaard L, Heegaard PMH, Larsen LE, Mortensen S, Schlegel M, Dürrwald R, et al. Late regulation of immune genes and microRNAs in circulating leukocytes in a pig model of influenza A (H1N2) infection. Sci. Rep. 2016;6:21812.
45. Chan MCW, Chan RWY, Yu WCL, Ho CCC, Yuen KM, Fong JHM, et al. Tropism and Innate Host Responses of the 2009 Pandemic H1N1 Influenza Virus in ex Vivo and in Vitro Cultures of Human Conjunctiva and Respiratory Tract. Am. J. Pathol. Elsevier; 2010;176:1828–40.
46. Van Reeth K, Nauwynck H. Proinflammatory cytokines and viral respiratory disease in pigs. Vet. Res. 2000;31:187–213.
47. Van Reeth K, Labarque G, Nauwynck H, Pensaert M. Differential production of proinflammatory cytokines in the pig lung during different respiratory virus infections: correlations with pathogenicity. Res. Vet. Sci. 1999;67:47–52.
48. Mackenzie A. The pathology of respiratory infections in pigs. Br. Vet. J. 1969;125:294–303.
49. Janke BH. Influenza A virus infections in swine: pathogenesis and diagnosis. Vet. Pathol. 2014;51:410–26.
50. Lyoo K-S, Kim J-K, Jung K, Kang B-K, Song D. Comparative pathology of pigs infected with Korean H1N1, H1N2, or H3N2 swine influenza A viruses. Virol. J. BioMed Central; 2014;11:170.
51. Iwasaki A, Pillai PS. Innate immunity to influenza virus infection. Nat. Rev. Immunol. Nature Publishing Group; 2014;14:315–28.
52. Delgado-Ortega M, Melo S, Punyadarsaniya D, Ramé C, Olivier M, Soubieux D, et al. Innate immune response to a H3N2 subtype swine influenza virus in newborn porcine trachea cells, alveolar macrophages, and precision-cut lung slices. Vet. Res. 2014;45:1–18.
53. Krishna VD, Roach E, Zaidman NA, Panoskaltsis-Mortari A, Rotschafer JH, O'Grady SM, et al. Differential induction of type I and type III interferons by swine and human origin H1N1 influenza a viruses in porcine airway epithelial cells. PLoS One. 2015;10.
54. Stegemann-Koniszewski S, Jeron A, Gereke M, Geffers R, Kröger A, Gunzer M. Alveolar Type II Epithelial Cells Contribute to the Anti-Influenza A Virus Response in the Lung by Integrating Pathogen- and Microenvironmen-Derived Signals. MBio. 2016;7:1–11.
55. Forero A, Fenstermacher K, Wohlgemuth N, Nishida A, Carter V, Smith EA, et al. Evaluation of the innate immune responses to influenza and live- attenuated influenza vaccine infection in primary differentiated human nasal epithelial cells. Vaccine. 2017;
56. Durbin RK, Kotenko S V., Durbin JE. Interferon induction and function at the mucosal surface. Immunol. Rev. 2013;255:25–39.
57. Mordstein M, Neugebauer E, Ditt V, Jessen B, Rieger T, Falcone V, et al. Lambda Interferon Renders Epithelial Cells of the Respiratory and Gastrointestinal Tracts Resistant to Viral Infections. J. Virol. 2010;84:5670–7.
58. Larsen DL, Karasin A, Zuckermann F, Olsen CW. Systemic and mucosal immune responses to H1N1 influenza virus infection in pigs. Vet. Microbiol. 2000. p. 117–31.
59. Kim HM, Lee Y-W, Lee K-J, Kim HS, Cho SW, van Rooijen N, et al. Alveolar Macrophages Are Indispensable for Controlling Influenza Viruses in Lungs of Pigs. J. Virol. American Society for Microbiology; 2008;82:4265–74.
60. Wang J, Nikrad MP, Travanty EA, Zhou B, Phang T, Gao B, et al. Innate Immune

Response of Human Alveolar Macrophages during Influenza A Infection. PLoS.One. 2012. p. e29879-.
61. Cardani A, Boulton A, Kim TS, Braciale TJ. Alveolar Macrophages Prevent Lethal Influenza Pneumonia By Inhibiting Infection Of Type-1 Alveolar Epithelial Cells. PLoS Pathog. 2017;13.
62. Forberg H, Hauge AG, Valheim M, Garcon F, Nunez A, Gerner W, et al. Early responses of natural killer cells in pigs experimentally infected with 2009 pandemic H1N1 influenza a virus. PLoS One. 2014;9.
63. Achdout H, Meningher T, Hirsh S, Glasner A, Bar-On Y, Gur C, et al. Killing of avian and Swine influenza virus by natural killer cells. J. Virol. American Society for Microbiology; 2010;84:3993–4001.
64. Hwang I, Scott JM, Kakarla T, Duriancik DM, Choi S, Cho C, et al. Activation Mechanisms of Natural Killer Cells during Influenza Virus Infection. PLoS One. 2012;7.
65. Herold S, Ludwig S, Pleschka S, Wolff T. Apoptosis signaling in influenza virus propagation, innate host defense, and lung injury. J. Leukoc. Biol. 2012;92:75–82.
66. Leymarie O, Meyer L, Tafforeau L, Lotteau V, Da Costa B, Delmas B, et al. Influenza virus protein PB1-F2 interacts with CALCOCO2 (NDP52) to modulate innate immune response. J. Gen. Virol. Microbiology Society; 2017;98:1196–208.
67. Schultz-Cherry S, Dybdahl-Sissoko N, Neumann G, Kawaoka Y, Hinshaw VS. Influenza virus ns1 protein induces apoptosis in cultured cells. J. Virol. American Society for Microbiology; 2001;75:7875–81.
68. Gannagé M, Dormann D, Albrecht R, Dengjel J, Torossi T, Rämer PC, et al. Matrix Protein 2 of Influenza A Virus Blocks Autophagosome Fusion with Lysosomes. Cell Host Microbe. Cell Press; 2009;6:367–80.
69. Tripathi S, Batra J, Cao W, Sharma K, Patel JR, Ranjan P, et al. Influenza A virus nucleoprotein induces apoptosis in human airway epithelial cells: implications of a novel interaction between nucleoprotein and host protein Clusterin. Cell Death Dis. 2013;4:e562.
70. Human Genome Sequencing Consortium I. Finishing the euchromatic sequence of the human genome. Nature. 2004;431:931–45.
71. Wilczynska A, Bushell M. The complexity of miRNA-mediated repression. Cell Death Differ. 2015;22:22–33.
72. Lee RC, Feinbaum RL, Ambros V. The C. elegans heterochronic gene lin-4 encodes small RNAs with antisense complementarity to lin-14. Cell. 1993;75:843–54.
73. Wightman B, Ha I, Ruvkun G. Posttranscriptional regulation of the heterochronic gene lin-14 by lin-4 mediates temporal pattern formation in C. elegans. Cell. 1993;75:855–62.
74. Bartel DP. MicroRNAs: Genomics, Biogenesis, Mechanism, and Function. Cell. 2004;116:281–97.
75. Li SC, Chan WC, Hu LY, Lai CH, Hsu CN, Lin W chang. Identification of homologous microRNAs in 56 animal genomes. Genomics. 2010;96:1–9.
76. Kozomara A, Griffiths-Jones S. MiRBase: Annotating high confidence microRNAs using deep sequencing data. Nucleic Acids Res. 2014;42:68–73.
77. Kim VN, Han J, Siomi MC. Biogenesis of small RNAs in animals. Nat. Rev. Mol. Cell Biol. 2009;10:126–39.
78. Daugaard I, Hansen TB. Biogenesis and Function of Ago-Associated RNAs. Trends Genet. Elsevier Ltd; 2017;33:208–19.
79. Han J, Lee Y, Yeom KH, Nam JW, Heo I, Rhee JK, et al. Molecular Basis for the Recognition of Primary microRNAs by the Drosha-DGCR8 Complex. Cell. 2006;125:887–901.
80. Kwon SC, Nguyen TA, Choi YG, Jo MH, Hohng S, Kim VN, et al. Structure of Human DROSHA. Cell. Elsevier Inc.; 2016;164:81–90.

81. Lund E, Güttinger S, Calado A, Dahlberg JE, Kutay U. Nuclear Export of MicroRNA Precursors. Science (80-.). 2004;303:95–8.
82. Meijer HA, Smith EM, Bushell M. Regulation of miRNA strand selection: follow the leader? Biochem. Soc. Trans. 2014;42:1135–40.
83. Kawamata T, Tomari Y. Making RISC. Trends Biochem. Sci. Elsevier Ltd; 2010;35:368–76.
84. Ambros V, Bartel B, Bartel DP, Burge CB, Carrington JC, Chen X, Dreyfuss G, Eddy SR, Griffiths-Jones S, Marshall M, Matzke M, Ruvkun G TT. A uniform system for microRNA annotation. Nucleic Acids Res. 2003;9:277–9.
85. Budak H, Bulut R, Kantar M, Alptekin B. MicroRNA nomenclature and the need for a revised naming prescription. Brief. Funct. Genomics. 2016;15:65–71.
86. Van Peer G, Lefever S, Anckaert J, Beckers A, Rihani A, Van Goethem A, et al. miRBase Tracker: keeping track of microRNA annotation changes. Database (Oxford). Oxford University Press; 2014;2014:1–8.
87. Bartel DP. MicroRNAs: Target Recognition and Regulatory Functions. Cell. 2009;136:215–33.
88. Park JH, Shin C. MicroRNA-directed cleavage of targets: Mechanism and experimental approaches. BMB Rep. 2014;47:417–23.
89. Liu J, Carmell MA, Rivas F V, Marsden CG, Thomson JM, Song J-J, et al. Argonaute2 is the catalytic engine of mammalian RNAi. Science (80-.). 2004;305:1437–41.
90. Meister G, Landthaler M, Patkaniowska A, Dorsett Y, Teng G, Tuschl T. Human Argonaute2 mediates RNA cleavage targeted by miRNAs and siRNAs. Mol. Cell. 2004;15:185–97.
91. Jonas S, Izaurralde E. Towards a molecular understanding of microRNA-mediated gene silencing. Nat. Rev. Genet. Nature Publishing Group; 2015;16:421–33.
92. Bartel DP, Chen C-Z. Micromanagers of gene expression: the potentially widespread influence of metazoan microRNAs. Nat. Rev. Genet. 2004;5:396–400.
93. Bracken CP, Scott HS, Goodall GJ. A network-biology perspective of microRNA function and dysfunction in cancer. Nat. Rev. Genet. Nature Publishing Group; 2016;17:719–32.
94. Vlachos IS, Paraskevopoulou MD, Karagkouni D, Georgakilas G, Vergoulis T, Kanellos I, et al. DIANA-TarBase v7.0: Indexing more than half a million experimentally supported miRNA:mRNA interactions. Nucleic Acids Res. 2015;43:D153–9.
95. Chou CH, Chang NW, Shrestha S, Hsu S Da, Lin YL, Lee WH, et al. miRTarBase 2016: Updates to the experimentally validated miRNA-target interactions database. Nucleic Acids Res. 2016;44:D239–47.
96. Thomson DW, Bracken CP, Goodall GJ. Experimental strategies for microRNA target identification. Nucleic Acids Res. 2011. p. 6845–53.
97. Peterson SM, Thompson JA, Ufkin ML, Sathyanarayana P, Liaw L, Congdon CB. Common features of microRNA target prediction tools. Front. Genet. 2014;5:1–10.
98. Maudet C, Mano M, Eulalio A. MicroRNAs in the interaction between host and bacterial pathogens. FEBS Lett. Federation of European Biochemical Societies; 2014;588:4140–7.
99. Tahamtan A, Inchley CS, Marzban M, Tavakoli-Yaraki M, Teymoori-Rad M, Nakstad B, et al. The role of microRNAs in respiratory viral infection: friend or foe? Rev. Med. Virol. 2016. p. 389–407.
100. Williams J, Smith F, Kumar S, Vijayan M, Reddy PH. Are microRNAs true sensors of ageing and cellular senescence? Ageing Res. Rev. Elsevier B.V.; 2017;35:350–63.
101. Heegaard NHH, Carlsen AL, Lilje B, Ng KL, Rønne ME, Jørgensen HL, et al. Diurnal Variations of Human Circulating Cell-Free Micro-RNA. PLoS One. 2016;11:e0160577.
102. Hayes J, Peruzzi PP, Lawler S. MicroRNAs in cancer: Biomarkers, functions and therapy. Trends Mol. Med. Elsevier Ltd; 2014;20:460–9.

103. Chen JQ, Papp G, Szodoray P, Zeher M. The role of microRNAs in the pathogenesis of autoimmune diseases. Autoimmun. Rev. Elsevier B.V.; 2016;15:1171–80.
104. Heegaard NHH, Carlsen AL, Skovgaard K, Heegaard PMH. Chapter 8 Circulating Extracellular microRNA in Systemic Autoimmunity. In: Igaz P, editor. Circ. microRNAs Dis. Diagnostics their Potential Biol. Relev. Springer; 2015. p. 171–95.
105. Cai M, Kolluru GK, Ahmed A. Small Molecule, Big Prospects: MicroRNA in Pregnancy and Its Complications. J. Pregnancy. Hindawi; 2017;2017.
106. Gray C, McCowan LM, Patel R, Taylor RS, Vickers MH. Maternal plasma miRNAs as biomarkers during mid-pregnancy to predict later spontaneous preterm birth: a pilot study. Sci. Rep. Springer US; 2017;7:815.
107. Ross SA, Davis CD. The Emerging Role of microRNAs and Nutrition in Modulating Health and Disease. Annu. Rev. Nutr. 2014;34:305–36.
108. Cruz KJC, de Oliveira ARS, Morais JBS, Severo JS, Marreiro, PhD D do N. Role of microRNAs on adipogenesis, chronic low-grade inflammation, and insulin resistance in obesity. Nutrition. 2017;35:28–35.
109. Chakraborty C, Sharma AR, Sharma G, Doss CGP, Lee S-S. Therapeutic miRNA and siRNA: Moving from Bench to Clinic as Next Generation Medicine. Mol. Ther. - Nucleic Acids. Elsevier Ltd.; 2017;8:132–43.
110. Rupaimoole R, Slack FJ. MicroRNA therapeutics: towards a new era for the management of cancer and other diseases. Nat. Rev. Drug Discov. Nature Publishing Group; 2017;16:203–22.
111. Jopling CL, Norman KL, Sarnow P. Positive and negative modulation of viral and cellular mRNAs by liver-specific MicroRNA miR-122. Cold Spring Harb. Symp. Quant. Biol. 2006;71:369–76.
112. Janssen HLA, Reesink HW, Lawitz EJ, Zeuzem S, Rodriguez-Torres M, Patel K, et al. Treatment of HCV Infection by Targeting MicroRNA. N. Engl. J. Med. 2013;368:1685–94.
113. Turchinovich A, Tonevitsky AG, Burwinkel B. Extracellular miRNA: A Collision of Two Paradigms. Trends Biochem. Sci. Elsevier Ltd; 2016;41:883–92.
114. Turchinovich A, Weiz L, Langheinz A, Burwinkel B. Characterization of extracellular circulating microRNA. Nucleic Acids Res. 2011;39:7223–33.
115. Mall C, Rocke DM, Durbin-Johnson B, Weiss RH. Stability of miRNA in human urine supports its biomarker potential. Biomark. Med. 2013;7:1–17.
116. Sauer E, Reinke AK, Courts C. Differentiation of five body fluids from forensic samples by expression analysis of four microRNAs using quantitative PCR. Forensic Sci. Int. Genet. Elsevier Ireland Ltd; 2016;22:89–99.
117. Fendler A, Stephan C, Yousef GM, Kristiansen G, Jung K. The translational potential of microRNAs as biofluid markers of urological tumours. Nat. Rev. Urol. 2016;13:734–52.
118. Glinge C, Clauss S, Boddum K, Jabbari R, Jabbari J, Risgaard B, et al. Stability of circulating blood-based microRNAs-Pre-Analytic methodological considerations. PLoS One. 2017;12:1–16.
119. Terrier O, Textoris J, Carron C, Marcel V, Bourdon J-C, Rosa-Calatrava M. Host microRNA molecular signatures associated with human H1N1 and H3N2 influenza A viruses reveal an unanticipated antiviral activity for miR-146a. J. Gen. Virol. 2013;94:985–95.
120. Zhao L, Zhu J, Zhou H, Zhao Z, Zou Z, Liu X, et al. Identification of cellular microRNA-136 as a dual regulator of RIG-I-mediated innate immunity that antagonizes H5N1 IAV replication in A549 cells. Sci. Rep. Nature Publishing Group; 2015;5:14991.
121. Ingle H, Kumar S, Raut AA, Mishra A, Kulkarni DD, Kameyama T, et al. The microRNA miR-485 targets host and influenza virus transcripts to regulate antiviral immunity and restrict viral replication. Sci. Signal. 2015;8:ra126-ra126.
122. Song L, Liu H, Gao S, Jiang W, Huang W. Cellular microRNAs inhibit replication of the

H1N1 influenza A virus in infected cells. J. Virol. 2010;84:8849–60.
123. Khongnomnan K, Makkoch J, Poomipak W, Poovorawan Y, Payungporn S. Human miR-3145 inhibits influenza A viruses replication by targeting and silencing viral PB1 gene. Exp Biol Med. 2015;1630–9.
124. Ma Y-J, Yang J, Fan X-L, Zhao H-B, Hu W, Li Z-P, et al. Cellular microRNA let-7c inhibits M1 protein expression of the H1N1 influenza A virus in infected human lung epithelial cells. J. Cell. Mol. Med. 2012;16:2539–46.
125. Zhang S, Wang R, Su H, Wang B, Sizhu S, Lei Z, et al. Sus scrofa miR-204 and miR-4331 negatively regulate swine H1N1/2009 influenza a virus replication by targeting viral HA and NS, respectively. Int. J. Mol. Sci. 2017;18:1–18.
126. Song H, Wang Q, Guo Y, Liu S, Song R, Gao X, et al. Microarray analysis of microRNA expression in peripheral blood mononuclear cells of critically ill patients with influenza A (H1N1). BMC Infect. Dis. BMC Infectious Diseases; 2013;13:257.
127. Tambyah PA, Sepramaniam S, Mohamed Ali J, Chai SC, Swaminathan P, Armugam A, et al. microRNAs in Circulation Are Altered in Response to Influenza A Virus Infection in Humans. PLoS One. 2013;8:e76811.
128. Zhu Z, Qi Y, Ge A, Zhu Y, Xu K, Ji H, et al. Comprehensive characterization of serum microRNA profile in response to the emerging avian influenza A (H7N9) virus infection in humans. Viruses. 2014;6:1525–39.
129. Peng F, He J, Loo JFC, Yao J, Shi L, Liu C, et al. Identification of microRNAs in throat swab as the biomarkers for diagnosis of influenza. Int. J. Med. Sci. 2016;13:77–84.
130. Saiki RK, Gelfand DH, Stoffel S, Scharf SJ, Horn GT, Mullis KB, et al. Primer-Directed Enzymatic Amplification of DNA with a Thermostable DNA Polymerase. Science (80-.). 1988;239:487–91.
131. Bustin SA, Benes V, Garson JA, Hellemans J, Huggett J, Kubista M, et al. The MIQE guidelines: minimum information for publication of quantitative real-time PCR experiments. Clin.Chem. Centre for Academic Surgery, Institute of Cell and Molecular Science, Barts and the London School of Medicine and Dentistry, London, UK. s.a.bustin@qmul.ac.uk; 2009;55:611–22.
132. Balcells I, Cirera S, Busk PK. Specific and sensitive quantitative RT-PCR of miRNAs with DNA primers. BMC Biotechnol. 2011;11:70.
133. Busk PK. A tool for design of primers for microRNA-specific quantitative RT-qPCR. BMC Bioinformatics. 2014;15:29.
134. Goodwin S, McPherson JD, McCombie WR. Coming of age: ten years of next-generation sequencing technologies. Nat. Rev. Genet. 2016;17:333–51.
135. Sanger F, Nicklen S, Coulson AR. DNA sequencing with chain-terminating inhibitors. Proc. Natl. Acad. Sci. 1977;74:5463–7.
136. Mardis ER. Next-Generation DNA Sequencing Methods. Annu. Rev. Genomics Hum. Genet. 2008;9:387–402.
137. Friedländer MR, Mackowiak SD, Li N, Chen W, Rajewsky N. miRDeep2 accurately identifies known and hundreds of novel microRNA genes in seven animal clades. Nucleic Acids Res. 2012;40:37–52.
138. Kanke M, Baran-Gale J, Villanueva J, Sethupathy P. miRquant 2.0: an Expanded Tool for Accurate Annotation and Quantification of MicroRNAs and their isomiRs from Small RNA-Sequencing Data. J. Integr. Bioinform. 2016;13:307.
139. Zhang Y, Zang Q, Zhang H, Ban R, Yang Y, Iqbal F, et al. DeAnnIso: a tool for online detection and annotation of isomiRs from small RNA sequencing data. Nucleic Acids Res. 2016;44:W166–75.
140. Zhang H, Vieira Resende e Silva B, Cui J. miRDis: a Web tool for endogenous and exogenous microRNA discovery based on deep-sequencing data analysis. Brief. Bioinform.

2017;bbw140.
141. Quek C, Jung C hee, Bellingham SA, Lonie A, Hill AF. iSRAP - A one-touch research tool for rapid profiling of small RNA-seq data. J. Extracell. Vesicles. 2015;4:1–10.
142. Trebbien R, Bragstad K, Larsen LE, Nielsen J, Bøtner A, Heegaard PMH, et al. Genetic and biological characterisation of an avian-like H1N2 swine influenza virus generated by reassortment of circulating avian-like H1N1 and H3N2 subtypes in Denmark. Virol. J. 2013;10:290.
143. Tannenbaum J, Bennett BT. Russell and Burch's 3Rs then and now: the need for clarity in definition and purpose. J. Am. Assoc. Lab. Anim. Sci. 2015;54:120–32.
144. Glorieux S, Van den Broeck W, van der Meulen KM, Van Reeth K, Favoreel HW, Nauwynck HJ. In vitro culture of porcine respiratory nasal mucosa explants for studying the interaction of porcine viruses with the respiratory tract. J. Virol. Methods. 2007;142:105–12.
145. Van Poucke SGM, Nicholls JM, Nauwynck HJ, Van Reeth K. Replication of avian, human and swine influenza viruses in porcine respiratory explants and association with sialic acid distribution. Virol. J. 2010;7:38.
146. Kirschner MB, Edelman JJB, Kao SCH, Vallely MP, Van Zandwijk N, Reid G. The impact of hemolysis on cell-free microRNA biomarkers. Front. Genet. 2013;4:1–13.
147. Wang Y, Brahmakshatriya V, Lupiani B, Reddy SM, Soibam B, Benham AL, et al. Integrated analysis of microRNA expression and mRNA transcriptome in lungs of avian influenza virus infected broilers. BMC Genomics. 2012. p. 1–15.
148. Rogers J V, Price J a, Wendling MQS, Long JP, Bresler HS. Preliminary microRNA analysis in lung tissue to identify potential therapeutic targets against H5N1 infection. Viral Immunol. 2012;25:3–11.
149. Wang Y, Brahmakshatriya V, Zhu H, Lupiani B, Reddy SM, Yoon B-J, et al. Identification of differentially expressed miRNAs in chicken lung and trachea with avian influenza virus infection by a deep sequencing approach. BMC Genomics. 2009;10:512.
150. Yan Y, Tan K Sen, Li C, Tran T, Chao SS, Sugrue RJ, et al. Human nasal epithelial cells derived from multiple subjects exhibit differential responses to H3N2 influenza virus infection in vitro. J. Allergy Clin. Immunol. 2016;138:276–281.
151. German RZ, Crompton AW, Thexton AJ. The coordination and interaction between respiration and deglutition in young pigs. J. Comp. Physiol. 1998;182:539–47.
152. Keck T, Leiacker R, Riechelmann H, Rettinger G. Temperature profile in the nasal cavity. Laryngoscope. 2000;110:651–4.
153. Davidson S, McCabe TM, Crotta S, Gad HH, Hessel EM, Beinke S, et al. IFNλ is a potent anti□influenza therapeutic without the inflammatory side effects of IFNα treatment. EMBO Mol. Med. 2016;8:1099–112.
154. Galani IE, Triantafyllia V, Eleminiadou E-E, Koltsida O, Stavropoulos A, Manioudaki M, et al. Interferon-λ Mediates Non-redundant Front-Line Antiviral Protection against Influenza Virus Infection without Compromising Host Fitness. Immunity. 2017;46:875–890.e6.
155. Li Y, Li J, Belisle S, Baskin CR, Tumpey TM, Katze MG. Differential microRNA expression and virulence of avian, 1918 reassortant, and reconstructed 1918 influenza A viruses. Virology. 2011;421:105–13.
156. Vela EM, Kasoji MD, Wendling MQ, Price JA, Knostman KAB, Bresler HS, et al. MicroRNA expression in mice infected with seasonal H1N1, swine H1N1 or highly pathogenic H5N1. J. Med. Microbiol. 2014;63:1131–42.

Paper 1

Animal models for host defense against influenza A virus infection: profound translational value of the porcine model

Review

SMR Starbæk, **L Brogaard**, H Dawson, A Smith, LE Larsen, PMH Heegaard, G Jungersen, K Skovgaard

Manuscript in preparation for submission to the *ILAR Journal*

Animal models for host defense against influenza A virus infection: profound translational value of the porcine model

Sofie M. R. Starbæk[1], Louise Brogaard[1], Harry Dawson[2], Allen Smith[2], Lars E. Larsen[3], Peter M. H. Heegaard[1], Gregers Jungersen[4], Kerstin Skovgaard[1]

[1] Division of Immunology and Vaccinology – Innate Immunology, National Veterinary Institute, Technical University of Denmark, 2800 Kgs. Lyngby, Denmark
[2] Diet, Genomics, Immunology Laboratory, Beltsville Human Nutrition Research Center, United States Department of Agriculture, Beltsville, MD 20705, USA
[3] Division of Diagnostics and Scientific Advice – Virology, National Veterinary Institute, Technical University of Denmark, 2800 Kgs. Lyngby, Denmark
[4] Division of Immunology and Vaccinology – Adaptive Immunology, National Veterinary Institute, Technical University of Denmark, 2800 Kgs. Lyngby, Denmark

Abstract

Influenza is a contagious respiratory disease causing major impact on public health. Influenza A virus (IAV) usually causes short-term, self-limiting disease in humans. However, in some population groups such as infants, the elderly, and individuals with underlying inflammatory conditions, IAV can cause severe illness. In this paper we review relevant small and large animal models for human IAV infection, including the pig, ferret, and mouse. We focus on the pig as a large animal model for human IAV infection and the subsequent innate immune response, as this model demonstrates extensive similarities with humans in many important areas related to IAV infection. Pigs are naturally infected with the same IAV subtypes as humans, they develop clinical disease which mirror human symptoms, and their respiratory physiology and host immune responses to IAV infection are remarkably similar to what is observed in humans. The swine model demonstrates high face and target validity for human IAV infection, making it suitable for modeling many different aspects of this disease including impaired vaccine response in settings of underlying pathologies, such as low-grade inflammation often associated with obesity and aging. Taken together, the pig is a promising intermediate animal model between mouse and human displaying substantial translational value with the ability to provide essential insights into IAV research.

Introduction

Influenza A virus (IAV) infections are a leading cause of morbidity and mortality in the human population, with estimates of annual epidemics resulting in 3-5 million cases of severe disease and 250,000-500,000 deaths worldwide [1]. IAV infection is a self-limiting disease in otherwise healthy individuals, who will usually recover within one to two weeks. However, vulnerable population groups such as pregnant women, infants, the elderly, or severely obese individuals, as well as individuals with chronic inflammatory and autoimmune conditions including diabetes mellitus, are at higher risk of increased morbidity and mortality from IAV infections [2–6]. Furthermore, these high risk groups tend to have more prolonged and invasive forms of IAV infections, and are likewise at higher risk of selection for drug resistant influenza strains due to prolonged infection and delayed viral clearance [7–10].

IAVs are enveloped, single stranded RNA viruses of the family *Orthomyxoviridae*. This family comprises different genera, including *Influenza virus A*, *B*, and *C*. IAVs are further classified into subtypes based on the antigenic surface glycoproteins hemagglutinin (HA) and neuraminidase (NA). Currently, 16 HA (H1–H16) and 9 NA subtypes (N1–N9) are found in the aquatic bird reservoir [11]. Due to their segmented genomes, IAV may undergo re-assortment where new subtypes are generated with new combinations of gene segments (antigenic shift). Additionally, the mutation rate of the IAV RNA genome is high, leading to amino acid changes in important viral epitopes (antigenic drift). Combined, antigenic shift and drift causes the development of new virus variants that may escape previously acquired host immunity and give rise to new epidemics or even pandemics. A wide range of subtypes have been found in wild aquatic birds, whereas IAV in humans and pigs mainly are restricted to the subtypes H1N1 (humans and pigs), H3N2 (humans and pigs), and H1N2 (pigs) [12]. Where the human seasonal influenza types are restricted to one variant of each of the H1N1 and the H3N2 subtypes, there is a vast number of different variants circulating in pigs globally, containing a huge variety of different genes originating from humans, pigs, and avian species [13]. In general, the endemic circulating IAV strains in humans and other mammalian species have a narrow host restriction. However, in connection to human pandemics there has been a spillover from humans to pigs resulting in new subtypes that over time haves adapted to pigs with impaired ability to be transmitted back to humans [14].

While substantial progress has been made toward understanding viral evolution, transmission, and determinants of viral proteins in pathogenicity, multiple aspects of IAV infection, such as host factor involvement in pathogenesis, control, and the ultimate clearance of infection, still remain to be fully understood. Disease severity varies markedly among patients, and this difference cannot exclusively be explained by viral factors but also involves host-specific determinants such as genetic susceptibility and host immune and inflammatory responses. Elucidation of the combined impact of viral and host mechanisms during IAV infection is paramount for the development of more effective vaccines and antiviral therapies.

Vaccination remains the most effective method for prevention of IAV infections and reduction of IAV related disease. However, responsiveness to seasonal IAV vaccination has been observed to vary between individuals. Lowered or even absent IAV vaccine responsiveness has been found to be pronounced in high-risk groups including the elderly and severely obese individuals, often associated with immunosenescence or low-grade chronic inflammation [15,16]. Vaccines and antiviral drugs are

often tested in healthy adults, thereby not addressing the challenge posed by reduced responsiveness in more vulnerable population groups. Antiviral agents can be used for treatment and prevention of IAV infections and can be paramount for immunocompromised patients. Two major classes of anti-influenza drugs have been approved by the US Food and Drug Administration (FDA) for clinical use, namely matrix-2 (M2) protein inhibitors and NA inhibitors. In the late 1960ies, the M2 inhibitor amantadine was approved as the first anti-influenza drug followed by the approval of rimantadine in 1993 [17]. Approximately a decade after the approval of the first anti-IAV drug, resistance to both drugs was described after the 1980 influenza season [18], and these two antivirals are no longer recommended for treatment and prophylaxis of IAV infection [19]. The first NA inhibitors oseltamivir and zanamivir were approved in the late 1990ies [17], but the emergence of IAV strains resistant to this type of drugs has likewise increased in recent years [20,21]. Thus, we are struggling to keep up with the IAV, as it continuously evades antiviral drugs and vaccines by its ability to rapidly mutate, leaving us chasing a moving target. This strongly underlines the need for excellent animal models in development of novel anti-IAV therapeutic and prophylactic agents [22] as well as universal vaccines targeting highly conserved epitopes of the influenza virus.
Animal models of human IAV infections are invaluable tools for studying pathogenesis and host immune mechanisms in settings resembling human conditions, thereby serving as a bridge for the translational gap to the clinic. Animal models allow research in physiologically relevant settings of a complex environment compared to traditional cell culture studies, with the additional benefit of enabling modeling of individual conditions as e.g. low-grade inflammation. When choosing an animal model, it is important to consider the validity and fit-for-purpose. Carefully selected and designed animal models for human IAV infection with a sufficient translational value are highly needed [23,24].

In this review we strive to summarize relevant characteristics of the ferret and mouse models in relation to IAV infection, both of which have provided extensive knowledge on basic immunology, pathology, and viral transmission [25]. Our main focus will, however, be on the pig as a large animal model for human IAV infection. The pig model excels in many translational aspects of IAV research, as it also does in many other areas of biomedical research.

Animal models for study of IAV infection

Several animal species have been used for IAV research, including guinea pigs, rodents, and non-human primates [26]. The most frequently used animal model in IAV research is the mouse. This model has been widely used, due to low experimental cost, low housing requirements, and availability of immunological reagents and genetically modified strains. Albeit the mouse model has provided us with extensive knowledge regarding basic immunology, differences in clinical manifestations and anatomy of the respiratory system should arouse the interest for novel models. As summarized in Table 1, mice are not naturally infected with human IAV strains nor do they show clinical signs similar to humans after IAV infection such as fever, nasal secretion, and coughing [27]. Although wild type mice are not natural host for IAV, there are several strains of IAV including the pandemic H1N1 (1918 and 2009) strains, H5N1, and several H7 strains that can replicate and cause disease in mice [26]. Other IAV strains require adaptation in order to effectively replicate and cause disease in mice. These adaptations include mutations in the receptor-binding site of the viral HA and NA proteins, loss of glycosylation sites, and other changes that may affect viral tissue tropism [28,29].

The mutations introduced in IAV genome during the process of adapting it to the mouse host could result in phenotypic changes that are important for pathogenesis in humans. The use of other animal species for IAV studies has thus increased, including the use of pigs and ferrets. These species are susceptible to infection with human IAV and show clinical signs resembling humans after infection. While ferrets and pigs can readily transmit infections to naïve animals, transmission between infected and naïve mice is inefficient [30,31]. Table 1 summarizes some of the most relevant features of the pig, ferret, and mouse models, highlighting their strengths and weaknesses in relation to their applicability for the study of human IAV infection.

Comparison of orthologous and non-orthologous proteins

Table 2 summarizes the comparative analysis of 103 proteins found to be involved in the antiviral immune response in humans, pigs, ferrets, and mice [32]. For these 103 proteins, 1:1 orthology could be established in all four species. Pig (82.9 %) and ferret (81.9 %) proteins were significantly more similar to human proteins than mice (78.4 %) and had a higher amino acid identity regardless of classification. No significant differences were found between the highly conserved and closely related families classified as DEAD (Asp-Glu-Ala-Asp) box polypeptide and DEXH (Asp-Glu-X-His) box polypeptide RNA helicases or inflammasome associated proteins in pig, ferret, and mouse proteins. Pig and ferret proteins classified as Cytokine Receptors, Interferons, RIG-I-Like Receptor, Toll-Like Receptors or TRIM superfamily (Table 2) exhibited significantly greater human similarities than mice. Pig proteins classified as Anti-Viral Restriction Factors had greater similarity to orthologous human proteins than either ferret or mouse whereas pig and ferret Toll-Like Receptor proteins were more similar to the orthologous human proteins than were the mouse orthologs (Table 2).

There was a number (24) of proteins where no 1:1 orthology could be established among all four species, as one or more of the orthologs have different structures or where the ortholog have diverged into one or more paralogs (Table 3). Notable differences between the four species were found in the following viral restriction factor superfamiles: oligoadenylate synthetase (OAS), Myxovirus (influenza virus) resistance (Mx), IFN-induced protein with tetratricopeptide repeats (IFIT) and Interferon-induced transmembrane protein (IFITM). The 2’–5’-oligoadenylate synthetases (OAS) constitute a family of anti-viral proteins that are important for controlling infections caused by IAV and other viruses. The enzyme initiates the degradation of viral RNA via synthesis of 2'-5'-oligoadenylates (2-5A) which activates a latent ribonuclease (RNASEL) leading to the degradation of viral RNA and inhibition of viral replication. Mx proteins are another family of antiviral proteins important for controlling IAV infection. Human, porcine, and mouse Mx1 inhibits the replication of swine influenza virus *in vitro* [33,34]. However, most inbred strains of mice carry Mx1 genes with a large deletion or a nonsense mutation as well as defective Mx2 genes [35]. Two additional families of IFN-induced antiviral proteins for which orthology could not be established are the tetratricopeptide repeats (IFIT) and IFN-induced transmembrane proteins (IFITM) families. Human and mouse IFIT1 proteins have no antiviral activity against IAV [36], but porcine IFIT1, IFIT2, and IFIT3 reportedly inhibit the replication of swine influenza virus *in vitro* [34].

Several genes with diverse antiviral functions are missing from one or more of the species reviewed here. The human natural cytotoxicity triggering receptors NKp44 (NCR2) [37] and (NCR1) NKp46 [38] bind to IAV HA. This binding is required for NK cell-mediated lysis of IAV infected cells. Pigs and ferrets, but not mice, have NCR2 [39] (Table 3), and T cells expressing NCR1, NCR2 and NCR3 have been found in the lungs of IAV infected animals [40]. Lastly, we and others have noted the lack of the AIM2 inflammasome in pigs [41], and here we extend this finding to ferrets.

Host defense against IAV infection

The antiviral innate defense is a multifactorial system encompassing a variety of cell types and cellular and secreted proteins working in concert to prevent viral invasion and replication and to control and fine-tune the inflammatory response. Every factor must play its role at the right time and place to ensure a balanced and efficient immune response resulting in the ultimate clearance of the virus with a minimal degree of host tissue damage.

Upon IAV infection, as summarized in Figure 1 and Table 4, the pulmonary host immune response is initiated by a rapid and transient induction of pro- and anti-inflammatory cytokines, type I and type III interferons, and interferon stimulated genes (ISGs), establishing an 'antiviral' state in the infected and neighboring host cells [42–46]. With a slightly shifted onset, the non-coding microRNA (miRNA) response sets in (Figure 1). miRNAs are involved in post-transcriptional regulation of antiviral target genes and persist throughout the infection and even after the virus has been cleared [47] (Brogaard *et al*., manuscript under review). The abundance of natural killer (NK) cells, an important innate cytotoxic lymphocyte, increases from the beginning of infection, and reaches its peak as the viral load is declining [48,49]. Within a week after influenza infection, IAV specific antibody responses emerge (Figure 1); however, by then the innate immune response will have controlled the infection in cases of uncomplicated disease.

Intrinsic and innate barriers against IAV infection in humans, pigs, ferrets, and mice

In order to successfully infect and replicate within a host, IAV has to traverse several physiological and chemical barriers. The first challenge facing IAV upon host contact is the respiratory mucus layer, a complex viscous gel-like fluid secreted from goblet cells and submucosal glands [50]. The distribution of goblet cells has been found to vary significantly in different species. As shown in Figure 2, the distribution of goblet cells in the upper respiratory tract of humans, pigs, and ferrets are relatively similar, whereas mucus secreting goblet cells are very rare in the upper respiratory tract of mice [51–55]. The two secreted mucins MUC5B and MUC5AC are major components of the mucus layer, and other important components of human and porcine mucus includes membrane-associated mucin (MUC1), pulmonary surfactants including SP-D, lysozymes, nitric oxide, and lactoferrin [56–58]. Furthermore, the respiratory mucus contains sialic acid 'decoy receptors' that can bind to the HA of the invading virus and thus hinder the penetration to the underlying epithelial cells [59,60]. Mucociliary clearance by ciliated epithelial cells ensures that inhaled and entrapped pathogens are continuously removed and swallowed. The percentage of ciliated respiratory epithelial cells varies among mice and other animal models for influenza (Figure 2). Similarly to humans, pigs and ferrets have a larger percentage of ciliated respiratory epithelial cells at the tracheal surface compared to mice [54,55,61,62].

SP-D is a soluble, sialic acid containing constituent of the respiratory mucus layer, and an important porcine defense lectin that has been demonstrated to reduce infection of H1N1, H3N2 and H5N1 of human, swine, and avian origin in MDCK cells with varying success [63]. Whereas SP-D has been found to be an important antiviral lectin in the mouse [64], it has recently been shown not to play a major role in inhibition of different types of IAV in ferrets [65,66]. We have recently found the SP-D gene (*SFTPD*) to be constitutively expressed but not induced in the porcine lung during swine IAV (H1N2) infection (Brogaard *et al*., manuscript in preparation), suggesting that SP-D is a factor of the intrinsic pulmonary antiviral defense rather than the innate. After breaching the mucus layer, the viral HA binds to the terminal sialic acid (SA) residues linked to host cell surface glycoproteins. Even

though the type of SA linkage is not the sole determinant of viral host and tissue tropism, the distribution of α-2,3 and α-2,6-linked sialic acid receptors is important for viral binding and infectivity. As can be seen in Figure 2 the distribution of SA-α-2,3 and SA-α-2,6 receptors in the nasal cavity, trachea, and lung has been shown to vary considerably between mice and humans, whereas less variation is seen between humans, pigs, and ferrets [67–72]. This might reflect the difference in the location of respiratory infection caused by less pathogenic IAV, which for mice locates in the lower respiratory tract rather than in the upper respiratory tract as observed in humans [27].

IAV infections in the pig model

Pulmonary host response in porcine models of low pathogenic IAV infection

After breaching the mucus layer and infecting the respiratory epithelial cells of the host, the receptor-mediated innate antiviral immune response takes over. For obvious reasons, lung tissue from patients with low pathogenic influenza virus infection is scarce, and characterization of the host response in IAV infected human lung has only been reported from fatal cases after infection with e.g. the 2009 pandemic H1N1 or highly pathogenic H5N1 [73–76]. While these case studies are of great importance for elucidation of the mechanisms responsible for fatal outcomes of IAV infection, they may be less relevant for characterization of the host innate response to low virulent and seasonal IAVs. Instead, *in vivo* experimental IAV infection in pigs as well as in sophisticated porcine *ex vivo* cultured respiratory tissue using low pathogenic seasonal and pandemic strains of both human and swine origin, have provided insight into the induction of the antiviral innate immune response at the site of viral infection and replication [46,77–83] (Brogaard *et al*., manuscript under review, Brogaard *et al*., manuscript in preparation).

High-throughput methods like microarrays, RNA sequencing, and microfluidic qPCR have been applied in several studies to obtain comprehensive transcriptional characterization of pig lung tissue after IAV challenge. By employing methods to identify pathway enrichment in differentially expressed genes, these studies commonly report genes involved in viral recognition, pro-inflammatory responses by means of cytokine induction, chemotaxis and immune cell recruitment, apoptosis, and the antiviral interferon and ISG response to be fundamental after IAV challenge [77–79,83]. Transcription of important viral pathogen recognition receptors (PRRs) such as Toll-like receptors 3 and 7 (*TLR3*, *TLR7*), RIG-I (*DDX58*) and MDA5 (*IFIH1*) are up-regulated in pig lungs (*in vivo*, *ex vivo*) in response to swine origin H1N1 and H1N2 infection [46,77,81] (Brogaard *et al*., manuscript under review). *In vivo* studies likewise report a strong chemokine response, dominated by CXCL10 (*CXCL10*) [46,77] (Brogaard *et al*., manuscript under review), accompanied by a balanced pro- and anti-inflammatory cytokine response exemplified by the up-regulation of IL-1β (*IL1B*), IL-6 (*IL6*), IL-1RA (*IL1RN*), and IL-10 (*IL10*) [46] (Brogaard *et al*., manuscript under review) (Figure 1). As described above, little is known about local pulmonary response to low pathogenic IAV infection in humans. However, the abovementioned chemokines and inflammatory cytokines found to be regulated in porcine models has likewise been found to be highly expressed in human lung tissue samples of fatal cases, caused by the 2009 pandemic influenza H1N1or avian H5N1 [73,75].

The major hallmark of antiviral immunity is the interferon response. Accordingly, transcriptional studies of the porcine respiratory system after IAV infection consistently report the induction of interferons and interferon stimulated genes (ISGs) (Table 4), such as ISG15 (*ISG15*), PKR (*EIF2AK2*), Mx1 (*MX1*), OAS1 (*OAS1*), OASL (*OASL*), and IFITM1 and 3 (*IFITM1*, *IFITM3*) [46,77,80–82] (Brogaard *et al*., manuscript under review). A marked type I interferon response is commonly reported in

porcine transcriptional studies of IAV infected lung tissue with IFN-β gene expression being the primary constituent (Table 4) [46,78] (Brogaard *et al*., manuscript under review, Brogaard *et al*., manuscript in preparation). Knowledge of type III interferon expression in the infected lung is however sparse. Type III interferons, or IFN-λ (Table 4), is the most recently identified family of interferons, and have been shown to induce a cellular antiviral state via intrinsic pathways and ISGs that are remarkably similar to those employed by type I interferons [80,82,84]. To date, one study has reported type III interferon expression (*IL28B*, the porcine gene encoding IFN-λ3) in porcine lung tissue after swine H1N2 challenge, demonstrating a massive induction of the transcriptional type III interferon response (Brogaard *et al*., manuscript under review). One other study has likewise demonstrated the ex vivo upregulation of *IL29* (porcine IFN-λ1) in precision-cut porcine lung slices after swine H3N2 infection [80]. Both studies showed that IFN-λ expression was accompanied by up-regulation of IFNB1 as well as a multitude of antiviral ISGs. In vitro investigation of the human type III interferon response to IAV has similarly demonstrated up-regulation of *IFNL1* and *IFNL2* in human alveolar type II epithelial cells after infection with human H1N1 and H3N2 [85] (Table 4). Type III interferons appear to be important contributors to the innate immune response in the IAV infected lung, but further studies are needed to elucidate the temporal dynamics of type I and III interferon expression and the interplay between these two important components of the antiviral immune response.

The porcine systemic response after IAV infection mirrors human findings

In contrast to the local pulmonary response, the systemic transcriptional response to IAV infection in humans has been studied extensively, often with the aim to elucidate blood-based IAV-specific (or respiratory virus-specific) 'signatures' or 'classifiers' [44,86–90]. Such a signature might prove a valuable diagnostic tool to determine disease etiology. The systemic response to IAV infection has a high degree of similarity to the local response including induction of PRR, IFNs and ISGs. Importantly, a substantial overlap of genes found to be up-regulated in circulating leukocytes in pigs and humans, including the PRRs *DDX58* (RIG-I), *IFIH1* (MDA5), *TLR7* (TLR7), *NOD1* (NOD1), the ISGs *MX1* (Mx1), *IFITM3* (IFITM3), and *OASL* (OASL) has recently been reported [91]. IFN-α serum protein levels have been found to be elevated in pigs after swine H1N1 infection [92], mirroring our own observations of transcriptional up-regulation of IFNA1 in circulating leukocytes from swine H1N2 infected pigs [91]. More comprehensive investigation of serum cytokine levels has been carried out in human patients with mild disease after pandemic H1N1 (2009) infection, with results likewise supporting our findings of transcriptional up-regulation of IFNA1, CXCL10, IL1RN, IL10, and CCL2 in circulation of pigs infected with IAV [91,93].

miRNAs are frequently heralded great potential as systemic biomarkers for various conditions, due to their stability and availability in circulation [94]. As such, systemic miRNA expression after IAV infection has received some attention in both pigs [91] and humans [95–97], and importantly, around 70 % of the miRNAs that were regulated in porcine leukocytes after experimental IAV infection are likewise reported to show altered expression in circulation of human patients after IAV infection [91]. So not only does the pig display a local antiviral immune responses at the sites of IAV infection that parallels the corresponding responses in the human host, but there is also a substantial overlap in the systemic transcriptional response of protein coding and non-coding genes.

microRNAs as a central component of the antiviral innate immune system in pigs and humans

Host-encoded microRNAs are most commonly described as endogenous regulators of cellular protein translation, but several reports also describe the interaction between host-encoded miRNAs and viral RNA of the IAV [98–101]. Some viruses including DNA and retroviruses encode their own miRNAs, as demonstrated by the annotated viral miRNAs included in the online miRNA repository; miRBase [102]. No influenza virus-encoded miRNAs can be found in miRBase as the IAV genome has not been shown to contain any canonical miRNAs. miRNAs are evolutionarily highly conserved across species, making it likely that the study of host miRNA in the pig model will have great translational value for induction and function of miRNAs in settings of human disease.

Host-encoded miRNA regulation of the innate antiviral response after IAV infection has received some attention in recent years. We recently presented results implicating ssc-miR-15a, ssc-miR-18a, ssc-miR-21, ssc-miR-29b, and hsa-miR-590-3p in the regulation of genes involved in viral pattern recognition, apoptosis, and inflammasome function in the lungs of pigs challenged with swine H1N2 (Brogaard *et al*., manuscript under review). Several of these, as well as other miRNAs found to be differentially expressed in pig lungs after IAV challenge, have likewise been found to be regulated in human lung epithelial A549 cells after H1N1 infection [103]. However, other studies again of IAV infected A549, demonstrate little or no overlap of differentially expressed miRNAs, with the study of miRNA regulation in pig lungs after IAV challenge [104,105] (Brogaard *et al*., manuscript under review). This calls for caution when interpreting miRNA expression results; their multifaceted role in regulation of translation likely causes their expression to be highly affected by different experimental setups.

Recently, porcine ssc-miR-204 and ssc-miR-4331 was demonstrated to target HA and NS encoding segments of IAV (swine H1N1) and inhibit viral replication in trachea cells isolated from newborn pigs [101]. ssc-miR-4331 has furthermore been shown to be up-regulated *in vivo* in porcine pulmonary alveolar macrophages [106], as well as in total lung tissue of IAV vaccinated pigs after swine H1N2 challenge (Brogaard *et al*., manuscript in preparation). However, host miRNA-IAV RNA interactions identified for one IAV strain is not necessarily applicable to other strains or subtypes, due to the high mutation rate and risk of losing a miRNA binding site through antigenic drift. It would be of great interest to generate a 'consensus genome' from a selection of IAVs of interest, and identify host miRNA binding sites in the highly conserved portion of the IAV genome. Such an approach would help determine if host miRNA-IAV RNA interaction is a defining factor for virulence, transmissibility, or host range.

Validity of the porcine model

The validity of animal models can be assessed through a number of different criteria such as face, target, and predictive validities [107,108]. In influenza research, face validity specifies how well the animal model mirrors human clinical condition and symptoms after IAV infection. Target validity specifies the similarity and homology of e.g. a certain signaling pathway or a protein central for IAV infection in humans and the animal model, and predictive validity refers to how accurately a certain animal model reflects the pharmacological effects of an antiviral drug or vaccine [23]. Models with high face validity for studies of IAV pathogenesis and host immunity, as well as models with high predictive validity for testing of vaccines and antiviral therapies must be prioritized [23,24]. Examination of the mouse as a model for human IAV infection reveals low face validity due to the low resemblance of clinical manifestations between human and mouse. The pig as a model, however,

reveals high face validity due to the high similarity in clinical manifestations in humans and pigs such as fever, nasal secretion, and cough. However, having high face validity does not necessarily mean that the underlying mechanisms of the disease are the same. Therefore, the underlying disease mechanisms including innate immune response to viral infection needs to be as similar as possible between the animal model and the human disease in order to reach high predictive validity. Genome and transcriptome comparison of immune and inflammatory related gene families and protein sequences strongly recommend the pig as an intermediate animal model between mice and humans [41] suggesting also a high target validity. Therefore, based on the high face validity and similar immune mechanisms in response to IAV infection the predictive validity of the pig model is in our opinion high.

Conclusion

Pigs are important in influenza ecology and are readily susceptible to infection with human IAV strains without the need for viral adaptation. They display higher sequence similarity to humans with regards to antiviral proteins than do both ferrets and mice, and present clinical signs and transcriptional immune responses which closely mirrors humans'. By using the pig as a model for IAV infection we will be able to investigate the local pulmonary immune response at the site of viral infection; this sample material is next to impossible to obtain from humans, but of great importance in elucidation of innate and adaptive antiviral immunity [109,110]. Several factors warrant caution when applying the mouse as a model for human IAV infection, e.g. its greater number of unique (non-orthologous) genes, its lower percentage of antiviral protein similarity to human proteins, the need for adapted IAV strains, and the natural resistance of mice to IAV infection. The mouse immune response does not always directly recapitulate the human response, thus increasing the possibility of drawing inappropriate conclusions based on mouse studies. The relative equivalence of the ferret and pig in regards to these factors, indicate that both could be used as satisfactory models. However, in-depth knowledge of the ferret innate and adaptive immune responses to IAV infections is currently limited.

Face and target validity of the porcine model is extensive, and although not yet fully investigated, a high predictive validity is anticipated as well. Last but not least, the pig is a suitable model for the study of IAV infection and impaired vaccine response in settings of underlying pathologies such as low-grade inflammation associated with obesity and aging, as this state is inducible and well characterized in the pig [111–115]. Taken together, the pig is of great translational value in IAV research, and will continue to provide essential insights into this important infection.

Figure and table legends

Figure 1. Schematic representation of different aspects of the antiviral host immune response against influenza. The x-axis shows the temporal progression of infection (days) and the y-axis denotes the relative magnitude of the different responses. The figure is adapted from several publications [46,48,109,116–118] as well as our own yet unpublished work (Brogaard *et al*., manuscript under review, Brogaard *et al*., manuscript in preparation).

Figure 2. Schematic illustration of the distribution of α-2,3 and α-2,6-linked sialic acid receptors in the nasal cavity, trachea, and lung of humans, pigs, ferrets, and mice. α-2,6-linked sialic acid receptors are demonstrated by white squares and α-2,3-linked sialic acid receptors as white

triangles. The relative sizes of squares and triangles outline the relative distribution of the sialic acid receptors at each of the three locations in the respiratory tract. Distribution of respiratory ciliated epithelial cells (red) and the proportion of mucus producing goblet cells (yellow) in humans, pigs, ferrets, and mice is shown in the trachea.

Table 1. Comparison of human, pig, ferret, and mouse clinical signs after IAV infection, morphology of the respiratory tract, and experimental requirements for these four species. The table is modified from that which appears in Brogaard et al. 2016 [91].

Table 2. Comparison of antiviral protein similarity between humans and pig, ferret, and mouse. Analyses were performed using data obtained from the Porcine Translational Research Database, the NCBI reference protein database and predicted sequences and NCBI blastp suite. 1:1 orthology of protein coding genes were determined by protein structure similarity (best reciprocal BLAST hit to the human protein) and the presence of a corresponding gene in the syntenic region of the pig, ferret, and/or mouse genome. Means that have no superscript in common are significantly different at a level of $p < 0.05$ by matched paired ANOVA (JMP® 12.2.0 SAS Institute Inc.). The type I interferon alpha superfamily was not compared because of previously noted difficulties establishing 1:1 orthology for these genes.

Table 3. Non-orthologous genes associated with an anti-IAV response in humans, pigs, ferrets, and mice. Analyses were performed using data obtained from the Porcine Translational Research Database and NCBI reference protein database and blastp suite.

Table 4. Overview of key features of the host intrinsic and innate antiviral response to IAV infection in humans, pigs, ferrets, and mice. Upwards arrows indicates up-regulation/high levels of this gene under the examined condition. A – indicates that the levels of this gene is unchanged in the examined condition.

References

1. WHO | Influenza (Seasonal) [Internet]. WHO. World Health Organization; 2017 [cited 2017 Oct 6]. Available from: http://www.who.int/mediacentre/factsheets/fs211/en/
2. Thompson WW, Shay DK, Weintraub E, Brammer L, Cox N, Anderson LJ. Mortality Associated With Influenza and Respiratory Syncytial Virus in the United States. J. Am. Med. Assoc. 2003;289:179–86.
3. McElhaney JE. The unmet need in the elderly: Designing new influenza vaccines for older adults. Vaccine. 2005;23:10–25.
4. Anar C, Bicmen C, Yapicioglu S, Unsal I, Halilcolar H, Yilmaz U. Evaluation of clinical data and antibody response following influenza vaccination in patients with chronic obstructive pulmonary disease. New Microbiol. 2010;33:117–27.
5. Glezen PW, Greenberg SB, Atmar RL, Pedro PA, Couch RB. Impact of Respiratory Virus Infections on Persons With Chronic Conditions. JAMA. 2000;283:499–505.
6. World Health Organization. A Manual for Estimating Disease Burden Associated with Seasonal Influenza. 2015;124.

7. To KKW, Hung IFN, Li IWS, Lee K-L, Koo C-K, Yan W-W, et al. Delayed Clearance of Viral Load and Marked Cytokine Activation in Severe Cases of Pandemic H1N1 2009 Influenza Virus Infection. Clin. Infect. Dis. 2010;50:850–9.
8. Meschi S, Selleri M, Lalle E, Bordi L, Valli MB, Ferraro F, et al. Duration of viral shedding in hospitalized patients infected with pandemic H1N1. BMC Infect. Dis. 2011;11:140.
9. Rajao DS, Loving CL, Waide EH, Gauger PC, Dekkers JCM, Tuggle CK, et al. Pigs with Severe Combined Immunodeficiency Are Impaired in Controlling Influenza A Virus Infection. J. Innate Immun. 2017;9:193–202.
10. van der Vries E, Stittelaar KJ, van Amerongen G, Veldhuis Kroeze EJB, de Waal L, Fraaij PLA, et al. Prolonged Influenza Virus Shedding and Emergence of Antiviral Resistance in Immunocompromised Patients and Ferrets. PLoS Pathog. 2013;9:e1003343.
11. Shi Y, Wu Y, Zhang W, Qi J, Gao GF. Enabling the “host jump”: structural determinants of receptor-binding specificity in influenza A viruses. Nat. Rev. Microbiol. 2014;12:822–31.
12. Janke BH. Influenza A virus infections in swine: pathogenesis and diagnosis. Vet. Pathol. 2014;51:410–26.
13. Vincent A, Awada L, Brown I, Chen H, Claes F, Dauphin G, et al. Review of Influenza A Virus in Swine Worldwide: A Call for Increased Surveillance and Research. Zoonoses Public Health. 2014;61:4–17.
14. Alexander DJ, Brown IH. Recent zoonoses caused by influenza A viruses. Rev. Sci. Tech. 2000;19:197–225.
15. Lang P, Govind S, Bokum A, Kenny N, Matas E, Pitts D, et al. Immune Senescence and Vaccination in the Elderly. Curr. Top. Med. Chem. 2013;13:2541–50.
16. Tagliabue C, Principi N, Giavoli C, Esposito S. Obesity: impact of infections and response to vaccines. Eur. J. Clin. Microbiol. Infect. Dis. 2016;35:325–31.
17. Drugs@FDA: FDA Approved Drug Products [Internet]. [cited 2017 Oct 6]. Available from: https://www.accessdata.fda.gov/scripts/cder/daf/
18. H Heider, B Adamczyk, HW Presber, C Schroeder, R Feldblum MI. Occurrence of amantadine- and rimantadine-resistant influenza A virus strains during the 1980 epidemic. Acta Virol. 1981;25.
19. Centers for Disease Control and Prevention NC for I and RD (NCIRD). Influenza Antiviral Drug Resistance. 2017.
20. Prachanronarong KL, Özen A, Thayer KM, Yilmaz LS, Zeldovich KB, Bolon DN, et al. Molecular Basis for Differential Patterns of Drug Resistance in Influenza N1 and N2 Neuraminidase. J. Chem. Theory Comput. 2016;12:6098–108.
21. Jiang L, Liu P, Bank C, Renzette N, Prachanronarong K, Yilmaz LS, et al. A Balance between Inhibitor Binding and Substrate Processing Confers Influenza Drug Resistance. J. Mol. Biol. 2016;428:538–53.
22. Król E, Rychłowska M, Szewczyk B. Antivirals - current trends in fighting influenza. Acta Biochim. Pol. 2014. p. 495–504.
23. Denayer T, Stöhr T, Van Roy M. Animal models in translational medicine: Validation and prediction. New Horizons Transl. Med. Elsevier; 2014;2:5–11.
24. Mcgonigle P, Ruggeri B. Animal models of human disease: Challenges in enabling translation (McGonigle and Ruggeri). Biochem. Pharmacol. 2014;87:162–71.
25. Thangavel RR, Bouvier NM. Animal models for influenza virus pathogenesis, transmission, and immunology. J. Immunol. Methods. Elsevier B.V.; 2014;410:60–79.

26. Margine I, Krammer F. Animal Models for Influenza Viruses: Implications for Universal Vaccine Development. Pathogens. 2014;3:845–74.
27. Radigan KA, Misharin A V, Chi M, Budinger GS. Modeling human influenza infection in the laboratory. Infect. Drug Resist. 2015;8:311–20.
28. Kamal RP, Katz JM, York IA. Molecular determinants of influenza virus pathogenesis in mice. Curr Top Microbiol Immunol. 2014;385:243–74.
29. Matsuoka Y, Swayne DE, Thomas C, Rameix-Welti MA, Naffakh N, Warnes C, et al. Neuraminidase stalk length and additional glycosylation of the hemagglutinin influence the virulence of influenza H5N1 viruses for mice. J Virol. 2009;83:4704–8.
30. Bouvier NM. Animal models for influenza virus transmission studies: A historical perspective. Curr. Opin. Virol. Elsevier B.V.; 2015;13:101–8.
31. Rajao DS, Vincent AL. Swine as a model for influenza A virus infection and immunity. ILAR J. 2015;56:44–52.
32. Dawson HD, Chen C, Gaynor B, Shao J, Urban JF. The porcine translational research database: a manually curated, genomics and proteomics-based research resource. BMC Genomics. BMC Genomics; 2017;18:643.
33. Haller O, Kochs G. Human MxA Protein: An Interferon-Induced Dynamin-Like GTPase with Broad Antiviral Activity. J. Interf. Cytokine Res. 2011;31:79–87.
34. Li Y, Wen Z, Zhou H, Wu S, Jia G, Qian W, et al. Porcine interferon-induced protein with tetratricopeptide repeats 3, poIFIT3, inhibits swine influenza virus replication and potentiates IFN-?? production. Dev. Comp. Immunol. 2015;50:49–57.
35. Iwasaki A, Pillai PS. Innate immunity to influenza virus infection. Nat. Rev. Immunol. Nature Publishing Group; 2014;14:315–28.
36. Pinto AK, Williams GD, Szretter KJ, White JP, Proença-Módena JL, Liu G, et al. Human and Murine IFIT1 Proteins Do Not Restrict Infection of Negative-Sense RNA Viruses of the Orthomyxoviridae, Bunyaviridae, and Filoviridae Families. J. Virol. 2015;89:9465–76.
37. Arnon TI, Lev M, Katz G, Chernobrov Y, Porgador A, Mandelboim O. Recognition of viral hemagglutinins by NKp44 but not by NKp30. Eur. J. Immunol. 2001;31:2680–9.
38. Mandelboim O, Lieberman N, Lev M, Paul L, Arnon TI, Bushkin Y, et al. Recognition of haemagglutinins on virus-infected cells by NKp46 activates lysis by human NK cells. Nature. 2001;409:1055–60.
39. Hollyoake M, Campbell RD, Aguado B. NKp30 (NCR3) is a pseudogene in 12 inbred and wild mouse strains, but an expressed gene in Mus caroli. Mol. Biol. Evol. 2005;22:1661–72.
40. Mair KH, Stadler M, Talker SC, Forberg H, Storset AK, Müllebner A, et al. Porcine CD3+NKp46+ lymphocytes have NK-cell characteristics and are present in increased frequencies in the lungs of influenza-infected animals. Front. Immunol. 2016;7:1–17.
41. Dawson HD, Smith AD, Chen C, Urban JF. An in-depth comparison of the porcine, murine and human inflammasomes; lessons from the porcine genome and transcriptome. Vet. Microbiol. Elsevier B.V.; 2017;202:2–15.
42. Galani IE, Triantafyllia V, Eleminiadou E-E, Koltsida O, Stavropoulos A, Manioudaki M, et al. Interferon-λ Mediates Non-redundant Front-Line Antiviral Protection against Influenza Virus Infection without Compromising Host Fitness. Immunity. 2017;46:875–890.e6.
43. Pomorska-Mol M, Markowska-Daniel I, Kwit K. Immune and acute phase response in pigs experimentally infected with H1N2 swine influenza virus. FEMS Immunol.Med.Microbiol. p.

44. Zhai Y, Franco LM, Atmar RL, Quarles JM, Arden N, Bucasas KL, et al. Host Transcriptional Response to Influenza and Other Acute Respiratory Viral Infections – A Prospective Cohort Study. PLoS Pathog. 2015;11:1–29.
45. Carolan LA, Rockman S, Borg K, Guarnaccia T, Reading P, Mosse J, et al. Characterization of the Localized Immune Response in the Respiratory Tract of Ferrets following Infection with Influenza A and B Viruses. J. Virol. 2016;90:2838–48.
46. Skovgaard K, Cirera S, Vasby D, Podolska A, Breum SØ, Dürrwald R, et al. Expression of innate immune genes, proteins and microRNAs in lung tissue of pigs infected experimentally with influenza virus (H1N2). Innate Immun. 2013;19:531–44.
47. Pociask DA, Robinson KM, Chen K, McHugh KJ, Clay ME, Huang GT, et al. Epigenetic and Transcriptomic Regulation of Lung Repair during Recovery from Influenza Infection. Am. J. Pathol. 2017;187:851–63.
48. Pommerenke C, Wilk E, Srivastava B, Schulze A, Novoselova N, Geffers R, et al. Global transcriptome analysis in influenza-infected mouse lungs reveals the kinetics of innate and adaptive host immune responses. PLoS One. 2012;7.
49. Forberg H, Hauge AG, Valheim M, Garcon F, Nunez A, Gerner W, et al. Early responses of natural killer cells in pigs experimentally infected with 2009 pandemic H1N1 influenza a virus. PLoS One. 2014;9.
50. Jeffery PK. Morphologic Features of Airway Surface Epithelial Cells and Glands. Am. Rev. Respir. Dis. 1983;128:S14–20.
51. Spicer SS, Schulte BA, Thomopoulos GN. Histochemical properties of the respiratory tract epithelium in different species. Am. Rev. Respir. Dis. 1983;128:S20-6.
52. Pavelka M. Organ culture of adult Rat and mouse tracheal epithelium: I. Ultrastructure following various culture periods. Cell Tissue Res. 1976;165.
53. DM Hyde, DA Samuelson, WH Blakeney PK. A correlative light microscopy, transmission and scanning electron microscopy study of the ferret lung. Scan. Electron Microsc. 1979;
54. Leigh MW, Cheng PW, Boat TF. Developmental Changes of Ferret Tracheal Mucin Composition and Biosynthesis. Biochemistry. 1989;28:9440–6.
55. Pack RJ, Al-Ugaily LH, Morris G, Widdicombe JG. The distribution and structure of cells in the tracheal epithelium of the mouse. Cell Tissue Res. 1980;208:65–84.
56. Ganesan S, Comstock AT, Sajjan US. Barrier function of airway tract epithelium. Tissue Barriers. 2013;1:e24997.
57. Dubin RF, Robinson SK, Widdicombe JH, Dajani R, Zhang Y, Taft PJ, et al. Secretion of lactoferrin and lysozyme by cultures of human airway epithelium Secretion of lactoferrin and lysozyme by cultures of human airway epithelium. Am. J. Physiol. - Lung Cell. Mol. Physiol. 2004;8664:750–5.
58. Ermund A, Meiss LN, Rodriguez-Pineiro AM, Bähr A, Nilsson HE, Trillo-Muyo S, et al. The normal trachea is cleaned by MUC5B mucin bundles from the submucosal glands coated with the MUC5AC mucin. Biochem. Biophys. Res. Commun. 2017;492:331–7.
59. Cohen M, Zhang X-Q, Senaati HP, Chen H-W, Varki NM, Schooley RT, et al. Influenza A penetrates host mucus by cleaving sialic acids with neuraminidase. Virol. J. 2013;10:321.
60. Yang X, Steukers L, Forier K, Xiong R, Braeckmans K, Van Reeth K, et al. A beneficiary role for neuraminidase in influenza virus penetration through the respiratory mucus. PLoS One. 2014;9:1–11.
61. Zhang L, Button B, Gabriel SE, Burkett S, Yan Y, Skiadopoulos MH, et al. CFTR delivery to 25% of surface epithelial cells restores normal rates of mucus transport to human cystic fibrosis airway epithelium. PLoS Biol. 2009;7.

62. Wallace P, Kennedy JR, Mendicino J. Transdifferentiation of outgrowth cells and cultured epithelial cells from swine trachea. Vitr. Cell. Dev. Biol. - Anim. 1994;3:168–80.
63. Hillaire MLB, van Eijk M, van Trierum SE, van Riel D, Saelens X, Romijn RA, et al. Assessment of the antiviral properties of recombinant porcine SP-D against various influenza A viruses in vitro. PLoS One. 2011;6.
64. Reading PC, Morey LS, Crouch EC. Collectin-mediated antiviral host defense of the lung : evidence from influenza virus infection of mice. J. Virol. 1997;71:8204–12.
65. Job ER, Deng Y-M, Tate MD, Bottazzi B, Crouch EC, Dean MM, et al. Pandemic H1N1 influenza A viruses are resistant to the antiviral activities of innate immune proteins of the collectin and pentraxin superfamilies. J. Immunol. 2010;185:4284–91.
66. Job ER, Pizzolla A, Nebl T, Short KR, Deng YM, Carolan L, et al. Neutralizing inhibitors in the airways of naïve ferrets do not play a major role in modulating the virulence of H3 subtype influenza A viruses. Virology. Elsevier; 2016;494:143–57.
67. Ning ZY, Luo MY, Qi WB, Yu B, Jiao PR, Liao M. Detection of expression of influenza virus receptors in tissues of BALB/c mice by histochemistry. Vet. Res. Commun. 2009;33:895–903.
68. Kirkeby S, Martel CJM, Aasted B. Infection with human H1N1 influenza virus affects the expression of sialic acids of metaplastic mucous cells in the ferret airways. Virus Res. 2009;144:225–32.
69. Xu Q, Wang W, Cheng X, Zengel J, Jin H. Influenza H1N1 A/Solomon Island/3/06 virus receptor binding specificity correlates with virus pathogenicity, antigenicity, and immunogenicity in ferrets. J. Virol. 2010;84:4936–45.
70. Trebbien R, Larsen LE, Viuff BM. Distribution of sialic acid receptors and influenza A virus of avian and swine origin in experimentally infected pigs. Virol. J. BioMed Central Ltd; 2011;8:434.
71. Shinya K, Ebina M, Yamada S, Ono M, Kasai N, Kawaoka Y. Avian flu: Influenza virus receptors in the human airway. Nature. 2006;440:435–6.
72. Nelli RK, Kuchipudi S V, White G a, Perez BB, Dunham SP, Chang K-C. Comparative distribution of human and avian type sialic acid influenza receptors in the pig. BMC Vet. Res. 2010;6:4.
73. Gao R, Bhatnagar J, Blau DM, Greer P, Rollin DC, Denison AM, et al. Cytokine and chemokine profiles in lung tissues from fatal cases of 2009 pandemic influenza A (H1N1): role of the host immune response in pathogenesis. Am. J. Pathol. 2013;183:1258–68.
74. Mauad T, Hajjar LA, Callegari GD, da Silva LFF, Schout D, Galas FRBG, et al. Lung Pathology in Fatal Novel Human Influenza A (H1N1) Infection. Am. J. Respir. Crit. Care Med. 2010;181:72–9.
75. Nakajima N, Van Tin N, Sato Y, Thach HN, Katano H, Diep PH, et al. Pathological study of archival lung tissues from five fatal cases of avian H5N1 influenza in Vietnam. Mod. Pathol. Nature Publishing Group; 2013;26:357–69.
76. Kongchanagul A, Suptawiwat O, Boonarkart C, Kitphati R, Puthavathana P, Uiprasertkul M, et al. Decreased expression of surfactant protein D mRNA in human lungs in fatal cases of H5N1 avian influenza. J. Med. Virol. 2011;83:1410–7.
77. Li Y, Zhou H, Wen Z, Wu S, Huang C, Jia G, et al. Transcription analysis on response of swine lung to H1N1 swine influenza virus. BMC Genomics. 2011;12:398.
78. Ma W, Belisle SE, Mosier D, Li X, Stigger-Rosser E, Liu Q, et al. 2009 pandemic H1N1 influenza virus causes disease and upregulation of genes related to inflammatory and immune responses, cell death, and lipid metabolism in pigs. J.Virol. 2011. p. 11626–37.

79. Go JT, Belisle SE, Tchitchek N, Tumpey TM, Ma W, Richt JA, et al. 2009 pandemic H1N1 influenza virus elicits similar clinical course but differential host transcriptional response in mouse, macaque, and swine infection models. BMC Genomics. 2012;13:627.
80. Delgado-Ortega M, Melo S, Punyadarsaniya D, Ramé C, Olivier M, Soubieux D, et al. Innate immune response to a H3N2 subtype swine influenza virus in newborn porcine trachea cells, alveolar macrophages, and precision-cut lung slices. Vet. Res. 2014;45:1–18.
81. Dobrescu I, Levast B, Lai K, Delgado-Ortega M, Walker S, Banman S, et al. In vitro and ex vivo analyses of co-infections with swine influenza and porcine reproductive and respiratory syndrome viruses. Vet. Microbiol. Elsevier B.V.; 2014;169:18–32.
82. Krishna VD, Roach E, Zaidman NA, Panoskaltsis-Mortari A, Rotschafer JH, O'Grady SM, et al. Differential induction of type I and type III interferons by swine and human origin H1N1 influenza a viruses in porcine airway epithelial cells. PLoS One. 2015;10.
83. Wilkinson JM, Gunvaldsen RE, Detmer SE, Dyck MK, Dixon WT, Foxcroft GR, et al. Transcriptomic and epigenetic profiling of the lung of influenza-infected pigs: A comparison of different birth weight and susceptibility groups. PLoS One. 2015;10:1–24.
84. Jung K, Chae C. Expression of Mx Protein and Interferon-α in Pigs Experimentally Infected with Swine Influenza Virus. Vet. Pathol. 2006;43:161–7.
85. Mason RJ, Nikrad M, Funk CJ, Hartshorn KL, Wang J, Oberley-Deegan R, et al. Differentiated Human Alveolar Type II Cells Secrete Antiviral IL-29 (IFN-?1) in Response to Influenza A Infection. J Immunol. 2009;182:1296–304.
86. Ramilo O, Allman W, Chung W, Mejias A, Ardura M, Glaser C, et al. Gene expression patterns in blood leukocytes discriminate patients with acute infections. Blood. 2007. p. 2066–77.
87. Zaas AK, Chen M, Varkey J, Veldman T, Hero III AO, Lucas J, et al. Gene expression signatures diagnose influenza and other symptomatic respiratory viral infections in humans. Cell Host.Microbe. 2009. p. 207–17.
88. Huang Y, Zaas AK, Rao A, Dobigeon N, Woolf PJ, Veldman T, et al. Temporal dynamics of host molecular responses differentiate symptomatic and asymptomatic influenza a infection. PLoS Genet. 2011;7.
89. Andres-Terre M, McGuire HM, Pouliot Y, Bongen E, Sweeney TE, Tato CM, et al. Integrated, Multi-cohort Analysis Identifies Conserved Transcriptional Signatures across Multiple Respiratory Viruses. Immunity. Elsevier Inc.; 2015;43:1199–211.
90. Sampson DL, Fox BA, Yager TD, Bhide S, Cermelli S, McHugh LC, et al. A Four-Biomarker Blood Signature Discriminates Systemic Inflammation Due to Viral Infection Versus Other Etiologies. Sci. Rep. 2017;7:2914.
91. Brogaard L, Heegaard PMH, Larsen LE, Mortensen S, Schlegel M, Dürrwald R, et al. Late regulation of immune genes and microRNAs in circulating leukocytes in a pig model of influenza A (H1N2) infection. Sci. Rep. 2016;6:21812.
92. Barbé F, Atanasova K, Van Reeth K. Cytokines and acute phase proteins associated with acute swine influenza infection in pigs. Vet. J. 2011;187:48–53.
93. Bradley-Stewart A, Jolly L, Adamson W, Gunson R, Frew-Gillespie C, Templeton K, et al. Cytokine responses in patients with mild or severe influenza A(H1N1)pdm09. J. Clin. Virol. Elsevier B.V.; 2013;58:100–7.
94. Turchinovich A, Tonevitsky AG, Burwinkel B. Extracellular miRNA: A Collision of Two Paradigms. Trends Biochem. Sci. Elsevier Ltd; 2016;41:883–92.

95. Tambyah PA, Sepramaniam S, Mohamed Ali J, Chai SC, Swaminathan P, Armugam A, et al. microRNAs in Circulation Are Altered in Response to Influenza A Virus Infection in Humans. PLoS One. 2013;8:e76811.
96. Song H, Wang Q, Guo Y, Liu S, Song R, Gao X, et al. Microarray analysis of microRNA expression in peripheral blood mononuclear cells of critically ill patients with influenza A (H1N1). BMC Infect. Dis. BMC Infectious Diseases; 2013;13:257.
97. Zhu Z, Qi Y, Ge A, Zhu Y, Xu K, Ji H, et al. Comprehensive characterization of serum microRNA profile in response to the emerging avian influenza A (H7N9) virus infection in humans. Viruses. 2014;6:1525–39.
98. Song L, Liu H, Gao S, Jiang W, Huang W. Cellular microRNAs inhibit replication of the H1N1 influenza A virus in infected cells. J. Virol. 2010;84:8849–60.
99. Khongnomnan K, Makkoch J, Poomipak W, Poovorawan Y, Payungporn S. Human miR-3145 inhibits influenza A viruses replication by targeting and silencing viral PB1 gene. Exp Biol Med. 2015;1630–9.
100. Ma Y-J, Yang J, Fan X-L, Zhao H-B, Hu W, Li Z-P, et al. Cellular microRNA let-7c inhibits M1 protein expression of the H1N1 influenza A virus in infected human lung epithelial cells. J. Cell. Mol. Med. 2012;16:2539–46.
101. Zhang S, Wang R, Su H, Wang B, Sizhu S, Lei Z, et al. Sus scrofa miR-204 and miR-4331 negatively regulate swine H1N1/2009 influenza a virus replication by targeting viral HA and NS, respectively. Int. J. Mol. Sci. 2017;18:1–18.
102. Kozomara A, Griffiths-Jones S. MiRBase: Annotating high confidence microRNAs using deep sequencing data. Nucleic Acids Res. 2014;42:68–73.
103. Terrier O, Textoris J, Carron C, Marcel V, Bourdon J-C, Rosa-Calatrava M. Host microRNA molecular signatures associated with human H1N1 and H3N2 influenza A viruses reveal an unanticipated antiviral activity for miR-146a. J. Gen. Virol. 2013;94:985–95.
104. Makkoch J, Poomipak W, Saengchoowong S, Khongnomnan K, Praianantathavorn K, Jinato T, et al. Human microRNAs profiling in response to influenza A viruses (subtypes pH1N1, H3N2, and H5N1). Exp. Biol. Med. 2016;241:409–20.
105. Loveday EK, Svinti V, Diederich S, Pasick J, Jean F. Temporal- and strain-specific host microRNA molecular signatures associated with swine-origin H1N1 and avian-origin H7N7 influenza A virus infection. J. Virol. 2012;86:6109–22.
106. Jiang P, Zhou N, Chen X, Zhao X, Li D, Wang F, et al. Integrative analysis of differentially expressed microRNAs of pulmonary alveolar macrophages from piglets during H1N1 swine influenza A virus infection. Sci. Rep. 2015;5:8167.
107. McKinney Jr WT, Bunney Jr WE. Animal model of depression: I. Review of evidence: implications for research. Arch. Gen. Psychiatry. 1969;21:240.
108. Willner P. The validity of animal models of depression. Psychopharmacology (Berl). 1984. p. 1–16.
109. Pomorska-Mól M, Kwit K, Markowska-Daniel I, Kowalski C, Pejsak Z. Local and systemic immune response in pigs during subclinical and clinical swine influenza infection. Res. Vet. Sci. Elsevier Ltd; 2014;97:412–21.
110. Tchilian E, Holzer B. Harnessing Local Immunity for an Effective Universal Swine Influenza Vaccine. Viruses. 2017;9:98.
111. Ludvigsen TP, Kirk RK, Christoffersen BØ, Pedersen HD, Martinussen T, Kildegaard J, et al. Göttingen minipig model of diet-induced atherosclerosis: influence of mild streptozotocin-induced

diabetes on lesion severity and markers of inflammation evaluated in obese, obese and diabetic, and lean control animals. J. Transl. Med. BioMed Central; 2015;13:1–12.
112. Boonen HCM, Moesgaard SG, Birck MM, Christoffersen B, Cirera S, Heegaard PMH, et al. Functional network analysis of obese and lean Göttingen minipigs elucidates changes in oxidative and inflammatory networks in obese pigs. Pflugers Arch. Eur. J. Physiol. 2014;466:2167–76.
113. Toedebusch RG, Roberts MD, Wells KD, Company JM, Kanosky KM, Padilla J, et al. Unique transcriptomic signature of omental adipose tissue in Ossabaw swine: a model of childhood obesity. Physiol Genomics. 2014;46:362–75.
114. Rødgaard T, Skovgaard K, Stagsted J, Heegaard PMH. Expression of innate immune response genes in liver and three types of adipose tissue in cloned pigs. Cell. Reprogram. 2012;14:407–17.
115. Mentzel CMJ, Alkan F, Keinicke H, Jacobsen MJ, Gorodkin J, Fredholm M, et al. Joint Profiling of miRNAs and mRNAs Reveals miRNA Mediated Gene Regulation in the Göttingen Minipig Obesity Model. PLoS One. 2016;11:1–16.
116. Crisci E, Mussá T, Fraile L, Montoya M. Review: influenza virus in pigs. Mol. Immunol. Elsevier Ltd; 2013;55:200–11.
117. Larsen DL, Karasin A, Zuckermann F, Olsen CW. Systemic and mucosal immune responses to H1N1 influenza virus infection in pigs. Vet. Microbiol. 2000. p. 117–31.
118. Pomorska-Mól M, Markowska-Daniel I, Kwit K. Immune and acute phase response in pigs experimentally infected with H1N2 swine influenza virus. FEMS Immunol. Med. Microbiol. 2012;66:334–42.
119. Bouvier NM, Lowen AC. Animal models for influenza virus pathogenesis and transmission. Viruses. 2010;2:1530–63.
120. KAPLAN MM, PAYNE AM. Serological survey in animals for type A influenza in relation to the 1957 pandemic. Bull. World Health Organ. 1959;20:465–88.
121. Smith W, Andrewes CH, Laidlaw PP, Timbury MC. A Virus obtained from influenza patients. Lancet. 1933;66–8.
122. Monto AS, Gravenstein S, Elliott M, Colopy M, Schweinle J. Clinical signs and symptoms predicting influenza infection. Arch.Intern.Med. 2000. p. 3243–7.
123. Carrat F, Tachet A, Rouzioux C, Housset B, Valleron AJ. Evaluation of clinical case definitions of influenza: detailed investigation of patients during the 1995-1996 epidemic in France. Clin. Infect. Dis. 1999;28:283–90.
124. Haesebrouck F, Pernsaert MB. Effect of intratracheal challenge of fattening pigs previously immunised with an activated influenza H1N1 vaccine. Vet. Microbiol. 1986;11:239–49.
125. Dybing JK, Schultz-Cherry S, Swayne DE, Suarez DL, Perdue ML. Distinct pathogenesis of hong kong-origin H5N1 viruses in mice compared to that of other highly pathogenic H5 avian influenza viruses. J. Virol. 2000;74:1443–50.
126. Janke BH. Clinicopathological Features of Swine Influenza. In: Richt JA, Webby RJ, editors. Swine Influ. Berlin, Heidelberg: Springer Berlin Heidelberg; 2013. p. 69–83.
127. Ohmit SE, Monto AS. Symptomatic predictors of influenza virus positivity in children during the influenza season. Clin. Infect. Dis. 2006;43:564–8.
128. S. L. S. The evaluation of compounds against influenza viruses. Ann NY Acad Sci. 1970;173:239–48.
129. Edenborough KM, Gilbertson BP, Brown LE. A Mouse Model for the Study of Contact-Dependent Transmission of Influenza A Virus and the Factors That Govern Transmissibility. J. Virol. 2012;86:12544–51.

130. Pabst R. Das lymphatische Gewebe der Nase (NALT) und des Kehlkopfes (LALT) im Speziesvergleich: Mensch, Ratte, Maus. Pneumologie. 2010;64:445–6.
131. Evans H, An NQ. Anatomy of the ferret. In: Fox JG, Robert MP, editors. Biol. Dis. Ferret. Third Edit. John Wiley & Sons, Inc.; 2014. p. 23–67.
132. Williams DM, Rowland AC. The palatine tonsils of the pig--an afferent route to the lymphoid tissue. J. Anat. 1972;113:131–7.
133. Casteleyn C, Breugelmans S, Simoens P, Van Den Broeck W. The tonsils revisited: Review of the anatomical localization and histological characteristics of the tonsils of domestic and laboratory animals. Clin. Dev. Immunol. 2011.
134. F. McLaughlin R, S.Tyler W, O.Canada R. A study of the subgross pulmonary anatomy in various mammals. Am. J. Anat. 1961. p. 149–65.
135. TYLER W. COMPARATIVE SUBGROSS ANATOMY OF LUNGS - PLEURAS, INTERLOBULAR SEPTA, AND DISTAL AIRWAYS. Am. Rev. Respir. Dis. 1983;128.
136. Peake JL, Pinkerton KE. Gross and Subgross Anatomy of Lungs, Pleura, Connective Tissue Septa, Distal Airways, and Structural Units. Second Edi. Comp. Biol. Norm. Lung Second Ed. Elsevier Inc.; 2015.
137. Schneberger D, Haronson-Raz K, Singh B. Pulmonary intravascular macrophages and lung health: what are we missing? Am.J.Physiol Lung Cell Mol.Physiol. 2012. p. L498–503.
138. Longworth KE. THE COMPARATIVE BIOLOGY OF PULMONARY INTRAVASCULAR MACROPHAGES. Front. Biosci. 1997;232–41.
139. Brain JD, Molina RM, DeCamp MM, Warner AE. Pulmonary intravascular macrophages: their contribution to the mononuclear phagocyte system in 13 species. Am.J.Physiol. p. L146–54.
140. Hartshorn KL, White MR, Shepherd V, Reid K, Jensenius JC, Crouch EC. Mechanisms of anti-influenza activity of surfactant proteins A and D: comparison with serum collectins. Am. J. Physiol. 1997;273:L1156–66.
141. Hawgood S, Brown C, Edmondson J, Stumbaugh A, Allen L, Goerke J, et al. Pulmonary Collectins Modulate Strain-Speci c In uenza A Virus Infection and Host Responses. Society. 2004;78:8565–72.
142. LeVine a M, Whitsett J a, Hartshorn KL, Crouch EC, Korfhagen TR. Surfactant protein D enhances clearance of influenza A virus from the lung in vivo. J. Immunol. 2001;167:5868–73.
143. Maines TR, Belser JA, Gustin KM, Van Hoeven N, Zeng H, Svitek N, et al. Local innate immune responses and influenza virus transmission and virulence in ferrets. J. Infect. Dis. 2012;205:474–85.
144. Stegemann-Koniszewski S, Jeron A, Gereke M, Geffers R, Kröger A, Gunzer M. Alveolar Type II Epithelial Cells Contribute to the Anti-Influenza A Virus Response in the Lung by Integrating Pathogen- and Microenvironmen-Derived Signals. MBio. 2016;7:1–11.
145. Rodriguez-Ramirez HG, Salinas-Carmona MC, Barboza-Quintana O, Melo-De La Garza A, Ceceñas-Falcon LA, Rangel-Martinez LM, et al. CD206+ Cell number differentiates influenza a (H1N1)PDM09 from seasonal influenza a virus in fatal cases. Mediators Inflamm. Hindawi; 2014;2014:1–8.
146. Huang SSH, Banner D, Degousee N, Leon AJ, Xu L, Paquette SG, et al. Differential pathological and immune responses in newly weaned ferrets are associated with a mild clinical outcome of pandemic 2009 H1N1 infection. J. Virol. 2012;86:13187–201.
147. León AJ, Banner D, Xu L, Ran L, Peng Z, Yi K, et al. Sequencing, annotation, and characterization of the influenza ferret infectome. J. Virol. 2013;87:1957–66.

148. Cameron CM, Cameron MJ, Bermejo-Martin JF, Ran L, Xu L, Turner P V, et al. Gene expression analysis of host innate immune responses during Lethal H5N1 infection in ferrets. J. Virol. 2008;82:11308–17.
149. Lee N, Wong CK, Hui DSC, Lee SKW, Wong RYK, Ngai KLK, et al. Role of human Toll-like receptors in naturally occurring influenza A infections. Influenza Other Respi. Viruses. 2013;7:666–75.
150. Le Goffic R, Balloy V, Lagranderie M, Alexopoulou L, Escriou N, Flavell R, et al. Detrimental contribution of the Toll-like receptor (TLR)3 to influenza A virus-induced acute pneumonia. PLoS Pathog. 2006;2:0526–35.
151. Jewell NA, Vaghefi N, Mertz SE, Akter P, Peebles RS, Bakaletz LO, et al. Differential Type I Interferon Induction by Respiratory Syncytial Virus and Influenza A Virus In Vivo. J. Virol. 2007;81:9790–800.

Figure 1. Schematic representation of different aspects of the antiviral host immune response against influenza. The x-axis shows the temporal progression of infection (days) and the y-axis denotes the relative magnitude of the different responses. The figure is adapted from several publications [46,48,109,116–118] as well as our own yet unpublished work (Brogaard *et al.*, manuscript under review, Brogaard *et al.*, manuscript in preparation).

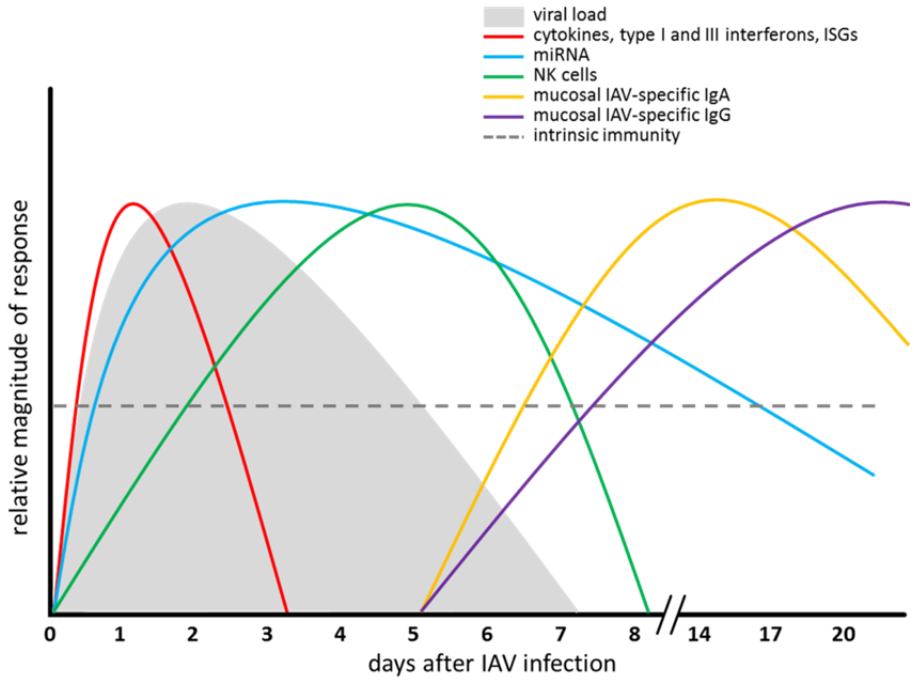

Figure 2. Schematic illustration of the distribution of α-2,3 and α-2,6-linked sialic acid receptors in the nasal cavity, trachea, and lung of humans, pigs, ferrets, and mice. α-2,6-linked sialic acid receptors are demonstrated by white squares and α-2,3-linked sialic acid receptors as white triangles. The relative sizes of squares and triangles outline the relative distribution of the sialic acid receptors at each of the three locations in the respiratory tract. Distribution of respiratory ciliated epithelial cells (red) and the proportion of mucus producing goblet cells (yellow) in humans, pigs, ferrets, and mice is shown in the trachea.

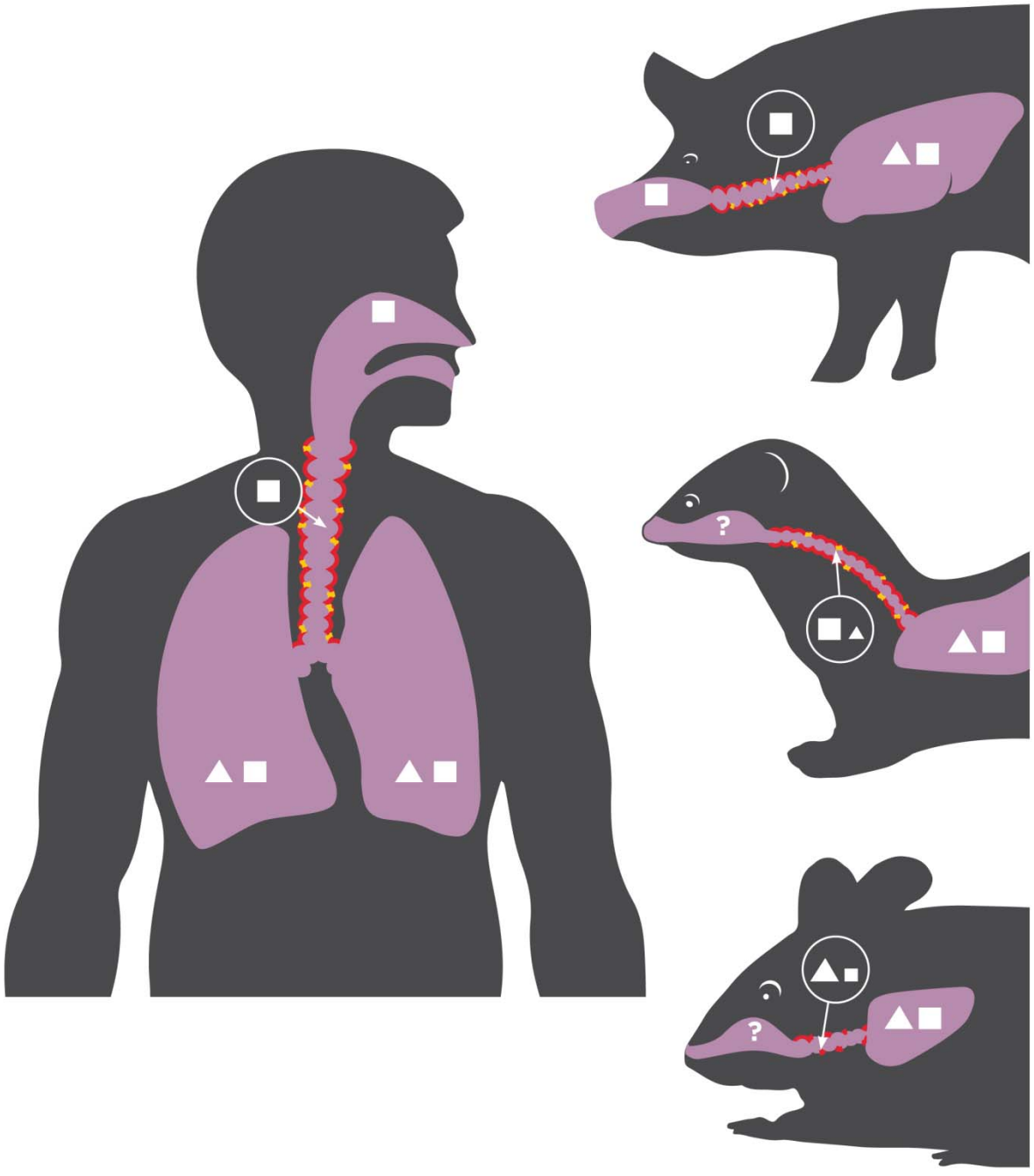

Table 1. Comparison of human, pig, ferret, and mouse clinical signs after IAV infection, morphology of the respiratory tract, and experimental requirements for these four species. The table is modified from that which appears in Brogaard et al. 2016 [91].

Feature	Human	Pig	Ferret	Mouse	Reference
Naturally infected with human influenza strains	Yes	Yes	Yes	No	[122-124]
Fever	Present	Present	Present	Absent	[27,124-128]
Nasal secretion	Present	Present	Present	Absent	[124,126,129]
Coughing	Present	Present	Present	Absent	[125,127,129-132]
Possess tonsils	Yes	Yes	Yes	No	[133-136]
Nature of pleura	Thick	Thick	Thin	Thin	[54,137-139]
Nature of connective tissue	Extensive and interlobular	Extensive and interlobular	Little	Little, if any	[137-139]
Pulmonary intravascular macrophages	Induced phagocytic cells	Constitutive phagocytic cells	Induced phagocytic cells	Induced phagocytic cells	[140-142]
Immunological reagents available	Many	Increasing	Few	Many	-
Housing requirements	-	Large	Medium	Small	-
Experimental costs	-	Moderate/high	Moderate/high	Low	-

Table 2. Comparison of antiviral protein similarity between humans and pig, ferret, and mouse. Analyses were performed using data obtained from the Porcine Translational Research Database, the NCBI reference protein database and predicted sequences and NCBI blastp suite. 1:1 orthology of protein coding genes were determined by protein structure similarity (best reciprocal BLAST hit to the human protein) and the presence of a corresponding gene in the syntenic region of the pig, ferret, and/or mouse genome. Means that have no superscript in common are significantly different at a level of $p < 0.05$ by matched paired ANOVA (JMP® 12.2.0 SAS Institute Inc.). The type I interferon alpha superfamily was not compared because of previously noted difficulties establishing 1:1 orthology for these genes.

		(mean %)		
Classification	Number of proteins	Pig	Ferret	Mouse
Cytokine Receptor	5	60.0^{A}	63.6^{A}	52.6^{B}
DEAD and DEXH	9	92.9^{A}	90.6^{A}	89.3^{A}
Inflammasome	3	78.3^{A}	76.0^{A}	74.0^{A}
Interferons	5	68.4^{A}	65.6^{A}	54.6^{B}
Miscellaneous	50	86.0^{A}	85.1^{A}	82.5^{B}
Restriction Factor	11	73.1^{A}	69.3^{B}	67.2^{B}
RIG-I-Like Receptor	3	81.7^{A}	82.3^{A}	78.7^{B}
Toll-Like Receptor	3	80.0^{A}	83.7^{AB}	77.3^{B}
Transcription Factor	9	87.9^{AB}	89.3^{A}	85.3^{B}
TRIM	9	84.6^{A}	84.7^{A}	81.3^{B}
Overall	103	82.9^{A}	81.9^{A}	78.4^{B}

Table 3. Non-orthologous genes associated with an anti-IAV response in humans, pigs, ferrets, and mice. Analyses were performed using data obtained from the Porcine Translational Research Database and NCBI reference protein database and blastp suite.

Gene	Human	Pig	Ferret	Mouse
OAS3	X		X	X
Oas1b				X
Oas1c				X
Oas1d				X
Oas1e				X
Oas1f				X
Oas1g				X
Oas1h				X
Oasl2				X
IFIT5	X	X	X	
ITIF1B	X		X	X
Ifit1bl2				X
IFIT1L1		X		
Ifit3b				X
IFIT5L			X	
Ifitm6				X
Ifitm7				X
IFITM1L1		X		
IFITM1L2		X		
IFITM1L3		X		
IFITM2	X	X		X
NCR2	X	X	X	
NCR3	X	X	X	
HERC5	X	X	X	

Table 4. Overview of key features of the host intrinsic and innate antiviral response to IAV infection in humans, pigs, ferrets, and mice. Upwards arrows indicates up-regulation/high levels of this gene under the examined condition. A – indicates that the levels of this gene is unchanged in the examined condition. * Not including pseudogenes. ** Partial cds. Table 4 is a work in progress.

Feature	Human	Pig	Ferret	Mouse
IAV neutralizing effect of pulmonary SP-D	Yes (*in vitro*) (huH1N1, huH3N2) [143]	Yes (*in vitro*) (huH1N1, huH3N2, swH1N1, swH3N2, avH1N1, avH3N2) [64]	Present in airways, but antiviral effect not demonstrated (H3N2, H3N1) [67]	Yes (*in vitro, in vivo*) (H3N2) [144,145]
Type I interferon genes	*IFNA1, IFNB1*	*IFNA1, IFNB1*	*IFNA***	*Ifna1, Ifnb1*
Type I interferon expression		↑ swH1N2 [47], [Brogaard *et al.* 2017, manuscript under review]	- huH3N2, huH1N1/09 [146] ↑ huH5N1 [146]	↑ H1N1 (PR8) [147] ↑ H1N1 *Ifnb* [151]
Type II interferon gene	*IFNG*	*IFNG*	*IFNG*	*Ifng*
Type II interferon expression	↑H1N1 pdm09 [148]	↑ swH1N2 [47]	- huH3N2, huH1N1/09 [146] ↑ huH5N1 [146]	
Type III interferon genes	*IFNL1, IFNL2, IFNL3, IFNL4*	*IL29* (IFN-λ1), *IL28A* (IFN-λ2), *IL28B* (IFN-λ3)	*IFNL1, IFNL3*	*Ifnl2, Ifnl3*
Type III interferon expression		↑ swH1N2 [Brogaard *et al.* 2017, manuscript under review]		↑ H1N1 (PR8) (IFN-λ2/3, protein, BAL) [43]
Dominating lung chemokine expression	*CXCL10* H1N1(pdm09) [74]	*CXCL10* – swH1N2 [47], [Brogaard *et al.* 2017, manuscript under review]	*CXCL10* – huH1N1/09 [149][150], huH5N1 [151][146]	*Cxcl10* – H1N1 (PR8) [147]
TLR genes*	*TLR1-TLR10*	*TLR1-TLR10*	*TLR1-TLR8, TLR10*	*Tlr1-Tlr9, Tlr11-Tlr13*
Expression of antiviral TLRs	↑ A/H1N1pdm09 + A/H3N2 – monocytes and dendritic cells, *TLR8, TLR9* [152]	↑ swH1N2 – lung, *TLR3, TLR7* [47], [Brogaard *et al.* 2017, manuscript under review]; circulating leukocytes, *TLR3, TLR7* [92]		↑ A/H3N2- pulmonary epithelial cells, *TLR3* (C57Bl/6 mice) [153]
RLR genes	*DDX58* (RIG-I), *IFIH1* (MDA5), *DHX58* (LGP2)	*DDX58* (RIG-I), *IFIH1* (MDA5), *DHX58* (LGP2)	*DDX58* (RIG-I), *IFIH1* (MDA5), *DHX58* (LGP2)	*Ddx58* (RIG-I), *Ifih1* (MDA5), *Dhx58* (LGP2)
Known mature miRNA (miRBase v. 21) [103]	2,588	411	None	1,915

Paper 2

Late regulation of immune genes and microRNAs in circulating leukocytes in a pig model of influenza A (H1N2) infection

Research article

L Brogaard, PMH Heegaard, LE Larsen, S Mortensen, M Schlegel, R Dürrwald, K Skovgaard

Published in *Scientific Reports* (2016)
6:21812 doi:10.1038/srep21812

All raw data is freely available upon request
loun@vet.dtu.dk

SCIENTIFIC REPORTS

OPEN

Late regulation of immune genes and microRNAs in circulating leukocytes in a pig model of influenza A (H1N2) infection

Received: 17 September 2015
Accepted: 01 February 2016
Published: 19 February 2016

Louise Brogaard[1], Peter M. H. Heegaard[1], Lars E. Larsen[2], Shila Mortensen[1,*], Michael Schlegel[3], Ralf Dürrwald[3] & Kerstin Skovgaard[1]

MicroRNAs (miRNAs) are a class of short regulatory RNA molecules which are implicated in modulating gene expression. Levels of circulating, cell-associated miRNAs in response to influenza A virus (IAV) infection has received limited attention so far. To further understand the temporal dynamics and biological implications of miRNA regulation in circulating leukocytes, we collected blood samples before and after (1, 3, and 14 days) IAV challenge of pigs. Differential expression of miRNAs and innate immune factor mRNA transcripts was analysed using RT-qPCR. A total of 20 miRNAs were regulated after IAV challenge, with the highest number of regulated miRNAs seen on day 14 after infection at which time the infection was cleared. Targets of the regulated miRNAs included genes involved in apoptosis and cell cycle regulation. Significant regulation of both miRNAs and mRNA transcripts at 14 days after challenge points to a protracted effect of IAV infection, potentially affecting the host's ability to respond to secondary infections. In conclusion, experimental IAV infection of pigs demonstrated the dynamic nature of miRNA and mRNA regulation in circulating leukocytes during and after infection, and revealed the need for further investigation of the potential immunosuppressing effect of miRNA and innate immune signaling after IAV infection.

Influenza A virus (IAV) infections are widespread in the human population and have great impact on human health and welfare. Significant resources are linked to influenza epidemics due to excess hospitalizations and lost productivity in workplaces, as well as the need for the production of yearly updated vaccines to cover the currently circulating influenza virus strains[1]. Otherwise healthy subjects will recover within 1–2 weeks without treatment, but the infection may also lead to severe morbidity and mortality, especially in elderly and immune compromised individuals[2]. New strains of influenza virus with pandemic potential will continue to emerge due to mutation, genetic reassortment, and a complex animal reservoir.

MicroRNAs (miRNAs) are a class of short (~22 nt), endogenous regulatory RNAs that have been identified in a wide range of organisms, including animals, plants, viruses, and fungi[3]. They modulate gene expression by interfering with mRNA translation most commonly by destabilising mRNA thereby facilitating degradation. miRNA-mRNA target interactions are complex; one miRNA may target a large number of genes, and the targets of a miRNA may belong to a variety of functional groups[3]. In turn, the 3′-UTR of a single mRNA transcript may be the target for several different miRNAs, lending another layer of complexity as well as flexibility to the system. miRNA-mediated regulation of gene expression has been found to affect many cellular functions, including innate and antiviral responses, e.g. key innate immune pathogen recognition receptors (PRRs) such as Toll-like receptors (TLR) and RIG-I-like receptors (RLR) and their associated pathways[4]. Additionally, a number of miRNAs have been demonstrated to bind to influenza virus PB1 mRNA and inhibit viral replication *in vitro*[5]. Recently, locally expressed miRNAs in lung tissue have been found to be regulated in response to IAV infection in pigs, chickens, mice, and macaques[6–10], but until now only three studies have investigated the role of circulating miRNAs during

[1]Section for Immunology and Vaccinology, National Veterinary Institute, Technical University of Denmark, 1870 Frederiksberg C, Denmark. [2]Section for Virology, National Veterinary Institute, Technical University of Denmark, 1870 Frederiksberg C, Denmark. [3]IDT Biologika GmbH, Dessau-Rosslau, Germany. *Present address: Department for Microbiological Diagnostics and Virology, Statens Serum Institut SSI, 2300 Copenhagen S, Denmark. Correspondence and requests for materials should be addressed to L.B. (email: loun@vet.dtu.dk)

Symptom/characteristic	Human	Pig	Mouse	Reference
Fever	Present	Present	Absent	19,54
Nasal secretion	Present	Present	Absent	54
Coughing	Present	Present	Absent	19,21
Major sialic acid receptor of the upper respiratory tract	α2-6-linked	α2-6-linked	α2-3-linked	25,55,56
Possess tonsils	Yes	Yes	No	57
Nature of connective tissue	Extensive and interlobular	Extensive and interlobular	Little if any	26,27
Nature of pleurae	Thick	Thick	Thin	26
Early cytokine response to IAV infection		Very similar to humans	Somewhat similar to humans	6,20,23,24,28
Pulmonary intravascular macrophages	Induced phagocytic cells	Constitutive phagocytic cells	Induced phagocytic cells	58
Lymph node structure		Inverted	As humans	17
Interleukin 8	Present	Present	No direct homolog	59,60
Immunological reagents available	Many	Increasing	Many	30,31

Table 1. Major differences and similarities of human, pig, and mouse disease signs, physiology, anatomy and immunology with regards to influenza A virus infection.

IAV infection[11–13]. These studies investigated human patients and each study employed a different type of sample material, namely whole blood[11], peripheral blood mononuclear cells (PBMCs)[12], and serum[13] from human patients, respectively. It is however important to recognize that circulating miRNAs may originate from different sources; white blood cells, red blood cells, and platelets all contain miRNAs. But miRNAs are also found extracellularly in protein complexes (Argonaute, RNA-induced silencing complex (RISC)), extracellular vesicles (EVs), and associated with high-density lipoprotein[14,15]. The origin of cell-free circulating miRNAs is still unclear; they may be breakdown products originating from lysed cells, or they may be actively secreted from cells to act in a paracrine manner, or perhaps a combination of the two[14]. Regulation of cell-associated and cell-free miRNAs in circulation in response to IAV infection may thus have different causes and functions. In PBMCs of critically ill patients with H1N1 infection, expression of hsa-miR-29a, -31, and -148a were all determined individually to have diagnostic potential[12], whereas the serum levels of hsa-miR-17, -20a, -106a, and -376c in combination could discriminate between avian influenza infected patients and healthy controls[13]. The third study, employing whole blood, reported some overlap with findings from the PBMC and serum studies, namely hsa-miR-29a and hsa-miR-17 and -106a, respectively[11]. Current knowledge on miRNAs in circulation in response to IAV is thus based on few studies representing both cell-free and cell-associated miRNAs.

All three studies have identified miRNAs that are regulated during IAV infection in human patients. An inherent challenge in such observational studies, however is that the timing of the infection is unknown; the infection could be widely differently progressed in the patients included. In contrast, animal models allow for precise control of parameters such as time and dose. An ideal animal model for human influenza should reproduce the clinical signs and pathogenesis observed in human influenza disease, and the host response should mimic that observed in humans, including an efficient antiviral immune response. The general potential of the pig as a large animal model for human disease including influenza has been reviewed several times[16–18]. Specifically, fever, fatigue, lassitude, and cough, which were the best indicators of human influenza in several studies[19–21], are all induced in IAV infected pigs within the first three days of infection as shown by us and others[6,22–24]. Pigs are susceptible to infection with human influenza A viruses, and have been demonstrated to be involved in influenza evolution and ecology[18,25]. Pigs additionally share many similarities with humans with respect to tracheobronchial tree structure, influenza virus receptor distribution, lung physiology, and innate immune cell infiltration of the respiratory system[26–29]. The pig is thus an obvious large animal model for human respiratory infections. However, the use of the mouse as an animal model for human IAV infection has been instrumental in influenza research due to its low cost, broad range of available reagents, and the availability of genetically modified mice[30,31]. Although this classical model has provided important information about basic biology during viral infection, mice are not natural hosts for IAV and many important clinical signs characteristic of human influenza virus infection are absent in mice[31]. The ferret model has also contributed substantially to the understanding of e.g. IAV pathogenicity, and transmission as well as species and cell tropism, in large part thanks to the ferret being susceptible to human IAV strains[30]. However, little is known about ferret specific innate immune response to IAV infection[30,31]. Table 1 summarizes some of the most important similarities and differences between man, pig, and mouse with regards to their clinical and immunological responses to IAV infection.

Despite the great potential of the pig as a large animal model and the importance of pigs in evolution and transmission of IAV, the immune response of pigs against IAV is not fully understood. This study aimed at providing a better understanding of the involvement of circulating miRNAs and innate immune factors in porcine blood leukocytes during and after active IAV infection. We focused on the cell-associated miRNA and mRNA expression. Cells in the lungs produce chemokines in response to IAV infection which direct the recruitment of various immune cells from the blood stream into the infected lung tissue[6,32]. miRNA expression profiles of circulating leukocytes may thus be important for immune regulation in the lung during IAV-infection, or even during subsequent secondary infections. Our experimental setup allowed us to perform highly controlled experimental IAV infection of pigs, and to study development of disease signs, viral titre, and fluctuations in miRNA and mRNA

levels as the disease progressed in time based on a statistically useful number of pigs, generating important information relevant for human disease, which would be difficult to obtain from human patients.

Results

Infection model and clinical signs. Clinical signs and results from virus specific qPCR from lung samples and nasal swabs of infected animals have been reported previously[6]. This included abrupt onset of disease with dyspnoea, fatigue, nasal secretion and nasal viral excretion on day 1 pi. Fever >40 °C was seen for all but one pig (39.6 °C) on day 1 pi. Clinical signs peaked between day 1 and 2 pi. Between day 3 and 7 pi coughing occurred in individual pigs. The infection and disease were completely cleared at day 14. Lung virus titres peaked at day 1 pi; mean $\log_{10}$ EID_{50}/g lung tissue was 4.23 and 3.35 at day 1 and 3 pi, respectively. No virus could be detected in the lungs by day 14 pi.

Quantification of leukocyte miRNAs in circulation. An initial screening for changes in miRNA expression in leukocytes at 24 and 72 h pi compared to before challenge was performed using the miRCURY LNA Human Panel I (Exiqon) assaying 375 human miRNAs. Of these, approx. one third was quantifiable in porcine leukocytes; however, only five were significantly differentially expressed (one-way ANOVA): hsa-miR-223-5p ($p = 3.20E-07$), hsa-miR-23a-3p ($p = 0.0001$), hsa-miR-30c-5p ($p = 1.10E-07$), hsa-miR-150-5p ($p = 0.0002$), and hsa-miR-92b-3p ($p = 0.0005$).

Results from the miRCURY LNA screening revealed the need for a more tailored approach; relevant miRNAs were selected for expression analysis in a larger set of samples, using the high-throughput RT-qPCR platform BioMark (Fluidigm). This selection included several of the miRNAs assayed in the miRCURY LNA Human Panel I, including four of the five miRNAs that were significant on the miRCURY platform. Using Student's *t*-test or Mann-Whitney *U* test ($p < 0.05$) to determine statistical significance of biologically relevant alterations in expression level ($> \pm 1.5$ fold up- or down-regulation) showed that results obtained from the two qPCR platforms were in agreement (data not shown).

Using high-throughput RT-qPCR we found a total of 20 miRNAs to be differentially expressed in IAV challenged pigs at minimum one of the three post-challenge sampling points compared to before challenge as depicted in the heat map in Fig. 1a; the precise expression levels relative to before challenge can be found in Supplementary Table S3. Only four miRNAs (hsa-miR-223-5p, ssc-miR-31, ssc-miR-29a, and ssc-miR-182) were differentially expressed at 24 h pi, whereas 10 miRNAs were differentially expressed at 72 h pi (ssc-miR-29b, hsa-miR-203a-3p, hsa-miR-449a, ssc-miR-21, ssc-miR-29a, hsa-miR-23a-3p, ssc-miR-23b, ssc-miR-30c-5p, ssc-miR-423-5p, and hsa-miR-150-5p). However, the highest number of significantly regulated miRNAs compared to before challenge was found at 14d pi, at which time point the infection had completely cleared (ssc-miR-15a, ssc-miR-29b, ssc-miR-29a, hsa-miR-449a, ssc-miR-186, ssc-miR-22-5p, ssc-miR-28-5p, hsa-miR-203a-3p, ssc-miR-146a-5p, hsa-miR-150-5p, ssc-miR-23b, hsa-miR-223-3p, hsa-miR-23a-3p, hsa-miR-16-5p). In all three post-challenge groups, at least three miRNAs were found to be unique for that particular time point, and only ssc-miR-29a was found to be differentially expressed at all three examined time points. Overlaps and differences in miRNA regulation at the three time points are summarised in Fig. 1b.

Leukocyte immune gene expression. In contrast to miRNA regulation, the major changes in immune gene expression were seen at 24 h pi. Levels of expression of interferon and interferon-induced genes, pattern recognition receptors (PRRs), chemokines, and pro- and anti-inflammatory cytokines before and after infection are listed in Table 2. We were able to verify expression of genes found to be regulated in human IAV infection such as *CCL2*, *CXCL10* (IP-10), *MX1*, *OASL*, *STAT1*, *IFIH1* (MDA5), and *DDX58* (RIG-I) in our porcine model. These genes have been previously reported to be of considerable diagnostic value in human influenza studies[33–36]. Remarkably, all of these genes but *CCL2* were among the most highly expressed immune factors in the present study at 24 h pi (Table 2). Several RNA virus associated PRRs, including *DDX58*, *IFIH1*, *TLR7*, and *TLR8*, were regulated according to infection status, being up-regulated at 24 h pi, and showing little or negligible change in expression during the rest of the study. Surprisingly, we found the PRR *TLR4*, recognising bacterial LPS, to be the most highly up-regulated TLR at 24 h pi. The up-regulation of *IDO1* (more than 100 fold after 24 h) was also highly significant and in agreement with the overall pattern of increased expression of pro-inflammatory genes, characterised by a fast and transient up-regulation peaking at 24 h pi (Table 2). Importantly, at day 14 pi all significant differentially expressed immune genes were down-regulated; these late down-regulated genes included *CCL3*, *CXCL2*, *IL1RAP*, *IL18*, *PTSG2*, *TNF*, *IDO1*, *TLR3*, and *TLR4*. The most significant down-regulation was seen for *IL18* at 24 h pi. This was also the only gene that was significantly down-regulated at all three time points.

Identification of targets of regulated leukocyte miRNA. KEGG pathway enrichment analysis of the validated gene targets of the 20 differentially expressed miRNAs revealed a big overlap in pathways enriched in the four subsets of target genes. Significantly enriched "p53 signaling", "Cell cycle", "Apoptosis", as well as pathways related to immune response and leukocyte extravasation, e.g. "Cytokine-cytokine receptor signaling", "Chemokine signaling", "Jak-STAT signaling", "Focal adhesion", "Adherens junction", and "Tight junction". In addition, several cancer related pathways were identified as significantly enriched as well, possibly due to many of the gene targets being involved in apoptotic and anti-apoptotic processes, as will be discussed later. A list of significantly enriched pathways can be found in Supplementary Table S4.

Differentially expressed miRNAs (human homologs) and experimentally validated MTIs (obtained from miRTarBase) were submitted to Cytoscape, creating interaction networks for all three post-infection time points. Of the 20 examined miRNAs, only two (hsa-miR-223-5p and hsa-miR-22-5p) did not have any MTIs registered in miRTarBase. At all three time point, we found a large number of genes to be targeted by only one of the regulated miRNAs (see Supplementary Fig. S1), but also genes targeted by two or more miRNAs were present in the

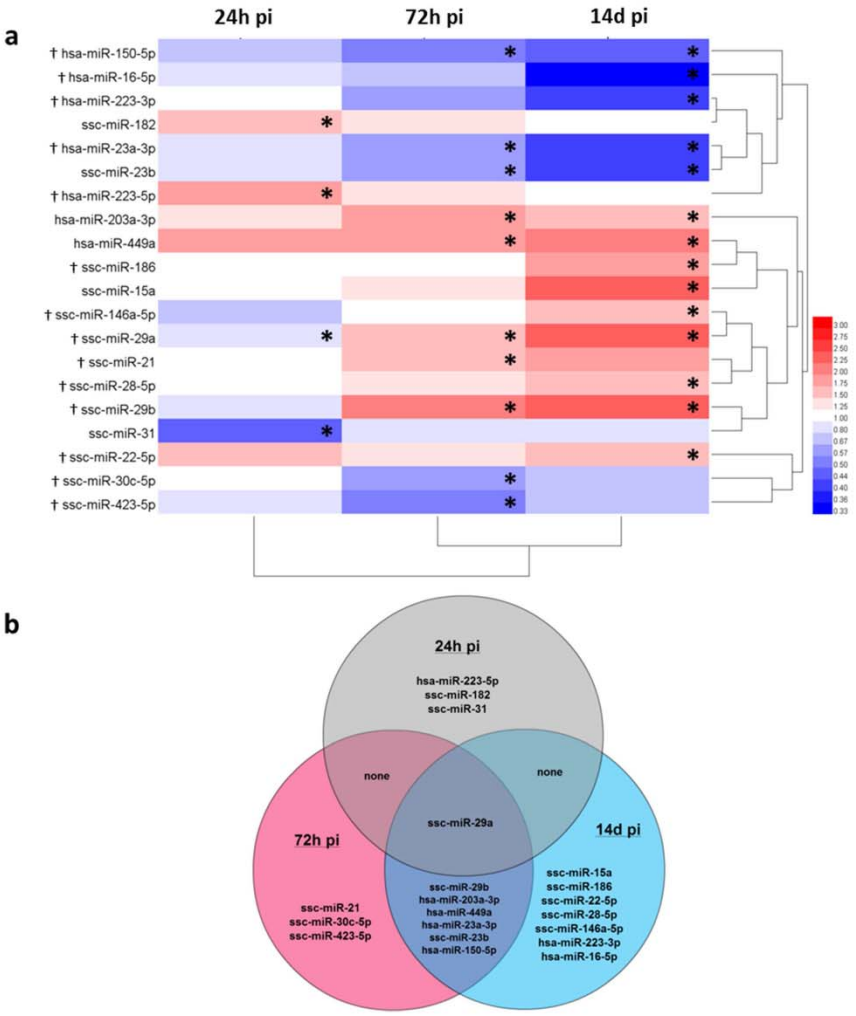

Figure 1. Expression of miRNA in porcine leukocytes after IAV challenge. (**a**) clustered heat map depicting up- and down-regulation (red and blue, respectively) at 24 h, 72 h, and 14d pi compared to before challenge. *Indicates statistical significance at that time point. †Indicates that the miRNA have previously been reported to be regulated in circulation in human patients after IAV infection[11–13]. Human (hsa-) miRNAs: hsa-miR-223-3p, hsa-miR-223-5p, hsa-miR-203a-3p, and hsa-miR-449a are not yet annotated in the porcine genome. hsa-miR-150-5p, hsa-miR-16-5p, and hsa-miR-23a-3p were not annotated in the pig genome at the time the assay was designed, but sequences have since become available and found to be 100% identical to the human homologs that were used for primer design. (**b**) Venn diagram showing at which post challenge time points miRNAs were regulated compared to before challenge.

interaction networks at all three time points. The number of genes with two or more experimentally validated MTIs comprised 6, 65, and 84 at 24 h, 72 h, and 14d pi, respectively (see Supplementary Fig. S1).

miRNA target gene expression. Following MTI analysis, a subset of genes found to be targets for regulated miRNAs were subjected to transcriptional analysis. A complete list of genes can be found in Supplementary Table S1. The following genes were found to be significantly (however less than 2-fold) up- or down-regulated compared to before challenge: at 24 h pi – *BCL2*, *MCL1*, and *SP1* (up-regulated), *IFNG, PTEN* and *CXCR4* (down-regulated); at 72 h pi – *VEGFA* (up-regulated), *CCNE2* (down-regulated); at 14d pi – *VEGFA* (up-regulated); *CCNE2* and *PTEN* (down-regulated). Additionally, the following genes showed no significant differential expression: *CDK2, CDK4, FOXO3A, TP53, CASP9, CHUK,* and *AKT2.*

Gene	Before challenge (n = 12)		24 h pi (n = 12)			72 h pi (n = 9)			14d pi (n = 6)		
	Rel. expr. level	±95% CI	Rel. expr. level	±95% CI	*p*-value	Rel. expr. level	±95% CI	*p*-value	Rel. expr. level	±95% CI	*p*-value
CASP1	1.00	0.13	7.21	1.78	4E-12	2.18	0.58	0.00022	0.94	0.36	NS
CASP3	1.00	0.09	5.91	1.07	3E-13	1.36	0.35	NS	1.13	0.30	NS
*CCL2**	1.00	0.41	2.34	0.50	0.0012	1.63	0.56	NS	1.53	0.70	NS
CCL3	1.00	0.24	0.59	0.22	0.030	1.07	0.70	NS	0.52	0.17	0.0067
CD163	1.00	0.47	3.58	1.50	0.00015	2.73	2.09	NS	0.48	0.18	0.047
CXCL2	1.00	0.35	0.96	0.18	NS	0.99	0.78	NS	0.39	0.16	0.019
*CXCL10**	1.00	0.33	283	92.56	7E-16	5.84	4.39	0.011	3.43	5.81	NS
*DDX58**	1.00	0.23	13.01	2.01	6E-13	1.53	0.66	NS	0.64	0.42	NS
FAS	1.00	0.11	5.52	1.02	4E-12	0.94	0.24	NS	0.73	0.19	0.018
FASLG	1.00	0.39	2.42	0.62	0.026	1.06	0.57	NS	0.65	0.23	NS
IDO1	1.00	0.30	133	98.20	8E-09	0.71	0.28	NS	0.55	0.27	0.035
IFITM1	1.00	0.27	5.66	0.98	2E-10	1.62	0.49	0.040	0.81	0.24	NS
IFITM3	1.00	0.40	3.93	0.69	7E-8	1.56	0.54	NS	0.78	0.27	NS
IFNA1	1.00	0.26	2.86	1.32	0.0022	0.72	0.23	NS	1.31	0.59	NS
IL8	1.00	0.32	1.86	0.60	0.018	1.37	0.44	NS	1.17	0.20	NS
IL10	1.00	0.39	4.49	1.04	2E-06	1.55	0.40	NS	0.93	0.23	NS
IL18	1.00	0.28	0.09	0.04	3E-08	0.60	0.52	0.020	0.50	0.28	0.028
IL1RAP	1.00	0.34	9.24	2.32	8E-09	0.70	0.32	NS	0.41	0.22	0.014
IL1RN	1.00	0.27	18.14	3.56	3E-14	1.10	0.29	NS	0.97	0.23	NS
IRF1	1.00	0.19	1.80	0.31	0.00030	0.57	0.13	0.0015	0.75	0.26	NS
IRF2	1.00	0.16	4.66	0.81	2E-10	1.09	0.25	NS	0.78	0.19	NS
IRF3	1.00	0.21	2.45	0.48	3E-06	0.99	0.18	NS	0.66	0.15	0.033
IRF9	1.00	0.25	1.88	0.25	0.00011	0.95	0.17	NS	0.72	0.22	NS
*IFIH1**	1.00	0.20	5.37	0.73	3E-11	1.15	0.22	NS	0.80	0.30	NS
JAK2	1.00	0.17	3.79	0.88	2E-8	1.35	0.30	NS	1.10	0.36	NS
MCL1	1.00	0.20	2.06	0.26	4E-06	0.90	0.17	NS	0.82	0.13	NS
*MX1**	1.00	0.23	13.72	2.09	1E-13	2.10	0.70	0.0018	0.87	0.65	NS
MYD88	1.00	0.28	1.58	0.39	0.031	0.90	0.44	NS	0.61	0.23	NS
NOD1	1.00	0.23	2.55	0.36	7E-5	1.08	0.25	NS	0.74	0.09	NS
*OASL**	1.00	0.26	20.40	4.14	7E-12	2.11	1.06	NS	1.20	1.10	NS
PTGS2	1.00	0.26	1.33	0.28	NS	0.87	0.23	NS	0.39	0.12	0.0012
*STAT1**	1.00	0.09	4.13	0.46	8E-14	1.11	0.25	NS	0.88	0.25	NS
TICAM1	1.00	0.25	2.47	0.66	0.00016	1.47	0.43	NS	1.08	0.29	NS
TICAM2	1.00	0.19	3.30	0.69	2E-08	0.84	0.14	NS	0.58	0.11	0.0017
TLR2	1.00	0.34	2.30	0.45	0.00035	1.12	0.52	NS	0.81	0.32	NS
TLR3	1.00	0.23	2.42	0.48	4E-05	1.40	0.35	NS	0.51	0.12	0.0078
TLR4	1.00	0.26	8.41	2.90	8E-09	1.32	0.64	NS	0.56	0.26	0.023
TLR7	1.00	0.14	4.23	0.51	4E-12	1.34	0.34	NS	1.09	0.34	NS
TLR8	1.00	0.22	2.17	0.59	0.00014	1.77	0.34	0.00065	1.11	0.22	NS
TNF	1.00	0.21	0.55	0.15	0.0027	0.79	0.42	NS	0.35	0.11	0.00024

Table 2. Relative expression levels of immune gene mRNA transcripts in porcine leukocytes before IAV challenge and at 24 h, 72 h, and 14d pi. Genes included are all statistically significantly > 2-fold up- or down-regulated at at least one time point after challenge ($p < 0.05$); NS: not significant. Genes marked with * have previously been reported as classifiers for human IAV infection (H1N1, H3N2)[33–37].

Discussion

Similarities and differences between human, pig, and mouse with regard to influenza and factors of importance for development of influenza are highlighted in Table 1. It is evident based on both physiological and immunological considerations, that the porcine model has the potential to provide valuable information in the study of IAV infection[18,28]. We did indeed observe clinical signs in the animals post challenge highly similar to those observed during human IAV infection[6]. We were able to reproduce key findings of human coding and non-coding transcriptional responses to IAV infection, consolidating the pig as a relevant large animal model for the study of IAV infection in controlled settings.

Early cytokine responses to IAV infection have been found to be remarkably similar between humans and pigs[6,20,23,24]. In the present study we found blood-based gene expression profiles of both coding and non-coding

RNA to be tightly regulated in accordance with progression of infection and disease in pigs experimentally infected with the H1N2 influenza virus. Expression of several protein coding genes in whole-blood RNA from human patients or volunteers have been found to be good predictors for IAV infection[33–37]. These genes include *CXCL10* (IP-10), *MX1*, *OASL*, *STAT1*, *IFIH1* (MDA5), and *DDX58* (RIG-I), and *CCL2*, which we also found to be highly expressed shortly after experimental IAV infection in pigs. Likewise, the expression of porcine interferon (*IFNA1* and *IFNG*) and interferon-related genes after viral infection were highly similar to those seen in human influenza cases[35–37].

We and others have reported locally produced miRNAs in lung tissue to be differentially expressed in response to IAV infection in a number of different animal models[6–10]. However, expression signatures of miRNAs in circulation after IAV infection have only been reported in a few studies[11–13]. These studies have employed whole blood, PBMCs, or serum supplied by hospitalised patients and healthy volunteers and the results therefore represent the circulating miRNA response to IAV infection collected from individuals that may have had widely differently progressed disease, and from blood fractions that may carry very different miRNA profiles even before IAV infection. However, 13 of the 20 differentially expressed miRNAs identified in the present study have been reported in the abovementioned human studies as relevant for distinguishing between healthy controls and IAV infected patients[11,12] (Fig. 1a). Almost complete sequence conservation is seen between human and porcine homologs of these miRNA, also within the important seed sequences (Supplementary Table S2). It is therefore reasonable to expect these conserved miRNAs to have the same biological function in response to IAV infection in pigs and humans.

Our experimental setup proved useful for demonstration of the temporal dynamics of miRNA expression after IAV challenge, from the first days of infection to after the IAV infection had cleared. In contrast to the human studies, the pig model allowed us to demonstrate that there is indeed a time factor to consider when assessing the regulation and involvement of cell-associated circulating miRNAs in response to IAV infection. This is made evident by our observations of e.g. ssc-miR-29a expression; this miRNA is initially down-regulated (24 h pi) but later up-regulated (72 h and 14d pi) (Fig. 1a), whereas human studies have reported only down-regulation of its homolog hsa-miR-29a-3p[11–13]. Another miRNA identified in human studies as regulated after H1N1 infection is hsa-miR-150-5p which was reported by one study to be up-regulated[11] while it was found to be down-regulated in another study[12]. We found that hsa-miR-150-5p was down-regulated in porcine leukocytes 72 h and 14d after H1N2 challenge in pigs (Fig. 1a). Many factors other than host species may contribute to these differences, e.g. the lack of control of the infection progression in human patient studies, patient heterogeneity, difference in IAV subtypes, and the application of different blood components in the analyses. Still, time course studies of miRNA expression in controlled experimental settings using standardised sampling methods are able to provide important data when studying the role of miRNAs in circulation in response to infection and in the search for valid biomarkers.

Genes for several well-known PRRs and pro-inflammatory factors were significantly down-regulated at day 14 pi, after the viral infection had cleared (Table 2). These data suggest a persisting lowered immune responsiveness in the animal. Critical illness and severe sepsis have previously been shown to leave patients in a protracted immunosuppressed stage after the illness has passed[38], but here we show that even a mild course of influenza disease may transcriptionally affect the immune competence of the recovered animal. Likewise, expression of miRNA at day 14 pi with the potential to subtly affect and regulate important apoptosis and cell survival related processes may have an essential function in the case of secondary infections following IAV infection. Upon secondary infection, circulating leukocytes will be recruited to the site of infection, and their built-in arsenal of apoptosis-regulating miRNAs could thus greatly influence disease progression.

Studies of secondary bacterial infections in mice after IAV infection have demonstrated a desensitisation to TLR ligands even several months after the IAV had cleared[39]. This appears to be a strategy for avoiding excessive inflammation, but the consequence of this lowered responsiveness may also be increased susceptibility to secondary infections. Here we show that ssc-miR-146a-5p is significantly up-regulated in circulating leukocytes only at 14d pi; the human homolog of this miRNA has been found to target important components of TLR signaling, such as *TLR2*, *TLR4*, *NFKB1*, *IRAK1*, *TRAF6*, and *IL8*. hsa-miR-203a-3p, which targets *MYD88*, is also up-regulated at 14d pi. These miRNAs might contribute to the reported lack of responsiveness to bacterial TLR ligands, by inhibiting translation or increasing degradation of mRNA transcripts of key components in the TLR signaling pathway. Strikingly, we did observe that *TLR4* and *TNF* (targets of and miR-146a-5p and miR-203a-3p, respectively) were significantly down-regulated in leukocytes at 14d pi. It is also worth noting, that in contrast to most other pathways found to be enriched in our analysis of miRNA target genes, the Toll-like receptor signaling pathway was only enriched in gene targets of up-regulated miRNAs, suggesting that TLR-mediated signaling may mostly be suppressed. The long-term effect of IAV-infection on the miRNA expression profile of circulating leukocytes thus potentially affects the individual's ability to combat secondary infections. This calls for future studies and focused investigation to elucidate if the miRNAs of circulating white blood cells truly affects the immune response to secondary infections, and offers a potential therapeutic target to avoid excess morbidity and mortality in vulnerable populations.

Both host and viral factors may contribute to the late regulation of miRNAs in circulating leukocytes at 14d pi. IAV is known to produce defective interfering (DI) virus particles during infection, i.e. virus particles that are unable to complete a full replication cycle but may be able to replicate in the host cell with the aid of a replication competent helper virus. DI particles have been demonstrated to persist in the lungs of SCID mice up to 16 days after challenge[40]. The persistence of such DI particles may explain the late regulation of miRNAs in the circulating leukocytes. Indeed, defective viral genomes (DVG) segments arising from especially the PA and PB1 gene segments have been shown to be recognised by RIG-I and may thus function as PAMPs, inducing a cytokine response (IFN-β, IL-6) through RIG-I also after the productive virus infection has vanished[41,42]. Although we did not observe significantly increased levels of *IFNB1* or *IL6* mRNA in the lungs of our animals at 14d pi (Skovgaard

et al. 2013), and we have found miRNAs in the lung tissue to primarily be regulated on days 1 and 3 (Brogaard *et al.*, manuscript in preparation) in contrast to on day 14 in leukocytes, we cannot rule out that DI particles have persisted in a small number of cells, influencing the lung environment and as a consequence affecting the miRNA response in circulation.

Numerous pathways are activated in the cell upon IAV infection, including the Toll-like receptor, RIG-I-like receptor, NFκB, and PI3K/AKT signaling pathways[43], many of which are important in the induction and control of apoptosis. IAV infection induces apoptosis in host cells *in vivo* and *in vitro* and different viral proteins have been found to manipulate apoptotic signaling, including the non-structural proteins NS1 and PB1-F2[44,45] and the nucleoprotein NP[46]. Several studies have shown that IAV has evolved strategies to benefit from host apoptosis, which might otherwise be considered a host defence mechanism to limit virus replication and spread. Our pathway enrichment analysis revealed that many of the same pathways may be affected in circulating leukocytes both during and after IAV infection, including pathways related to apoptosis and cell cycle regulation. These pathways were enriched in gene target subsets of both up- and down-regulated miRNA, demonstrating that miRNA regulation of these pathways is complex and allows for both down-regulation as well as expression or even up-regulation of their target genes/pathways. Consequently, only small or even non-significant changes were observed in the expression of the genes selected as highly targeted by differentially expressed miRNAs, suggesting a role for miRNAs in fine-tuning gene expression rather than causing dramatic changes.

MTI analysis of miRNAs found to be significantly regulated in porcine leukocytes revealed that several of the most highly targeted genes are relevant for apoptosis and cell survival, including *BCL2*, *MCL1*, *PTEN*, *AKT2*, *BRCA1*, and *TP53*. This suggests that miRNA play a role in regulating apoptotic pathways after IAV infection, e.g. by targeting components of some of the same pathways that are directly affected by viral protein interaction. Consistent with this emphasis on apoptosis was the fact that we found caspase-1 and caspase-3 transcription to be up-regulated within the first 72 hours of infection. The pro-apoptotic transcription factor p53 (*TP53*) has previously been implicated in IAV-induced apoptosis, mediated by direct interaction with viral NP[46]. In accordance with the importance of this transcription factor, we found miRNAs targeting *TP53* to be significantly regulated in circulating leukocytes. Other genes that were highly targeted by differentially expressed miRNAs include *PTEN* and *BCL2*, central players in cell survival and apoptosis[44,47,48]. *BCL2* was heavily targeted by up-regulated miRNAs, whereas *PTEN* targeting was balanced between up- and down-regulated miRNAs. ssc-miR-29a was the only miRNA to be regulated at all three time points. The miR-29 family is well characterised and commonly described to be involved in cancers as tumor suppressors[49]. Among the targets for hsa-miR-29a-3p is *PTEN*, which was significantly down-regulated at both 24 h and 14 d pi. This is consistent with up-regulation of ssc-miR-29a at 14 d pi, whereas up-regulation of ssc-miR-182 – another *PTEN*-targeting miRNA – may be a contributing factor to *PTEN* down-regulation at 24 h pi given that ssc-miR-29a is itself down-regulated at this time point.

In a previous study inhibition of miR-29a(-3p) in human hepatoma cell lines was shown to lead to up-regulation of *PTEN* at mRNA and protein levels, whereas overexpression of miR-29a down-regulated *PTEN* mRNA and protein[50]. Moreover, miR-29a inhibition negatively regulated phosphorylation of Akt (Protein Kinase B), which is an important step in the PI3K/AKT signaling pathway[50].

Akt family member *AKT2* as well as *FOXO3A*, a pro-apoptotic transcription factor (FoxO) downstream of PTEN and Akt, are also among the targets for hsa-miR-29a-3p. Despite being heavily targeted by up-regulated miRNAs at both 72 h and 14 d pi (Supplementary Fig. S1), we saw no regulation of these two genes. It is however possible that Akt and FoxO protein functions are still affected by ssc-miR-29a regulation, given the effect that down-regulation of *PTEN* is likely to have on PTEN protein levels. Additionally, we observed up-regulation of hsa-miR-29a-3p targets *BCL2* and *MCL1* at 24 h pi, where ssc-miR-29a was down-regulated. Collectively, our results highlight the importance of ssc-miR-29a in relation also to influenza, especially after infection, where it is involved in regulation of apoptosis, as has been described previously primarily in cancers[49].

In a previous study, we investigated mRNA expression in the lung tissue of the same animals as employed in the present study[6], and could demonstrate that the chemokine transcripts *CCL2*, *CCL3*, and *CXCL10* were highly up-regulated at 24 h and 72 h pi. This is in accordance with an expected need for recruitment of various immune cells to the affected lung tissue, in order to combat and contain the IAV infection. Here we show that the leukocytes available for extravasation display a miRNA expression profile specialised towards contributing to the control of cell survival and apoptosis in response to IAV infection.

Materials and Methods

Experimental design. This study employed blood samples from a previously described experimental challenge study[6]. All procedures and animal care activities were conducted in accordance with the guidelines and under approval of Good Clinical Practice (VICH GL9, CVMP/VICH/595/98), the Directive 2001/82/EC on the Community code relating to veterinary medicinal products and German Animal Protection Law. The protocol IDT A 03/2004 was approved by the Landesverwaltungsamt Sachsen-Anhalt, Germany (Reference Number: AZ 42502-3-401 IDT). All pigs (cross-bred Large White x German Landrace) were found seronegative for the following influenza virus strains by hemagglutination inhibition assay: A/sw/Haselünne/IDT2617/03 (H1N1), A/sw/Bakum/1832/00 (H1N2), A/sw/Bakum/IDT1769/03 (H3N2), A/sw/Denmark/13850/03 (H1N1), A/sw/Denmark/12687/03 (H1N2). A/sw/Denmark/12687/03 (H1N2) was used as challenge strain; this virus has a European avian-like H1, and a European swine-like N2[29]. This reassortant has been circulating in the Danish pig population since 2003, and has also been found in Germany, Poland, and Italy[25]. Briefly, a group of 12-week-old pigs were challenged by aerosol exposure to 6.0 l nebulised culture supernatant containing $10^{4.55}$ $TCID_{50}$/ml of the challenge strain. Blood samples were collected 2–4 hours (h) before challenge (n = 12), and at three time points after challenge: 24 h post infection (pi) (n = 12), 72 h pi (n = 9), and 14 days (d) pi (n = 6). Blood samples were stabilised by heparin (HEP tubes, Terumo). Lung material was collected for virus titration at 24 h (n = 3), 72 h (n = 3), and 14 d pi (n = 6) and stored in RNA*later* (Qiagen) at −20 °C.

Clinical signs and virus detection. Clinical signs and rectal temperature were recorded morning and afternoon until 72 h pi. A composite dyspnoea score was determined based on the following clinical signs as described previously[6]: 0 = breathing unaffected; 1 = increased respiratory frequency and moderate flank movement; 2 = marked pumping breathing and severe flank movement; 3 = laboured breathing affecting the entire body, pronounced flank movement and substantial movements of the snout, 4 = severe breathing reflecting substantial lack of oxygen. Virus content of the lungs was quantified by titration in embryonated hens' eggs on day one, three, and 14 after challenge as described previously[51]. The individual titers expressed in EID_{50}/g lung tissue were determined in samples of pools from all lung lobes.

RNA extraction. Heparin stabilised whole blood samples were depleted of red blood cells using QIAamp hypotonic EL buffer (Qiagen), followed by centrifugation at 400 × g at 4 °C for 10 min. Pellets containing leukocytes were resuspended in 600 µl RLT buffer (Qiagen) and stored at −80 °C, stabilising the RNA until extraction. For extraction, 300 µl leukocyte suspension was mixed with 1 ml Trizol (Invitrogen) and incubated for 5 min at room temperature. RNA extraction was performed according to the manufacturer's instructions (Invitrogen). Purity of extracted total RNA was assessed using UV absorption measured on a NanoDrop ND-1000 spectrophotometer (Saveen and Werner AB); average $A_{260/280}$ and $A_{260/230}$ ratios were 1.87 and 1.70, respectively. Total RNA was quantified by measuring the sample absorption at 260 nm; average RNA yield was 272 ng/µl. RNA integrity was measured on an Agilent 2100 Bioanalyzer (Agilent Technologies) using the RNA 6000 Nano Kit (Agilent), yielding an average RNA integrity number (RIN) of 8.9.

miRCURY LNA Universal RT microRNA PCR. Initial screening for differentially expressed miRNAs during the course of infection was performed on a subset of the samples from the experimentally challenged pigs: before challenge: n = 10; 24 h pi: n = 10; 72 h pi: n = 6. Screening was carried out using the Human Panel I, miRCURY LNA™ (Exiqon). 20 ng total RNA was reverse transcribed in 20 µl reactions using the miRCURY LNA™ Universal RT microRNA PCR, polyadenylation, and cDNA synthesis kit (Exiqon). Negative controls (minus RT) where the reverse transcriptase was replaced with water were included to check for contaminating genomic DNA. Diluted (1:100) cDNA was assayed in 10 µl PCR reactions according to the protocol for miRCURY LNA™ Universal RT microRNA PCR (Exiqon). Each miRNA was assayed once by qPCR in the Human Panel I containing 375 miRNA assays including a non-template control (NTC). Amplification was performed in a LightCycler® 480 Real-Time PCR System (Roche) in 384 well plates. LightCycler® 480 software was used to determine the quantification cycle (C_q) values and inspect amplification and melting curves. Data was normalised to the mean expression value of all miRNAs expressed in the individual sample.

cDNA synthesis, pre-amplification, and qPCR of miRNA. Reverse transcription of 100 ng total RNA was performed as described previously[52]. Briefly, reaction volumes of 10 µl containing 1 µM universal RT primer (5′caggtccagttttttttttttttvn3′), 100 ng total RNA, 1 µl of 10X poly(A) polymerase buffer (New England BioLabs), 0.1 mM of ATP (New England BioLabs), 0.1 µM of each deoxynucleotide (dATP, dCTP, dGTP, and dTTP) (Sigma-Aldrich), 100 units of MuLV reverse transcriptase (replaced with water for the minus RT control) (New England BioLabs), 1 unit of poly(A) polymerase (New England Biolabs, USA), and RNase-free water were prepared. cDNA was synthesised at 42 °C for 1 hour followed by enzyme inactivation at 95 °C for 5 min. Two replicates of cDNA synthesis were performed per RNA sample (technical replicates). All primers used in this study, including the universal RT primer, were designed using the specifications described previously[52] and purchased from Sigma-Aldrich. Relevant miRNAs were defined based on the miRCURY LNA™ panel screening, published findings, and database searches (miRTarBase v. 4.5 and TarBase v. 6.0) for miRNAs experimentally confirmed to target antiviral immune mediators previously found to be regulated during influenza infection. Whenever an annotated porcine miRNA ("ssc-miR-") sequence was available in miRBase, this was used for primer design. If no porcine sequence was available, the corresponding human sequence homolog ("hsa-miR-") was used. Primer sequences are shown in Supplementary Table S1. Pre-amplification was performed using TaqMan PreAmp Master Mix (Applied Biosystems). 200 nM pooled qPCR primer mix was prepared by combining each miRNA primer pair used in the qPCR setup. 5 µl TaqMan PreAmp Master Mix, 2.5 µl 200 nM pooled primer mix, and 2.5 µl cDNA was incubated at 95 °C for 10 min followed by 18 cycles of 95 °C for 15 s and 60 °C for 4 min. Residual primers were digested by adding 16 U of Exonuclease I (New England BioLabs), and incubated at 37 °C for 30 min followed by 80 °C for 15 min. qPCR was performed in Dynamic Array Integrated Fluidic Circuit chips (Fluidigm) in the BioMark HD real-time PCR instrument (Fluidigm). Pre-sample mix was prepared using the following components per sample: 3 µl ABI TaqMan Gene Expression Master Mix (Applied Biosystems), 0.3 µl 20X DNA Binding Dye Sample Loading Reagent (Fluidigm), 0.3 µl 20X EvaGreen (Biotium, VWR – Bie & Berntsen), and 0.9 µl low EDTA TE Buffer (VWR – Bie & Berntsen). Pre-sample mix (4.5 µl) was mixed with 1.5 µl pre-amplified cDNA diluted 1:10 in low-EDTA TE-buffer (VWR – Bie & Berntsen), including a non-template control (cDNA replaced with water). Primer mix was prepared for each assay by mixing 3 µl primer pair (forward and reverse, each 10 µM) with 3 µl 2X Assay Loading Reagent (Fluidigm). The following cycling parameters were used: 2 min at 50 °C, 10 min at 95 °C, followed by 35 cycles with denaturing for 15 s at 95 °C and annealing/elongation for 1 min at 60 °C. Melting curves were generated after each run (from 60 °C to 95 °C, increasing 1°C/3 s).

Primer efficiencies were calculated for each assay based on three independent 5-fold dilution series made from a pool of all pre-amplified cDNA samples. C_q values were acquired using the Fluidigm Real-Time PCR Analysis software 3.0.2 (Fluidigm) and exported to GenEx5 (MultiD) for data processing including interplate calibration, correction for PCR efficiency, normalisation to mean expression of all miRNAs included in this study, and averaging of cDNA technical repeats.

cDNA synthesis, pre-amplification, and qPCR of mRNA. Extracted total RNA was converted into cDNA by reverse transcription of 50 ng RNA using the QuantiTect Reverse Transcription Kit (Qiagen) as described previously[6], including minus RT controls. cDNA was diluted 1:3 in low-EDTA TE-buffer (VWR – Bie & Berntsen) prior to 15 cycles of pre-amplification followed by exonuclease treatment as described previously[6]. Pre-amplified cDNA was diluted 1:10 in low-EDTA TE-buffer (VWR – Bie & Berntsen) for use in qPCR. A panel of immune genes were chosen for transcriptional analysis based on published findings. Subsequently, based on target identification of the miRNAs found to be significantly regulated, additional transcriptional analysis was performed for the identified genes. qPCR primers were designed using Primer3 (http://bioinfo.ut.ee/primer3-0.4.0/) as described previously[53], and purchased from Sigma-Aldrich. Primer sequences and PCR efficiencies are shown in Supplementary Table S1.

qPCR was carried out in Dynamic Array Integrated Fluidic Circuit chips on the BioMark HD real-time PCR platform (Fluidigm) as described previously[6]. C_q values were acquired using the Fluidigm Real-Time PCR Analysis software 3.0.2 (Fluidigm) and exported to GenEx5 (MultiD) for data processing, including interplate correction, correction for PCR efficiency, normalisation to reference genes, and averaging of cDNA technical repeats. Using geNorm and NormFinder algorithms (in GenEx), peptidylprolyl isomerase A (*PPIA*), hypoxanthine phosphoribosyltransferase I (*HRPT1*), ribosomal protein L13a (*RPL13A*), TATA-box binding protein (*TBP*), and tyrosine 3-monooxygenase/tryptophan 5-monooxygenase activation protein, zeta polypeptide (*YWHAE*) where identified as the most stably expressed reference genes out of six candidates and used for mRNA data normalisation.

Analysis for differential gene expression. For the initial screening study, normalised miRCURY LNA™ data was $\log_2$ transformed before one-way ANOVA and Sidak correction ($p < 0.0007$) was employed to correct for multiple testing.

Normalised miRNA and mRNA qPCR expression data from Dynamic Array chips (Fluidigm) was $\log_2$ transformed and tested for normal distribution prior to Student's *t*-test (or Mann-Whitney *U* test if normality of data could not be demonstrated). miRNA and mRNA expression in sample groups (group means) from time points after challenge (24 h, 72 h, and 14d pi) was compared to expression in samples from before challenge (group mean); fold changes of expression was determined by dividing the mean expression level of a post-challenge group with the mean expression of the pre-challenge group. A change in expression level was considered statistically and biologically significant if $p < 0.05$ and the relative gene expression difference was >1.5-fold (up or down) (miRNA) or >2-fold (up- or down) (mRNA) between the groups compared.

A clustered heatmap was constructed to visualise miRNA gene expression, using the HemI 1.0.2 Heatmap Illustrator Toolkit employing hierarchical clustering.

miRNA target identification. Information on experimentally validated miRNA-target (i.e. mRNA) interactions (MTIs) was available from miRTarBase v. 6.0. An initial overview of potentially affected cellular pathways was gained from performing KEGG pathway enrichment analysis by submitting the list of target genes obtained from miRTarBase to DAVID Bioinformatics Resources v. 6.7 tool. The Benjamini-Hochberg procedure was applied to control the false discovery rate ($p < 0.05$). Pathway enrichment analysis was performed on four subsets of target genes: target genes for 1) miRNAs up-regulated at 24 h and 72 h pi (i.e. during active infection), 2) miRNAs down-regulated at 24 h and 72 h pi, 3) miRNAs up-regulated at 14d pi (i.e. after infection had cleared), and 4) miRNAs down-regulated at 14d pi.

MTIs for the sets of differentially expressed miRNAs in the three post-challenge groups were visualised using Cytoscape v. 3.2.1. This was achieved using the Cytoscape app CyTargetLinker v. 3.0.1; a CyTargetLinker RegIN containing only MTIs supported by strong experimental evidence as defined by miRTarBase was created, and applied for visualisation of MTI interaction networks in Cytoscape. KEGG pathway enrichment analysis and MTI networks were created using human miRNA and mRNA homologs, as miRTarBase does not contain porcine MTIs.

As available literature and miRNA databases are almost exclusively concerned with human miRNAs, a comparison of human and porcine miRNA sequences was made (miRBase v. 21) (summarised in Supplementary Table S2).

References

1. Molinari, N. A. *et al.* The annual impact of seasonal influenza in the US: measuring disease burden and costs. *Vaccine* **25,** 5086–5096 (2007).
2. Mauskopf, J., Klesse, M., Lee, S. & Herrera-Taracena, G. The burden of influenza complications in different high-risk groups: a targeted literature review. *J. Med. Econ.* **16,** 264–77 (2013).
3. Bartel, D. P. MicroRNAs: Target Recognition and Regulatory Functions. *Cell* **136,** 215–233 (2009).
4. Li, Y. & Shi, X. MicroRNAs in the regulation of TLR and RIG-I pathways. *Cell. Mol. Immunol.* **10,** 65–71 (2013).
5. Song, L., Liu, H., Gao, S., Jiang, W. & Huang, W. Cellular microRNAs inhibit replication of the H1N1 influenza A virus in infected cells. *J. Virol.* **84,** 8849–60 (2010).
6. Skovgaard, K. *et al.* Expression of innate immune genes, proteins and microRNAs in lung tissue of pigs infected experimentally with influenza virus (H1N2). *Innate Immun.* **19,** 531–44 (2013).
7. Jiang, P. *et al.* Integrative analysis of differentially expressed microRNAs of pulmonary alveolar macrophages from piglets during H1N1 swine influenza A virus infection. *Sci. Rep.* **5,** 8167 (2015).
8. Wang, Y. *et al.* Integrated analysis of microRNA expression and mRNA transcriptome in lungs of avian influenza virus infected broilers. *BMC Genomics* **13,** 278 (2012).
9. Peng, X. *et al.* Integrative deep sequencing of the mouse lung transcriptome reveals differential expression of diverse classes of small RNAs in response to respiratory virus infection. *MBio.* **2** (2011).
10. Li, Y. *et al.* Differential microRNA expression and virulence of avian, 1918 reassortant, and reconstructed 1918 influenza A viruses. *Virology* **421,** 105–113 (2011).

11. Tambyah, P. a. *et al.* microRNAs in Circulation Are Altered in Response to Influenza A Virus Infection in Humans. *PLoS One* **8,** e76811 (2013).
12. Song, H. *et al.* Microarray analysis of microRNA expression in peripheral blood mononuclear cells of critically ill patients with influenza A (H1N1). *BMC Infect. Dis.* **13,** 257 (2013).
13. Zhu, Z. *et al.* Comprehensive characterization of serum microRNA profile in response to the emerging avian influenza A (H7N9) virus infection in humans. *Viruses* **6,** 1525–1539 (2014).
14. Turchinovich, A., Weiz, L., Langheinz, A. & Burwinkel, B. Characterization of extracellular circulating microRNA. *Nucleic Acids Res.* **39,** 7223–7233 (2011).
15. Vickers, K. C., Palmisano, B. T., Shoucri, B. M., Shamburek, R. D. & Remaley, A. T. MicroRNAs are transported in plasma and delivered to recipient cells by high-density lipoproteins. *Nat. Cell Biol.* **13,** 423–433 (2011).
16. Rajao, D. S. & Vincent, a. L. Swine as a Model for Influenza A Virus Infection and Immunity. *ILAR J.* **56,** 44–52 (2015).
17. Rothkötter, H. J. Anatomical particularities of the porcine immune system-A physician's view. *Dev. Comp. Immunol.* **33,** 267–272 (2009).
18. Meurens, F., Summerfield, A., Nauwynck, H., Saif, L. & Gerdts, V. The pig: a model for human infectious diseases. *Trends Microbiol.* **20,** 50–57 (2012).
19. Monto, A. S., Gravenstein, S., Elliott, M., Colopy, M. & Schweinle, J. Clinical signs and symptoms predicting influenza infection. *Arch. Intern. Med.* **160,** 3243–3247 (2000).
20. Kaiser, L., Fritz, R. S., Straus, S. E., Gubareva, L. & Hayden, F. G. Symptom pathogenesis during acute influenza: interleukin-6 and other cytokine responses. *J. Med. Virol.* **64,** 262–268 (2001).
21. Ohmit, S. E. & Monto, A. S. Symptomatic predictors of influenza virus positivity in children during the influenza season. *Clin. Infect. Dis.* **43,** 564–568 (2006).
22. Van Reeth, K., Van Gucht, S. & Pensaert, M. Correlations between lung proinflammatory cytokine levels, virus replication, and disease after swine influenza virus challenge of vaccination-immune pigs. *Viral Immunol.* **15,** 583–594 (2002).
23. Van Reeth, K., Nauwynck, H. & Pensaert, M. Bronchoalveolar interferon-alpha, tumor necrosis factor-alpha, interleukin-1, and inflammation during acute influenza in pigs: a possible model for humans? *J. Infect. Dis.* **177,** 1076–1079 (1998).
24. Hayden, F. G. *et al.* Local and systemic cytokine responses during experimental human influenza A virus infection. Relation to symptom formation and host defense. *J. Clin. Invest* **101,** 643–649 (1998).
25. Simon, G. *et al.* European Surveillance Network for Influenza in Pigs: Surveillance Programs, Diagnostic Tools and Swine Influenza Virus Subtypes Identified in 14 European Countries from 2010 to 2013. *PLoS One* **9,** e115815 (2014).
26. McLaughlin, F. R., Tyler, W. S. & O.Canada, R. A study of the subgross pulmonary anatomy in various mammals. *Am. J. Anat.* **108,** 149–165 (1961).
27. Tyler, W. S. Comparative subgross anatomy of lungs. Pleuras, interlobular septa, and distal airways. *Am.Rev.Respir.Dis.* **128,** S32–S36 (1983).
28. Khatri, M. *et al.* Swine influenza H1N1 virus induces acute inflammatory immune responses in pig lungs: a potential animal model for human H1N1 influenza virus. *J. Virol.* **84,** 11210–8 (2010).
29. Trebbien, R. *et al.* Genetic and biological characterisation of an avian-like H1N2 swine influenza virus generated by reassortment of circulating avian-like H1N1 and H3N2 subtypes in Denmark. *Virol. J.* **10,** 290 (2013).
30. Thangavel, R. R. & Bouvier, N. M. Animal models for influenza virus pathogenesis, transmission, and immunology. *J. Immunol. Methods* **410,** 60–79 (2014).
31. Margine, I. & Krammer, F. Animal Models for Influenza Viruses: Implications for Universal Vaccine Development. *Pathogens* **3,** 845–874 (2014).
32. Gao, R. *et al.* Cytokine and chemokine profiles in lung tissues from fatal cases of 2009 pandemic influenza A (H1N1): role of the host immune response in pathogenesis. *Am. J. Pathol.* **183,** 1258–68 (2013).
33. Woods, C. W. *et al.* A host transcriptional signature for presymptomatic detection of infection in humans exposed to influenza H1N1 or H3N2. *PLoS.One.* **8,** e52198 (2013).
34. Zaas, A. K. *et al.* Gene expression signatures diagnose influenza and other symptomatic respiratory viral infections in humans. *Cell Host.Microbe* **6,** 207–217 (2009).
35. Zaas, A. K. *et al.* A host-based RT-PCR gene expression signature to identify acute respiratory viral infection. *Sci.Transl.Med.* **5,** 203ra126 (2013).
36. Ramilo, O. *et al.* Gene expression patterns in blood leukocytes discriminate patients with acute infections. *Blood* **109,** 2066–2077 (2007).
37. Parnell, G. P. *et al.* A distinct influenza infection signature in the blood transcriptome of patients with severe community-acquired pneumonia. *Crit. Care* **16,** R157 (2012).
38. Hotchkiss, R. S., Coopersmith, C. M., McDunn, J. E. & Ferguson, T. a. The sepsis seesaw: tilting toward immunosuppression. *Nat. Med.* **15,** 496–497 (2009).
39. Didierlaurent, A. *et al.* Sustained desensitization to bacterial Toll-like receptor ligands after resolution of respiratory influenza infection. *J. Exp. Med.* **205,** 323–329 (2008).
40. Scott, P. D., Meng, B., Marriott, A. C., Easton, A. J. & Dimmock, N. J. Defective interfering influenza virus confers only short-lived protection against influenza virus disease: evidence for a role for adaptive immunity in DI virus-mediated protection *in vivo*. *Vaccine* **29,** 6584–6591 (2011).
41. Baum, A., Sachidanandam, R. & Garcia-Sastre, A. Preference of RIG-I for short viral RNA molecules in infected cells revealed by next-generation sequencing. *Proc Natl Acad Sci USA* **107,** 16303–16308 (2010).
42. Tapia, K. *et al.* Defective viral genomes arising *in vivo* provide critical danger signals for the triggering of lung antiviral immunity. *PLoS Pathog.* **9,** e1003703 (2013).
43. Gaur, P., Munjhal, A. & Lal, S. K. Influenza virus and cell signaling pathways. *Med. Sci. Monit.* **17,** RA148–A154 (2011).
44. Ehrhardt, C. *et al.* Influenza A virus NS1 protein activates the PI3K/Akt pathway to mediate antiapoptotic signaling responses. *J. Virol.* **81,** 3058–3067 (2007).
45. Herold, S., Ludwig, S., Pleschka, S. & Wolff, T. Apoptosis signaling in influenza virus propagation, innate host defense, and lung injury. *J. Leukoc. Biol.* **92,** 75–82 (2012).
46. Nailwal, H., Sharma, S., Mayank, a. K. & Lal, S. K. The nucleoprotein of influenza A virus induces p53 signaling and apoptosis via attenuation of host ubiquitin ligase RNF43. *Cell Death Dis.* **6,** e1768 (2015).
47. Hinshaw, V. S., Olsen, C. W., Dybdahl-Sissoko, N. & Evans, D. Apoptosis: a mechanism of cell killing by influenza A and B viruses. *J. Virol.* **68,** 3667–3673 (1994).
48. Olsen, C. W., Kehren, J. C., Dybdahl-Sissoko, N. R. & Hinshaw, V. S. Bcl-2 Alters Influenza Virus Yield, Spread, and Hemagglutinin Glycosylation. *J. Virol.* **70,** 663–666 (1996).
49. Schmitt, M. J., Margue, C., Behrmann, I. & Kreis, S. MiRNA-29: a microRNA family with tumor-suppressing and immune-modulating properties. *Curr. Mol. Med.* **13,** 572–85 (2013).
50. Kong, G. *et al.* Upregulated microRNA-29a by hepatitis B virus X protein enhances hepatoma cell migration by targeting PTEN in cell culture model. *PLoS One* **6,** 1–10 (2011).
51. Lange, J. *et al.* Reassortants of the pandemic (H1N1) 2009 virus and establishment of a novel porcine H1N2 influenza virus, lineage in Germany. *Vet. Microbiol.* **167,** 345–356 (2013).

52. Balcells, I., Cirera, S. & Busk, P. K. Specific and sensitive quantitative RT-PCR of miRNAs with DNA primers. *BMC Biotechnol.* **11,** 70 (2011).
53. Skovgaard, K. *et al.* Rapid and widely disseminated acute phase protein response after experimental bacterial infection of pigs. *Vet. Res.* **40,** 23 (2009).
54. Carrat, F., Tachet, a, Rouzioux, C. & Housset, B. & Valleron, a J. Evaluation of clinical case definitions of influenza: detailed investigation of patients during the 1995-1996 epidemic in France. *Clin. Infect. Dis.* **28,** 283–290 (1999).
55. Trebbien, R., Larsen, L. E. & Viuff, B. M. Distribution of sialic acid receptors and influenza A virus of avian and swine origin in experimentally infected pigs. *Virol. J.* **8,** 434 (2011).
56. Ning, Z. Y. *et al.* Detection of expression of influenza virus receptors in tissues of BALB/c mice by histochemistry. *Vet. Res. Commun.* **33,** 895–903 (2009).
57. Pabst, R. Das lymphatische Gewebe der Nase (NALT) und des Kehlkopfes (LALT) im Speziesvergleich: Mensch, Ratte, Maus. *Pneumologie* **64,** 445–446 (2010).
58. Schneberger, D., Haronson-Raz, K. & Singh, B. Pulmonary intravascular macrophages and lung health: what are we missing? *Am. J. Physiol Lung Cell Mol.Physiol* **302,** L498–L503 (2012).
59. Hol, J., Wilhelmsen, L. & Haraldsen, G. The murine IL-8 homologues KC, MIP-2, and LIX are found in endothelial cytoplasmic granules but not in Weibel-Palade bodies. *J. Leukoc. Biol.* **87,** 501–508 (2010).
60. Goodman, R. B. *et al.* Molecular cloning of porcine alveolar macrophage-derived neutrophil chemotactic factors I and II; identification of porcine IL-8 and another intercrine-alpha protein. *Biochemistry* **31,** 10483–10490 (1992).

Acknowledgements

The authors wish to thank Kerstin Wieczorek and Roswitha Ulrich for technical assistance, Dr Guntram Hagemann is thanked for providing the influenza A virus antibody negative pigs, and Renè Rau for assistance during the animal trial (all IDT Biologika GmbH, Dessau-Roßlau, Germany). Karin Tarp (National Veterinary Institute, Frederiksberg C, Denmark) is thanked for technical assistance with sample collection and RT-qPCR.

Author Contributions

L.B. performed miRNA and mRNA qPCR analysis, including data processing, miRNA target prediction analyses, and main manuscript text. P.M.H.H. contributed to manuscript preparation. L.E.L. and S.M. contributed to the experimental design. R.D. and M.S. contributed to the experimental design, carried out animal experiments and supervised serological and virological investigations. K.S. contributed to the experimental design, miRNA and mRNA qPCR data analysis, and main manuscript text. All authors reviewed the manuscript.

Additional Information

Supplementary information accompanies this paper at http://www.nature.com/srep

Competing financial interests: The authors declare no competing financial interests.

How to cite this article: Brogaard, L. *et al.* Late regulation of immune genes and microRNAs in circulating leukocytes in a pig model of influenza A (H1N2) infection. *Sci. Rep.* **6,** 21812; doi: 10.1038/srep21812 (2016).

1 Supplementary material for:

2

3 **Late regulation of immune genes and microRNAs in circulating leukocytes in a pig model of**

4 **influenza A (H1N2) infection**

5 Louise Brogaard, Peter M. H. Heegaard, Lars E. Larsen, Shila Mortensen, Michael Schlegel, Ralf

6 Dürrwald, Kerstin Skovgaard

7

Supplementary Table S1. qPCR primer sequences and experimentally determined PCR efficiencies for all reported genes and miRNAs in the present study.

Gene/miRNA	Forward primer	Reverse primer	PCR eff.
CASP1	GAAGGACAAACCCAAGGTGA	TGGGCTTTCTTAATGGCATC	101 %
CASP3	AGCAGTTTTATTTGCGTGCTT	CAACAGGTCCATTTGTTCCA	99 %
CASP9	CTGTGAGGACCTGCTGACC	CGGAGGAAATTAAAACAGCCAGG	104 %
CCL2	CTTCTGCACCCAGGTCCTT	CGCTGCATCGAGATCTTCTT	90 %
CCL3	CCAGGTCTTCTCTGCACCAC	GCTACGAATTTGCGAGGAAG	104 %
CD163	CACATGTGCCAACAAAATAAGAC	CACCACCTGAGCATCTTCAA	117 %
CXCL2	GAAGATGCTAAACAAGAGCAGTG	AGCCAAATGCATGAAACACA	112 %
CXCL10	CCCACATGTTGAGATCATTGC	GCTTCTCTCTGTGTTCGAGGA	97 %
DDX58	ACGAAAGGGGAAGGTTGTCT	ATGCCTGCAACTTTGTACCC	96 %
FAS	CACTGTAACCCTTGCACCAC	TGGAACACTTCTCTGCATTTGG	109 %
FASLG	TTCTGGTGGCCCTGGTTG	CTTTGGCTGGCAGACTCTCT	106 %
IDO1	GGGCCCATGACTTACAAGAA	TTTCCACCAATAGCGAAACC	97 %
IFITM1	GCTTTCGCCTACTCCGTGA	CCAGGATCAGAGCCCAGATG	106 %
IFITM3	TGAACTGCGCTTCCCAGC	CACCTCGTGCTCCTCCTTG	104 %
IFNA1	TTCCAGCTCTTCAGCACAGA	AGCTGCTGATCCAGTCCAGT	101 %
IFNG	CCATTCAAAGGAGCATGGAT	TTCAGTTTCCCAGAGCTACCA	94 %
IL8	TTGCCAGAGAAATCACAGGA	TGCATGGGACACTGGAAATA	89 %
IL10	TACAACAGGGGCTTGCTCTT	GCCAGGAAGATCAGGCAATA	108 %
IL18	CAATTGCATCAGCTTTGTGG	TCCAGGTCCTCATCGTTTTC	100 %
IL1RAP	TGCATCTTTGACCGAGACAG	GGGCTCAGGACAACAATCAT	93 %
IL1RN	TGCCTGTCCTGTGTCAAGTC	GTCCTGCTCGCTGTTCTTTC	103 %
IRF1	TGAAGCTGCAACAGATGAGG	CTTCCCATCCACGTTTGTCT	102 %
IRF2	GATGCTGCCCTTATCTGAGC	TGTGCTTCACTCTGTCTTCCTT	91 %
IRF3	GCTACACCCTCTGGTTCTGC	GAGACACATGGGGACAACCT	96 %
IRF9	CATTCAGACTTGGGGAGCAG	AAAGGGGCCTCAGTGGTAAC	101 %
IFIH1	CAGTGTGCTAGCCTGCTCTG	GCAGTGCCTTGTTTCCTCTC	97 %
JAK2	CTCAGATATGCAAGGGTATGGAGT	CCACCAATATATTCCTTGTTGCCA	104 %
MCL1	GAGGCTGGGATGGGTTTGTG	TGCCAAACCAGCTCCTACTC	103 %
MX1	CCTCCACAGAACTGCCAAG	GCAGTACACGATCTGCTCCA	98 %
MYD88	AGCTGTAGGGGGAATGTGTG	TCAGCTGGTCTGTGGATGTG	98 %
NOD1	CTCGACCTGGACAACAACAA	TGAGTCTGATGACCGTGAGG	105 %
OASL	TGGTACCTGAAGTACGTGAAAGC	TACCCACTTCCCAGGCATAG	90 %
PTGS2	AGGCTGATACTGATAGGAGAAACG	GCAGCTCTGGGTCAAACTTC	96 %
STAT1	CCTTGCAGAATAGAGAACATGATAC	CCTTTCTCTTGTTGTCAAGCATT	98 %
TICAM1	CTGCCTTCCCACAGCCTC	AGCCCCAGTTGTACCATTTGA	90 %
TICAM2	TCTGCTGCAAAATGACTTCGG	AGCCATTGACAGCATCGTCT	90 %
TLR2	GTTTTACGGAAATTGTGAAACTG	TCCACATTACCGAGGGATTT	92 %
TLR3	ATTGTGCAAAAGATTCAAGGTG	TCTTCGCAAACAGAGTGCAT	104 %
TLR4	TTTCCACAAAAGTCGGAAGG	CAACTTCTGCAGGACGATGA	95 %
TLR7	GGAAATAGCATCAGCCAAGCTC	TTCCAGGTTGCGTAGCTCTT	87 %
TLR8	GCAAAGACCACCACCAAC	ATCCGTCAGTCTGGGAAT	95 %
TNF	CCCCCAGAAGGAAGAGTTTC	CGGGCTTATCTGAGGTTTGA	94 %
Genes identified as targeted in MTI network analysis			
AKT2	CTGCTTAAGAAGGACCCAAAGC	CTTCTGTACCACGTCCTGCC	95 %
BCL2	GACTCCCTTCACCGCGAG	CTCTCCACACACATGACCCC	90 %
CDK2	TTGCTGAGATGGTGACCCG	GGGTCCCAAGAGTCCGAAAG	106 %
CDK4	GGCCAGAATCTACAGCTACCAG	TCCACAGGTGTTGCATACGT	90 %

CCNE2	ATGGTGCTTGCAGTGAAGAGG	TGGAGGAAGAGATTTAGCCAGG	107 %
CXCR4	CTGCTGGCTGCCATACTACA	TCAAACTCACACCCTTGCTG	97 %
FOS	GGAACAGTTGTCCCCAGAAG	TGTCAGTCAGCTCCCTCCTC	100 %
FOXO3A	CCAGTCTATGCAAACCCTCTCG	CAAGTCGCTGGGGAACTTCT	90 %
PTEN	AGCAAATAAAGACAAGGCCAACC	GTTGAACTGCTAGCCTCTGGA	103 %
SP1	AAGATAGTGAAGGAAGGGGCTC	TACTTTGCCACAACCTTGCATG	106 %
TP53	TAAGCGAGCACTGCCCAC	TCTCGGAACATCTCGAAGCG	101 %
VEGFA	CGAAGGTCTGGAGTGTGTGC	TCTCTCCTATGTGCTGGCCT	90 %
hsa-miR-223-5p	GCGTGTATTTGACAAGCTG	GTCCAGTTTTTTTTTTTTTTTAACTCAG	97 %
ssc-miR-182	AGTTTGGCAATGGTAGAACTC	GTCCAGTTTTTTTTTTTTTTTAGTGTG	96 %
ssc-miR-29a	GCTAGCACCATCTGAAATCG	TCCAGTTTTTTTTTTTTTTTAACCGA	100 %
ssc-miR-31	GGCAAGATGCTGGCA	CCAGTTTTTTTTTTTTTTTCAGCTATG	92 %
ssc-miR-29b	CAGTAGCACCATTTGAAATCAG	GGTCCAGTTTTTTTTTTTTTTTAACACT	96 %
hsa-miR-203a-3p	AGGTGAAATGTTTAGGACCAC	GTCCAGTTTTTTTTTTTTTTTCTAGTG	99 %
hsa-miR-449a	AGTGGCAGTGTATTGTTAGC	GTCCAGTTTTTTTTTTTTTTTACCAG	90 %
ssc-miR-21	TCAGTAGCTTATCAGACTGATG	CGTCCAGTTTTTTTTTTTTTTTCAAC	101 %
hsa-miR-23a-3p	CATCACATTGCCAGGGAT	CGTCCAGTTTTTTTTTTTTTTGGAA	109 %
ssc-miR-23b	AGATCACATTGCCAGGGA	CCAGTTTTTTTTTTTTTTTGGTAATCC	104 %
ssc-miR-30c-5p	CAGTGTAAACATCCTACACTCTC	CCAGTTTTTTTTTTTTTTTGCTGAG	109 %
ssc-miR-423-5p	GGGCAGAGAGCGAGAC	GGTCCAGTTTTTTTTTTTTTTTAAAGTC	90 %
hsa-miR-150-5p	GTCTCCCAACCCTTGTAC	GTCCAGTTTTTTTTTTTTTTCACTG	115 %
ssc-miR-15a	CAGTAGCAGCACATAATGGT	TCCAGTTTTTTTTTTTTTTTACAAACC	97 %
ssc-miR-186	CGCAGCAAAGAATTCTCCT	GGTCCAGTTTTTTTTTTTTTTTAAGC	102 %
ssc-miR-22-5p	CAGAGTTCTTCAGTGGCAAG	GGTCCAGTTTTTTTTTTTTTTTAAAGC	90 %
ssc-miR-28-5p	CAGAAGGAGCTCACAGTCT	GGTCCAGTTTTTTTTTTTTTTTCTCA	97 %
ssc-miR-146a-5p	GCAGTGAGAACTGAATTCCA	GGTCCAGTTTTTTTTTTTTTTTAACC	92 %
hsa-miR-223-3p	CGCAGTGTCAGTTTGTCA	CCAGTTTTTTTTTTTTTTTGGGGTA	101 %
hsa-miR-16-5p	GCAGTAGCAGCACGTA	CAGTTTTTTTTTTTTTTTCGCCAA	96 %

10

11

Supplementary Table S2. Sequence comparison of human and porcine homologs of the miRNAs reported regulated in the present study. Underlined nucleotides: nucleotides 2-7, i.e. the seed sequence.

miRBase accession number	miRNA	miRNA sequence
MIMAT0000086	hsa-miR-29a-3p	uagcaccaucugaaaucgguua
MIMAT0013870	ssc-miR-29a	cuagcaccaucugaaaucgguua
MIMAT0000089	hsa-miR-31-5p	aggcaagaugcuggcauagcu
MIMAT0025360	ssc-miR-31	aggcaagaugcuggcauagcug
MIMAT0000100	hsa-miR-29b-3p	uagcaccauuugaaaucaguguu
MIMAT0002137	ssc-miR-29b	uagcaccauuugaaaucaguguu
MIMAT0000076	hsa-miR-21-5p	uagcuuaucagacugauguuga
MIMAT0002165	ssc-miR-21	uagcuuaucagacugauguuga
MIMAT0000078	hsa-miR-23a-3p	aucacauugccagggauuucc
MIMAT0002133	ssc-miR-23a	aucacauugccagggauuucc
MIMAT0000244	hsa-miR-30c-5p	uguaaacauccuacacucucagc
MIMAT0002167	ssc-miR-30c-5p	uguaaacauccuacacucucagc
MIMAT0004748	hsa-miR-423-5p	ugaggggcagagagcgagacuuu
MIMAT0013880	ssc-miR-423-5p	ugaggggcagagagcgagacuuu
MIMAT0000451	hsa-miR-150-5p	ucucccaacccuuguaccagug
MIMAT0025365	ssc-miR-150	ucucccaacccuuguaccagug
MIMAT0000456	hsa-miR-186-5p	caaagaauucuccuuuugggcu
MIMAT0002162	ssc-miR-186	caaagaauucuccuuuugggcuu
MIMAT0004495	hsa-miR-22-5p	aguucuucaguggcaagcuuua
MIMAT0015709	ssc-miR-22-5p	aguucuucaguggcaagcuuua
MIMAT0000085	hsa-miR-28-5p	aaggagcucacagucuauugag
MIMAT0002136	ssc-miR-28-5p	aaggagcucacagucuauugag
MIMAT0000449	hsa-miR-146a-5p	ugagaacugaauuccauggguu
MIMAT0022963	ssc-miR-146a-5p	ugagaacugaauuccauggguu
MIMAT0000069	hsa-miR-16-5p	uagcagcacguaaauauuggcg
MIMAT0007754	ssc-miR-16	uagcagcacguaaauauuggcg
MIMAT0000259	hsa-miR-182-5p	uuuggcaaugguagaacucacacu
MIMAT0025366	ssc-miR-182	uuuggcaaugguagaacucacacu
MIMAT0000418	hsa-miR-23b-3p	aucacauugccagggauuacc
MIMAT0013893	ssc-miR-23b	aucacauugccagggauuacca
MIMAT0000068	hsa-miR-15a-5p	uagcagcacauaaugguuugug
MIMAT0007753	ssc-miR-15a	uagcagcacauaaugguuugu

Supplementary Table S3. Expression levels of miRNA in porcine leukocytes after IAV challenge.

Expression is shown as relative levels compared to before challenge.

miRNA	Rel. expression level	±95 % CI	*p*-value
24h pi (n = 12)			
hsa-miR-223-5p	1.94	0.41	0.00030
ssc-miR-182	1.70	0.47	0.020
ssc-miR-29a	0.65	0.18	0.028
ssc-miR-31	0.45	0.28	0.0027
72h pi (n = 9)			
ssc-miR-29b	2.16	0.46	0.000048
hsa-miR-203a-3p	1.82	0.28	0.00024
hsa-miR-449a	1.80	0.74	0.038
ssc-miR-21	1.60	0.47	0.033
ssc-miR-29a	1.55	0.36	0.0071
hsa-miR-23a-3p	0.63	0.18	0.036
ssc-miR-23b	0.60	0.16	0.024
ssc-miR-30c-5p	0.59	0.10	0.0074
ssc-miR-423-5p	0.53	0.11	0.011
hsa-miR-150-5p	0.52	0.15	0.042
14d pi (n = 6)			
ssc-miR-15a	2.31	0.98	0.022
ssc-miR-29b	2.30	0.78	0.0057
ssc-miR-29a	2.29	0.76	0.0032
hsa-miR-449a	2.05	0.82	0.028
ssc-miR-186	1.84	0.52	0.010
ssc-miR-22-5p	1.64	0.47	0.013
ssc-miR-28-5p	1.60	0.47	0.0076
hsa-miR-203a-3p	1.56	0.31	0.010
ssc-miR-146a-5p	1.52	0.24	0.010
hsa-miR-150-5p	0.50	0.21	0.022
ssc-miR-23b	0.44	0.15	0.017
hsa-miR-223-3p	0.42	0.15	0.010
hsa-miR-23a-3p	0.42	0.14	0.0076
hsa-miR-16-5p	0.35	0.26	0.022

Supplementary Table S4. KEGG Pathway enrichment analysis of experimentally validated targets of the miRNAs found to be differentially expressed in the present study. Pathways highlighted in bold text are enriched in at least three of the four gene subsets. Many pathways related to specific cancer types were also enriched in all four gene subsets; these have not been included in the table.

KEGG pathway	Number of genes involved	Percentage of investigated genes involved	P-Value	Benjamini-Hochberg adjusted P-Value
1) Enriched in target genes for up-regulated miRNAs at 24h and 72h pi				
Pathways in cancer	55	19,3	1,60E-27	1,80E-25
Focal adhesion	36	12,6	2,30E-18	8,50E-17
Cell cycle	20	7	3,20E-09	3,50E-08
p53 signaling pathway	15	5,3	7,70E-09	7,70E-08
MAPK signaling pathway	26	9,1	2,30E-07	1,80E-06
Apoptosis	13	4,6	8,40E-06	5,50E-05
Neurotrophin signaling pathway	15	5,3	1,60E-05	9,70E-05
Cytokine-cytokine receptor interaction	22	7,7	2,70E-05	1,60E-04
ErbB signaling pathway	12	4,2	4,70E-05	2,60E-04
TGF-beta signaling pathway	12	4,2	4,70E-05	2,60E-04
T cell receptor signaling pathway	13	4,6	7,70E-05	4,00E-04
Adherens junction	11	3,9	8,30E-05	4,20E-04
ECM-receptor interaction	11	3,9	1,70E-04	8,40E-04
Toll-like receptor signaling pathway	12	4,2	1,90E-04	8,50E-04
Regulation of actin cytoskeleton	17	6	6,10E-04	2,70E-03
Progesterone-mediated oocyte maturation	10	3,5	9,70E-04	4,10E-03
Gap junction	10	3,5	1,20E-03	5,00E-03
Dilated cardiomyopathy	10	3,5	1,60E-03	5,90E-03
Jak-STAT signaling pathway	13	4,6	2,10E-03	7,80E-03
GnRH signaling pathway	10	3,5	2,40E-03	8,60E-03
Hypertrophic cardiomyopathy (HCM)	9	3,2	3,60E-03	1,20E-02
B cell receptor signaling pathway	8	2,8	6,70E-03	2,20E-02
VEGF signaling pathway	8	2,8	6,70E-03	2,20E-02
Fc gamma R-mediated phagocytosis	9	3,2	7,10E-03	2,30E-02
2) Enriched in target genes for down-regulated miRNAs at 24h and 72h pi				
Pathways in cancer	37	19,1	8,60E-16	9,70E-14
p53 signaling pathway	14	7,2	3,80E-09	1,40E-07
Focal adhesion	22	11,3	5,50E-09	1,50E-07
Tight junction	12	6,2	2,80E-04	2,20E-03
Adherens junction	9	4,6	4,10E-04	2,80E-03
Cell cycle	11	5,7	6,60E-04	4,20E-03
ECM-receptor interaction	9	4,6	7,40E-04	4,50E-03

Notch signaling pathway	7	3,6	7,40E-04	4,20E-03
Apoptosis	9	4,6	9,40E-04	5,10E-03
Jak-STAT signaling pathway	11	5,7	3,40E-03	1,70E-02
Chemokine signaling pathway	12	6,2	4,40E-03	2,10E-02
Epithelial cell signaling in Helicobacter pylori infection	7	3,6	5,10E-03	2,40E-02
Viral myocarditis	7	3,6	6,30E-03	2,80E-02
Cysteine and methionine metabolism	5	2,6	7,90E-03	3,40E-02
Neurotrophin signaling pathway	9	4,6	8,60E-03	3,50E-02
Wnt signaling pathway	10	5,2	8,90E-03	3,60E-02
3) Enriched in target genes for up-regulated miRNAs at 14d pi				
Pathways in cancer	63	24,8	8,80E-37	9,50E-35
Focal adhesion	39	15,4	8,10E-22	2,90E-20
Cell cycle	25	9,8	4,90E-14	5,30E-13
Toll-like receptor signaling pathway	22	8,7	4,20E-13	4,10E-12
Neurotrophin signaling pathway	21	8,3	2,10E-10	1,60E-09
MAPK signaling pathway	28	11	6,30E-09	4,00E-08
Apoptosis	16	6,3	1,80E-08	1,10E-07
p53 signaling pathway	14	5,5	4,60E-08	2,60E-07
T cell receptor signaling pathway	17	6,7	5,50E-08	3,00E-07
ErbB signaling pathway	15	5,9	1,30E-07	6,90E-07
Chemokine signaling pathway	21	8,3	3,00E-07	1,50E-06
B cell receptor signaling pathway	13	5,1	1,20E-06	5,60E-06
Adherens junction	13	5,1	1,60E-06	7,10E-06
Fc gamma R-mediated phagocytosis	14	5,5	2,60E-06	1,10E-05
VEGF signaling pathway	12	4,7	8,10E-06	3,20E-05
Regulation of actin cytoskeleton	20	7,9	1,10E-05	4,10E-05
Cytokine-cytokine receptor interaction	22	8,7	1,60E-05	6,10E-05
Progesterone-mediated oocyte maturation	12	4,7	3,10E-05	1,10E-04
Wnt signaling pathway	15	5,9	1,00E-04	3,50E-04
Epithelial cell signaling in Helicobacter pylori infection	10	3,9	1,30E-04	4,30E-04
Leukocyte transendothelial migration	13	5,1	1,30E-04	4,30E-04
Fc epsilon RI signaling pathway	10	3,9	3,70E-04	1,20E-03
ECM-receptor interaction	10	3,9	6,40E-04	2,00E-03
mTOR signaling pathway	8	3,1	6,60E-04	2,00E-03
TGF-beta signaling pathway	10	3,9	8,30E-04	2,40E-03
Gap junction	10	3,9	9,80E-04	2,80E-03
Axon guidance	12	4,7	1,20E-03	3,20E-03
Jak-STAT signaling pathway	13	5,1	1,60E-03	4,20E-03
NOD-like receptor signaling pathway	8	3,1	1,90E-03	4,90E-03
Type II diabetes mellitus	7	2,8	2,10E-03	5,30E-03
Insulin signaling pathway	11	4,3	5,40E-03	1,30E-02
GnRH signaling pathway	9	3,5	7,10E-03	1,70E-02
Hypertrophic cardiomyopathy (HCM)	8	3,1	1,10E-02	2,60E-02

Intestinal immune network for IgA production	6	2,4	1,30E-02	2,90E-02
Oocyte meiosis	9	3,5	1,40E-02	3,10E-02
Natural killer cell mediated cytotoxicity	10	3,9	1,40E-02	3,10E-02
Tight junction	10	3,9	1,50E-02	3,20E-02
RIG-I-like receptor signaling pathway	7	2,8	1,60E-02	3,40E-02
Dilated cardiomyopathy	8	3,1	1,70E-02	3,40E-02
Endocytosis	12	4,7	1,70E-02	3,40E-02
Prion diseases	5	2	1,80E-02	3,50E-02
4) Enriched in target genes for down-regulated miRNAs at 14d pi				
Pathways in cancer	35	23,6	1,40E-16	1,20E-14
p53 signaling pathway	12	8,1	7,30E-08	2,60E-06
Jak-STAT signaling pathway	14	9,5	1,10E-05	1,10E-04
Cell cycle	12	8,1	3,40E-05	3,00E-04
Cytokine-cytokine receptor interaction	16	10,8	2,00E-04	1,20E-03
Insulin signaling pathway	11	7,4	3,30E-04	2,00E-03
Focal adhesion	13	8,8	6,20E-04	3,50E-03
Chemokine signaling pathway	12	8,1	1,20E-03	6,30E-03
NOD-like receptor signaling pathway	7	4,7	1,40E-03	7,10E-03
Dorso-ventral axis formation	5	3,4	1,40E-03	6,80E-03
ErbB signaling pathway	8	5,4	1,70E-03	7,70E-03
Apoptosis	8	5,4	1,70E-03	7,70E-03
Adipocytokine signaling pathway	7	4,7	2,10E-03	9,30E-03
Notch signaling pathway	6	4,1	2,30E-03	9,90E-03
Neurotrophin signaling pathway	9	6,1	3,20E-03	1,30E-02
VEGF signaling pathway	7	4,7	3,70E-03	1,50E-02
Tight junction	9	6,1	5,20E-03	2,00E-02
MAPK signaling pathway	13	8,8	6,70E-03	2,50E-02
Progesterone-mediated oocyte maturation	7	4,7	7,20E-03	2,60E-02
Wnt signaling pathway	9	6,1	1,00E-02	3,50E-02

24

Supplementary Figure S1. miRNA-target interaction networks at A) 24h pi, B) 72h pi, and c) 14d pi. Red circles represent down-regulated miRNAs; green circles represent up-regulated miRNAs; hexagons represent experimentally validated gene targets. Hexagons with solid grey fill are genes that interact with two or more of the regulated miRNAs. Experimentally validated interactions are indicated with arrows from miRNA to target. The number of genes with two or more experimentally validated MTIs comprised 6, 65, and 84 at 24h, 72h, and 14d pi, respectively.

a) 24h pi

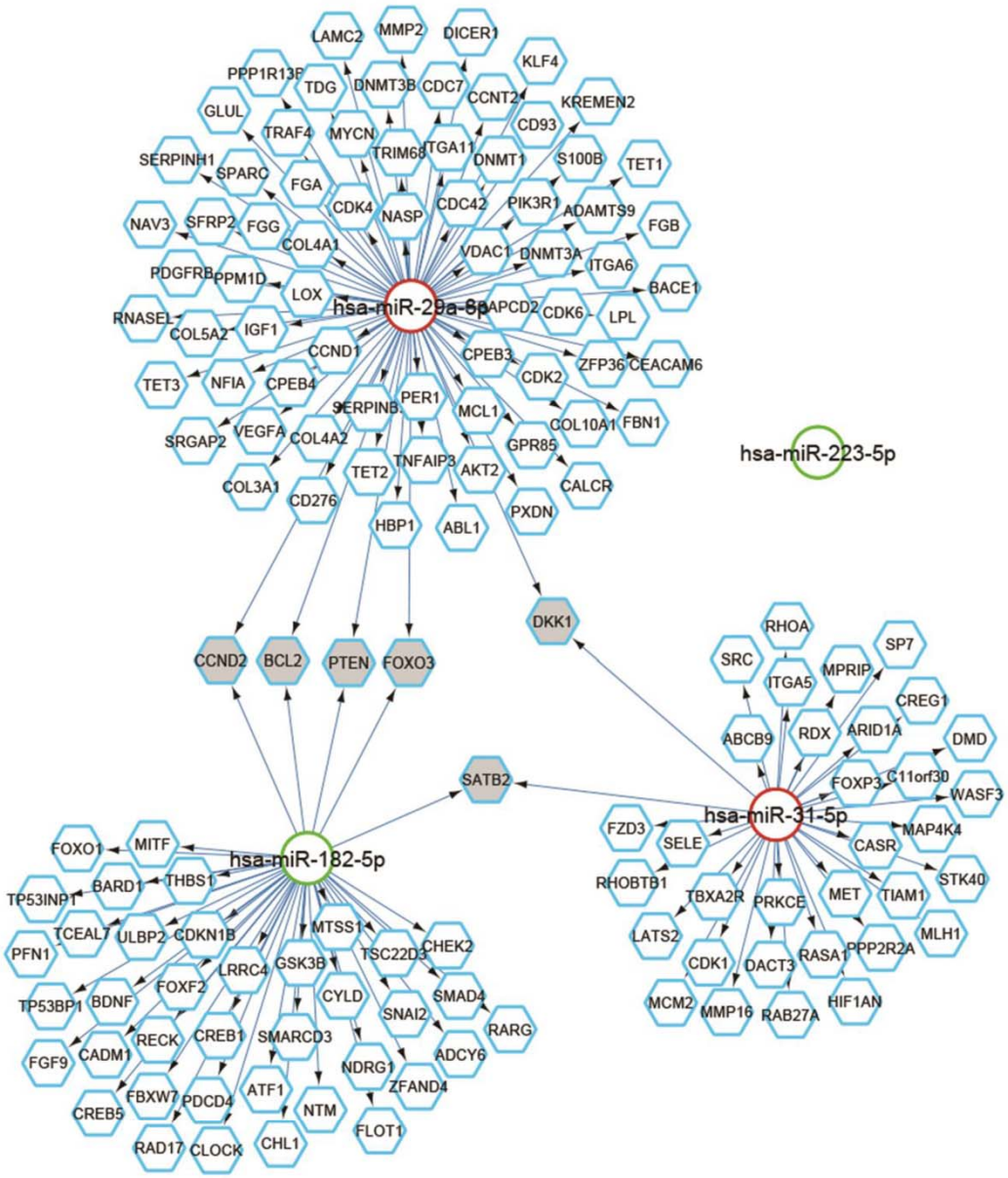
hsa-miR-29a-8p
hsa-miR-223-5p
hsa-miR-31-5p
hsa-miR-182-5p
LAMC2
MMP2
DICER1
KLF4
PPP1R13P
TDG
DNMT3B
CDC7
CCNT2
KREMEN2
GLUL
CD93
TRAF4
MYCN
TRIM68
ITGA11
DNMT1
S100B
TET1
SERPINH1
SPARC
FGA
CDK4
NASP
CDC42
PIK3R1
ADAMTS9
FGB
NAV3
SFRP2
FGG
COL4A1
VDAC1
DNMT3A
ITGA6
PDGFRB
PPM1D
LOX
BACE1
RNASEL
COL5A2
IGF1
APCD2
CDK6
LPL
CCND1
CPEB3
ZFP36
CEACAM6
TET3
NFIA
CPEB4
CDK2
PER1
SERPINB
MCL1
COL10A1
FBN1
SRGAP2
VEGFA
COL4A2
GPR85
COL3A1
TET2
TNFAIP3
AKT2
CALCR
CD276
HBP1
ABL1
PXDN
DKK1
CCND2
BCL2
PTEN
FOXO3
RHOA
SRC
SP7
ITGA5
MPRIP
CREG1
ABCB9
RDX
ARID1A
DMD
FOXP3
C11orf30
WASF3
SATB2
FZD3
SELE
MAP4K4
CASR
RHOBTB1
STK40
TBXA2R
PRKCE
MET
TIAM1
LATS2
MLH1
CDK1
DACT3
RASA1
PPP2R2A
MCM2
MMP16
RAB27A
HIF1AN
FOXO1
MITF
THBS1
BARD1
TP53INP1
TCEAL7
ULBP2
CDKN1B
MTSS1
CHEK2
TSC22D3
PFN1
LRRC4
GSK3B
FOXF2
CYLD
SMAD4
TP53BP1
BDNF
SNAI2
RARG
RECK
CREB1
SMARCD3
ADCY6
FGF9
CADM1
NDRG1
ZFAND4
FBXW7
PDCD4
ATF1
NTM
CREB5
FLOT1
RAD17
CLOCK
CHL1

b) 72h pi

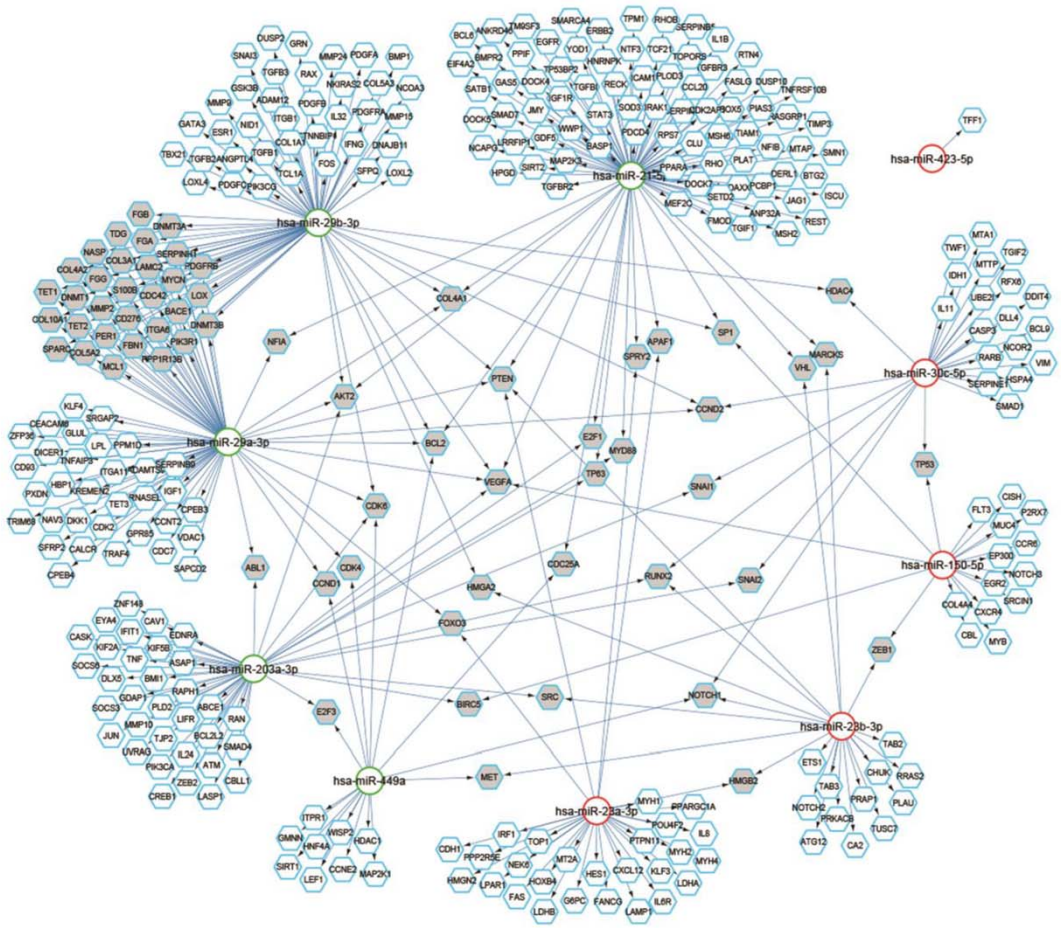
hsa-miR-29b-3p
hsa-miR-21-5p
hsa-miR-423-5p
hsa-miR-30c-5p
hsa-miR-29a-3p
hsa-miR-150-5p
hsa-miR-203a-3p
hsa-miR-23b-3p
hsa-miR-449a
hsa-miR-23a-3p
AKT2
PTEN
BCL2
CCND2
VEGFA
TP63
SNAI1
CDK6
CDK4
CCND1
ABL1
HMGA2
CDC25A
RUNX2
SNAI2
FOXO3
BIRC5
SRC
NOTCH1
E2F3
ZEB1
TP53
HDAC4
SP1
APAF1
SPRY2
MARCKS
VHL
COL4A1
NFIA
MET
HMGB2
E2F1
MYD88

c) 14d pi

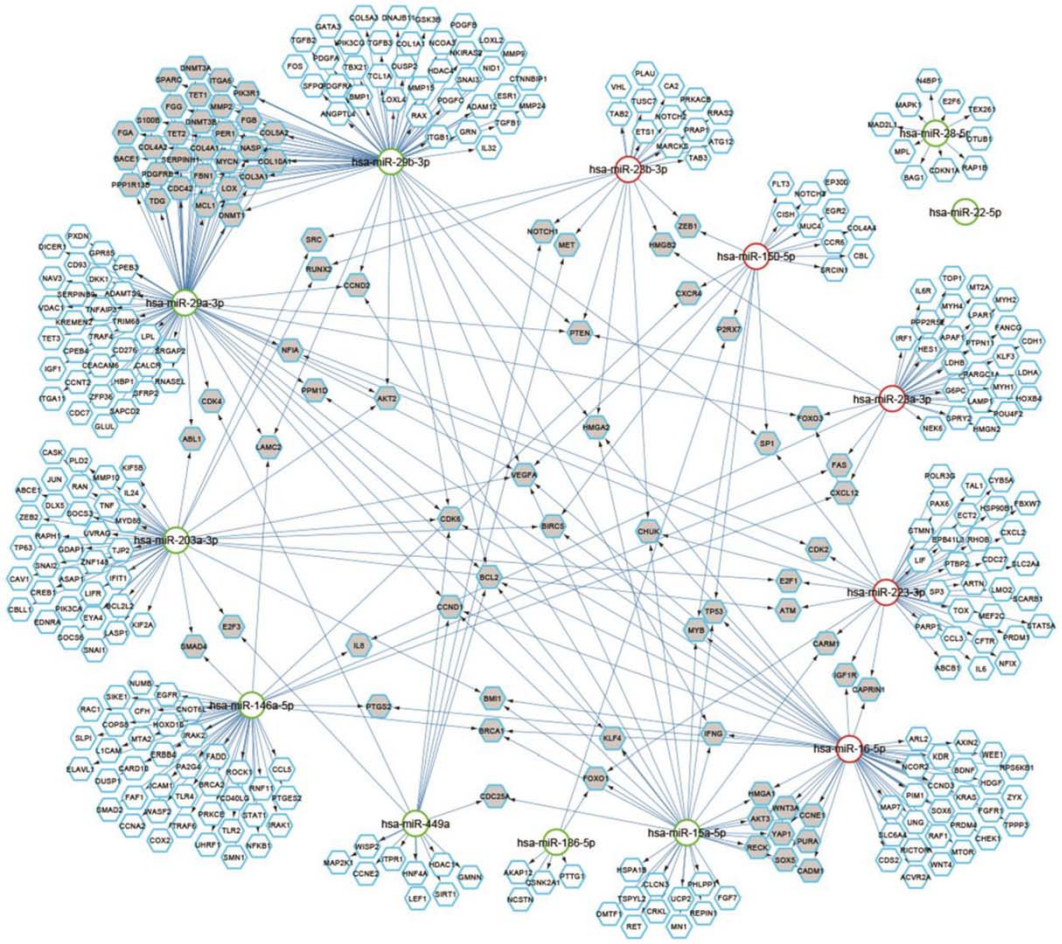
hsa-miR-29b-3p
hsa-miR-29a-3p
hsa-miR-203a-3p
hsa-miR-146a-5p
hsa-miR-449a
hsa-miR-186-5p
hsa-miR-15a-5p
hsa-miR-16-5p
hsa-miR-223-3p
hsa-miR-21a-3p
hsa-miR-150-5p
hsa-miR-28b-3p
hsa-miR-28-5p
hsa-miR-22-5p

Paper 3

IFN-λ and microRNAs are important modulators of the pulmonary innate immune response against influenza A (H1N2) infection in pigs

Research article

L Brogaard, LE Larsen, PMH Heegaard, C Anthon, J Gorodkin, R Dürrwald, K Skovgaard

Submitted for publication in *PLOS ONE* (August 28th 2017)
Under review at the time of thesis submission

All raw data is freely available upon request
It is not feasible to print Supplementary Tables 3-6 due to their format; they are available upon request
loun@vet.dtu.dk

IFN-λ and microRNAs are important modulators of the pulmonary innate immune response against influenza A (H1N2) infection in pigs

Louise Brogaard[1]*, Lars E. Larsen[2], Peter M. H. Heegaard[1], Christian Anthon[3], Jan Gorodkin[3], Ralf Dürrwald[4,#a], Kerstin Skovgaard[1]

[1] Division of Immunology and Vaccinology – Innate Immunology, National Veterinary Institute, Technical University of Denmark, Kongens Lyngby, Denmark
[2] Division of Diagnostics and Scientific Advice – Virology, National Veterinary Institute, Technical University of Denmark, Kongens Lyngby, Denmark
[3] Center for non-coding RNA in Technology and Health (RTH), Department of Veterinary and Animal Science, University of Copenhagen, Frederiksberg, Denmark
[4] IDT Biologika GmbH, Dessau-Rosslau, Germany
[#a] Current address: Department of Infectious Diseases, Robert Koch Institute, Berlin, Germany

*Corresponding author
Email: loun@vet.dtu.dk (LB)

Abstract

The innate immune system is paramount in the response to and clearance of influenza A virus (IAV) infection in non-immune individuals. Known factors include type I and III interferons and antiviral pathogen recognition receptors, and the cascades of antiviral and pro- and anti-inflammatory gene expression they induce. MicroRNAs (miRNAs) are increasingly recognized to participate in post-transcriptional modulation of these responses, but the temporal dynamics of how these players of the antiviral innate immune response collaborate to combat infection remain poorly characterized. We quantified the expression of miRNAs and protein coding genes in the lungs of pigs 1, 3, and 14 days after challenge with swine IAV (H1N2). Through RT-qPCR we observed a 400-fold relative increase in IFN-λ3 gene expression on day 1 after challenge, and a strong interferon-mediated antiviral response was observed on days 1 and 3 accompanied by up-regulation of genes related to the pro-inflammatory response and apoptosis.

Using small RNA sequencing and qPCR validation we found 27 miRNAs that were differentially expressed after challenge, with the highest number of regulated miRNAs observed on day 3. In contrast, the number of protein coding genes found to be regulated due to IAV infection peaked on day 1. Pulmonary miRNAs may thus be aimed at fine-tuning the initial rapid inflammatory response after IAV infection. Specifically, we found five miRNAs (ssc-miR-15a, ssc-miR-18a, ssc-miR-21, ssc-miR-29b, and hsa-miR-590-3p) – four known porcine miRNAs and one novel porcine miRNA candidate – to be potential modulators of viral pathogen recognition and apoptosis. A total of 11 miRNAs remained differentially expressed 14 days after challenge, at which point the infection had cleared. In conclusion, the results suggested a role for miRNAs both during acute infection as well as later, with the potential to influence lung homeostasis and susceptibility to secondary infections in the lungs of pigs after IAV infection.

Introduction

Influenza A is an RNA virus of the *Orthomyxoviridae* family with a single-stranded, negative sense segmented genome causing highly contagious respiratory infections in many species, including humans and pigs. Seasonal influenza in humans is a self-limiting disease, and healthy individuals usually recover within a week. However, in vulnerable individuals, such as the elderly, the immunocompromised, or individuals with chronic low-grade inflammation, the course of disease may be more severe, with a higher incidence of secondary infections and fatalities [1]. New variant viruses emerge continuously due to accumulation of mutations in the viral genome during replication. Due to these continuous antigenic changes, immunity that is acquired during one influenza season (either by natural infection or vaccination) often provide insufficient protection against the strains that dominate the following seasons [2]. Control of the IAV infection is therefore highly dependent on an efficient innate immune response [3].

It has been documented that IAV infection induces a rapid interferon response dominated by type I interferons (IFN-α, IFN-β) and the more recently described type III interferons (IFN-λ) [4,5]. Interferons are responsible for the induction of a multitude of genes termed interferon-stimulated genes (ISGs), including PKR, Mx1, IFITMs, and ISG15. These ISGs establish an antiviral state within the cell that effectively combats the infection and spreads to neighboring cells via secreted interferon [5]. This innate antiviral response is initiated by pathogen recognition receptors (PRRs) that recognize viral RNA, such as the cytoplasmic Toll-like receptors (TLRs) 3 and 7 and the RIG-I-like receptors (RLRs) RIG-I and MDA5 [3]. Upon PRR recognition of IAV, adapter proteins such as MyD88, MAVS, and TRIF initiate signaling cascades that ultimately lead to the production of cytokines such as IL-1, IL-6, and TNF, as well as chemokines IL-8, CXCL2, and CXCL10 that recruit monocytes and macrophages to the infected tissue [6–8].

The pig has proven to be a valid model for human IAV infection; the pathogenesis of IAV infection is highly similar in pigs and humans, pigs are natural hosts for IAV and have extensive immunological and physiological similarities to humans, and pigs present clinical signs upon IAV infection that are comparable to humans' [9]. Porcine models for human IAV infection have been receiving increasing attention in recent years, but many aspects of the porcine local pulmonary tissue response are still unresolved. Particularly, there is a lack of knowledge regarding the role of microRNA (miRNA) involvement in the innate immune response against viral infections. Since their discovery in the early 1990ies, miRNAs have been demonstrated to be associated with a multitude of cellular and developmental processes [10–12]. miRNAs are a class of short (~22 nt) non-coding RNA molecules that regulate translation via antisense complementarity to target mRNA transcripts. miRNA-mRNA interaction will typically lead to destabilization and degradation of the mRNA target, thereby effectively inhibiting the protein output [13,14].

A vast range of pathologies have been found to induce changes in host miRNA expression, including many viral infections [15,16]. This has prompted research into the field of therapeutic and biomarker potential for miRNAs in viral infections and many other diseases. In recent years, several studies describing miRNA expression during IAV infection have emerged. Among these are studies in both animal [17,18] and *in vitro* [19–21] models demonstrating that different IAV strains and subtypes of varying virulence induce distinct miRNA responses in the host. Given the potential importance of miRNAs in the modulation of inflammatory responses [22,23], miRNAs are likely to play an important role in the refinement of the innate immune defense against IAV.

Investigations into miRNA regulation of innate immune processes have provided experimental evidence for a large number of miRNA-target interactions [24]. A number of *in silico* resources for miRNA target prediction are likewise available [25]. Combined, the large number of miRNAs that are experimentally validated or computationally predicted to target immune-related transcripts yields a long list of miRNAs for which the function in relation to IAV infection is important to clarify. miRNAs exert their function within the context of an intricate network, where each miRNA has the potential to target several mRNA transcripts, and in turn each mRNA may contain binding sites for many different miRNAs. Despite the availability of information on previously experimentally validated (e.g. [26,27]) as well as predicted miRNA-target interactions (e.g. [27,28]), it is therefore difficult to put forward hypotheses on miRNA expression and regulation. Small RNA sequencing (RNAseq) offers a hypothesis-free approach for researchers to investigate miRNA expression, as this method does not require any sequence specific primers or probes in order to perform miRNA quantification, in contrast to more traditional gene expression methodologies such as microarrays or reverse transcription quantitative real-time PCR (RT-qPCR). However, studies that comprehensively compare and validate miRNA expression results obtained by RNAseq and qPCR are scarce but greatly needed in order to generate valid and reproducible data in miRNA research.

Materials and methods

Animals and challenge

The challenge experiment will be described briefly, as details have been described previously [8]. All procedures and animal care was carried out in accordance with Good Clinical Practice (VICH GL9, CVMP/VICH/595/98), the Directive 2001/82/EC on the Community code relating to veterinary medicinal products, and German Animal Protection Law. The protocol IDT A 03/2004 was approved by the Landesverwaltungsamt Sachsen-Anhalt, Germany (Reference Number: AZ 42502-3-401 IDT). 25 pigs were included in the present study. 20 pigs were experimentally infected by aerosol exposure (6.0 l cell culture supernatant containing $10^{4.55}$ $TCID_{50}$/ml) to the Danish swine IAV strain A/sw/Denmark/12687/03 (H1N2) [29], and 5 unchallenged animals were used as controls; all animals were confirmed seronegative for IAV H1N1, H1N2, and H3N2 subtypes. Clinical signs (body temperature and dyspnea) were recorded during the first 72 h after challenge. Dyspnea was scored as described previously [8]: 0 = breathing unaffected; 1 = increased respiratory frequency and moderate flank movement; 2 = marked pumping breathing and severe flank movement; 3 = labored breathing affecting the entire body, pronounced flank movement and substantial movements of the snout; 4 = severe breathing reflecting substantial lack of oxygen. Infected animals were euthanized at 1 day (n = 6), 3 days (n = 6), and 14 days (n = 8) after challenge. Control animals (n = 5) were euthanized on day 14. Lung tissue samples of 500 mg were collected from the left cranial lobe from regions with no gross lesions, and immediately stabilized in RNA*later* (Qiagen) and stored at -20 °C. IAV content in lungs and nasal swabs was determined by RT-qPCR at several time points after challenge as previously described [8].

RNA extraction

Total RNA was isolated using M-tubes and a gentleMACS Octo Dissociator (Miltenyi Biotec) for tissue homogenization and the miRNeasy Mini Kit (Qiagen) for extraction, according to the manufacturer's specifications. For each sample, approx. 35 mg lung tissue was homogenized in 1 ml QIAzol Lysis Reagent (Qiagen). The lysate was mixed with 200 µl chloroform and centrifuged at 4 °C and 12,000xg

for 15 min. The rest of the procedure was carried out at room temperature. 300 µl of the upper aqueous phase was removed and mixed with 450 µl 99.9 % ethanol (ratio 1:1.5), and processed in the RNeasy Mini Spin Columns (supplied in kit) as specified by the manufacturer. An on-column DNase treatment was incorporated, using RNase-Free DNase Set (Qiagen); 80 µl DNase solution was pipetted directly onto the column membrane and incubated 15 min. Prior to elution, an additional centrifugation was performed at 12,000xg for 2 min to prevent any carryover of buffers to the elution. RNA was eluted in 50 µl RNase-free water by centrifugation at 8,000xg for 2 min.
RNA purity and concentration was determined using a NanoDrop ND-1000 UV spectrophotometer (Thermo Scientific); mean A260/280 ratio for all RNA samples was 2.1 and mean A260/230 ratio was 2.0, RNA yields ranged from 396 to 1158 ng/µl, mean yield was 753.1 ng/µl. RNA quality was estimated by measuring RNA integrity numbers (RIN) for each extraction, using Agilent RNA 6000 Nano Chips and Agilent RNA 6000 Nano reagents on an Agilent 2100 Bioanalyzer (Agilent Technologies); RIN varied from 5.4 to 8.7, with the mean RIN value being 6.4. The same RNA extractions were applied in both RNAseq and RT-qPCR.

Small RNA sequencing

All procedures related to library preparation, sequencing, and quality control was carried out by the sequencing provider Exiqon A/S (Vedbaek, Denmark). The RNA was diluted to 250 ng/µl in RNase-free water and a total of 8 µl (2 µg RNA) from each sample was supplied to Exiqon A/S for analysis. For each RNA sample, 1 µg of total RNA was converted into miRNA NGS libraries using the NEBNext Small RNA Library Prep Set for Illumina (New England BioLabs) according to the manufacturer's instructions. Each individual RNA sample had adaptors ligated to its 3' (AGATCGGAAGAGCACACGTCTGAACTCCAGTCACNNNNNATCTCGTATGCCGTCTTCTGCTTG) and 5' (AATGATACGGCGACCACCGAGATCACACGTTCAGAGTTCTACAGTCCGACGATC) ends and was converted into cDNA. The cDNA was pre-amplified by PCR (protocol and reagents supplied with NEBNext kit) using the following cycling parameters: initial denaturation at 94 °C for 30 seconds, 15 cycles of denaturation at 94 °C for 15 seconds, annealing at 62 °C for 20 seconds, and extension at 70 °C for 15 seconds, and concluded with final extension at 70 °C for 5 min. The 3' PCR primer was associated with a barcode sequence that was unique for each original RNA sample, thus allowing for differentiation of reads from different samples in the subsequent multiplex sequencing procedure of pooled cDNA samples. Libraries were purified using the QIAquick PCR Purification Kit (Qiagen), and the insert efficiency evaluated on a Bioanalyzer 2100 instrument on high sensitivity DNA chips (Agilent Technologies) to confirm a peak at ~140 nt corresponding to the length of adapter-ligated miRNAs. The miRNA cDNA libraries were size fractionated on a LabChip XT (Caliper Inc.) and a band representing adaptors and 15-40 nt insert (i.e. the size range covering miRNAs) excised according to the manufacturer's instructions. Samples were quantified using qPCR and subsequently pooled in equimolar concentrations. The library pool was used to generate clusters on the surface of a flow cell before sequencing using v3 sequencing methodology in accordance with manufacturer instructions (Illumina). Samples were sequenced on the Illumina NextSeq 500 system, yielding 50 nt single-ended reads of high quality (Q-score above 30). Raw sequencing data were supplied to the authors as compressed FASTQ files.

Small RNA sequencing data analysis

Adaptor sequences from the library preparation and sequencing were trimmed from the reads using Cutadapt v. 1.8 [30] (options applied: -a [3' adapter sequence, see above] -q 20 -m 16) thus retaining

only reads with a minimum length of 16 nt. Modules from the miRDeep2 package v. 2.0.0.5 was applied for the remaining sequencing data processing [31]. The mapper module was run to collapse trimmed reads with the following options: -e -h -i -j -m, supplying trimmed sequencing reads in .fq format and specifying an .fa output file with collapsed reads. Bowtie v. 1.0.0 was run with the following options [32]: -p 16 -f -n 1 -e 80 -l 16 -a -m 5 --best –strata [indexed genome file] --sam, using a pre-built indexed porcine genome from the iGenomes collection from Illumina ('susScr3' from UCSC built on the Sscrofa10.2 genome assembly [33], downloaded January 27th 2015 from here: https://support.illumina.com/sequencing/sequencing_software/igenome.html). The miRDeep2 module was supplied with .fa files with trimmed collapsed sequencing reads and the indexed porcine genome (see above), .arf file with reads mapped to the genome, and .fa files with known porcine miRNA sequences and known Homo sapiens, Bos taurus, and Mus musculus miRNA sequences, respectively.The latter was applied for the identification of potential novel (not yet annotated) porcine miRNAs candidates by comparing the obtained read sequences to known mature miRNAs from other species. All miRNA sequences were acquired from miRBase v. 21 [34].
Data was normalized individually for each sample using the number (millions) of mapped reads in that particular sample as normalization factor (performed by the quantifier module contained in miRDeep2). Normalized read counts were obtained from the miRDeep2 output file (.csv), and the remaining analysis for differential expression and statistical analysis was performed in Microsoft Excel. miRNA regulation was calculated as $\log_2$(fold change) ($\log_2$FC) of expression levels in a post-challenge group relative to the control group. A miRNA was considered to be differentially expressed if it was ≥50 % up- or down-regulated, i.e. $\log_2FC > 0.585$ or $\log_2FC < -0.585$, and significant in a *t*-test ($p < 0.05$, $\log_2$ transformed data), using the T.TEST() function in Microsoft Excel (two-tailed, equal variance).

miRNA RT-qPCR

RNA obtained from IAV infected porcine lung samples were reverse transcribed into cDNA and pre-amplified prior to high-throughput qPCR. 100 ng total RNA was applied in each cDNA synthesis in a reaction volume of 10 µl also containing 1 µM universal RT primer (5' CAGGTCCAGTTTTTTTTTTTTTTTVN 3'), 1 µl 10X poly(A) polymerase buffer (New England BioLabs), 0.1 mM ATP (New England BioLabs), 0.1 µM of each deoxynucleotide (dATP, dTTP, dGTP, and dCTP) (Sigma-Aldrich), 100 units MuLV reverse transcriptase (replaced with water in –RT control (no reverse transcriptase)) (New England BioLabs), 1 unit poly(A) polymerase (replaced with water in –poly(A) control (no poly(A) polymerase)) (New England BioLabs), and RNase-free water. The cDNA synthesis was carried out at 42 °C for 60 min followed by 95 °C for 5 min. Two cDNA replicates were synthesized from each RNA sample. All cDNA samples were pre-amplified prior to qPCR. Pre-amplification reactions contained 2.5 µl cDNA (diluted 1:10 in low-EDTA TE buffer (VWR – Bie & Berntsen)), 5 µl TaqMan PreAmp Master Mix (Applied Biosystems), and 2.5 µl 200 nM pre-amplification primer pool. The primer pool contained all primers to be included in the subsequent qPCR (at 200 nM each). Pre-amplification parameters were as follows: 95 °C for 10 min followed by 14 cycles of 95 °C for 15 seconds and 60 °C for 4 min. Residual primers were digested by adding 16 units of Exonuclease I (New England BioLabs) at 37 °C for 30 min followed by 80 °C for 15 min. All miRNA primers, including the universal RT primer, were designed as described previously [35] and purchased from Sigma-Aldrich. Whenever a porcine version of a miRNA was and available in miRBase at the time of primer design, this sequence was used (indicated by the prefix ssc). Otherwise, the sequence of the human (hsa) (or mouse, mmu, in the case of novel miRNAs from sequencing data)

homolog was used instead. Sequences and qPCR efficiencies for all primers can be found in S1 Table. The majority of miRNAs assayed by RT-qPCR were chosen based on RNAseq results. Additional miRNAs not detected by sequencing were also included in the qPCR analysis, based on our previous work and literature studies. qPCR was carried out in 96.96 Dynamic Array IFC chips using the high-throughput BioMark HD real-time platform (Fluidigm). For each sample, 1.5 µl pre-amplified cDNA (diluted 1:10 in low-EDTA TE buffer (VWR – Bie & Berntsen)) was combined with 3 µl ABI TaqMan Gene Expression Master Mix (Applied Biosystems), 0.3 µl 20X DNA Binding Dye Sample Loading Reagent (Fluidigm), 0.3 µl 20X EvaGreen (Biotium, VWR – Bie & Berntsen), and 0.9 µl low-EDTA TE buffer (VWR – Bie & Berntsen). qPCR primers were prepared by mixing 3 µl primer pair (forward and reverse, 10 µM each) with 3 µl 2X Assay Loading Reagent (Fluidigm). 96 sample mixes (including a non-template control, using water instead of cDNA) and 96 primer mixes were added to the 96.96 Dynamic Array IFC chip, and a total of 9,216 qPCR reactions were carried out in parallel. Dilution series were prepared from a pool of all samples (except –RT and –poly(A) controls) and included in the qPCR to assess primer efficiency. The following thermal protocol was applied: a thermal mix phase consisting of 2 min at 50 °C, 30 min at 70 °C, and 10 min at 25 °C; a hot start phase consisting of 2 min at 50 °C and 10 min at 95 °C; 35 cycles of denaturing for 15 seconds at 95 °C and annealing/elongation for 1 min at 60 °C, with fluorescence being recorded at the end of each cycle. Melting curve analysis was performed lastly by increasing the temperature form 60 to 95 °C at a speed of 1 °C/3 seconds.

miRNA qPCR data analysis

All amplification and melting curves were visually inspected using the Fluidigm Real-Time PCR Analysis software (v. 4.1.3). Primer efficiency was assessed for each assay from the standard curves produced from the included dilution series and subsequently used to adjust the C_q values in the individual assays. Primer efficiencies ranged from 92 to 119 %. miRNA qPCR data was normalized using the global mean expression method [36] and cDNA replicates were averaged. C_q values were converted to relative quantities on the linear scale. miRNA regulation was calculated as $\log_2$FC of expression levels in a post-challenge group relative to the control group. A miRNA was considered to be differentially expressed if it was ≥50 % up- or down-regulated, i.e. $\log_2 FC > 0.585$ or $\log_2 FC < -0.585$, and significant in a *t*-test ($p < 0.05$, $\log_2$ transformed data), using the T.TEST() function in Microsoft Excel (two-tailed, equal variance).

RT-qPCR of protein coding genes

For mRNA, the cDNA synthesis was performed with 500 ng RNA using the QuantiTect Reverse Transcription Kit (Qiagen). Any residual genomic DNA was removed from the RNA sample by incubating with 2 µl gDNA Wipeout Buffer (Qiagen) in a total reaction volume of 14 µl (in RNase-free water) at 42 °C for 2 min. Next, 6 µl reverse transcription master mix containing 0.75 µl Quantiscript Reverse Transcriptase (replaced with water in –RT control), 1 µl RT Primer Mix (mix of oligo-dT and random primers), 4 µl Quantiscript RT Buffer, and 0.25 µl RNase-free water was added to each sample. cDNA was synthesized at 42 °C for 15 min followed by 95 °C for 3 min. Two cDNA replicates were synthesized from each RNA sample. cDNA was diluted 1:10 in low-EDTA TE buffer prior to pre-amplification and exonuclease treatment, which was carried out as described above (section 'miRNA RT-qPCR') using 16 cycles of amplification. Highly specific mRNA primers were designed according to specification previously described [37] using Primer3 (http://bioinfo.ut.ee/primer3-0.4.0/). Included in the panel of assayed genes were a number of potential reference genes ('housekeeping genes')

that would later be evaluated for their suitability for data normalization. Dilution series were prepared from a pool of all samples and included in the qPCR (except the –RT control) to assess primer efficiency. Sequences and qPCR efficiencies for all primers can be found in S1 Table. High-throughput qPCR was carried out on the BioMark HD real-time instrument (Fluidigm) in a setup identical to that described for miRNA (section 'miRNA RT-qPCR').

mRNA qPCR data analysis

All amplification and melting curves were visually inspected using the Fluidigm Real-Time PCR Analysis software (v. 4.1.3). Primer efficiency was assessed from the standard curves used to adjust the C_q values in the individual assays. Primer efficiencies ranged from 95 to 113 %. Potential reference genes were evaluated using the algorithms geNorm [38] and NormFinder [39], and β-actin (*ACTB*), β2 microglobulin (*B2M*), glyceraldehyde 3-phosphate dehydrogenase (*GAPDH*), peptidylprolyl isomerase A (*PPIA*), 60S ribosomal protein L13A (*RPL13A*), and tyrosine 3-monooxygenase/tryptophan 5-monooxygenase activation protein, zeta polypeptide (*YWHAZ*) were applied for mRNA qPCR data normalization. cDNA replicates were averaged and C_q values were converted to relative quantities on the linear scale. mRNA regulation was calculated as $\log_2$FC of expression levels in a post-challenge group relative to the control group. A protein coding gene was considered to be differentially expressed if it was ≥100 % up- or down-regulated, i.e. $\log_2 FC > 1$ or $\log_2 FC < -1$, and significant in a *t*-test ($p < 0.05$, $\log_2$ transformed data), using the T.TEST() function in Microsoft Excel (two-tailed, equal variance).

miRNA-mRNA interactions

Using online tools and databases (see below), potential mRNA targets among the assayed protein coding genes were identified for miRNAs found to be differentially expressed after IAV challenge. As very little experimental target validation has been performed for porcine miRNAs, the human miRNA homologs as well as protein coding genes were applied for target identification and prediction. A comparison of porcine and human miRNA sequences applied in miRNA-mRNA interaction analysis can be found in S1 Table. One differentially expressed miRNA was excluded from these analyses, as no human homolog has yet been annotated (ssc-miR-7134-5p, first identified in a previous study of ours [40]). Using each miRNA as input in a 'single name' search in the RAIN database v. 1.0 [27], which integrates non-coding RNA interactions and associations with the protein-protein interaction database STRING v. 10.5 [41], previously experimentally validated and computationally predicted targets were identified by applying the following settings: 'active interaction sources' – only 'experiments' and 'databases'; 'minimum required interaction score' – 'low confidence (0.150)'; 'max number of interactions to show' – custom value of 300 for 1st shell (300 was chosen as this number proved to exceed the final number of nodes in the resulting network for any of the miRNAs, thus ensuring that all possible interactions were shown). No 2nd shell interactions were included. As RAIN due to licensing restrictions does not integrate information from TarBase or target predictions by microT-CDS from DIANA Lab, previously experimentally validated and computationally predicted targets were likewise identified from these two sources. Searches in TarBase v. 7.0 [26] were made using the following settings: 'species' – '*Homo sapiens*'; 'validation type' – 'direct'; 'validated as' – 'positive'. Targets were predicted with microT-CDS v. 5.0 [28] by applying the default score threshold of 0.7. For all validated or predicted miRNA-mRNA interactions obtained from RAIN, TarBase, and microT-CDS, Pearson's correlation coefficient (Pearson's *r*) was calculated for miRNA and mRNA expression data (qPCR) on day 1 and 3 post challenge. If a negative correlation of $r < -0.532$ ($p < 0.05$)

was seen, that particular miRNA-mRNA interaction was regarded as potentially relevant in the regulation of innate immune response in pigs during active IAV infection.
The RAIN database v. 1.0 [27] was likewise applied to identify cellular pathways that could potentially be affected by the differentially expressed miRNAs. Two subsets of differentially expressed miRNAs were applied as input in 'multiple names' search in RAIN: 1) miRNAs up-regulated during acute infection on day 1 and/or 3 after challenge and 2) miRNAs down-regulated during acute infection on day 1 and/or 3 after challenge. The following settings were applied to obtain miRNA-target interaction networks in STRING [41]: 'active interaction sources' – only 'experiments' and 'databases'; 'minimum required interaction score' – 'medium confidence (0.400)'; 'max number of interactions to show' – custom value of 300 for 1st shell (300 was chosen as this number proved to exceed the final number of nodes in the resulting network for any of the four sets of miRNAs, thus ensuring that all possible interactions were shown). No 2nd shell interactions were included. KEGG Pathway enrichment analysis [42] (integrated in STRING) was performed on the collection of targets identified for each set of the differentially expressed miRNAs.

Results

Animals and challenge

Clinical signs of IAV infection were observed in infected animals during the three first days following challenge. Fever peaked on day 1 after challenge with a mean temperature of 41 °C, which dropped to 39.9 °C on day 3. Dyspnea was likewise most severe on day 1 with a mean score of 2.4, decreasing to 0.8 on day 3. No clinical signs were observed in control animals. As reported previously [8], the challenge strain could be detected by qPCR in lung tissue on day 1 and 3 after challenge and in nasal swabs on day 1, 3, 5, and 7 after challenge. No IAV could be detected on day 14 in nasal swabs or lung tissue [8].

Small RNA sequencing

Length distribution of reads (after adapter trimming) showed an expected peak around 18-23 nt, corresponding to typical miRNA length. The total number of reads obtained after sequencing ranged from 10.5 to 26.2 million per sample, averaging on 19.5 million. Of these, an average of 14.9 million reads mapped to the porcine genome, with an average of 7.5 million reads mapping to known miRNAs. A total of 238 mature annotated porcine miRNAs could be detected in all of the samples (see S2 Table).
61 novel mature miRNA candidate sequences were obtained from the miRDeep2 pipeline and subjected to BLASTN search in the miRBase database (v. 21) [34] to identify miRNA homologs in other species. The best matching human homolog was chosen (highest score, lowest *E*-value), unless a homolog from another species was a better match than the human homolog (higher score, lower *E*-value). Of the 61 candidate sequences, human homologs were identified for 12, mouse homologs for two, and a bovine homolog for one sequence, respectively (Table 1). More details (including candidate hairpin sequences and scores and E-values from BLASTN) can be found in S3 Table. These 15 miRNA homologs were subsequently included in qPCR analyses.
Fold changes of miRNA expression (known and novel candidates) in lung tissue of infected animals relative to the uninfected control animals were calculated. These results are shown in volcano plots in Fig 1, highlighting the number of differentially expressed miRNAs at each of the post-challenge time points, i.e. statistically significant up- or down-regulation. Log_2FC of all detected miRNAs are

summarized in S4 Table. A total of 49 miRNAs were found to be differentially expressed at one or more time points ($p < 0.05$) (Fig 2).

Table 1. Predicted novel porcine miRNA candidates and their known miRNA homologs.

Novel porcine miRNA candidate	Novel porcine miRNA candidate sequence identified in RNAseq data	Homolog miRNA	Homolog accession number	Homolog miRNA sequence
ssc-miR-novel-1	uucaaguaauucaggauaguu	bta-miR-26b	MIMAT0003531	uucaaguaauucaggauaguu
ssc-miR-novel-2	aaucacuaauuccacugccauc	mmu-miR-34b-3p	MIMAT0000382	aaucacuaacuccacugccauc
ssc-miR-novel-3*	aggcaguguaauuagcugauug**u**	mmu-miR-34b-5p	MIMAT0004581	aggcaguguaauuagcugauug
ssc-miR-novel-4*	uaacacugucugguaaagaug	hsa-miR-141-3p	MIMAT0000432	uaacacugucugguaaagaug**g**
ssc-miR-novel-5	caucuuccagcacaguguugga	hsa-miR-141-5p	MIMAT0004598	caucuuccaguacaguguugga
ssc-miR-novel-6	caucccuugcaugguggaggg	hsa-miR-188-5p	MIMAT0000457	caucccuugcaugguggaggg
ssc-miR-novel-7	uaauacugccugguaaugauga	hsa-miR-200b-3p	MIMAT0000318	uaauacugccugguaaugauga
ssc-miR-novel-8	caucuuacugggcagcauugga	hsa-miR-200b-5p	MIMAT0004571	caucuuacugggcagcauugga
ssc-miR-novel-9	uaauacugccggguaaugaugga	hsa-miR-200c-3p	MIMAT0000617	uaauacugccggguaaugaugga
ssc-miR-novel-10	uuuguucguucggcucgcguga	hsa-miR-375	MIMAT0000728	uuuguucguucggcucgcguga
ssc-miR-novel-11	uggcaguguauuguuagcuggu	hsa-miR-449a	MIMAT0001541	uggcaguguauuguuagcuggu
ssc-miR-novel-12	aggcaguguauuguuagcuggc	hsa-miR-449b-5p	MIMAT0003327	aggcaguguauuguuagcuggc
ssc-miR-novel-13	uagugcaauauugcuuauagggu	hsa-miR-454-3p	MIMAT0003885	uagugcaauauugcuuauagggu
ssc-miR-novel-14	uaauuuuauguauaagcuagu	hsa-miR-590-3p	MIMAT0004801	uaauuuuauguauaagcuagu
ssc-miR-novel-15	uacccauugcauaucggaguug	hsa-miR-660-5p	MIMAT0003338	uacccauugcauaucggaguug

When equally identical homologs were found in several species, the human homolog is shown here. Species specific prefixes are as follows: ssc - *Sus scrofa*, hsa - *Homo sapiens*, bta - *Bos taurus*, and mmu - *Mus musculus*. * indicates that the novel porcine sequence is not 100 % identical to its matching homolog (see underlined bold nucleotides).

Fig 1. Volcano plots showing miRNA expression changes as obtained by RNAseq. A) day 1 after challenge, B) day 3 after challenge, C) day 14 after challenge. x-axes show the $\log_2$FC values of post-challenge time points vs. unchallenged controls. 50 % up- or down-regulation is denoted by vertical dotted lines ($\log_2$FC > 0.585, $\log_2$FC < -0.585). y-axes show the $-\log_{10}$ transformed p-values obtained from *t*-tests. $p = 0.05$ is denoted by a horizontal red line. miRNAs that pass the criteria for differential expression are marked with a number denoting their identity; miRNAs that appear in more than one

volcano plot are marked with the same number in all plots. All log_2FC values can be found in S4 Table. 1 ssc-miR-205; 2 ssc-miR-146b; 3 ssc-miR-34c; 4 ssc-miR-671-5p; 5 ssc-miR-708-3p; 6 mmu-miR-34b-5p; 7 ssc-miR-129a; 8 ssc-miR-339-3p; 9 ssc-miR-193a-3p; 10 ssc-miR-187; 11 ssc-miR-1296-5p; 12 ssc-miR-129b; 13 ssc-miR-2320-3p; 14 ssc-miR-183; 15 ssc-miR-328; 16 ssc-miR-128; 17 hsa-miR-449a; 18 ssc-miR-139-3p; 19 ssc-miR-551a; 20 ssc-miR-671-3p; 21 ssc-miR-92b-5p; 22 ssc-miR-184; 23 ssc-miR-190b; 24 mmu-miR-34b-3p; 25 ssc-miR-1343; 26 ssc-miR-7134-5p; 27 ssc-miR-92b-3p; 28 hsa-miR-375; 29 ssc-miR-296-3p; 30 ssc-miR-744; 31 ssc-miR-20a; 32 ssc-miR-142-5p; 33 ssc-miR-504; 34 ssc-miR-29b; 35 ssc-miR-221-5p; 36 ssc-miR-144; 37 mmu-miR-34b-3p; 38 ssc-miR-486; 39 ssc-miR-451; 40 ssc-miR-365-5p; 41 ssc-miR-326; 42 ssc-miR-217; 43 ssc-miR-196-5p; 44 ssc-miR-183; 45 ssc-miR-139-5p; 46 ssc-miR-30c-1-3p; 47 ssc-miR-7139-3p; 48 ssc-miR-1249; 49 ssc-miR-133b.

Fig 2. Venn diagram comparing differentially expressed miRNAs identified by and qPCR and RNAseq. Overlap of miRNAs found to be differentially expressed at one or more post-challenge time points by RNAseq (yellow) and qPCR (blue). †miRNAs assayed by qPCR but not detected by sequencing; *miRNAs detected by sequencing, but not assayed by qPCR. When a known porcine (ssc) sequence for a given miRNA was not available in miRBase (v. 21), human (hsa) or mouse (mmu) names are applied in accordance with the homolog that best matched the novel porcine miRNA discovered in the RNAseq data, and these homolog sequences were likewise used for qPCR primer design.

Comparison of RNAseq and qPCR results

qPCR expression data was obtained for a total of 80 miRNA (see S5 Table); 27 of these met the criteria for being differentially expressed (log_2FC > 0.585 or log_2FC < -0.585, $p < 0.05$ (*t*-test)) (Table 2). Generally, good agreement was found between RNAseq and qPCR results. For those miRNAs found to be differentially expressed at one or more time points after challenge by at least one of the methods, a significant positive sample-wise correlation (Pearson's *r*, $p < 0.05$) of normalized RNAseq and qPCR expression values was seen for 74 % of the miRNAs. Expression patterns for miRNAs found to be differentially expressed at one or more time points after challenge obtained with the two methods are compared in Fig 3. Linear regression showed an R^2 of 0.6244, and a highly significant positive correlation (Pearson's *r*) ($r = 0.8$, $p < 0.01$).

Results from both methods concur that day 3 is the time point where there is the highest number of differentially expressed miRNAs (Table 2). qPCR analysis on day 3 showed 19 miRNAs to be differentially expressed relative to the control group; only roughly half as many were differentially expressed on day 1 and 14. Only two miRNAs were significantly changed throughout the whole experiment: ssc-miR-34c and ssc-miR-92b-3p. Both were down-regulated at very similar levels at all post-challenge time points.

Table 2. Differential expression of miRNAs measured by qPCR in pig lungs after IAV challenge relative to unchallenged controls.

	Day 1 after challenge relative to control group		Day 3 after challenge relative to control group		Day 14 after challenge relative to control group	
miRNA	log_2FC (lower 95 % CI; upper 95 % CI)	*p* (*t*-test)	log_2FC (lower 95 % CI; upper 95 % CI)	*p* (*t*-test)	log_2FC (lower 95 % CI; upper 95 % CI)	*p* (*t*-test)

ssc-miR-7	**1.2 (0.79; 1.5)**	**0.0019**	0.70 (0.15; 1.1)	0.065	-0.43 (-0.67; -0.22)	0.13
ssc-miR-15a†	0.41 (0.25; 0.56)	0.0070	**0.63 (0.53; 0.73)**	**8.9E-05**	0.23 (0.049; 0.39)	0.10
ssc-miR-18a	0.12 (-0.16; 0.37)	0.57	**0.65 (0.45; 0.81)**	**0.0033**	0.36 (0.18; 0.53)	0.043
ssc-miR-21	-0.12 (-0.39; 0.11)	0.50	**0.75 (0.65; 0.84)**	**0.00016**	0.27 (0.085; 0.44)	0.096
ssc-miR-29b	0.37 (0.17; 0.54)	0.020	**0.58 (0.38; 0.76)**	**0.0014**	-0.12 (-0.30; 0.038)	0.28
mmu-miR-34b-3p	-0.76 (-1.5; -0.28)	0.058	**-1.0 (-1.3; -0.85)**	**0.0019**	-0.56 (-0.93; -0.26)	0.079
ssc-miR-34c	**-1.0 (-1.5; -0.67)**	**0.0026**	**-2.2 (-3.3; -1.6)**	**0.00026**	**-0.95 (-1.3; -0.66)**	**0.0029**
ssc-miR-92b-3p	**-0.85 (-1.2; -0.57)**	**0.0045**	**-2.2 (-2.6; -1.9)**	**3.4E-06**	**-1.2 (-1.4; -0.98)**	**9.4E-05**
ssc-miR-146a-5p	**-0.58 (-0.91; -0.30)**	**0.034**	-0.43 (-0.86; -0.098)	0.10	-0.087 (-0.35; 0.13)	0.65
ssc-miR-184	-0.60 (-1.9; 0.072)	0.27	**-1.1 (-1.5; -0.78)**	**0.047**	-0.25 (-0.70; 0.094)	0.74
ssc-miR-193a-3p	**0.58 (0.36; 0.78)**	**0.0028**	**0.73 (0.43; 0.97)**	**0.0017**	0.16 (-0.10; 0.38)	0.46
ssc-miR-205	**-1.1 (-1.8; -0.64)**	**0.028**	**-2.2 (-2.7; -1.8)**	**0.00021**	0.088 (-0.41; 0.46)	0.84
ssc-miR-221-5p	**1.1 (0.56; 1.5)**	**0.0066**	**1.1 (0.15; 1.7)**	**0.040**	-0.31 (-1.2; 0.22)	0.27
hsa-miR-223-5p†	0.57 (0.32; 0.79)	0.023	**1.1 (0.86; 1.4)**	**0.00042**	0.17 (-0.068; 0.37)	0.40
ssc-miR-296-3p	-0.12 (-0.38; 0.10)	0.58	**-0.67 (-0.96; -0.43)**	**0.016**	**-0.57 (-0.82; -0.36)**	**0.015**
ssc-miR-363	0.20 (-0.057; 0.42)	0.40	**0.69 (0.44; 0.90)**	**0.011**	-0.10 (-0.33; 0.095)	0.76
hsa-miR-375	**-0.82 (-1.1; -0.61)**	**0.00031**	**-0.78 (-1.2; -0.43)**	**0.0053**	-0.11 (-0.26; 0.023)	0.30
ssc-miR-378	-0.28 (-0.40; -0.17)	0.18	-0.42 (-0.47; -0.38)	0.042	**-0.62 (-0.91; -0.37)**	**0.018**
hsa-miR-449a	-0.28 (-0.78; 0.086)	0.25	-0.50 (-1.1; -0.059)	0.10	**0.77 (0.47; 1.0)**	**0.0060**
hsa-miR-449b-5p	-0.38 (-0.90; 0.0040)	0.18	-0.59 (-1.2; -0.16)	0.076	**0.73 (0.48; 0.95)**	**0.0058**
ssc-miR-451	0.84 (-0.71; 1.6)	0.20	1.4 (-1.2; 2.3)	0.080	**1.4 (0.37; 2.0)**	**0.045**
ssc-miR-551a	-0.15 (-0.40; 0.059)	0.35	**-0.82 (-1.1; -0.57)**	**0.0035**	**-1.0 (-1.3; -0.75)**	**0.00022**
hsa-miR-590-3p†	0.36 (0.049; 0.61)	0.14	**0.74 (0.23; 1.1)**	**0.027**	-0.026 (-0.35; 0.24)	0.86
ssc-miR-671-3p	-0.43 (-0.69; -0.21)	0.021	-0.36 (-0.66; -0.11)	0.057	**-0.58 (-0.69; -0.48)**	**6.7E-05**
ssc-miR-708-5p	**-0.74 (-0.90: -0.60)**	**0.0022**	-0.43 (-0.88; -0.080)	0.14	-0.67 (-1.0; -0.41)	**0.014**

ssc-miR-1343	-0.40 (-0.69; -0.15)	0.073	**-0.91 (-1.2; -0.66)**	**0.0016**	-0.21 (-0.38; -0.058)	0.23
ssc-miR-7134-5p	-0.46 (-0.82; -0.17)	0.040	**-0.98 (-1.2; -0.79)**	**0.00013**	**-0.73 (-0.91; -0.57)**	**0.00035**

Log_2FC of miRNA expression on day 1, 3, and 14 after IAV challenge relative to unchallenged controls. Lower and upper limits for 95 % confidence interval are given in parentheses. Data in bold text are those that meet the criteria for differential expression (see text). *p*-values were obtained from *t*-test between the control group and a post-challenge group. †miRNAs that were not identified in RNAseq data.

Fig 3. Comparison of miRNA log_2FC as measured by RNAseq and qPCR. Log_2FC (challenged group vs. control group) obtained by qPCR is plotted against the corresponding log_2FC obtained by RNAseq. Each point represents log_2FC of one miRNA on day 1 (black), day 3 (white), or day 14 (grey) after challenge.

qPCR of protein coding genes

Analysis of differential expression of protein coding genes was focused primarily on factors of the antiviral innate immune system and apoptosis, thus gathering a thorough characterization of the processes that are engaged to combat the IAV infection locally in the lung of our pig model. A total of 49 genes were identified by RT-qPCR as being differentially expressed (log_2FC > 1 or log_2FC < -1, p < 0.05 (*t*-test)) in the lung at one or more time points after infection (Table 3).

A dramatic interferon response dominated on day 1 after challenge, demonstrated by a log_2FC of 8.7 and 6.3 for *IFNL3* (IFN-λ3) and *IFNB1* (IFN-β), respectively. The most strongly up-regulated PRRs were the two cytoplasmic RLRs RIG-I (*DDX58*) and MDA5 (*IFIH1*) (log_2FC 6.1 and 3.5 on day 1 after challenge, respectively). Other up-regulated PRRs included TLRs 3 and 7 (log_2FC 2.5 and 1.8 on day 1 after challenge, respectively). These four PRRs all remained significantly up-regulated on day 3 after challenge. Several cytokines with both pro- and anti-inflammatory functions were also up-regulated on day 1 and (partly) day 3 after challenge, including *IL1B* (IL-1β), *IL6* (IL-6), *IL1RN* (IL-1RA), and *IL10* (IL-10). The only cytokine to demonstrate down-regulation in response to IAV infection was the pro-inflammatory *IL18* (IL-18). A strong chemokine response, especially by *CCL2* (CCL2) and *CXCL10* (CXCL10), was also detected on day 1 after challenge. Additionally, the importance of apoptosis in the response to IAV infection was clearly demonstrated by the early up-regulation of e.g. genes related to the Jak/STAT signaling pathway (*STAT1*, *STAT2*, *JAK2*, *IRF2*, *IRF7*, *SOCS1*), as well as caspases 1 and 3 (*CASP1*, *CASP3*), Bcl-2 (*BLC2*), Mcl-1 (*MCL1*), and protein kinase R (*EIF2AK2*).

Only one of the assayed protein coding genes was regulated on day 14 after challenge: the positive acute-phase protein (APP) serum amyloid A (*SAA*) showed a log_2FC of -2.6 at this time point. SAA was not differentially expressed at earlier time points; however, transferrin (*TF*) and PAI-1 (*SERPINE1*) were regulated on day 3 after challenge in accordance with their roles as negative and positive APPs (log_2FC -1.4 and 2.2, respectively).

Table 3. Differential expression of protein coding genes in pig lungs after IAV infection relative to unchallenged controls.

		Day 1 after challenge relative to control group		Day 3 after challenge relative to control group		Day 14 after challenge relative to control group	
Gene product	Gene	log_2(FC)	*p* (*t*-test)	log_2(FC)	*p* (*t*-	log_2(FC)	*p* (*t*-

		(lower 95 % CI; upper 95 % CI)		(lower 95 % CI; upper 95 % CI)	test)	(lower 95 % CI; upper 95 % CI)	test)
Pathogen recognition receptors and downstream signaling							
TLR3 (Toll-like receptor 3)	*TLR3*	**2.5 (2.1; 2.8)**	**2.30E-06**	**1.4 (1.0; 1.7)**	**0.00021**	0.35 (0.16; 0.52)	0.063
TLR7 (Toll-like receptor 7)	*TLR7*	**1.8 (1.2; 2.2)**	**0.00030**	0.84 (0.28; 1.2)	0.066	-0.25 (-0.78; 0.13)	0.38
RIG-I (retinoic acid-inducible gene I)	*DDX58*	**6.1 (5.7; 6.5)**	**2.30E-07**	**3.8 (2.4; 4.4)**	**0.0028**	0.33 (-1.9; 1.2)	0.86
MDA5 (melanoma differentiation-associated protein 5)	*IFIH1*	**3.5 (3.1; 3.8)**	**0.0000010**	**1.7 (0.67; 2.3)**	**0.025**	-0.18 (-2.1; 0.62)	0.31
MYD88 (myeloid differentiation primary response gene 88)	*MYD88*	**1.1 (0.83; 1.3)**	**0.0095**	0.24 (-0.039; 0.47)	0.23	-0.44 (-0.74; -0.20)	0.71
IRAK1 (interleukin-1 receptor-associated kinase 1)	*IRAK1*	0.63 (0.25; 0.93)	0.085	**1.0 (0.61; 1.3)**	**0.023**	0.085 (-0.42; 0.46)	0.59
TRAM (TIR domain-containing adapter molecule 2)	*TICAM2*	**2.0 (1.1; 2.6)**	**0.0012**	0.31 (-0.61; 0.67)	0.36	-0.63 (-0.76; -0.50)	0.000021
IKK-β (inhibitor of nuclear factor kappa-B kinase subunit beta)	*IKBKB*	**1.9 (1.6; 2.1)**	**0.000013**	**1.1 (0.80; 1.4)**	**0.0016**	0.081 (-0.20; 0.32)	0.76
Cytokines and chemokines							
TNF (tumor necrosis factor)	*TNF*	**1.5 (1.0; 1.8)**	**0.0026**	0.46 (0.085; 0.76)	0.15	0.73 (0.24; 1.1)	0.15
IL-1β (interleukin 1β)	*IL1B*	**3.1 (1.4; 3.9)**	**0.0018**	0.86 (-1.2; 1.7)	0.65	-0.82 (-1.1; -0.57)	0.0087
IL-1RA (interleukin 1 receptor antagonist)	*IL1RN*	**4.6 (4.0; 5.1)**	**2.2E-07**	**2.9 (1.7; 3.5)**	**0.00099**	0.077 (-0.4; 0.44)	0.96
IL-6 (interleukin 6)	*IL6*	**4.7 (3.3; 5.4)**	**0.000046**	**2.7 (1.4; 3.4)**	**0.0021**	0.51 (-0.096; 0.93)	0.25
IL-10 (interleukin 10)	*IL10*	**2.0 (1.7; 2.2)**	**0.000033**	0.69 (-0.27; 1.3)	0.24	-0.19 (-0.69; 0.18)	0.50

IL-12β (interleukin 12 subunit β)	*IL12B*	**2.3 (1.6; 2.8)**	**0.00036**	-0.028 (-0.78; 0.46)	0.81	-0.081 (-0.46; 0.22)	0.90
IL-15 (interleukin 15)	*IL15*	**1.5 (0.93; 1.9)**	**0.0017**	-0.029 (-0.55; 0.35)	0.87	-0.55 (-0.83; -0.32)	0.036
IL-18 (interleukin 18)	*IL18*	**-1.2 (-2.1; -0.59)**	**0.043**	-0.61 (-1.8; 0.028)	0.23	0.075 (-0.40; 0.43)	0.73
CCL2 (chemokine (C-C motif) ligand 2)	*CCL2*	**3.3 (2.4; 3.9)**	**0.000054**	**1.7 (0.54; 2.4)**	**0.028**	0.15 (-0.13; 0.38)	0.48
CCL3 (chemokine (C-C motif) ligand 3)	*CCL3*	**1.7 (0.75; 2.2)**	**0.0017**	0.36 (-0.50; 0.90)	0.64	-0.53 (-1.6; 0.067)	0.091
CXCL2 (chemokine (C-X-C motif) ligand 2)	*CXCL2*	**2.5 (1.7; 3.0)**	**0.0013**	1.2 (0.0023; 1.8)	0.11	0.38 (-0.073; 0.73)	0.30
CXCL10 (chemokine (C-X-C motif) ligand 10)	*CXCL10*	**5.5 (4.7; 6.0)**	**3.0E-06**	2.7 (0.72; 3.6)	0.057	-0.37 (-3.5; 0.54)	0.32
Interferon and interferon stimulated genes							
IFN-λ3 (interferon-λ3)	*IFNL3*	**8.7 (7.8; 9.2)**	**2.2E-08**	**6.1 (3.3; 7.0)**	**0.0014**	1.2 (0.33; 1.7)	0.098
IFN-β (interferon-β)	*IFNB1*	**6.3 (5.3; 6.9)**	**1.5E-06**	**4.6 (3.2; 5.3)**	**0.00057**	0.71 (-0.15; 1.2)	0.43
ISG15 (interferon-stimulated gene 15)	*ISG15*	**6.3 (5.9; 6.7)**	**6.3E-07**	**4.0 (2.6; 4.7)**	**0.012**	1.1 (0.0; 2.6)	0.50
IFITM1 (interferon-induced transmembrane protein 1)	*IFITM1*	**3.6 (3.2; 3.9)**	**7.4E-07**	**2.0 (1.2; 2.5)**	**0.0057**	0.25 (-2.7; 1.1)	0.74
IFITM3 (interferon-induced transmembrane protein 3)	*IFITM3*	**3.3 (2.7; 3.7)**	**0.000010**	**2.1 (1.3; 2.6)**	**0.0025**	0.23 (0.0; 1.2)	0.59
IRF2 (interferon regulatory factor 2)	*IRF2*	**1.8 (1.4; 2.1)**	**0.000060**	0.59 (0.013; 1.0)	0.086	-0.094 (-0.21; 0.012)	0.41
IRF7 (interferon regulatory factor 7)	*IRF7*	**4.7 (4.4; 5.0)**	**1.5E-07**	**3.0 (2.0; 3.6)**	**0.0064**	0.22 (-5.0; 1.2)	0.63
SOCS1 (suppressor of cytokine signalling 1)	*SOCS1*	**3.0 (2.4; 3.4)**	**0.000027**	**1.8 (0.91; 2.3)**	**0.0063**	-0.15 (-0.32; 0.013)	0.61
Mx1 (interferon-	*MX1*	**5.5 (5.1;**	**1.6E-07**	**3.4 (2.2;**	**0.012**	0.67 (0.0;	0.54

induced GTP-binding protein Mx1)		**5.8)**		**4.1)**		1.9)	
OASL (59 kDa 2'-5'-oligoadenylate synthetase-like protein)	*OASL*	**5.3 (4.9; 5.5)**	**2.5E-07**	**4.3 (3.2; 4.9)**	**0.018**	0.47 (0.0; 1.5)	0.73
OAS1 (2'-5'-oligoadenylate synthetase 1)	*OAS1*	**3.5 (3.2; 3.8)**	**3.8E-06**	**1.6 (0.90; 2.1)**	**0.022**	-0.74 (-2.9; 0.091)	0.09
PKR (protein kinase R)	*EIF2AK2*	**3.3 (3.0; 3.6)**	**1.8E-06**	**1.9 (1.1; 2.4)**	**0.015**	-0.16 (-1.3; 0.48)	0.52
RNase L (ribonuclease L)	*RNASEL*	**3.4 (3.0; 3.8)**	**9.6E-06**	1.4 (0.23; 2.0)	0.074	-0.24 (-0.76; 0.14)	0.62
STAT1 (signal transducer and activator of transcription 1)	*STAT1*	**3.4 (3.0; 3.7)**	**1.7E-07**	**2.1 (1.3; 2.5)**	**0.00020**	0.45 (0.10; 0.73)	0.15
STAT2 (signal transducer and activator of transcription 2)	*STAT2*	**2.7 (2.3; 3.0)**	**3.2E-06**	0.94 (0.17; 1.4)	0.11	-0.28 (-0.92; 0.17)	0.20
JAK2 (Janus kinase 2)	*JAK2*	**2.0 (1.6; 2.3)**	**0.0000097**	**1.2 (0.92; 1.4)**	**0.000016**	0.32 (0.13; 0.48)	0.047
Apoptosis							
CASP1 (caspase-1)	*CASP1*	**1.7 (1.3; 2.1)**	**0.0025**	0.69 (-0.075; 1.2)	0.26	-0.45 (-1.1; 0.0071)	0.39
CASP3 (caspase-3)	*CASP3*	**1.8 (1.4; 2.1)**	**0.00014**	**1.1 (0.90; 1.3)**	**0.000046**	0.42 (0.059; 0.70)	0.18
Bcl-2 (B-cell lymphoma 2)	*BCL2*	**2.3 (1.8; 2.7)**	**0.000061**	0.90 (0.45; 1.2)	0.012	0.31 (-0.19; 0.68)	0.45
Mcl-1 (induced myeloid leukemia cell differentiation protein Mcl-1)	*MCL1*	**1.5 (1.1; 1.9)**	**0.00015**	0.69 (0.37; 0.95)	0.0032	0.25 (0.63; 0.41)	0.079
FasR (FAS receptor)	*FAS*	**2.1 (1.4; 2.5)**	**0.00028**	0.93 (0.43; 1.3)	0.018	0.23 (-0.049; 0.47)	0.34
FasL (FAS ligand)	*FASLG*	**1.8 (1.5; 2.0)**	**0.00018**	0.82 (0.10; 1.3)	0.062	-0.16 (-0.45; 0.085)	0.79
GZMB (granzyme B)	*GZMB*	**1.7 (1.5; 1.9)**	**0.00062**	**1.0 (0.64; 1.3)**	**0.017**	-0.12 (-0.30; 0.043)	0.82
Acute phase proteins							
SAA (serum amyloid A)	*SAA*	0.90 (0.43; 1.3)	0.061	-0.12 (-1.0; 0.44)	0.80	**-2.6 (-3.2; -2.1)**	**0.00011**

PAI-1 (plasminogen activator inhibitor-1)	*SERPINE 1*	**2.5 (1.9; 3.0)**	**0.000038**	**2.2 (0.70; 2.9)**	**0.0063**	-0.016 (-0.80; 0.49)	0.60
TF (transferrin)	*TF*	-0.90 (-1.3; -0.59)	0.014	**-1.4 (-2.3; -0.85)**	**0.013**	-0.83 (-1.3; -0.45)	0.018
Others							
HMGB1 (high mobility group box 1)	*HMGB1*	**-1.1 (-1.3; 0.95)**	**0.000016**	-0.65 (-0.80; -0.52)	0.00026	-0.11 (-0.26; 0.028)	0.38
SEPT4 (septin-4)	*SEPT4*	**-1.2 (-1.7; -0.79)**	**0.0044**	-0.79 (-1.0; -0.60)	0.0098	-0.29 (-0.62; -0.018)	0.29
MUC1 (mucin-1)	*MUC1*	**1.6 (1.4; 1.8)**	**0.00018**	0.47 (-0.16; 0.90)	0.30	0.16 (-0.44; 0.58)	0.66

Log_2FC of mRNA expression on day 1, 3, and 14 after IAV challenge relative to unchallenged controls. Lower and upper limits for 95 % confidence interval are given in parentheses. Data in bold text are those that meet the criteria for differential expression (see text). *p*-values were obtained from *t*-test between the control group and a post-challenge group.

Target identification of differentially expressed miRNAs

Previously experimentally validated or computationally predicted targets (obtained with RAIN, TarBase, and microT-CDS) for the differentially expressed miRNAs among the protein coding genes assayed in the present study was identified using the RAIN database [27], TarBase v. 7.0 [26], and microT-CDS v. 5.0 [28]. For a number of these miRNA-mRNA interactions, a significant negative correlation ($r < -0.532$, $p < 0.05$) was seen for the expression during active viral infection on day 1 and 3 post challenge. These interactions are summarized in Fig 4. Potential functional implications of miRNA regulation was assessed by KEGG Pathway enrichment analysis of genes identified with RAIN to be validated or predicted targets of the subsets of miRNAs found to be up- or down-regulated during acute infection on day 1 and 3 after challenge. Substantial overlap of enriched pathways was seen for those two sets of target genes, including 'Influenza A' (ID 5164), 'Apoptosis' (ID 4210), 'Jak-STAT signaling' (ID 4630), 'NF-κB signaling' (ID 4064), 'Cytokine-cytokine receptor interaction' (ID 4060), 'Chemokine signaling' (ID 4062), and 'Endocytosis' (4144). Among the enriched pathways of relevance to IAV infection, the following were found to be enriched only in one of sets of target genes: 'B cell receptor signaling' (ID 4662), 'Natural killer cell mediated cytotoxicity' (ID 4650), and 'Antigen processing and presentation' (ID 4612) were enriched only in targets of up-regulated miRNAs on day 1 and 3 after challenge, and 'Toll-like receptor signaling' (4620), 'NOD-like receptor signaling' (ID 4621), and 'RIG-I-like receptor signaling' (ID 4622) were enriched only in targets of down-regulated miRNAs on day 1 and 3 after challenge. The miRNA-target interaction networks that form the basis for the KEGG Pathway enrichment analysis can be viewed in S1 and S2 Figs.

Fig 4. Potential miRNA-mRNA interactions. Expression of eight of the assayed miRNAs showed significant negative correlation with expression of protein coding genes that were identified (using RAIN v1.0 [27], TarBase v. 7.0 [26], and/or microT-CDS [28]) to be experimentally validated targets of the miRNA (solid lines), computationally predicted targets of the miRNA (dotted lines), or both (solid lines, underlined gene names).

Discussion

Temporal dynamics of the antiviral response

Transcriptional analysis showed several known miRNAs and novel miRNA candidates to be differentially expressed in the lungs of pigs experimentally infected with H1N2 swine IAV relative to lung tissue from healthy controls. Differentially expressed miRNAs were identified at all examined post-challenge time points (day 1, 3, and 14 after challenge). To the best of our knowledge, this is the first study to present global characterization of miRNA expression in pig lungs after IAV infection. However, several of the miRNAs we found to be differentially expressed have previously been reported to display similar regulation in mouse lung tissue during acute infection after challenge with seasonal H1N1 [18,43] or pandemic (2009) H1N1 [44]. These include ssc-miR-7 [44], ssc-miR-15a [18], ssc-miR-18a [18,44], ssc-miR-21 [43,44], mmu-miR-34b-3p [18], ssc-miR-34c [18], ssc-miR-92b-3p [18], ssc-miR-193a-3p [43], hsa-miR-449a [18], and ssc-miR-671-3p [18]. Three of the up-regulated miRNAs (ssc-miR-7, ssc-miR-221-5p, and ssc-miR-451) likewise overlapped with miRNAs we have previously found to be up-regulated in necrotic lung tissue compared to visually unaffected lung tissue of pigs experimentally infected with the Gram-negative bacterium *Actinobacillus pleuropneumoniae* [40], suggesting a potential common function of these during both viral and Gram-negative bacterial pulmonary infection in pigs.

The majority of differential miRNA expression was found to occur at day 3 after challenge; this is in contrast to our previous findings of miRNA expression in circulating leukocytes of the same animals, where the number of differentially expressed miRNAs peaked after viral clearance, 14 days after challenge [45]. The role of miRNAs expressed in the lung may thus be more focused on modulating transcripts related to the active viral infection. However, in both infected lung tissue and circulating leukocytes the lowest number of differentially expressed miRNAs was seen on day 1 after challenge, whereas the number of differentially expressed protein coding genes related to the antiviral immune response was at its highest at this time point. The miRNA response in the porcine lung may thus be a secondary response with the aim of containing and balancing the rapid inflammatory response upon IAV infection, which if left unchecked may cause massive tissue damage [46].

In terms of clinical symptoms, IAV infection is a short-lived disease in otherwise healthy individuals. However, we here demonstrated in a relevant porcine model that even on day 14 after challenge (when the virus had been cleared), remodeling of the miRNA expression of the lung tissue persisted. Similar results of miRNA regulation in the lungs of mice at late time points after IAV (H1N1) infection were recently published [47]. These authors demonstrated significantly altered expression of miRNAs at 21 days after IAV challenge, including up-regulation of miR-449a which is in agreement with our results 14 days after challenge in the pig lung. Recuperation from IAV infection thus appears to be a protracted process involving miRNAs both locally at the infection site as well as systemically. Such lingering remodeling of the miRNA landscape after viral infection may have important consequences for lung homeostasis and susceptibility to secondary infections. Additional evidence of long term effects of IAV infection locally in the pig lung is seen in the down-regulation of *SAA* 14 days after challenge. This peculiar finding confirms results we have previously published [8]. This conventionally positive APP showed no significant pulmonary regulation during the acute phase of the disease in the lung of IAV infected pigs. However, several reports confirm elevated levels of SAA in serum from pigs within 2-3 days after IAV (H1N1, H1N2, H3N2) infection [48–50]. Thus, there appear to be a role for hepatically produced SAA during the acute phase of IAV infection in pigs, rather than locally produced pulmonary SAA. SAA has been reported to have chemotactic and pro-inflammatory effects

[51]; down-regulation of *SAA* during recuperation may thus be a means to restore lung homeostasis after IAV infection.

Pulmonary type III interferon in pigs

Despite the important role for type III interferon in IAV infection, the pulmonary IFN-λ response remains uncharacterized in the pig. To the best of our knowledge, the present study is the first to report the regulation of IFN-λ in pigs in response to IAV infection. Type III interferons (IFN-λ1, IFN-λ2, IFN-λ3, and IFN-λ4) are the most recently described members of the interferon family [52]. Like their type I interferon (IFN-α and IFN-β) counterparts, they have been shown to be crucial inducers of the antiviral response upon IAV infection in mice and *in vitro* systems [5]. However, in contrast to the type I interferon receptor, which is expressed on the surface of a wide variety of cells, the type III interferon receptor is considered to be largely restricted to epithelial cell surfaces [52,53]. Lung-infiltrating neutrophils in mice have also been demonstrated to respond to type III interferon [54]. Nevertheless, type III and type I interferon signaling through their respective receptors do activate the same ISGs. Mouse experiments have demonstrated IFN-λ to be important for restriction of viral replication and to be the earliest type of interferons produced in response to IAV infection [54,55]. This antiviral function is mediated via ISGs such as Mx1, PKR, and ISG15 [56], which were all found to be up-regulated in the present study.

Fang *et al*. showed that protein levels of IFN-λ1 were elevated in serum in an influenza patient cohort compared to healthy controls. They furthermore demonstrated that hsa-miR-29 (especially hsa-miR-29b-3p) indirectly mediate *IFNL1* up-regulation by controlling DNA methyltransferase (*DNMT3A* and *DNMT3B*) activity in human pulmonary epithelial cells (A549) and a subsequent IRF3/IRF7 dependent transcription of *IFNL1* via COX2 (*PTGS2*), a potent inflammatory protein in IAV infection [57]. Our results mirror these findings in human patients and cells: IFN-λ (*IFNL3*) was >400-fold up-regulated (log_2FC 8.7) in the porcine lung 1 day after IAV challenge, and remained up-regulated on day 3. IRF7 was also highly up-regulated at these time points. Finally, we also found ssc-miR-29b to be modestly up-regulated on day 1 and 3 after challenge, suggesting that ssc-miR-29b mediated up-regulation of *IFNL3* via COX2 and IRF7 may also contribute to the antiviral response in IAV infection in our pig model.

The prominent up-regulation of type III interferon gene expression compared to type I interferon suggested that the antiviral interferon response may be somewhat tailored to epithelial cells, as these are the cells that primarily express the type III interferon receptor. This suggests a preferred targeting of cells that actually contain the virus, as respiratory epithelial cells are the main site for IAV replication *in vivo* [58]. This tailored approach could contribute to lowered tissue damage and disease severity than what might be expected from a dominating type I interferon response as type I receptors are present on a wider range of cells. Corroborating results were recently published by Galani *et al*., who found that pulmonary type I interferon mediated a stronger pro-inflammatory response and increased immunopathology compared to type III interferons in H1N1 IAV infected mice [54]. Here, in our pig model inducing relatively mild IAV disease, we accordingly found the type III interferon to be the dominating response. It can be speculated that the severity of IAV infection relates to the balance between the type I and III interferon responses, with the more severe clinical and immunopathological manifestations being associated with at higher type I interferon response.

miRNA modulation of the antiviral response

In addition to the abovementioned possible involvement of ssc-miR-29b in the IFN-λ3 response, our results likewise suggested miRNA-mediated modulation of other branches of the innate response to IAV infection in the pig. A number of the assayed protein coding genes were found to be targets (either previously experimentally validated or computationally predicted) of the miRNAs found to be differentially expressed after IAV infection in pigs. Our results supported that some of these interactions are potentially important for the porcine pulmonary response to IAV infection, given that the expression of eight of these miRNAs and their target mRNAs was significantly and negatively correlated during active infection (day 1 and 3 after challenge only). Prominent among the miRNA targeted genes were antiviral PRRs (*IFIH1* and *TLR3*) and genes related to apoptosis (*BCL2*, *MCL1*, *CASP1*, *CASP3*, *FASLG*, and *EIF2AK2*). It is well established that apoptosis occurs in the host during IAV infection, both as a host response to limit viral replication and spread, but also directly induced by viral proteins for the benefit of the virus [58–60]. Common to all five miRNAs found to correlate negatively with apoptosis-related gene expression (ssc-miR-15a, ssc-miR-18a, ssc-miR-21, ssc-miR-29b, and hsa-miR-590-3p) is that they were significantly up-regulated on day 3 after challenge, and not regulated at other time points. This concurs with the expression of the apoptosis-related genes, all down-regulated at day 3 compared to their initial up-regulation on day 1. The same pattern holds true for the expression *IFIH1* and *TLR3* and the miRNAs that target them (ssc-miR-29b, ssc-miR-18a, and hsa-miR-590-3p). This negative correlation between miRNA expression and their target transcripts thus suggest the specific involvement of ssc-miR-15a, ssc-miR-18a, ssc-miR-21, ssc-miR-29b, and hsa-miR-590-3p in the modulation of important signaling cascades of apoptosis and viral recognition. Given the likely suppressive effect of these miRNAs on their target genes' protein output, the miRNA-mediated down-regulation of *IFIH1* and *TLR3* may be way of limiting the pro-inflammatory effects of viral PRR signaling upon IAV infection in order to limit immunopathology. Concordantly, the pro-inflammatory factors *IL1B* and *CXCL10* are likewise among the miRNA-targeted genes showing significant negative correlation with one or more miRNAs and a strong up-regulation on day 1 after challenge but not on day 3.

Gene targets for the differentially expressed miRNAs were identified using online databases and prediction tools, and subjected to KEGG Pathway enrichment analysis. A large overlap of enriched pathways relevant to IAV infection was seen for genes targeted by either up- or down-regulated miRNAs on day 1 and 3 after challenge, including 'Influenza A', 'Apoptosis', 'Endocytosis', 'Jak-STAT signaling', 'NF-κB signaling', 'Cytokine-cytokine receptor interaction', and 'Chemokine signaling'. This coinciding up- and down-regulation of miRNAs that target such central pathways activated during IAV infection exemplifies the role of miRNAs in balancing and fine-tuning the antiviral innate immune response. Interestingly, we found the pathways 'Toll-like receptor signaling', 'NOD-like receptor signaling', and 'RIG-I-like receptor signaling' to be enriched only in targets of miRNAs down-regulated on day 1 and 3 after challenged. Based on KEGG Pathway enrichment analysis, viral recognition thus appears to be one general aspect of the antiviral response that is not subject miRNA fine-tuning during active IAV infection.

qPCR validation of RNAseq results

In the present study RNAseq miRNA expression results were validated using high-throughput qPCR. Generally, we found the agreement between RNAseq and qPCR results to be good with respect to directionality of miRNA regulation (up, down, or unchanged). These expression patterns were largely identical in both datasets with only two noticeable exceptions: ssc-miR-339-3p, which was

significantly up-regulated in RNAseq but unchanged in qPCR, and mmu-miR-34b-5p, which was significantly down-regulated in RNAseq but also unchanged in qPCR. This lack of agreement could be caused by factors inherent to either method, e.g. poorly designed qPCR primers or the presence of isomiRs which would be detected by RNAseq but not qPCR and would thus contribute to expression levels in one dataset but not the other [61]. However, although there is a general agreement on the regulation patterns of the miRNAs between the two platforms, levels of regulation (i.e. fold change of expression) and statistical significance did not always concur. The relatively small changes that are typically observed when measuring differential miRNA expression combined with considerable animal-to-animal variation and difference in platform sensitivity makes it challenging to produce consistent statistically significant results.

To our knowledge, few studies of large-scale qPCR validation of RNAseq miRNA expression results have yet been published. One such study by Blondal *et al*. described the quantification of miRNAs in serum of hepatitis B and C patients [62], and reported a linear correlation (R2) of 0.6054 between fold changes obtained with the two platforms, which is highly comparable to our own findings (R2 = 0.6244). Also consistent with our observations is the fact that Blondal et al. found the levels of fold change to differ between the two platforms for many of the assayed miRNAs, even though the directionality of regulation was in agreement. Another study of miRNA quantification in the urine of rats with renal tubular injury reported minimal agreement between RNAseq and qPCR results [63]. The authors detected 14 differentially expressed miRNAs with RNAseq and 32 with RT-qPCR; of these, an overlap of only three miRNAs that were supported by both platforms. Our findings as well as the available literature thus suggest that extensive validation of results obtained with RNAseq should be performed with an independent platform, in order to produce consistent and reliable miRNA expression results.

Acknowledgements

The authors wish to thank Karin Tarp (National Veterinary Institute, Kongens Lyngby, Denmark) for technical assistance with sample collection and RT-qPCR. Dr Michael Schlegel is thanked for his contributions during the animal challenge experiments; Kerstin Wieczorek and Roswitha Ulrich are thanked for technical assistance; Dr Guntram Hagemann is thanked for supplying IAV antibody negative pigs; Renè Rau is thanked for assistance during challenge experiment (all affiliated with IDT Biologika GmbH, Dessau-Rosslau, Germany at the time of the challenge experiment).

References

1. Mauskopf J, Klesse M, Lee S, Herrera-Taracena G. The burden of influenza complications in different high-risk groups: a targeted literature review. J. Med. Econ. 2013;16:264–77.
2. Wiersma L, Rimmelzwaan G, de Vries R. Developing Universal Influenza Vaccines: Hitting the Nail, Not Just on the Head. Vaccines. 2015;3:239–62.
3. Tripathi S, White MR, Hartshorn KL. The amazing innate immune response to influenza A virus infection. Innate Immun. 2013;21:73–98.
4. Kotenko S V, Gallagher G, Baurin V V, Lewis-Antes A, Shen M, Shah NK, et al. IFN-lambdas mediate antiviral protection through a distinct class II cytokine receptor complex. Nat. Immunol. 2003;4:69–77.
5. Syedbasha M, Egli A. Interferon Lambda: Modulating immunity in infectious diseases. Front. Immunol. 2017;8.

6. Khatri M, Dwivedi V, Krakowka S, Manickam C, Ali A, Wang L, et al. Swine influenza H1N1 virus induces acute inflammatory immune responses in pig lungs: a potential animal model for human H1N1 influenza virus. J. Virol. 2010;84:11210–8.
7. Barbé F, Atanasova K, Van Reeth K. Cytokines and acute phase proteins associated with acute swine influenza infection in pigs. Vet. J. 2011;187:48–53.
8. Skovgaard K, Cirera S, Vasby D, Podolska A, Breum SO, Durrwald R, et al. Expression of innate immune genes, proteins and microRNAs in lung tissue of pigs infected experimentally with influenza virus (H1N2). Innate Immun. 2013;19:531–44.
9. Rajao DS, Vincent AL. Swine as a Model for Influenza A Virus Infection and Immunity. ILAR J. 2015;56:44–52.
10. Lee RC, Feinbaum RL, Ambros V. The C. elegans heterochronic gene lin-4 encodes small RNAs with antisense complementarity to lin-14. Cell. 1993;75:843–54.
11. Wightman B, Ha I, Ruvkun G. Posttranscriptional regulation of the heterochronic gene lin-14 by lin-4 mediates temporal pattern formation in C. elegans. Cell. 1993;75:855–62.
12. Alipoor SD, Adcock IM, Garssen J, Mortaz E, Varahram M, Mirsaeidi M, et al. The roles of miRNAs as potential biomarkers in lung diseases. Eur. J. Pharmacol. 2016;791:395–404.
13. Guo H, Ingolia NT, Weissman JS, Bartel DP. Mammalian microRNAs predominantly act to decrease target mRNA levels. Nature. 2010;466:835–40.
14. Bartel DP. MicroRNAs: Target Recognition and Regulatory Functions. Cell. 2009;136:215–33.
15. Foster PS, Plank M, Collison A, Tay HL, Kaiko GE, Li J, et al. The emerging role of microRNAs in regulating immune and inflammatory responses in the lung. Immunol. Rev. 2013;253:198–215.
16. Samir M, Vaas LAI, Pessler F. MicroRNAs in the Host Response to Viral Infections of Veterinary Importance. Front. Vet. Sci. 2016;3:1–17.
17. Li Y, Li J, Belisle S, Baskin CR, Tumpey TM, Katze MG. Differential microRNA expression and virulence of avian, 1918 reassortant, and reconstructed 1918 influenza A viruses. Virology. 2011;421:105–13.
18. Vela EM, Kasoji MD, Wendling MQ, Price JA, Knostman KAB, Bresler HS, et al. MicroRNA expression in mice infected with seasonal H1N1, swine H1N1 or highly pathogenic H5N1. J. Med. Microbiol. 2014;63:1131–42.
19. Terrier O, Textoris J, Carron C, Marcel V, Bourdon J-C, Rosa-Calatrava M. Host microRNA molecular signatures associated with human H1N1 and H3N2 influenza A viruses reveal an unanticipated antiviral activity for miR-146a. J. Gen. Virol. 2013;94:985–95.
20. Makkoch J, Poomipak W, Saengchoowong S, Khongnomnan K, Praianantathavorn K, Jinato T, et al. Human microRNAs profiling in response to influenza A viruses (subtypes pH1N1, H3N2, and H5N1). Exp. Biol. Med. 2016;241:409–20.
21. Loveday EK, Svinti V, Diederich S, Pasick J, Jean F. Temporal- and strain-specific host microRNA molecular signatures associated with swine-origin H1N1 and avian-origin H7N7 influenza A virus infection. J. Virol. 2012;86:6109–22.
22. Li Y, Shi X. MicroRNAs in the regulation of TLR and RIG-I pathways. Cell. Mol. Immunol. 2013;10:65–71.
23. Oglesby IK, McElvaney NG, Greene CM. MicroRNAs in inflammatory lung disease--master regulators or target practice? Respir. Res. 2010;11:148.
24. Forero A, So L, Savan R. Re-evaluating Strategies to Define the Immunoregulatory Roles of miRNAs. Trends Immunol. Elsevier; 2017;
25. Oulas A, Karathanasis N, Louloupi A, Pavlopoulos GA, Poirazi P, Kalantidis K, et al. Prediction of miRNA Targets. In: Picardi E, editor. RNA Bioinforma. New York, NY: Springer New York; 2015. p. 207–29.
26. Vlachos IS, Paraskevopoulou MD, Karagkouni D, Georgakilas G, Vergoulis T, Kanellos I, et al. DIANA-TarBase v7.0: Indexing more than half a million experimentally supported miRNA:mRNA interactions. Nucleic Acids Res. 2015;43:D153–9.

27. Junge A, Refsgaard JC, Garde C, Pan X, Santos A, Alkan F, et al. RAIN: RNA-protein Association and Interaction Networks. Database. 2017;2017:1–9.
28. Paraskevopoulou MD, Georgakilas G, Kostoulas N, Vlachos IS, Vergoulis T, Reczko M, et al. DIANA-microT web server v5.0: service integration into miRNA functional analysis workflows. Nucleic Acids Res. 2013;41:169–73.
29. Trebbien R, Bragstad K, Larsen LE, Nielsen J, Bøtner A, Heegaard PMH, et al. Genetic and biological characterisation of an avian-like H1N2 swine influenza virus generated by reassortment of circulating avian-like H1N1 and H3N2 subtypes in Denmark. Virol. J. 2013;10:290.
30. Martin M. Cutadapt removes adapter sequences from high-throughput sequencing reads. EMBnet.journal. 2011;17:10–2.
31. Friedländer MR, Mackowiak SD, Li N, Chen W, Rajewsky N. miRDeep2 accurately identifies known and hundreds of novel microRNA genes in seven animal clades. Nucleic Acids Res. 2012;40:37–52.
32. Langmead B, Trapnell C, Pop M, Salzberg S. Ultrafast and memory-efficient alignment of short DNA sequences to the human genome. Genome Biol. 2009;10:R25.
33. Groenen MAM, Archibald AL, Uenishi H, Tuggle CK, Takeuchi Y, Rothschild MF, et al. Analyses of pig genomes provide insight into porcine demography and evolution. Nature. Nature Publishing Group; 2012;491:393–8.
34. Kozomara A, Griffiths-Jones S. MiRBase: Annotating high confidence microRNAs using deep sequencing data. Nucleic Acids Res. 2014;42:68–73.
35. Balcells I, Cirera S, Busk PK. Specific and sensitive quantitative RT-PCR of miRNAs with DNA primers. BMC Biotechnol. 2011;11:70.
36. Mestdagh P, Van Vlierberghe P, De Weer A, Muth D, Westermann F, Speleman F, et al. A novel and universal method for microRNA RT-qPCR data normalization. Genome Biol. 2009;10:R64.
37. Skovgaard K, Mortensen S, Boye M, Poulsen KT, Campbell FM, Eckersall PD, et al. Rapid and widely disseminated acute phase protein response after experimental bacterial infection of pigs. Vet.Res. 2009;40:23.
38. Vandesompele J, De PK, Pattyn F, Poppe B, Van RN, De PA, et al. Accurate normalization of real-time quantitative RT-PCR data by geometric averaging of multiple internal control genes. Genome Biol. 2002;3:RESEARCH0034.
39. Andersen CL, Jensen JL, Ørntoft TF. Normalization of Real-Time Quantitative Reverse Transcription-PCR Data: A Model-Based Variance Estimation Approach to Identify Genes Suited for Normalization, Applied to Bladder and Colon Cancer Data Sets. Cancer Res. 2004;64:5245–50.
40. Podolska A, Anthon C, Bak M, Tommerup N, Skovgaard K, Heegaard PM, et al. Profiling microRNAs in lung tissue from pigs infected with Actinobacillus pleuropneumoniae. BMC Genomics. 2012;13:459.
41. Szklarczyk D, Franceschini A, Wyder S, Forslund K, Heller D, Huerta-Cepas J, et al. STRING v10: Protein-protein interaction networks, integrated over the tree of life. Nucleic Acids Res. 2015;43:D447–52.
42. Kanehisa M, Furumichi M, Tanabe M, Sato Y, Morishima K. KEGG: New perspectives on genomes, pathways, diseases and drugs. Nucleic Acids Res. 2017;45:D353–61.
43. Li Y, Chan EY, Li J, Ni C, Peng X, Rosenzweig E, et al. MicroRNA expression and virulence in pandemic influenza virus-infected mice. J. Virol. 2010;84:3023–32.
44. Wu Z, Hao R, Li P, Zhang X, Liu N, Qiu S, et al. MicroRNA expression profile of mouse lung infected with 2009 pandemic H1N1 influenza virus. PLoS One. 2013;8:e74190.
45. Brogaard L, Heegaard PMH, Larsen LE, Mortensen S, Schlegel M, Dürrwald R, et al. Late regulation of immune genes and microRNAs in circulating leukocytes in a pig model of influenza A (H1N2) infection. Sci. Rep. 2016;6:21812.
46. Kash JC, Taubenberger JK. The role of viral, host, and secondary bacterial factors in influenza pathogenesis. Am. J. Pathol. Elsevier; 2015;185:1528–36.

47. Pociask DA, Robinson KM, Chen K, McHugh KJ, Clay ME, Huang GT, et al. Epigenetic and Transcriptomic Regulation of Lung Repair during Recovery from Influenza Infection. Am. J. Pathol. 2017;187:851–63.
48. Pomorska-Mól M, Markowska-Daniel I, Kwit K. Immune and acute phase response in pigs experimentally infected with H1N2 swine influenza virus. FEMS Immunol. Med. Microbiol. 2012;66:334–42.
49. Pomorska-Mól M, Krzysztof K, Pejsak Z, Markowska-Daniel I. Analysis of the acute-phase protein response in pigs to clinical and subclinical infection with H3N2 swine influenza virus. Influenza Other Respi. Viruses. 2014;8:228–34.
50. Pomorska-Mól M, Markowska-Daniel I, Kwit K, Czyżewska E, Dors A, Rachubik J, et al. Immune and inflammatory response in pigs during acute influenza caused by H1N1 swine influenza virus. Arch. Virol. 2014;159:2605–14.
51. Ye RD, Sun L. Emerging functions of serum amyloid A in inflammation. J. Leukoc. Biol. 2015;98:923–9.
52. Durbin RK, Kotenko S V., Durbin JE. Interferon induction and function at the mucosal surface. Immunol. Rev. 2013;255:25–39.
53. Mordstein M, Neugebauer E, Ditt V, Jessen B, Rieger T, Falcone V, et al. Lambda Interferon Renders Epithelial Cells of the Respiratory and Gastrointestinal Tracts Resistant to Viral Infections. J. Virol. 2010;84:5670–7.
54. Galani IE, Triantafyllia V, Eleminiadou E-E, Koltsida O, Stavropoulos A, Manioudaki M, et al. Interferon-λ Mediates Non-redundant Front-Line Antiviral Protection against Influenza Virus Infection without Compromising Host Fitness. Immunity. 2017;46:875–890.e6.
55. Davidson S, McCabe TM, Crotta S, Gad HH, Hessel EM, Beinke S, et al. IFNλ is a potent anti-influenza therapeutic without the inflammatory side effects of IFNα treatment. EMBO Mol. Med. 2016;8:1099–112.
56. Sedger LM. MicroRNA control of interferons and interferon induced anti-viral activity. Mol. Immunol. 2013;56:781–93.
57. Fang J, Hao Q, Liu L, Li Y, Wu J, Huo X, et al. Epigenetic changes mediated by microRNA miR29 activate cyclooxygenase 2 and lambda-1 interferon production during viral infection. J.Virol. 86:1010–20.
58. Janke BH. Influenza A virus infections in swine: pathogenesis and diagnosis. Vet. Pathol. 2014;51:410–26.
59. Arora S, Lim W, Bist P, Perumalsamy R, Lukman HM, Li F, et al. Influenza A virus enhances its propagation through the modulation of Annexin-A1 dependent endosomal trafficking and apoptosis. Cell Death Differ. 2016;23:1243–56.
60. Mayank AK, Sharma S, Nailwal H, Lal SK. Nucleoprotein of influenza A virus negatively impacts antiapoptotic protein API5 to enhance E2F1-dependent apoptosis and virus replication. Cell Death Dis. 2015;6:e2018.
61. Moldovan L, Batte KE, Trgovcich J, Wisler J, Marsh CB, Piper M. Methodological challenges in utilizing miRNAs as circulating biomarkers. J. Cell. Mol. Med. 2014;18:371–90.
62. Blondal T, Brunetto MR, Cavallone D, Mikkelsen M, Thorsen M, Mang Y, et al. Genome-Wide Comparison of Next-Generation Sequencing and qPCR Platforms for microRNA Profiling in Serum. In: Dalmay T, editor. MicroRNA Detect. Target Identif. Methods Protoc. New York, NY: Springer New York; 2017. p. 21–44.
63. Nassirpour R, Mathur S, Gosink MM, Li Y, Shoieb AM, Wood J, et al. Identification of tubular injury microRNA biomarkers in urine: comparison of next-generation sequencing and qPCR-based profiling platforms. BMC Genomics. 2014;15:485.

Supporting information

S1 Table. Sequences and qPCR efficiencies of primers used in the present study.

S2 Table. Comparison of porcine and human miRNA sequences for those applied in miRNA-mRNA interaction analysis. Underlined, bold nucleotides highlights differences between porcine and human sequences.

S3 Table. Normalized RNAseq read counts. Normalized read counts for all known porcine (n = 238) as well as potential novel porcine miRNA candidates (n = 15) detected with RNAseq (total n = 253) in 25 porcine lung samples.

S4 Table. Novel porcine miRNA candidate sequences. Mature and hairpin sequences of novel porcine miRNA candidates identified in RNAseq data, for which homologs could be identified in other species.

S5 Table. Expression changes of miRNAs determined by RNAseq. Log2FC of all known porcine (n = 238) as well as potential novel porcine miRNA candidates (n = 15) detected with RNAseq (total n = 253) in lungs of pigs at 1, 3, and 14 days after IAV challenge relative to unchallenged controls.

S6 Table. Expression changes of miRNAs measured with qPCR. Log2FC of miRNAs determined with qPCR (n = 80) in lungs of pigs at 1, 3, and 14 days after IAV challenge relative to unchallenged controls.

S1 Fig. miRNA-target interaction network, up-regulated miRNAs day 1 and 3. Pink edges – experimentally determined interaction. Blue edges – information from curated database. Yellow edges – computationally predicted interaction.

S2 Fig. miRNA-target interaction network, down-regulated miRNAs day 1 and 3. Pink edges – experimentally determined interaction. Blue edges – information from curated database. Yellow edges – computationally predicted interaction.

Author contributions

Conceptualization: LB, KS

Formal analysis: LB

Investigation: LB, LEL, PMHH, RD, KS

Methodology: LB, LEL, PMHH, CA, JG, RD, KS

Resources: LEL, PMHH, CA, JG, RD, KS

Software: CA, JG

Visualization: LB

Writing – original draft preparation: LB

Writing – reviewing and editing: LB, LEL, PMHH, CA, JG, RD, KS

Fig1. Volcano plots showing miRNA expression changes as obtained by RNAseq. A) day 1 after challenge, B) day 3 after challenge, C) day 14 after challenge. x-axes show the log_2FC values of post-challenge time points vs. unchallenged controls. 50 % up- or down-regulation is denoted by vertical dotted lines ($log_2FC > 0.585$, $log_2FC < -0.585$). y-axes show the $-log_{10}$ transformed *p*-values obtained from *t*-tests. $p = 0.05$ is denoted by a horizontal red line. miRNAs that pass the criteria for differential expression are marked with a number denoting their identity; miRNAs that appear in more than one volcano plot are marked with the same number in all plots. All log_2FC values can be found in S4 Table. 1 ssc-miR-205; 2 ssc-miR-146b; 3 ssc-miR-34c; 4 ssc-miR-671-5p; 5 ssc-miR-708-3p; 6 mmu-miR-34b-5p; 7 ssc-miR-129a; 8 ssc-miR-339-3p; 9 ssc-miR-193a-3p; 10 ssc-miR-187; 11 ssc-miR-1296-5p; 12 ssc-miR-129b; 13 ssc-miR-2320-3p; 14 ssc-miR-183; 15 ssc-miR-328; 16 ssc-miR-128; 17 hsa-miR-449a; 18 ssc-miR-139-3p; 19 ssc-miR-551a; 20 ssc-miR-671-3p; 21 ssc-miR-92b-5p; 22 ssc-miR-184; 23 ssc-miR-190b; 24 mmu-miR-34b-3p; 25 ssc-miR-1343; 26 ssc-miR-7134-5p; 27 ssc-miR-92b-3p; 28 hsa-miR-375; 29 ssc-miR-296-3p; 30 ssc-miR-744; 31 ssc-miR-20a; 32 ssc-miR-142-5p; 33 ssc-miR-504; 34 ssc-miR-29b; 35 ssc-miR-221-5p; 36 ssc-miR-144; 37 mmu-miR-34b-3p; 38 ssc-miR-486; 39 ssc-miR-451; 40 ssc-miR-365-5p; 41 ssc-miR-326; 42 ssc-miR-217; 43 ssc-miR-196-5p; 44 ssc-miR-183; 45 ssc-miR-139-5p; 46 ssc-miR-30c-1-3p; 47 ssc-miR-7139-3p; 48 ssc-miR-1249; 49 ssc-miR-133b.

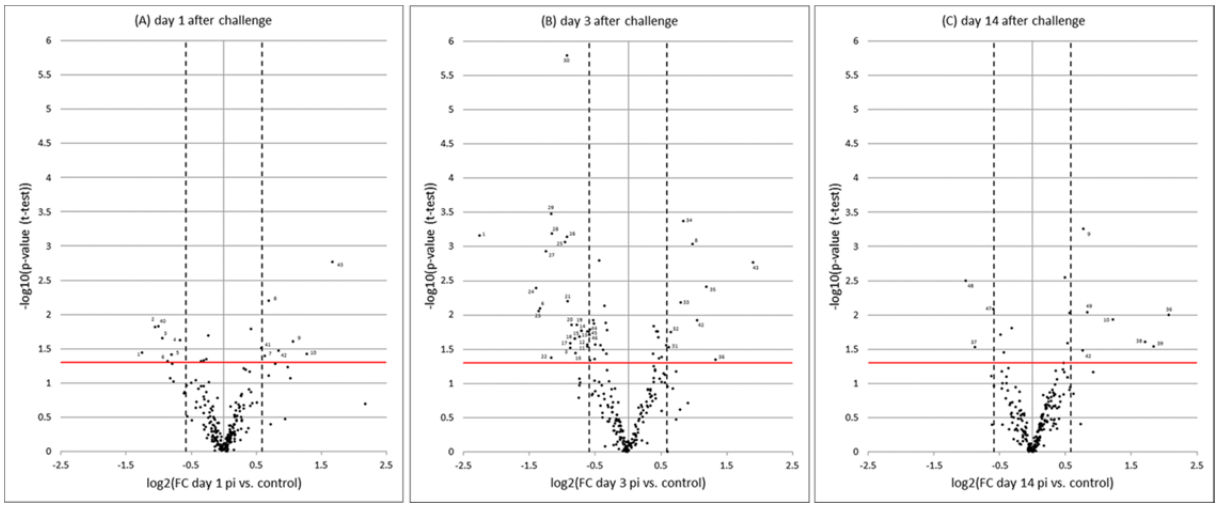

Fig 2. Venn diagram comparing differentially expressed miRNAs identified by and qPCR and RNAseq. Overlap of miRNAs found to be differentially expressed at one or more post-challenge time points by RNAseq (yellow) and qPCR (blue). †miRNAs assayed by qPCR but not detected by sequencing; *miRNAs detected by sequencing, but not assayed by qPCR. When a known porcine (ssc) sequence for a given miRNA was not available in miRBase (v. 21), human (hsa) or mouse (mmu) names are applied in accordance with the homolog that best matched the novel porcine miRNA discovered in the RNAseq data, and these homolog sequences were likewise used for qPCR primer design.

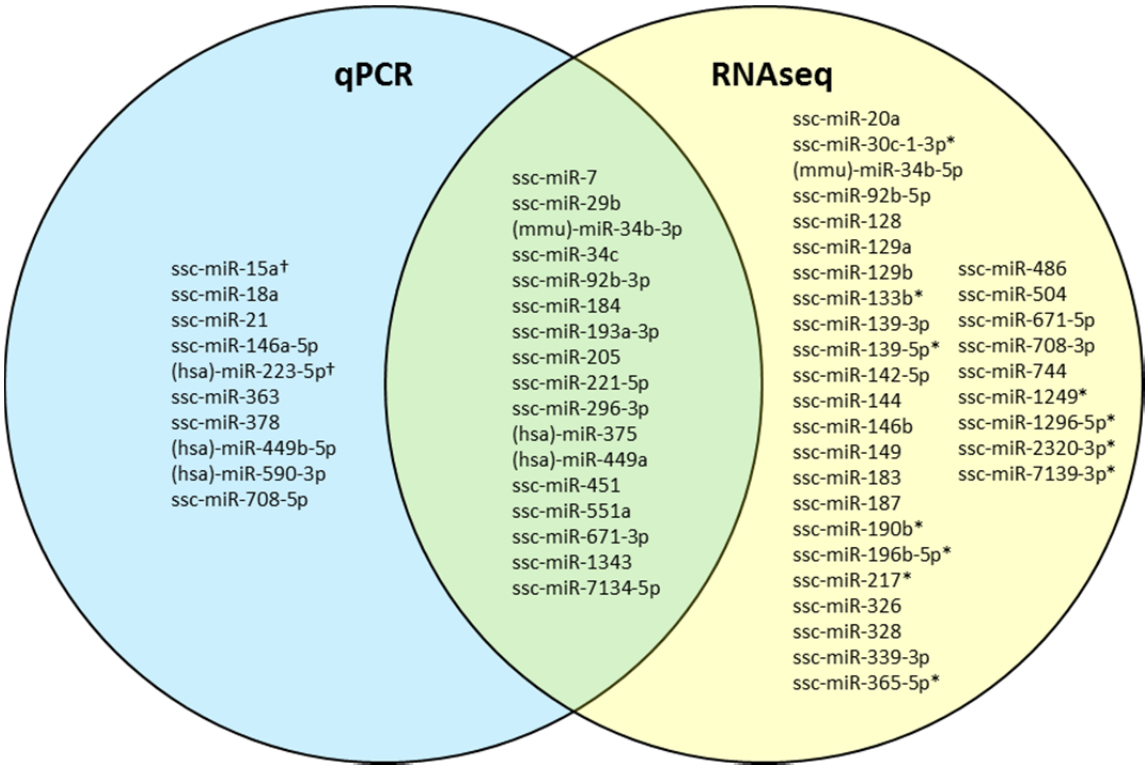

Fig 3. Comparison of miRNA log_2FC as measured by RNAseq and qPCR. Log_2FC (challenged group vs. control group) obtained by qPCR is plotted against the corresponding log_2FC obtained by RNAseq. Each point represents log_2FC of one miRNA on day 1 (black), day 3 (white), or day 14 (grey) after challenge.

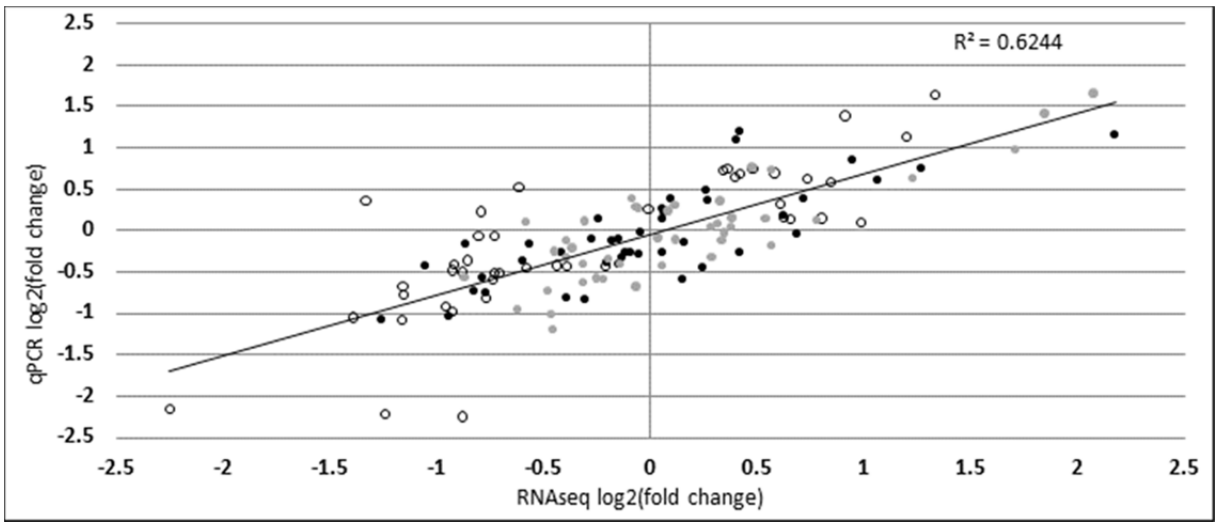

Fig 4. Potential miRNA-mRNA interactions. Expression of eight of the assayed miRNAs showed significant negative correlation with expression of protein coding genes that were identified (using RAIN v1.0 [27], TarBase v. 7.0 [26], and/or microT-CDS [28]) to be experimentally validated targets of the miRNA (solid lines), computationally predicted targets of the miRNA (dotted lines), or both (solid lines, underlined gene names).

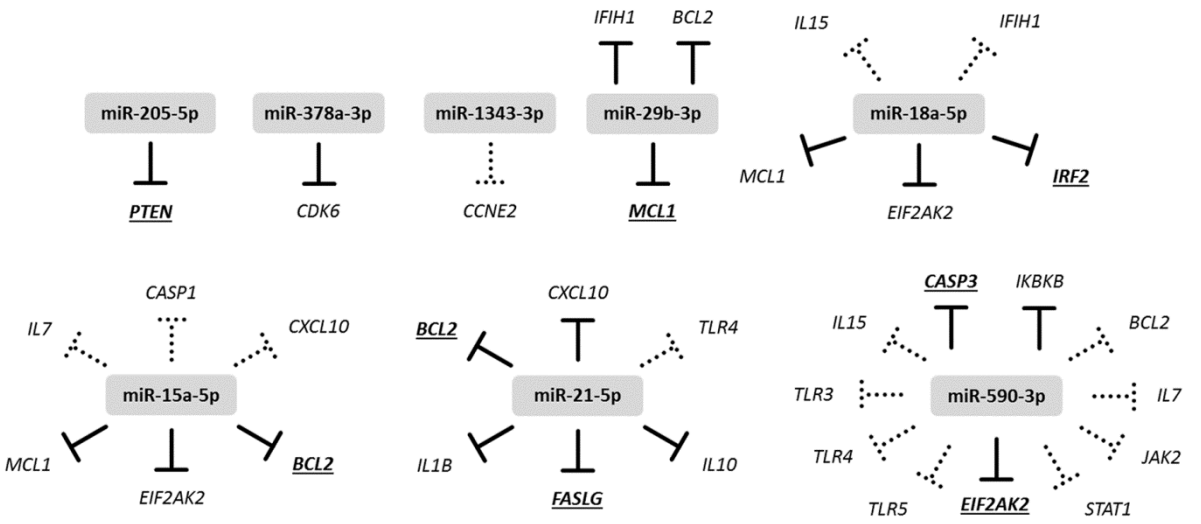

S1 Fig. miRNA-target interaction network, up-regulated miRNAs day 1 and 3. Pink edges – experimentally determined interaction. Blue edges – information from curated database. Yellow edges – computationally predicted interaction.

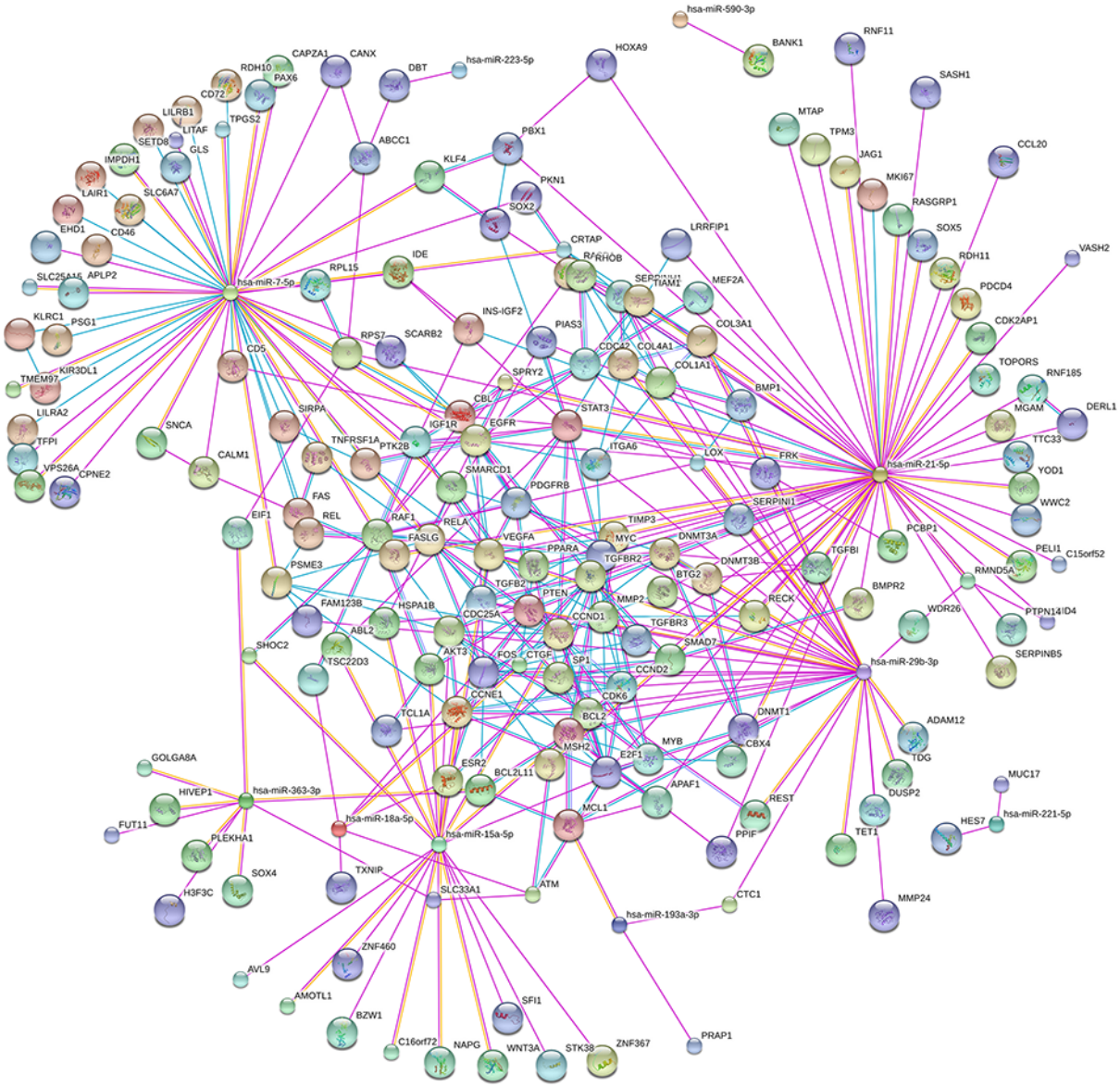

S2 Fig. miRNA-target interaction network, down-regulated miRNAs day 1 and 3. Pink edges – experimentally determined interaction. Blue edges – information from curated database. Yellow edges – computationally predicted interaction.

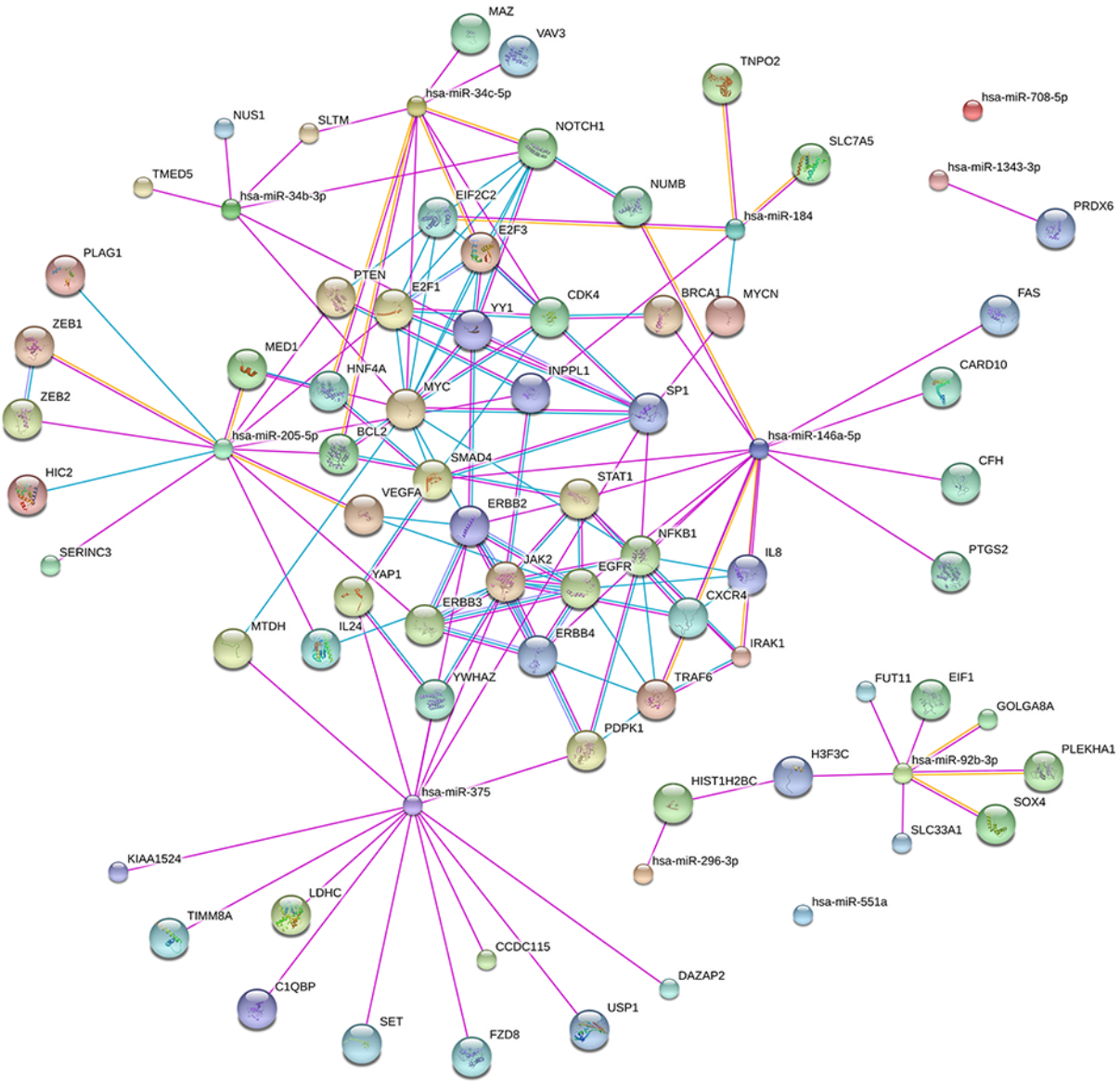

S1 Table. Sequences and qPCR efficiencies of primers used in the present study.

Gene	Forward primer 5´-3´	Reverse primer 5´-3´	qPCR efficiency
ACTB	CTACGTCGCCCTGGACTTC	GCAGCTCGTAGCTCTTCTCC	1,09
B2M	TGAAGCACGTGACTCTCGAT	CTCTGTGATGCCGGTTAGTG	0,99
GAPDH	ACCCAGAAGACTGTGGATGG	AAGCAGGGATGATGTTCTGG	0,97
PPIA	CAAGACTGAGTGGTTGGATGG	TGTCCACAGTCAGCAATGGT	1,03
RPL13A	ATTGTGGCCAAGCAGGTACT	AATTGCCAGAAATGTTGATGC	1,05
YWHAZ	GCTGCTGGTGATGATAAGAAGG	AGTTAAGGGCCAGACCCAAT	1,01
BCL2	CCCTGTGGATGACTGAGTACC	AACCACACATGCACCTACCC	0,98
CASP1	GAAGGACAAACCCAAGGTGA	TGGGCTTTCTTAATGGCATC	1,02
CASP3	AGCAGTTTTATTTGCGTGCTT	CAACAGGTCCATTTGTTCCA	1,03
CCL2	CTTCTGCACCCAGGTCCTT	CGCTGCATCGAGATCTTCTT	1,07
CCL3	CCAGGTCTTCTCTGCACCAC	GCTACGAATTTGCGAGGAAG	1,02
CXCL10	CCCACATGTTGAGATCATTGC	GCTTCTCTCTGTGTTCGAGGA	0,99
CXCL2	GAAGATGCTAAACAAGAGCAGTG	AGCCAAATGCATGAAACACA	1,00
DDX58	ACGAAAGGGGAAGGTTGTCT	ATGCCTGCAACTTTGTACCC	1,01
EIF2AK2	AGGCTGGCGTCTTAGATGTATT	AGGTCGTTTCTTGGGGTCATT	1,03
FAS	CACTGTAACCCTTGCACCAC	TGGAACACTTCTCTGCATTTGG	1,01
FASLG	TTCTGGTGGCCCTGGTTG	CTTTGGCTGGCAGACTCTCT	0,99
GZMB	CCAGGACCAGGATAATCGAA	GGGTGACGTTGATTGAGCTT	1,01
HMGB1	CAAGGCCCGTTATGAAAGAG	ATCTGCAGCGGTGTTATTCC	1,08
IFIH1	CAGTGTGCTAGCCTGCTCTG	GCAGTGCCTTGTTTCCTCTC	1,08
IFITM1	CACCACGGTGATCACCATCC	GCACCAGTTCAGGAAGAGGG	1,04
IFITM3	ACCACGGTGATCAACATCCG	AGCACCAGTTCATGAAGAGGG	1,10
IFNB1	AGCACTGGCTGGAATGAAAC	TCCAGGATTGTCTCCAGGTC	1,00
IFNL3	CCTGGAAGCCTCTGTCATGT	TCTCCACTGGCGACACATT	0,95
IKBKB	TGGGATCACATCGGACAAACTG	CTTCACCTCGTTCTCCCGTC	1,00
IL10	TACAACAGGGGCTTGCTCTT	GCCAGGAAGATCAGGCAATA	1,05
IL12B	GACCAGAAAGAGCCCAAAAAC	AGGTGAAACGTCCGGAGTAA	1,13
IL15	GCTCATCCCAATTGCAAAGTA	TGGACTCTTGCAAAATGACG	1,00
IL18	CTGCTGAACCGGAAGACAAT	TCCGATTCCAGGTCTTCATC	1,10
IL1B	TCTCTCACCCCTTCTCCTCA	GACCCTAGTGTGCCATGGTT	1,07
IL1RN	TGCCTGTCCTGTGTCAAGTC	GTCCTGCTCGCTGTTCTTTC	1,05
IL6	TGGGTTCAATCAGGAGACCT	CAGCCTCGACATTTCCCTTA	1,12
IRAK1	GGATGGGGTTCTGGACAGC	TTCATCACTCTCTTCGGGCC	1,04
IRF2	GATGCTGCCCTTATCTGAGC	TGTGCTTCACTCTGTCTTCCTT	1,03
IRF7	GTGTGCTCCTGTACGGGTCT	CTGCAGCAGCTTCTCTGTGT	0,96
ISG15	AGTTCTGGCTGACTTTCGAGG	GGTGCACATAGGCTTGAGGT	1,12
JAK2	CTCAGATATGCAAGGGTATGGAGT	CCACCAATATATTCCTTGTTGCCA	1,04
MCL1	GAGGCTGGGATGGGTTTGTG	TGCCAAACCAGCTCCTACTC	1,00
MUC1	GGATTTCTGAATTGTTTTTGCAG	ACTGTCTTGGAAGGCCAGAA	1,00
MX1	GCCGAGATCTTTCAGCACCT	CGGAGGATGAAGAACTGGATGA	1,09
MYD88	CCAGACTAAGTTTGCACTCAGC	AGGATGCTGGGGAACTCTTT	1,01
OAS1	AAGAAACCCAGGCCTGTGATTC	TAGTGCCCCTTCTACCAGCT	1,10
OASL	TGGTACCTGAAGTACGTGAAAGC	TACCCACTTCCCAGGCATAG	1,11

RNASEL	TAGAGGCCCTAGGATTGCTGG	GGAGAGCCTTGAATCACCTCT	1,00
SEPT4	CCAGTTCCCAGACTGTGACTC	CCTCTACCACGGTGTTGCTG	1,04
SERPINE1	CCTGCAAAAGGTGAAGATCG	ATCACTTGGCCCATGAAAAG	1,12
SOCS1	CCAGCGCATTGTGGCTAC	GCGGCCGATCATATCTGGAA	1,01
STAT1	CCTTGCAGAATAGAGAACATGATAC	CCTTTCTCTTGTTGTCAAGCATT	0,98
STAT2	TTTGCCCCATGATCTGAGACAC	ACGTTGGTGTTCTGGCTAGC	1,02
SAA	CAGAGATGGGCATCATTCCT	TGGCATCGCTGATCACTTTA	1,03
TF	CTCAACCTCAAAACTCCTGGAA	CCGTCTCCATCAGGTGGTA	0,99
TICAM2	TCTGCTGCAAAATGACTTCGG	AGCCATTGACAGCATCGTCT	1,11
TLR3	ATTGTGCAAAAGATTCAAGGTG	TCTTCGCAAACAGAGTGCAT	1,09
TLR7	AGAAGCCCCTTCAGAAGTCC	GGTGAGCCTGTGGATTTGTT	1,00
TNF	CCCCCAGAAGGAAGAGTTTC	CGGGCTTATCTGAGGTTTGA	0,99
hsa-let-7a	GCAGTGAGGTAGTAGGTTGT	GTCCAGTTTTTTTTTTTTTTTAACT	1,04
hsa-let-7c	GCAGTGAGGTAGTAGGTTGTA	GTCCAGTTTTTTTTTTTTTTTAACCA	0,99
ssc-let-7e	CAGTGAGGTAGGAGGTTGT	GGTCCAGTTTTTTTTTTTTTTTAACTATAC	1,07
ssc-miR-1	CGCAGTGGAATGTAAAGAAGT	GGTCCAGTTTTTTTTTTTTTTTACATAC	1,11
ssc-miR-7	CGCAGTGGAAGACTAGTG	GTCCAGTTTTTTTTTTTTTTTAACAACA	1,02
ssc-miR-15a	CAGTAGCAGCACATAATGGT	TCCAGTTTTTTTTTTTTTTTACAAACC	0,96
ssc-miR-17-3p	TGCAGTGAAGGCACTTG	GGTCCAGTTTTTTTTTTTTTTTCTACA	1,05
ssc-miR-18a	GCAGTAAGGTGCATCTAGTG	GGTCCAGTTTTTTTTTTTTTTTATCTG	1,06
hsa-miR-20a	ACAGTAAAGTGCTTATAGTGCA	GTCCAGTTTTTTTTTTTTTTTCTACCT	0,99
ssc-miR-20b	AGCAAAGTGCTCACAGTG	GTCCAGTTTTTTTTTTTTTTTCTACCT	1,05
ssc-miR-21	TCAGTAGCTTATCAGACTGATG	CGTCCAGTTTTTTTTTTTTTTTCAAC	1,19
ssc-miR-23a	AGATCACATTGCCAGGGA	CCAGTTTTTTTTTTTTTTTGGAAATCC	1,11
ssc-miR-24-3p	GTGGCTCAGTTCAGCAG	CCAGTTTTTTTTTTTTTTTCTGTTCCT	1,05
ssc-miR-29a	GCAGCTAGCACCATCTG	GGTCCAGTTTTTTTTTTTTTTTAACC	1,04
ssc-miR-29b	CAGTAGCACCATTTGAAATCAG	GGTCCAGTTTTTTTTTTTTTTTAACACT	1,00
ssc-miR-30a-5p	GCAGTGTAAACATCCTCGAC	CCAGTTTTTTTTTTTTTTTCTTCCAG	0,98
ssc-miR-30c-3p	CTGGGAGAAGGCTGTTTAC	AGGTCCAGTTTTTTTTTTTTTTTAGAG	1,08
ssc-miR-31	GGCAAGATGCTGGCATAG	GGTCCAGTTTTTTTTTTTTTTTCAG	1,04
ssc-miR-34a	GTGGCAGTGTCTTAGCTG	CCAGTTTTTTTTTTTTTTTACAACCAG	0,98
hsa-miR-34b-3p	GCAATCACTAACTCCACTGC	TCCAGTTTTTTTTTTTTTTTATGGCA	1,05
hsa-miR-34b-5p	GTAGGCAGTGTCATTAGCTG	GTCCAGTTTTTTTTTTTTTTTCAATCAG	0,92
ssc-miR-34c	GAGGCAGTGTAGTTAGCTG	CCAGTTTTTTTTTTTTTTTGCAATCAG	1,03
ssc-miR-92b-3p	CGCAGTATTGCACTCGTC	GTCCAGTTTTTTTTTTTTTTTGGAG	1,13
ssc-miR-92b-5p	GGACGCGGTGCAGT	GGTCCAGTTTTTTTTTTTTTTTAACACT	1,00
ssc-miR-99a	CAGAACCCGTAGATCCGA	TCCAGTTTTTTTTTTTTTTTCACAAGA	1,11
hsa-miR-103	AGAGCAGCATTGTACAGG	AGGTCCAGTTTTTTTTTTTTTTTCAT	1,10
ssc-miR-128	CACAGTGAACCGGTCTC	GGTCCAGTTTTTTTTTTTTTTTAAAGAG	1,07
ssc-miR-129a-3p	AAGCCCTTACCCCAAAAAG	GGTCCAGTTTTTTTTTTTTTTTATGCT	0,99
ssc-miR-129b	TTGCGGTCTGGGCT	CCAGTTTTTTTTTTTTTTTGCAAGC	1,00
ssc-miR-135	CGCAGTATGGCTTTTTATTCCT	GTCCAGTTTTTTTTTTTTTTTCACATAG	1,03
ssc-miR-139-3p	GCGGCCCTGTTGG	GGTCCAGTTTTTTTTTTTTTTTACTC	1,00
hsa-miR-142-3p	GCAGTGTAGTGTTTCCTACT	GTCCAGTTTTTTTTTTTTTTTCCAT	0,98
ssc-miR-142-5p	GCAGCATAAAGTAGAAAGCAC	GTCCAGTTTTTTTTTTTTTTTAGTAGTG	1,02
ssc-miR-144	CAGCGCAGTACAGTATAGATG	GGTCCAGTTTTTTTTTTTTTTTGTACAT	1,00

ssc-miR-145-3p	AGGGATTCCTGGAAATACTGT	GGTCCAGTTTTTTTTTTTTTTTAGAACA	1,06
ssc-miR-145-5p	GTCCAGTTTTCCCAGGAATC	GGTCCAGTTTTTTTTTTTTTTTAAGG	1,14
ssc-miR-146a-5p	CGCAGTGAGAACTGAATTCC	CAGGTCCAGTTTTTTTTTTTTTTTAAC	1,07
ssc-miR-146b	GCAGTGAGAACTGAATTCCA	CCAGTTTTTTTTTTTTTTTGCCTATG	0,99
ssc-miR-148b-5p	GCAGGAAGTTCTGTTATACACTC	CAGTTTTTTTTTTTTTTTGCCTGAG	0,98
ssc-miR-149	GGCTCCGTGTCTTCAC	GTCCAGTTTTTTTTTTTTTTTTGGGA	1,02
ssc-miR-150	CTCCCAACCCTTGTACCA	GGTCCAGTTTTTTTTTTTTTTTCACT	1,05
ssc-miR-181a	CATTCAACGCTGTCGGT	GTCCAGTTTTTTTTTTTTTTTTAACTCAC	1,03
ssc-miR-181b	GAACATTCATTGCTGTCGGT	GGTCCAGTTTTTTTTTTTTTTTTAACC	1,10
ssc-miR-182	AGTTTGGCAATGGTAGAACTC	GTCCAGTTTTTTTTTTTTTTTTAGTGTG	1,00
ssc-miR-183	GCAGTATGGCACTGGTAGA	TCCAGTTTTTTTTTTTTTTTCAGTGA	1,01
ssc-miR-184	CAGTGGACGGAGAACTGA	GTCCAGTTTTTTTTTTTTTTTACCCT	1,00
ssc-miR-187	TCGTGTCTTGTGTTGCAG	GTTTTTTTTTTTTTTCCGGCTG	0,98
ssc-miR-193a-3p	GAACTGGCCTACAAAGTCC	CCAGTTTTTTTTTTTTTTTACTGGGA	0,94
ssc-miR-200c	AGTAATACTGCCGGGTAATG	GGTCCAGTTTTTTTTTTTTTTTCCA	1,03
ssc-miR-205	CCTTCATTCCACCGGAGT	GTCCAGTTTTTTTTTTTTTTTCAGAC	1,05
ssc-miR-206	GCAGTGGAATGTAAGGAAGTG	CCAGTTTTTTTTTTTTTTTCACACAC	0,93
ssc-miR-221-5p	AGACCTGGCATACAATGTAGA	GGTCCAGTTTTTTTTTTTTTTTACAGA	0,99
ssc-miR-222	CTACATCTGGCTACTGGGT	GGTCCAGTTTTTTTTTTTTTTTGAG	1,07
hsa-miR-223-3p	CGCAGTGTCAGTTTGTC	CCAGTTTTTTTTTTTTTTTGGGGTA	1,04
hsa-miR-223-5p	GCGTGTATTTGACAAGCTG	GTCCAGTTTTTTTTTTTTTTTAACTCAG	1,00
ssc-miR-296-3p	GTTGGGCGGAGGCT	GTCCAGTTTTTTTTTTTTTTTGGAAAG	1,02
ssc-miR-323	GCAGGCACATTACACGGT	GTCCAGTTTTTTTTTTTTTTTAGAGGT	1,00
ssc-miR-328	GCCCTCTCTGCCCTTC	GTCCAGTTTTTTTTTTTTTTTACGGA	1,01
ssc-miR-335	GCAGTCAAGAGCAATAACGA	GTCCAGTTTTTTTTTTTTTTTCATTTTTC	1,02
ssc-miR-339-3p	GCTCCTCGAGGCCAG	GTTTTTTTTTTTTTTGGGCTCTG	0,98
ssc-miR-345-5p	AGGCTGACTCCTAGTCCA	CAGTTTTTTTTTTTTTTTGCACTGG	1,03
ssc-miR-363	CAGAATTGCACGGTATCCA	GGTCCAGTTTTTTTTTTTTTTTACAG	1,06
hsa-miR-375	CAGTTTGTTCGTTCGGCT	GGTCCAGTTTTTTTTTTTTTTTCAC	1,03
ssc-miR-378	GACTGGACTTGGAGTCAGA	CCAGTTTTTTTTTTTTTTTGCCTTCT	0,96
hsa-miR-449a	AGTGGCAGTGTATTGTTAGC	GTCCAGTTTTTTTTTTTTTTTACCAG	1,01
hsa-miR-449b-5p	CAGAGGCAGTGTATTGTTAGC	TCCAGTTTTTTTTTTTTTTTGCCA	1,01
ssc-miR-451	CAGAAACCGTTACCATTACTGA	GGTCCAGTTTTTTTTTTTTTTTAACTCA	1,04
hsa-miR-454-3p	GCAGTAGTGCAATATTGCTTATAG	GTCCAGTTTTTTTTTTTTTTTACCCT	1,04
ssc-miR-486	GCAGTCCTGTACTGAGCTG	GTCCAGTTTTTTTTTTTTTTTCTCG	1,06
ssc-miR-491	GTGGGGAACCCTTCCA	GGTCCAGTTTTTTTTTTTTTTTCCT	1,07
ssc-miR-500	GCACCTGGGCAAGGA	GGTCCAGTTTTTTTTTTTTTTTAGAATC	1,03
ssc-miR-504	AGACCCTGGTCTGCAC	GGTCCAGTTTTTTTTTTTTTTTAGATAGAG	0,93
ssc-miR-551a	GCGACCCACTCTTGG	CAGTTTTTTTTTTTTTTTGGAAACCA	1,08
hsa-miR-590-3p	GCAGCGCAGTAATTTTATGTATAAG	TCCAGTTTTTTTTTTTTTTTACTAGCTT	0,97
ssc-miR-671-3p	GCAGTCCGGTTCTCAGG	GGTCCAGTTTTTTTTTTTTTTTGGT	0,98
ssc-miR-708-5p	CGCAGAAGGAGCTTACAATC	GTCCAGTTTTTTTTTTTTTTTCCCA	1,01
ssc-miR-744	CGGGGCTAGGGCTAAC	GTCCAGTTTTTTTTTTTTTTTGCTG	1,07
ssc-miR-874	CCTGGCCCGAGGGA	CCAGTTTTTTTTTTTTTTTGTCGGT	1,10
ssc-miR-1343	GGGCCCGCACTCT	TCCAGTTTTTTTTTTTTTTTGCGA	1,03
ssc-miR-7134-5p	CCGCGGGTTCCCT	CCAGTTTTTTTTTTTTTTTGGATAGG	1,08

S2 Table. Comparison of porcine and human miRNA sequences for those applied in miRNA-mRNA interaction analysis. Underlined, bold nucleotides highlights differences between porcine and human sequences.

miRBase accession number	miRNA name	miRNA sequence
MIMAT0002141	ssc-miR-7	uggaagacuagugauuuuguugu**u**
MIMAT0000252	hsa-miR-7-5p	uggaagacuagugauuuuguugu
MIMAT0007753	ssc-miR-15a	uagcagcacauaaugguuugu
MIMAT0000068	hsa-miR-15a-5p	uagcagcacauaaugguuugu**g**
MIMAT0002161	ssc-miR-18a	uaaggugcaucuagugcagaua
MIMAT0000072	hsa-miR-18a-5p	uaaggugcaucuagugcagaua**g**
MIMAT0002165	ssc-miR-21	uagcuuaucagacugauguuga
MIMAT0000076	hsa-miR-21-5p	uagcuuaucagacugauguuga
MIMAT0002137	ssc-miR-29b	uagcaccauuugaaaucaguguu
MIMAT0000100	hsa-miR-29b-3p	uagcaccauuugaaaucaguguu
	No porcine homolog annotated in miRBase	
MIMAT0004676	hsa-miR-34b-3p	caaucacuaacuccacugccau
MIMAT0013916	ssc-miR-34c	aggcaguguaguuagcugauugc
MIMAT0000686	hsa-miR-34c-5p	aggcaguguaguuagcugauugc
MIMAT0013909	ssc-miR-92b-3p	uauugcacucgucccggccucc
MIMAT0003218	hsa-miR-92b-3p	uauugcacucgucccggccucc
MIMAT0022963	ssc-miR-146a-5p	ugagaacugaauuccauggguu
MIMAT0000449	hsa-miR-146a-5p	ugagaacugaauuccauggguu
MIMAT0002127	ssc-miR-184	uggacggagaacugauaagggu
MIMAT0000454	hsa-miR-184	uggacggagaacugauaagggu
MIMAT0013895	ssc-miR-193a-3p	aacuggccuacaaagucccagu
MIMAT0000459	hsa-miR-193a-3p	aacuggccuacaaagucccagu
MIMAT0002146	ssc-miR-205	uccuucauuccaccggagucug
MIMAT0000266	hsa-miR-205-5p	uccuucauuccaccggagucug
MIMAT0022949	ssc-miR-221-5p	accuggcauacaauguagauuu**cugu**
MIMAT0004568	hsa-miR-221-5p	accuggcauacaauguagauuu
	No porcine homolog annotated in miRBase	
MIMAT0004570	hsa-miR-223-5p	cguguauuugacaagcugaguu
MIMAT0022958	ssc-miR-296-3p	aggguugggcggaggcuuucc
MIMAT0004679	hsa-miR-296-3p	gaggguuggguggaggcucucc
MIMAT0015711	ssc-miR-363	aauugcacgguauccaucugua**a**
MIMAT0000707	hsa-miR-363-3p	aauugcacgguauccaucugua
	No porcine homolog annotated in miRBase	
MIMAT0000728	hsa-miR-375	uuuguucguucggcucgcguga
MIMAT0013868	ssc-miR-378	acuggacuuggagucagaaggc
MIMAT0000732	hsa-miR-378a-3p	acuggacuuggagucagaaggc
	No porcine homolog annotated in miRBase	
MIMAT0001541	hsa-miR-449a	uggcaguguauuguuagcuggu
	No porcine homolog annotated in miRBase	
MIMAT0003327	hsa-miR-449b-5p	aggcaguguauuguuagcuggc

MIMAT0018382	ssc-miR-451	aaaccguuaccauuacugaguu
MIMAT0001631	hsa-miR-451a	aaaccguuaccauuacugaguu
MIMAT0025379	ssc-miR-551a	gcgacccacucuugguuucc
MIMAT0003214	hsa-miR-551a	gcgacccacucuugguuucc**a**
	No porcine homolog annotated in miRBase	
MIMAT0004801	hsa-miR-590-3p	uaauuuuauguauaagcuagu
MIMAT0025382	ssc-miR-671-3p	uccgguucucagggcuccacc
MIMAT0004819	hsa-miR-671-3p	uccgguucucagggcuccacc
MIMAT0013945	ssc-miR-708-5p	aaggagcuuacaaucuagcuggg
MIMAT0004926	hsa-miR-708-5p	aaggagcuuacaaucuagcuggg
MIMAT0020596	ssc-miR-1343	cuccuggggcccgcacucucgc
MIMAT0019776	hsa-miR-1343-3p	cuccuggggcccgcacucucgc
MIMAT0028143	ssc-miR-7134-5p	auguccgcggguucccuaucc
	No human homolog annotated in miRBase	

Paper 4

Clinical outcome after influenza A virus challenge affects the pulmonary microRNA response in vaccinated and unvaccinated pigs

(WORKING TITLE)

Research article

L Brogaard, PMH Heegaard, LE Larsen, R Dürrwald, K Skovgaard

Manuscript in preparation

IAV detection by qPCR in the applied porcine lung samples will be included prior to manuscript submission

All raw data is freely available upon request

loun@vet.dtu.dk

Clinical outcome after influenza A virus challenge affects the pulmonary microRNA response in vaccinated and unvaccinated pigs

Louise Brogaard[1]*, Peter M. H. Heegaard[1], Lars E. Larsen[2], Ralf Dürrwald[3], Kerstin Skovgaard[1]

[1] Division of Immunology and Vaccinology – Innate Immunology, National Veterinary Institute, Technical University of Denmark, Kongens Lyngby, Denmark
[2] Division of Diagnostics and Scientific Advice – Virology, National Veterinary Institute, Technical University of Denmark, Kongens Lyngby, Denmark
[3] Department of Infectious Diseases, Robert Koch Institute, Berlin, Germany

* Corresponding author, loun@vet.dtu.dk

ABSTRACT

microRNAs (miRNAs) are short non-coding RNA molecules which exert post-transcriptional modulation of gene expression by binding to target mRNA via sequence complementarity. They are involved in a multitude of cellular processes, including lung inflammation, innate immunity, and the induction of the adaptive immune response. Here, we investigated the involvement of miRNAs in the host response to influenza A virus (IAV) challenge in vaccinated and unvaccinated pigs. 30 8-weeks-old pigs received a commercially available 2-step (day 0 and 21) inactivated swine IAV vaccine. All vaccinated pigs as well as 20 unvaccinated pigs were challenged with swine IAV (H1N2) by aerosol exposure one week after second administration of the vaccine.

Vaccinated pigs displayed significantly lower degrees of clinical disease in comparison with unvaccinated pigs. Transcriptional profiling of protein coding gene expression in the lungs of pigs revealed several innate viral pathogen recognition receptors (*TLR3*, *TLR7*, *DDX58*, and *IFIH1*), components of the antiviral interferon response (*IL28B*, *MX1*, *ISG15*, *ISG20*, *IFITM1*, *IFITM3*, *SOCS1*, *OAS1*, *EIF2AK2*, and *IRF7*), pro-inflammatory cytokines (*IL6*, *CCL2*, and *CXCL10*), and apoptosis-related genes (*BCL2*, *FAS*, and *FASLG*) to be significantly higher expressed in unvaccinated pigs compared to vaccinated pigs during the acute phase of IAV infection. *IL1A*, *IL18*, *IL8*, and *CSF2* were all significantly higher expressed in vaccinated pigs. Furthermore, a distinct pulmonary miRNA response in vaccinated and unvaccinated animals was seen at all examined time point after IAV challenge. GO Term (Biological Process) enrichment analysis of validated target genes for the differentially expressed miRNAs revealed distinct roles for miRNA regulation of the host response against influenza A virus infection in vaccinated and unvaccinated pigs. Many immune response related GO Terms were significantly enriched in targets for the subset of miRNAs most highly expressed in the vaccinated pigs, indicating miRNA involvement in the rapid induction of immune response after vaccination and IAV infection. In contrast, apoptosis-related GO Terms were enriched in gene targets for miRNAs most highly expressed in unvaccinated pigs. The pulmonary miRNA profiles remained significantly different between vaccinated and unvaccinated pigs at 14 days after IAV challenge. Targets of the differentially expressed miRNAs at day 14 were found to include GO Terms associated with activation of different mechanisms for lung regeneration and reestablishment of pulmonary immune homeostasis in both vaccinated and unvaccinated pigs.

INTRODUCTION

Influenza A virus (IAV) infections are responsible for considerable morbidity and mortality in humans, as well as in several other animal hosts including pigs and poultry. The European Center for Disease Prevention and Control (ECDC) estimates that 15,000-70,000 influenza-associated deaths occur each year in European citizens in addition to 4-50 million symptomatic cases [1]. Vaccination is the most effective method of preventing influenza, and the majority of current IAV vaccines administered to humans today are trivalent inactivated vaccines [2]. The he selection of IAV strains for seasonal IAV vaccines needs to be reevaluated every year as the process of antigenic drift continuously causes major viral surface antigens to mutate and escape recognition by neutralizing antibodies induced by vaccines and natural infection from previous seasons [3]. Substantial resources and effort have been devoted to creating a universal IAV vaccine, effective against a broad range of influenza strains. One approach to develop a universal IAV vaccine is to target highly conserved epitopes on the stem of HA in order to establish a B cell response that confers broad heterosubtypic immunity [4,5].

Development of a universal influenza vaccine is a highly coveted goal, and would be a scientific achievement with global implications for both human and animal health. In individuals that do not harbor immunity from vaccination or previous infection, initial control of IAV infection is highly dependent on a rapid innate immune response. The primary IAV-specific adaptive immune response will typically not set in until approx. one week after infection, leaving the host highly dependent on an efficient local pulmonary antiviral intrinsic and innate response in order to restrict viral spread and prevent excessive tissue damage [6] (Starbæk *et al*. 2017 (manuscript in preparation); Brogaard *et al*. 2017 (manuscript under review)). Insight into the local pulmonary immune response after IAV vaccination and infection is paramount for the understanding of how the host efficiently clears the virus and mounts protective immunity. The pig has proven valuable for the study of human IAV infection due to its remarkable similarity to humans in many aspects relevant for IAV infection. This includes highly similar morphology of the respiratory system including composition of the respiratory epithelial cell layer and influenza receptor distribution [7–9] (Starbæk *et al*. 2017 (manuscript in preparation)). Furthermore, the porcine innate immune response to IAV infection locally in the lung as well as systemically mirrors the sparse results described in human IAV studies [10] (Starbæk *et al*. 2017 (manuscript in preparation); Brogaard *et al*. 2017 (manuscript under review)).

Over the last couple of decades, microRNAs (miRNAs) have emerged as endogenous regulators of a multitude of cellular processes, including lung inflammation [11], innate immunity [12], and the induction of the adaptive immune response after vaccination [13]. miRNAs are short (~22 nt) non-coding RNA molecules which exercise post-transcriptional control of gene expression by binding to target mRNA via sequence complementarity [14]. The ubiquitous nature of miRNAs has by now made them an integrated part of a holistic view of the host transcriptional response to infection, and made them the focus of extensive research regarding their potential therapeutic and biomarker applications in a variety of settings [15,16]. The local pulmonary miRNA response to IAV infection has received some attention in recent years, and reports from IAV infections in pigs [17,18] (Brogaard *et al*. 2017 (manuscript under review)), non-human primates [19], and mice [20–23] have shed light on the involvement of miRNA in fine-tuning the local antiviral innate immune response in the lung. miRNAs have been shown to be differentially expressed during and after IAV infection, and to be putatively involved in regulation of IAV induced inflammation, apoptosis, and lung repair after IAV infection [10,21,24–26]. There is however a gap in our knowledge of miRNA involvement in the host response to IAV infection in vaccinated individuals. In general, we know very little of the host

transcriptional response associated with the lowered IAV disease severity observed in vaccinated individuals. The induction of local pulmonary immunity by IAV vaccination is regarded paramount for achieving sufficient protection [27–29], and knowledge of miRNA involvement in the regulation of the host response to IAV infection in the lung of vaccinated individuals may reveal novel mechanisms responsible for eliciting a protective vaccine-induced immune response.

In this study we compare the transcriptional response in lung tissue of pigs which had been immunized with a trivalent inactivated swine IAV vaccine (Respiporc FLU3, IDT Biologika) prior to IAV challenge (H1N2) with that of pigs naïve to IAV prior to challenge. We demonstrate that the ameliorated clinical manifestations observed in vaccinated pigs were associated with a significantly lowered antiviral interferon and pro-inflammatory cytokine response. Extensive miRNA profiling revealed distinct expression patterns in vaccinated and unvaccinated pigs both during acute infection and after the virus had been cleared. IAV vaccination thus greatly impacts the host pulmonary miRNA response to IAV infection, suggesting that miRNAs may potentially be involved in fine tuning and maintaining protective immunity after vaccination and reestablishment of lung immune homeostasis after viral clearance.

MATERIALS AND METHODS

Animals and challenge

All procedures and animal care was carried out in accordance with Good Clinical Practice (VICH GL9, CVMP/VICH/595/98), the Directive 2001/82/EC on the Community code relating to veterinary medicinal products, and German Animal Protection Law. The protocol IDT A 03/2004 was approved by the Landesverwaltungsamt Sachsen-Anhalt, Germany (Reference Number: AZ 42502-3-401 IDT). 50 pigs (Large White x German Landrace) were included in the present study; the pigs were 8-weeks-old at the time of first vaccination and 12-weeks-old at the time of IAV challenge. All animals were obtained from a farm which had had no IAV infections during the previous year. 30 pigs received 2-step vaccination against IAV with a commercially available trivalent inactivated vaccine (Respiporc FLU3 vaccine (IDT Biologika GmbH); vaccine strains: A/sw/Bakum/IDT1769/03(H3N2), A/sw/Haselünne/IDT2617/03(H1N1), and A/sw/Bakum/1832/00(H1N2)) by intramuscular injection behind the ear on the right side of the neck. First vaccination was given on day 0; booster shot was given on day 21. The remaining 20 pigs received no vaccination. On day 28 after the first vaccination, all 50 pigs were challenged by aerosol exposure to 6.0 l cell culture supernatant containing $10^{4.55}$ $TCID_{50}$/ml of the IAV strain A/sw/Denmark/12687/03(H1N2). Clinical signs of IAV infection were recorded during the first three days after challenge (rectal temperature and dyspnoea). Dyspnoea was scored according to the following scale as described previously [17]: 0 = breathing unaffected; 1 = increased respiratory frequency and moderate flank movement; 2 = marked pumping breathing and severe flank movement; 3 = labored breathing affecting the entire body, pronounced flank movement and substantial movements of the snout; 4 = severe breathing reflecting substantial lack of oxygen. Pigs were slaughtered at three time points after challenge: 1 day post challenge (dpc): 10 pigs from the vaccinated group and 6 pigs from the unvaccinated group; 3 dpc: 10 pigs from the vaccinated group and 6 pigs from the unvaccinated group; 14 dpc: 10 pigs from the vaccinated group and 8 pigs from the unvaccinated group. 500 mg of lung tissue was harvested from the left cranial lobe from regions without gross lesions and stored in RNAlater (Qiagen) at -20 °C. Blood samples were collected in Vacuette Tubes from all available animals before challenge and at 0.5, 1, 2, 3, 4, 5,

6, 7, and 14 dpc for quantification of C-reactive protein (CRP) in serum. Serum was obtained from the blood samples by centrifugation (3000 rpm) within four hours after collection and stored at -20 °C thereafter.

RNA extraction

For each pig, approx. 35 mg lung tissue was applied for total RNA extraction using the miRNeasy Mini Kit (Qiagen). Lung tissue was homogenized in M-tubes (Miltenyi Biotec) using a gentleMACS Octo Dissociator (Miltenyi Biotec) in 1 ml QIAzol Lysis Reagent (Qiagen). The lysate was mixed with chloroform (200 µl) and centrifuged at 12,000 x g for 15 minutes at 4 °C. The rest of the extraction procedure was carried out at room temperature. The upper aqueous phase was removed (300 µl) and mixed with 99.9 % ethanol (450 µl) and processed in RNeasy Mini Spin Columns (Qiagen). On-column DNase treatment was carried out using the RNase-free DNase Set (Qiagen) according to manufacturer's specifications. After DNase treatments, an extra centrifugation of the column was carried out (8,000 x g, 2 minutes) to prevent carryover of reagents from the extraction to the elution. RNA was eluted in 50 µl RNase-free water by centrifugation (8,000 x g, 2 minutes). Purity and concentration of the RNA extractions were measured with a NanoDrop ND-1000 UV spectrophotometer (Thermo Scientific). RNA concentrations ranged from 396 to 1,099 ng/µl, mean concentration was 727 ng/µl. A260/280 and A260/230 ratios showed acceptable purity of the extractions, with mean ratios of 2.11 and 2.10, respectively. RNA integrity numbers (RIN) were assessed by chip electrophoresis using Agilent RNA 6000 Nano Chips and Agilent RNA 6000 reagents with an Agilent 2100 Bioanalyzer (Agilent Technologies). RIN values varied from 5.4 to 8.9; mean RIN was 6.8.

RT-qPCR of miRNA

Two cDNA replicates were made from each RNA extraction using the method originally described by Balcells, Cirera, and Busk [30]. 100 ng RNA was reverse transcribed into cDNA in reaction volumes of 10 µl containing 1 µM universal RT primer (5' CAGGTCCAGTTTTTTTTTTTTTTTVN 3'), 1 µl 10X poly(A) polymerase buffer (New England BioLabs), 0.1 mM ATP (New England BioLabs), 0.1 µM of each deoxynucleotide (dATP, dTTP, dGTP, and dCTP) (Sigma-Aldrich), 100 units MuLV reverse transcriptase (replaced with water in -RT control (no reverse transcriptase)) (New England BioLabs), 1 unit poly(A) polymerase (replaced with water in -poly(A) control (no poly(A) polymerase)) (New England BioLabs), and RNase-free water. The reaction was carried out at 42 °C for 60 minutes followed by 95 °C for 5 minutes. cDNA samples were pre-amplified using a mix of all miRNA qPCR primer pairs which would be included in the subsequent qPCR. Pre-amplification was carried out in reaction volumes of 10 µl containing 2.5 µl cDNA (diluted 1:10 in low-EDTA TE buffer (VWR – Bie & Berntsen)), 2.5 µl 200 nM miRNA qPCR primer mix, 1 µl TaqMan PreAmp Master Mix (Applied Biosystems), and 4 µl RNase-free water. Pre-amplification cycling parameters were as follows: 95 °C for 10 minutes followed by 14 cycles of 95 °C for 15 seconds and 60 °C for 4 minutes. Pre-amplification was followed by exonuclease digestion of residual miRNA qPCR primers; 16 units of Exonuclease I (New England BioLabs) was added to each sample of pre-amplified cDNA and incubated at 37 °C for 30 minutes followed by 80 °C for 15 minutes. The universal RT primer and miRNA qPCR primers were designed as described previously [30], and purchased from Sigma-Aldrich. If possible, the porcine sequence of a given miRNA was used for primer design, which is indicated by the use of the ssc (*Sus scrofa*) prefix. If a porcine version of a miRNA of interest was not included in miRBase [31] at the time of primer design, then the corresponding human miRNA sequence was used for primer design instead,

indicated by the use of the hsa (*Homo sapiens*) prefix. Primer sequences and qPCR efficiencies for all miRNA assays can be found in Supplementary Table 1. miRNA levels were quantified in the pre-amplified cDNA samples by qPCR on the high-throughput platform BioMark HD (Fluidigm) in 96.96 Dynamic Array IFC chips (Fluidigm). Sample mix was prepared by combining 1.5 µl pre-amplified cDNA (diluted 1:10 in low-EDTA TE buffer (VWR – Bie & Berntsen)), 3 µl ABI TaqMan Gene Expression Master Mix (Applied Biosystems), 0.3 µl 20X DNA Binding Dye Sample Loading Reagent (Fluidigm), 0.3 µl 20X EvaGreen (Biotium, VWR – Bie & Berntsen), and 0.9 µl low-EDTA TE buffer (VWR – Bie & Berntsen). Samples included a non-template control (NTC) and triplicate 6-step 4-fold dilution series made from a pool of all pre-amplified cDNA samples (not -RT and -poly(A) controls) to assess qPCR efficiency for each miRNA assay. Assay mix was prepared by combining 3 µl primer pair (forward and reverse, 10 µM each) and 3 µl 2X Assay Loading Reagent (Fluidigm). Sample mixes and assay mixes were added to the appropriate inlets on the 96.96 Dynamic Array IFC chips, and the following thermal protocol was applied: a thermal mix phase consisting of 2 minutes at 50 °C, 30 minutes at 70 °C, and 10 minutes at 25 °C; a hot start phase consisting of 2 minutes at 50 °C and 10 minutes at 95 °C; 35 cycles of denaturing for 15 seconds at 95 °C and annealing/elongation for 1 minute at 60 °C, with fluorescence being recorded at the end of each cycle. Melting curve analysis was performed lastly by increasing the temperature from 60 to 95 °C at a speed of 1 °C/3 seconds. Amplification and melting curves were inspected visually and qPCR efficiency was calculated for each miRNA assay using the Fluidigm Real-Time PCR Analysis software (v. 4.1.3). Expression data was obtained for 65 different miRNAs (full list in Supplementary Table 1). miRNA qPCR data was processed using the GenEx software (v. 6), including efficiency correction, data normalization using the global mean expression method [32], and conversion of C_q values to relative quantities. Relative quantities of miRNA data was $\log_2$ transformed prior to statistical testing (Student's *t*-test), hierarchical clustering, and principal component analysis (PCA). miRNA expression data was moreover mean centered prior to PCA, carried out with the GenEx software (v. 6). Two-way agglomerative hierarchical clustering of miRNA expression data in combination with heat map generation was carried out using the online tool Morpheus [33] (accessed on October 1st 2017) using 'one minus Pearson's correlation' as distance measure.

RT-qPCR of protein coding genes

Two cDNA replicates were made from each RNA sample. 500 ng total RNA was reverse transcribed into cDNA using the QuantiTect Reverse Transcription Kit (Qiagen). First, a second DNase treatment was carried out to remove any residual genomic DNA; RNA was incubated with 2 µl gDNA Wipeout Buffer (Qiagen) in a total reaction volume of 14 µl (in RNase-free water) at 42 °C for 2 minutes. 6 µl reverse transcription master mix comprised of 0.75 µl Quantiscript Reverse Transcriptase (replaced with water in –RT control), 1 µl RT Primer Mix (mix of oligo-dT and random primers), 4 µl Quantiscript RT Buffer, and 0.25 µl RNase-free water was added to each sample after DNase treatment, and cDNA was synthesized at 42 °C for 15 minutes followed by 95 °C for 3 minutes. cDNA was diluted 1:10 in low-EDTA TE buffer prior to pre-amplification and exonuclease digestion, which was carried out as described above for miRNA, using 16 pre-amplification cycles. qPCR primers for protein coding genes were designed as described previously [34] using the Primer3 online tool (http://bioinfo.ut.ee/primer3-0.4.0/) and purchased from Sigma-Aldrich. Primer sequences and qPCR efficiencies for all assays for protein coding genes can be found in Supplementary Table 1. qPCR of protein coding genes was carried out as described above for miRNA, using 96.96 Dynamic Array IFC chips on the BioMark platform (Fluidigm). An NTC and triplicate dilution series (6-step 4-fold dilution)

from a pool of all pre-amplified cDNA samples (except the -RT control) were included to assess qPCR efficiency. All amplification and melting curves were inspected visually and qPCR efficiencies for each assay were calculated using the Fluidigm Real-Time PCR Analysis software (v. 4.1.3). qPCR data was processed using the GenEx software (v. 6), including efficiency correction, reference gene identification and data normalization, and conversion of C_q values to relative quantities. Stable reference genes were identified using the algorithms geNorm [35] and NormFinder [36], and the following genes were used for data normalization: β-actin (*ACTB*), β2 microglobulin (*B2M*), glyceraldehyde 3-phosphate dehydrogenase (*GAPDH*), peptidylprolyl isomerase A (*PPIA*), 60S ribosomal protein L13A (*RPL13A*), and tyrosine 3-monooxygenase/tryptophan 5-monooxygenase activation protein, zeta polypeptide (*YWHAZ*). Gene expression data was $\log_2$ transformed prior to statistical testing (Student's *t*-test).

CRP quantification in serum

Levels of C-reactive protein (CRP) were quantified in serum of all animals before challenge and at 0.5, 1, 2, 3, 4, 5, 6, 7, and 14 dpc by sandwich ELISA using dendrimer-coupled cytidine diphosphocholine in the coating layer [37] using polyclonal rabbit anti-human antibodies (Dako) with cross-reactivity to porcine CRP [38]. Detection was done with peroxidase-conjugated goat anti-rabbit antibodies (Dako). Pooled pig serum calibrated against a human CRP calibrator (Dako A0073) was used as standard. The detection limit was 0.35 mg/l (human equivalents). Plates were developed with a tetramethylbenzidine (TMB) peroxide color substrate according to manufacturer's instructions (Kem-En-Tec), reading optical densities of wells at 490 nm subtracting unspecific coloration at 650 nm using an automatic plate reader (Thermo Multiskan Ex spectrophotometer, Thermo Scientific). All samples including standards were assayed in duplicate. Sample values were calculated from the curve fitted to the readings of the standard using Ascent software (v. 2.6) (Thermo Scientific).

miRNA target identification and GO Term enrichment analysis

Gene Ontology (GO) Term (Biological Process) [39] enrichment analysis in sets of target genes for miRNAs found to be regulated, was performed to investigate potential functional implications of the observed differences in miRNA expression between vaccinated and unvaccinated pigs. As available databases of validated miRNA-target interactions do not include interactions validated in the pig, the human homologs were applied in target identification searches. An overview of porcine and the human homolog miRNA sequences applied in these searches can be seen in Supplementary Table 2. Prior to GO Term enrichment analyses, previously experimentally validated gene targets for the relevant miRNAs were retrieved from the online database TarBase (v. 7.0) [40] using the following settings: 'species' – '*Homo sapiens*'; 'validation type' – 'direct'; 'validated as' – 'positive'. GO Term enrichment was restricted to networks of genes that included 1) the target genes whose expression at 1 and 3 dpc was significantly negatively correlated (taking sample size into account to determine critical values of Pearson's *r* at $p < 0.05$) with the expression of the miRNA they were a target for, combined with 2) other proteins that the miRNA targets were identified to interact with (via STRING). GO Term enrichment analysis was carried out using the STRING database (v. 10.0) [41]. Input was the selected sets of target genes using the following settings: 'Organism' – '*Homo sapiens*', 'active interaction sources' – 'Experiments', 'minimum required interaction score' – 'highest confidence (0.900)', maximum number of interactions to show' – '1st shell: custom value, max interactions 500'. The maximum number of 1st shell interactions was arbitrarily set to 500 as this was found to exceed the number of interactions found with the given confidence score, thus ensuring that all available

interactions were shown. This generated protein networks including the targets of the differentially expressed miRNAs as well as proteins validated to interact with the miRNA targets. These networks are visualized in Supplementary Figures 1 and 2.
Similarly to the abovementioned process, subsets of miRNAs were identified which were differentially expressed in the lungs of vaccinated and unvaccinated pigs at 14 dpc when the infection had cleared. GO Term enrichment analysis was again carried out using the STRING database [41], however this time STRING was accessed via the database RAIN (v. 1.0) [42] which integrates with STRING and allows sets of miRNAs as input rather than protein coding genes. As such, for the 14 dpc analyses, sets of differentially expressed miRNAs were used as query input in RAIN (multiple names search), and the analysis settings in STRING were set to 'active interaction sources' – 'Experiments' and 'Databases', 'minimum required interaction score' – 'medium confidence (0.400)', maximum number of interactions to show' – '1st shell: custom value, max interactions 150'.
A lower confidence score was applied for analyses at 14 days after challenge compared to 1 and 3 days after challenge as some of the interactions used in STRING to build the network for enrichment analysis stems from miRNA target prediction algorithms (in addition to including experimentally validated targets), and such an interaction is in STRING assigned lower confidence than experimentally validated interactions.

RESULTS

Vaccinated pigs show milder clinical signs and altered innate antiviral and inflammatory transcriptional response after IAV challenge

Rectal temperature and dyspnoea scores were recorded for all pigs at 12, 24, 36, 48, and 72 hours post challenge (hpc) (Figure 1, A). Rectal temperature was significantly higher in unvaccinated pigs during the first 24 hpc compared to vaccinated pigs. Likewise, unvaccinated pigs had a significantly higher score of dyspnoea during the first 48 hpc after challenge compared to vaccinated pigs (Figure 1, B). However, the more severe clinical signs observed in unvaccinated pigs were not associated with elevated levels of CRP in their serum (Figure 1, C). A tendency towards higher CRP levels in vaccinated pigs compared to unvaccinated pigs was seen at 2-4 dpc, but level were not significantly different (Student's *t*-test) at any of the examined time points.
Transcriptional profiling of protein coding gene expression in the lungs of pigs after IAV challenge revealed several innate viral pathogen recognition receptors (PRRs) (*TLR3*, *TLR7*, *DDX58*, and *IFIH1*), components of the antiviral interferon response (*IL28B*, *MX1*, *ISG15*, *ISG20*, *IFITM1*, *IFITM3*, *SOCS1*, *OAS1*, *EIF2AK2*, and *IRF7*), pro- and anti-inflammatory cytokines (*IL1A*, *IL6*, *IL18*, *IL8*, *CCL2*, *CXCL10*, and *CSF2*), and apoptosis-related genes (*BCL2*, *FAS*, and *FASLG*) to be significantly differentially expressed ($p < 0.05$, Student's *t*-test; ≥2-fold higher levels in one group compared to the other) between vaccinated and unvaccinated animals during the acute phase of infection (Figure 2). *IL1A*, *IL18*, *IL8*, and *CSF2* were all more highly expressed (~2-4 fold) in vaccinated pigs; all other mentioned genes were more highly expressed in unvaccinated pigs (~2-7 fold). No significant differences in expression of protein coding genes between vaccinated and unvaccinated pigs were seen at 14 dpc. The expression of other genes commonly described to be mediators of the innate immune and antiviral host responses to IAV infection such as *IFNA1*, *IL1B*, *TNF*, *IL10*, and components of the NF-κB and JAK-STAT signaling pathways was easily detectable by qPCR, but these genes showed no differential expression between vaccinated and unvaccinated pigs at any of the examined time points.

Vaccination was associated with a distinct miRNA response in the porcine lung after IAV challenge

Initial investigation of the overall variation of miRNA expression profiles in the lungs of IAV challenged pigs was carried out by performing principal component analysis (PCA) on expression data for all assayed miRNAs (n = 65). Based on similarities and differences in miRNA expression patterns this analysis resulted in a clear separation of vaccinated and unvaccinated pigs (Figure 3), however no separate clusters were seen according to the three sampling time points. Less inter-sample variation was seen within the cluster of vaccinated pigs compared to the cluster of unvaccinated pigs.
To identify which miRNAs contributed to this clear distinction between vaccinated and unvaccinated pigs, hierarchical clustering of samples and miRNAs was performed, and visualized as a heat map in Figure 4. Again, pigs grouped together according to their vaccination status, with the distinction between sampling time points being less clear-cut. Two subsets of miRNAs were identified based on their different levels of expression in vaccinated and unvaccinated animals (Figure 4): subset 1 which generally showed lower expression levels in vaccinated pigs compared to unvaccinated pigs, and subset 2 which generally showed higher expression levels in vaccinated pigs compared to unvaccinated pigs. The potential functional implications of the differential expression of these two subsets of miRNAs in vaccinated and unvaccinated pigs was investigated by applying GO Term (Biological Process) [39] enrichment analysis of previously experimentally validated target genes retrieved from TarBase (v. 7.0) [40]. The set of target genes supplied to STRING [41] to generate gene networks for GO Term enrichment analysis for subset 1 included *BCL2*, *CASP3*, *CCNE2*, *CDK6*, *EIF2AK2*, *FAS*, *IFITM3*, *MCL1*, *MYC*, *NFE2L1*, *NFKBIA*, *PIK3R2*, *PRDM1*, *PTEN*, and *TP53*, and the target gene set for miRNA subset 2 included *BCL2*, *CDK6*, *JUN*, *MCL1*, *MYC*, *MYD88*, *NFE2L1*, *PIK3R1*, *PRDM1*, *PTEN*, *PTGS2*, and *STAT1*. The networks generated for GO Term enrichment analysis can be seen in Supplementary Figures 1 and 2; the networks for miRNA subsets 1 and 2 comprised 221 and 162 genes, respectively. Figure 5 shows the top ten most significantly enriched GO Terms (Biological Process) for the interaction networks for the two sets of target genes. For targets of miRNAs most highly expressed in unvaccinated pigs based on hierarchical clustering, enriched GO Terms were primarily associated with metabolic processes and apoptosis. For targets of miRNAs most highly expressed in vaccinated pigs based on hierarchical clustering, enriched GO Terms were primarily associated with immune response processes.

Different long-term effects on the pulmonary miRNA landscape were observed in vaccinated and unvaccinated pigs

26 miRNAs were found to be expressed at significantly different ($p < 0.05$, Student's *t*-test) levels in the lungs of vaccinated and unvaccinated pigs at 14 dpc. Importantly, IAV had not been detectable in lung tissue or nasal swabs of unvaccinated animals since 7 dpc [17]. Of these miRNAs, 9 were expressed at ≥1.5-fold higher levels in vaccinated pigs compared to unvaccinated pigs, and the remaining 17 miRNAs were expressed at ≥1.5-fold higher levels in unvaccinated pigs compared to vaccinated pigs (Figure 6). GO Term (Biological Process) [39] enrichment analysis of miRNA gene targets was performed using the integrated RAIN (v. 1.0) and STRING (v. 10.5) databases [41,42]. Search input for RAIN comprised the two sets of miRNAs found differentially expressed between vaccinated and unvaccinated animals at 14 dpc (Figure 6). These two inputs yielded two miRNA-target gene interaction networks which are shown in Supplementary Figures 3 and 4. The interaction

network for miRNAs most highly expressed in vaccinated and unvaccinated pigs included 54 and 141 genes, respectively. The top ten most significantly enriched GO Terms (Biological Process) in the two target gene sets are shown in Figure 7.

DISCUSSION

In the present study we employed transcriptional analysis of miRNAs and protein coding genes in the lungs of pigs that had been experimentally challenged with IAV infection. We could demonstrate that immunization with a commercially available trivalent inactivated porcine IAV vaccine conferred protection from disease as evident by the significantly lowered clinical signs observed in vaccinated pigs compared to unvaccinated pigs upon IAV challenge. These differences in clinical outcome was associated with a marked difference in lung miRNA expression in vaccinated and unvaccinated pigs, indicating that different miRNAs may potentially be involved in inducing, fine-tuning, and maintaining protective immunity after vaccination .

In a naïve humans or animals, limiting viral replication and disease severity is mediated by the innate immune response. This is achieved by a fast and transient induction of an interferon mediated antiviral response by type I and III interferons and interferon stimulated genes (ISGs), as well as a balanced pro- and anti-inflammatory response [17,43–46] (Brogaard *et al*. 2017 (manuscript under review)). Prior immunization with inactivated vaccines will induce a humoral response within days after IAV infection [47], which will reduce the viral load of the lung via neutralization or other antibody-dependent mechanisms such as antibody-dependent cellular cytotoxicity (ADCC) and complement dependent lytic (CDL) antibodies [48–50].

By hierarchical clustering of lung miRNA expression data from vaccinated and unvaccinated pigs after IAV challenge, we identified two clusters of miRNAs which showed markedly different expression patterns. GO Term (Biological Process) enrichment analysis of previously experimentally validated target genes, and their interacting genes, revealed distinct potential roles for miRNA regulation of the host response against IAV infection in vaccinated and unvaccinated pigs within the first three days after challenge. GO Terms related to immune response, including antibody based responses, were among the most significantly enriched biological processes in the protein coding gene targets for the subset of miRNAs which were more highly expressed in the vaccinated pigs shortly after challenge. In contrast, GO Terms associated with metabolic processes and apoptosis were most significantly enriched in target genes of miRNAs that were more highly expressed in unvaccinated animals. This is in accordance with the known importance of apoptosis both as a host defense mechanism during IAV infection, but also as a strategy by which IAV enhances its replication [51,52], and the fact that apoptosis-related genes (*BCL2*, *FAS*, *FASLG*) were more highly expressed in unvaccinated animals. The miRNA expression profiles locally in the lungs of IAV challenged pigs suggest that these non-coding RNAs might be involved in early modulation and induction of both innate and adaptive responses in vaccinated pigs. Given the lowered disease severity observed in vaccinated pigs, the induced immune responses were effective in limiting the impact of IAV infection. This was likewise reflected by the lower expression levels of several genes known to contribute to antiviral and pro-inflammatory responses in vaccinated pigs during acute infection. These responses were however more highly induced in the unvaccinated animals, which relied on strong pro-inflammatory, apoptotic, and interferon-induced antiviral responses for the early control of IAV infection. Lung tissue gross pathology and histopathology was not recorded for these animals, so it is not possible to assess the correlation between histopathological changes, pro-inflammatory

response, and miRNA expression profiles. No significantly elevated levels of serum CRP were observed in the unvaccinated pigs compared to the less clinically affected vaccinated pigs, despite the fact that this acute phase protein previously has been shown to be elevated in swine IAV infected pigs [53,54]. Thus, even though vaccination was associated with reduced clinical signs and lowered the expression of several well-known ISG such as *MX1*, *ISG15*, *ISG20*, and *CXCL10* locally in the lung, no systemic differences of CRP were seen in these pigs.

Significant differences in miRNA expression levels between vaccinated and unvaccinated pigs were even found on day 14 after challenge by which time the IAV infection had been cleared in unvaccinated pigs [17]. We have previously shown that alterations to the miRNA landscape persists in the lungs and in circulating leukocytes in pigs at 14 days after IAV challenge, despite the fact that the infection is cleared and the animals have returned to normal health [10,17] (Brogaard et al. 2017 (manuscript under review)). Similar observations have been made in mice [21]. Here we show that IAV vaccination prior to infection may have consequences for the composition of the protracted pulmonary miRNA response. However, whether the differential miRNA expression in the lungs of vaccinated and unvaccinated pigs is a direct consequence of vaccination status, or an effect mediated by the difference in disease severity and related local pulmonary pro-inflammatory response after IAV challenge remains unanswered. Most likely, both vaccination status and magnitude of the innate response to infection influence the protracted pulmonary miRNA response, and differentiation between the two is not easily determined. GO Term enrichment analysis of the target genes of the subsets of miRNAs which were differently expressed in vaccinated and unvaccinated pigs at 14 dpc revealed that both subsets of miRNAs are likely involved in regenerative functions, evident by the enrichment of processes associated with cell proliferation and differentiation, organ development, and metabolic and biosynthetic processes. Thus, miRNAs appear to participate in the efforts to reestablish lung homeostasis after IAV infection regardless of vaccination status. Vaccination and/or differences in the severity of disease may however influence the progression of these events after infection, giving rise to differences in the miRNAs involved in this important task.

FIGURE AND TABLE TEXTS

Figure 1. Clinical signs and serum CRP in pigs after IAV challenge. A) rectal temperature of vaccinated pigs (dashed line) at 12 (n = 30), 24 (n = 20), 36 (n = 20), 48 (n = 20), and 72 (n = 20) hpc, and unvaccinated pigs (solid line) at 12 (n = 20), 24 (n = 14), 36 (n = 14), 48 (n = 14), and 72 (n = 14) hpc. ** $p < 0.0001$, * $p < 0.01$ (Student's *t*-test). Error bars show standard deviation (SD). B) dyspnoea score of vaccinated pigs (hatched bars) at 12 (n = 30), 24 (n = 20), 36 (n = 20), 48 (n = 20), and 72 (n = 20) hpc, and unvaccinated pigs (solid bars) at 12 (n = 20), 24 (n = 14), 36 (n = 14), 48 (n = 14), and 72 (n = 14) hpc. ** $p < 0.0001$, * $p < 0.01$ (Mann-Whitney *U* test). Error bars show SD. C) Serum CRP levels in vaccinated pigs (dashed line) before challenge (n = 30) and 0.5 (n = 30), 1 (n = 20), 2 (n = 20), 3 (n = 20), 4 (n = 10), 5 (n = 10), 6 (n = 10), 7 (n = 10), and 14 (n = 10) dpc, and unvaccinated pigs (solid line) before challenge (n = 20) and 0.5 (n = 20), 1 (n = 14), 2 (n = 14), 3 (n = 14), 4 (n = 6), 5 (n = 6), 6 (n = 6), 7 (n = 6), and 14 (n = 6) dpc. Error bars show SD. VAC – vaccinated. UNVAC – unvaccinated.

Figure 2. Differential pulmonary expression of protein coding genes in unvaccinated compared to vaccinated pigs. Expression level ratios of protein coding genes in lungs at 1, 3, and 14 dpc in

unvaccinated pigs is shown relative to vaccinated pigs. * $p < 0.05$ (Student's *t*-test). Horizontal dashed black lines denote 2-fold up- and down-regulation. VAC – vaccinated. UNVAC – unvaccinated.

Figure 3. PCA of miRNA expression data in lungs of IAV challenged pigs. PCA of expression data generated from 65 different pulmonary miRNAs at 1 (red), 3 (blue), and 14 (grey) dpc. Group labeled 1 – vaccinated pigs; group labeled 2 – unvaccinated pigs. Expression data was $\log_2$ transformed and mean centered prior to PCA. Each square represents one lung tissue sample from an IAV challenged pig.

Figure 4. Hierarchical clustering of samples and miRNAs based on gene expression data. Agglomerative hierarchical clustering was carried out on $\log_2$ transformed expression data using the 'one minus Pearson's correlation' distance measure. Each column represents a lung tissue sample from an IAV challenged pig; each sample is named according to the pig's vaccination status (VAC/UNVAC), sampling time point (1/3/14 dpc), and a unique three digit animal ID. Each row represents expression levels of a miRNA; a relative color scheme is employed for each individual row to show the expression pattern for that miRNA across all samples. Dark red – highest relative levels of miRNA expression; dark blue – lowest relative levels of miRNA expression. Subset 1 – miRNAs which are expressed at lower levels in vaccinated pigs and at higher levels in unvaccinated pigs. Subset 2 – miRNAs which are expressed at higher levels in vaccinated pigs and at lower levels in unvaccinated pigs.

Figure 5. GO Term enrichment in target gene networks of differentially expressed miRNAs. A) Top ten most significantly enriched GO Terms (Biological Process) in the protein interaction network of target genes for miRNAs found to be more highly expressed in unvaccinated pigs compared to vaccinated pigs. Bars depict the percentage of the total number of genes (n = 221) which are associated with the individual GO Terms. B) Top ten most significantly enriched GO Terms (Biological Process) in the protein interaction network of target genes for miRNAs found to be more highly expressed in vaccinated pigs compared to unvaccinated pigs. Bars depict the percentage of the total number of genes (n = 162) which are associated with the individual GO Terms.

Figure 6. miRNA profiles in lungs after IAV clearance. All depicted miRNAs are expressed at significantly different levels at 14 dpc in the lungs of unvaccinated compared to vaccinated pigs ($p < 0.05$, Student's *t*-test; ≥1.5-fold higher levels). VAC – vaccinated. UNVAC – unvaccinated.

Figure 7. GO Term enrichment in target genes of miRNAs differentially expressed 14 dpc. A) Top ten most significantly enriched GO Terms (Biological Process) in the target genes for miRNAs found to be more highly expressed in unvaccinated pigs compared to vaccinated pigs at 14 dpc. Bars depict the percentage of the total number of genes (n = 141) which are associated with the individual GO Terms. B) Top ten most significantly enriched GO Terms (Biological Process) in the target genes for miRNAs found to be more highly expressed in vaccinated pigs compared to unvaccinated pigs at 14 dpc. Bars depict the percentage of the total number of genes (n = 54) which are associated with the individual GO Terms.

Supplementary Figure 1. Protein coding gene interaction network generated in STRING, obtained for target genes of miRNAs found to be more highly expressed in unvaccinated pigs compared to vaccinated pigs after IAV challenge based on hierarchical clustering.

Supplementary Figure 2. Protein coding gene interaction network generated in STRING, obtained for target genes of miRNAs found to be more highly expressed in vaccinated pigs compared to unvaccinated pigs after IAV challenge based on hierarchical clustering.

Supplementary Figure 3. Protein coding gene interaction network obtained for target genes of miRNAs found to be significantly more expressed in unvaccinated pigs compared to vaccinated pigs at 14 dpc.

Supplementary Figure 4. Protein coding gene interaction network obtained for target genes of miRNAs found to be significantly more expressed in vaccinated pigs compared to unvaccinated pigs at 14 dpc.

Supplementary Table 1. qPCR primer sequences and experimentally obtained qPCR efficiencies for the assayed miRNAs and protein coding genes.

Supplementary Table 2. Porcine miRNA sequences and their human homolog sequences applied in the retrieval of previously experimentally validated gene targets from TarBase (v. 7.0). Differences between porcine and human sequences are highlighted by bold, underlined nucleotides.

REFERENCES

1. European Centre for Disease Prevention and Control. Factsheet about seasonal influenza [Internet]. 2017 [cited 2017 Oct 1]. Available from: https://ecdc.europa.eu/en/seasonal-influenza/facts/factsheet
2. Schotsaert M, García-Sastre A. Inactivated influenza virus vaccines: the future of TIV and QIV. Curr. Opin. Virol. 2017;23:102–6.
3. Wiersma L, Rimmelzwaan G, de Vries R. Developing Universal Influenza Vaccines: Hitting the Nail, Not Just on the Head. Vaccines. 2015;3:239–62.
4. Fu Y, Zhang Z, Sheehan J, Avnir Y, Ridenour C, Sachnik T, et al. A broadly neutralizing anti-influenza antibody reveals ongoing capacity of haemagglutinin-specific memory B cells to evolve. Nat. Commun. 2016;7:12780.
5. Andrews SF, Joyce MG, Chambers MJ, Gillespie RA, Kanekiyo M, Leung K, et al. Preferential induction of cross-group influenza A hemagglutinin stem–specific memory B cells after H7N9 immunization in humans. Sci. Immunol. 2017;2.
6. Tripathi S, White MR, Hartshorn KL. The amazing innate immune response to influenza A virus infection. Innate Immun. 2013;21:73–98.
7. Trebbien R, Larsen LE, Viuff BM. Distribution of sialic acid receptors and influenza A virus of avian and swine origin in experimentally infected pigs. Virol. J. BioMed Central Ltd; 2011;8:434.
8. Wallace P, Kennedy JR, Mendicino J. Transdifferentiation of outgrowth cells and cultured epithelial cells from swine trachea. Vitr. Cell. Dev. Biol. - Anim. 1994;3:168–80.

9. Jeffery PK. Morphologic Features of Airway Surface Epithelial Cells and Glands. Am. Rev. Respir. Dis. 1983;128:S14–20.
10. Brogaard L, Heegaard PMH, Larsen LE, Mortensen S, Schlegel M, Dürrwald R, et al. Late regulation of immune genes and microRNAs in circulating leukocytes in a pig model of influenza A (H1N2) infection. Sci. Rep. 2016;6:21812.
11. Foster PS, Plank M, Collison A, Tay HL, Kaiko GE, Li J, et al. The emerging role of microRNAs in regulating immune and inflammatory responses in the lung. Immunol. Rev. 2013;253:198–215.
12. O'Connell RM, Rao DS, Chaudhuri AA, Baltimore D. Physiological and pathological roles for microRNAs in the immune system. Nat. Rev. Immunol. Nature Publishing Group; 2010;10:111–22.
13. de Candia P, Torri A, Gorletta T, Fedeli M, Bulgheroni E, Cheroni C, et al. Intracellular Modulation, Extracellular Disposal and Serum Increase of MiR-150 Mark Lymphocyte Activation. PLoS One. 2013;8:1–13.
14. Bartel DP. MicroRNA Target Recognition and Regulatory Functions. Cell. 2009;136:215–33.
15. Correia CN, Nalpas NC, McLoughlin KE, Browne JA, Gordon S V., MacHugh DE, et al. Circulating microRNAs as potential biomarkers of infectious disease. Front. Immunol. 2017;8:1–17.
16. Rupaimoole R, Slack FJ. MicroRNA therapeutics: towards a new era for the management of cancer and other diseases. Nat. Rev. Drug Discov. Nature Publishing Group; 2017;16:203–22.
17. Skovgaard K, Cirera S, Vasby D, Podolska A, Breum SO, Durrwald R, et al. Expression of innate immune genes, proteins and microRNAs in lung tissue of pigs infected experimentally with influenza virus (H1N2). Innate Immun. 2013;19:531–44.
18. Jiang P, Zhou N, Chen X, Zhao X, Li D, Wang F, et al. Integrative analysis of differentially expressed microRNAs of pulmonary alveolar macrophages from piglets during H1N1 swine influenza A virus infection. Sci. Rep. 2015;5:8167.
19. Li Y, Li J, Belisle S, Baskin CR, Tumpey TM, Katze MG. Differential microRNA expression and virulence of avian, 1918 reassortant, and reconstructed 1918 influenza A viruses. Virology. 2011;421:105–13.
20. Preusse M, Schughart K, Pessler F. Host genetic background strongly affects pulmonary microRNA expression before and during influenza A virus infection. Front. Immunol. 2017;8:1–18.
21. Pociask DA, Robinson KM, Chen K, McHugh KJ, Clay ME, Huang GT, et al. Epigenetic and Transcriptomic Regulation of Lung Repair during Recovery from Influenza Infection. Am. J. Pathol. 2017;187:851–63.
22. Tan K, Choi H, Jiang X, Yin L, Seet J, Patzel V, et al. Micro-RNAs in regenerating lungs: an integrative systems biology analysis of murine influenza pneumonia. BMC Genomics. 2014;15:587.
23. Vela EM, Kasoji MD, Wendling MQ, Price JA, Knostman KAB, Bresler HS, et al. MicroRNA expression in mice infected with seasonal H1N1, swine H1N1 or highly pathogenic H5N1. J. Med. Microbiol. 2014;63:1131–42.
24. Terrier O, Textoris J, Carron C, Marcel V, Bourdon J-C, Rosa-Calatrava M. Host microRNA molecular signatures associated with human H1N1 and H3N2 influenza A viruses reveal an unanticipated antiviral activity for miR-146a. J. Gen. Virol. 2013;94:985–95.
25. Guan Z, Shi N, Song Y, Zhang X, Zhang M, Duan M. Induction of the cellular microRNA-29c by influenza virus contributes to virus-mediated apoptosis through repression of antiapoptotic factors BCL2L2. Biochem. Biophys. Res. Commun. Elsevier Inc.; 2012;425:662–7.
26. Bao Y, Gao Y, Jin Y, Cong W, Pan X, Cui X. MicroRNA expression profiles and networks in mouse lung infected with H1N1 influenza virus. Mol. Genet. Genomics. Springer Berlin Heidelberg; 2015;290:1885–97.

27. Morgan SB, Hemmink JD, Porter E, Harley R, Shelton H, Aramouni M, et al. Aerosol Delivery of a Candidate Universal Influenza Vaccine Reduces Viral Load in Pigs Challenged with Pandemic H1N1 Virus. J. Immunol. 2016;196:5014–23.
28. Tchilian E, Holzer B. Harnessing Local Immunity for an Effective Universal Swine Influenza Vaccine. Viruses. 2017;9:98.
29. Adachi Y, Onodera T, Yamada Y, Daio R, Tsuiji M, Inoue T, et al. Distinct germinal center selection at local sites shapes memory B cell response to viral escape. J. Exp. Med. Rockefeller University Press; 2015;212:1709–23.
30. Balcells I, Cirera S, Busk PK. Specific and sensitive quantitative RT-PCR of miRNAs with DNA primers. BMC Biotechnol. 2011;11:70.
31. Kozomara A, Griffiths-Jones S. MiRBase: Annotating high confidence microRNAs using deep sequencing data. Nucleic Acids Res. 2014;42:68–73.
32. Mestdagh P, Van Vlierberghe P, De Weer A, Muth D, Westermann F, Speleman F, et al. A novel and universal method for microRNA RT-qPCR data normalization. Genome Biol. 2009;10:R64.
33. Morpheus [Internet]. [cited 2017 Oct 1]. Available from: https://software.broadinstitute.org/morpheus/
34. Skovgaard K, Mortensen S, Boye M, Poulsen KT, Campbell FM, Eckersall PD, et al. Rapid and widely disseminated acute phase protein response after experimental bacterial infection of pigs. Vet.Res. 2009;40:23.
35. Vandesompele J, De PK, Pattyn F, Poppe B, Van RN, De PA, et al. Accurate normalization of real-time quantitative RT-PCR data by geometric averaging of multiple internal control genes. Genome Biol. 2002;3:RESEARCH0034.
36. Andersen CL, Jensen JL, Ørntoft TF. Normalization of Real-Time Quantitative Reverse Transcription-PCR Data: A Model-Based Variance Estimation Approach to Identify Genes Suited for Normalization, Applied to Bladder and Colon Cancer Data Sets. Cancer Res. 2004;64:5245–50.
37. Heegaard PM, Klausen J, Nielsen JP, Gonzalez-Ramon N, Pineiro M, Lampreave F, et al. The porcine acute phase response to infection with Actinobacillus pleuropneumoniae. Haptoglobin, C-reactive protein, major acute phase protein and serum amyloid A protein are sensitive indicators of infection. Comp Biochem. B Biochem. 1998;119:365–73.
38. Heegaard PM, Pedersen HG, Jensen AL, Boas U. A robust quantitative solid phase immunoassay for the acute phase protein C-reactive protein (CRP) based on cytidine 5'-diphosphocholine coupled dendrimers. J.Immunol.Methods. 2009;343:112–8.
39. The Gene Ontology in 2010: extensions and refinements. Nucleic Acids Res. 2010;38.
40. Vlachos IS, Paraskevopoulou MD, Karagkouni D, Georgakilas G, Vergoulis T, Kanellos I, et al. DIANA-TarBase v7.0: Indexing more than half a million experimentally supported miRNA:mRNA interactions. Nucleic Acids Res. 2015;43:D153–9.
41. Szklarczyk D, Franceschini A, Wyder S, Forslund K, Heller D, Huerta-Cepas J, et al. STRING v10: Protein-protein interaction networks, integrated over the tree of life. Nucleic Acids Res. 2015;43:D447–52.
42. Junge A, Refsgaard JC, Garde C, Pan X, Santos A, Alkan F, et al. RAIN: RNA-protein Association and Interaction Networks. Database. 2017;2017:1–9.
43. Delgado-Ortega M, Melo S, Punyadarsaniya D, Ramé C, Olivier M, Soubieux D, et al. Innate immune response to a H3N2 subtype swine influenza virus in newborn porcine trachea cells, alveolar macrophages, and precision-cut lung slices. Vet. Res. 2014;45:1–18.

44. Galani IE, Triantafyllia V, Eleminiadou E-E, Koltsida O, Stavropoulos A, Manioudaki M, et al. Interferon-λ Mediates Non-redundant Front-Line Antiviral Protection against Influenza Virus Infection without Compromising Host Fitness. Immunity. 2017;46:875–890.e6.
45. Wilkinson JM, Gunvaldsen RE, Detmer SE, Dyck MK, Dixon WT, Foxcroft GR, et al. Transcriptomic and epigenetic profiling of the lung of influenza-infected pigs: A comparison of different birth weight and susceptibility groups. PLoS One. 2015;10:1–24.
46. Vidaña B, Martínez J, Martínez-Orellana P, García Migura L, Montoya M, Martorell J, et al. Heterogeneous pathological outcomes after experimental pH1N1 influenza infection in ferrets correlate with viral replication and host immune responses in the lung. Vet. Res. 2014;45:1–14.
47. Krammer F, Palese P. Advances in the development of influenza virus vaccines. Nat. Rev. Drug Discov. 2015;14:167–82.
48. Kim JH, Reber AJ, Kumar A, Ramos P, Sica G, Music N, et al. Non-neutralizing antibodies induced by seasonal influenza vaccine prevent, not exacerbate A(H1N1)pdm09 disease. Sci. Rep. 2016;6:37341.
49. Zhong W, Gross FL, Holiday C, Jefferson SN, Bai Y, Liu F, et al. Vaccination with 2014-15 Seasonal Inactivated Influenza Vaccine Elicits Cross-Reactive Anti-HA Antibodies with Strong ADCC Against Antigenically Drifted Circulating H3N2 Virus in Humans. Viral Immunol. 2016;29:259–62.
50. Co MDT, Cruz J, Takeda A, Ennis FA, Terajima M. Comparison of complement dependent lytic, hemagglutination inhibition and microneutralization antibody responses in influenza vaccinated individuals. Hum. Vaccines Immunother. 2012;8:1218–22.
51. Tripathi S, Batra J, Cao W, Sharma K, Patel JR, Ranjan P, et al. Influenza A virus nucleoprotein induces apoptosis in human airway epithelial cells: implications of a novel interaction between nucleoprotein and host protein Clusterin. Cell Death Dis. 2013;4:e562.
52. Jorgensen I, Rayamajhi M, Miao EA. Programmed cell death as a defence against infection. Nat. Rev. Immunol. 2017;17:151–64.
53. Pomorska-Mól M, Markowska-Daniel I, Kwit K, Czyżewska E, Dors A, Rachubik J, et al. Immune and inflammatory response in pigs during acute influenza caused by H1N1 swine influenza virus. Arch. Virol. 2014;159:2605–14.
54. Pomorska-Mól M, Markowska-Daniel I, Kwit K. Immune and acute phase response in pigs experimentally infected with H1N2 swine influenza virus. FEMS Immunol. Med. Microbiol. 2012;66:334–42.

Figure 1. Clinical signs and serum CRP in pigs after IAV challenge. A) rectal temperature of vaccinated pigs (dashed line) at 12 (n = 30), 24 (n = 20), 36 (n = 20), 48 (n = 20), and 72 (n = 20) hpc, and unvaccinated pigs (solid line) at 12 (n = 20), 24 (n = 14), 36 (n = 14), 48 (n = 14), and 72 (n = 14) hpc. ** $p < 0.0001$, * $p < 0.01$ (Student's *t*-test). Error bars show standard deviation (SD). B) dyspnoea score of vaccinated pigs (hatched bars) at 12 (n = 30), 24 (n = 20), 36 (n = 20), 48 (n = 20), and 72 (n = 20) hpc, and unvaccinated pigs (solid bars) at 12 (n = 20), 24 (n = 14), 36 (n = 14), 48 (n = 14), and 72 (n = 14) hpc. ** $p < 0.0001$, * $p < 0.01$ (Mann-Whitney *U* test). Error bars show SD. C) Serum CRP levels in vaccinated pigs (dashed line) before challenge (n = 30) and 0.5 (n = 30), 1 (n = 20), 2 (n = 20), 3 (n = 20), 4 (n = 10), 5 (n = 10), 6 (n = 10), 7 (n = 10), and 14 (n = 10) dpc, and unvaccinated pigs (solid line) before challenge (n = 20) and 0.5 (n = 20), 1 (n = 14), 2 (n = 14), 3 (n = 14), 4 (n = 6), 5 (n = 6), 6 (n = 6), 7 (n = 6), and 14 (n = 6) dpc. Error bars show SD. VAC – vaccinated. UNVAC – unvaccinated.

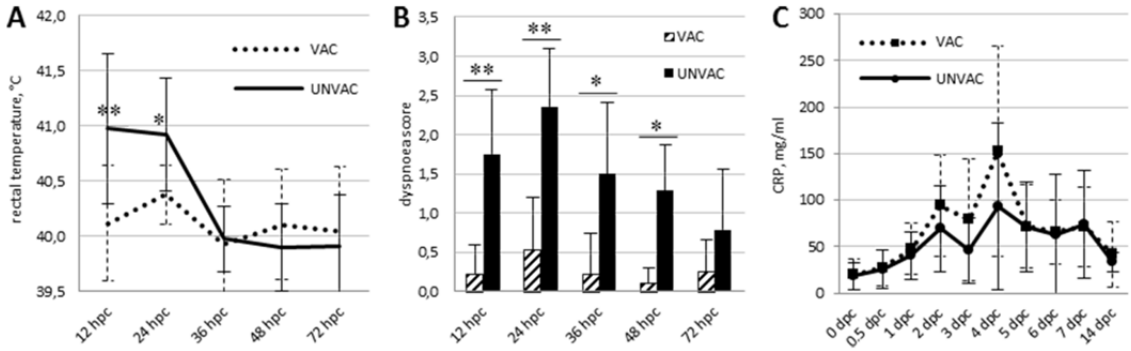

Figure 2. Differential pulmonary expression of protein coding genes in unvaccinated compared to vaccinated pigs. Expression level ratios of protein coding genes in lungs at 1, 3, and 14 dpc in unvaccinated pigs is shown relative to vaccinated pigs. * $p < 0.05$ (Student's *t*-test). Horizontal dashed black lines denote 2-fold up- and down-regulation. VAC – vaccinated. UNVAC – unvaccinated.

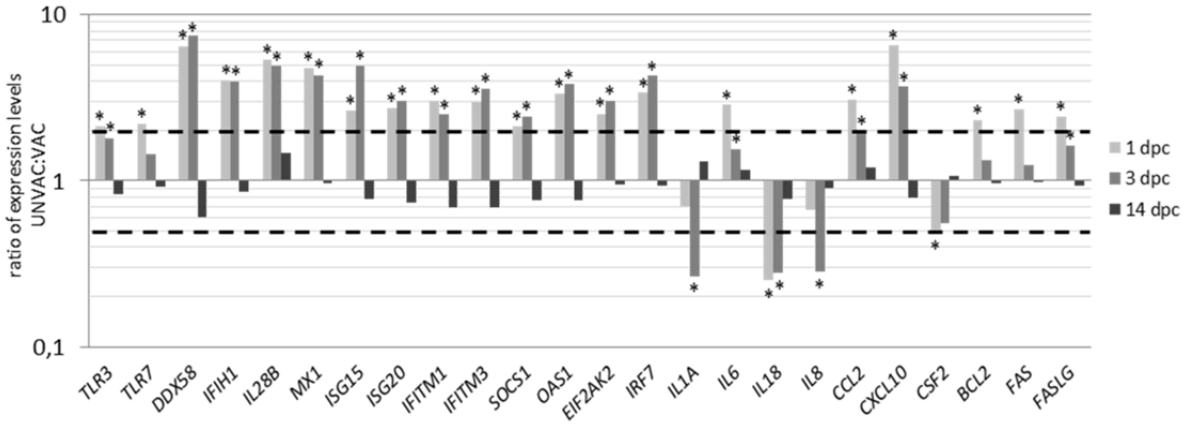

Figure 3. PCA of miRNA expression data in lungs of IAV challenged pigs. PCA of expression data generated from 65 different pulmonary miRNAs at 1 (red), 3 (blue), and 14 (grey) dpc. Group labeled 1 – vaccinated pigs; group labeled 2 – unvaccinated pigs. Expression data was $\log_2$ transformed and mean centered prior to PCA. Each square represents one lung tissue sample from an IAV challenged pig.

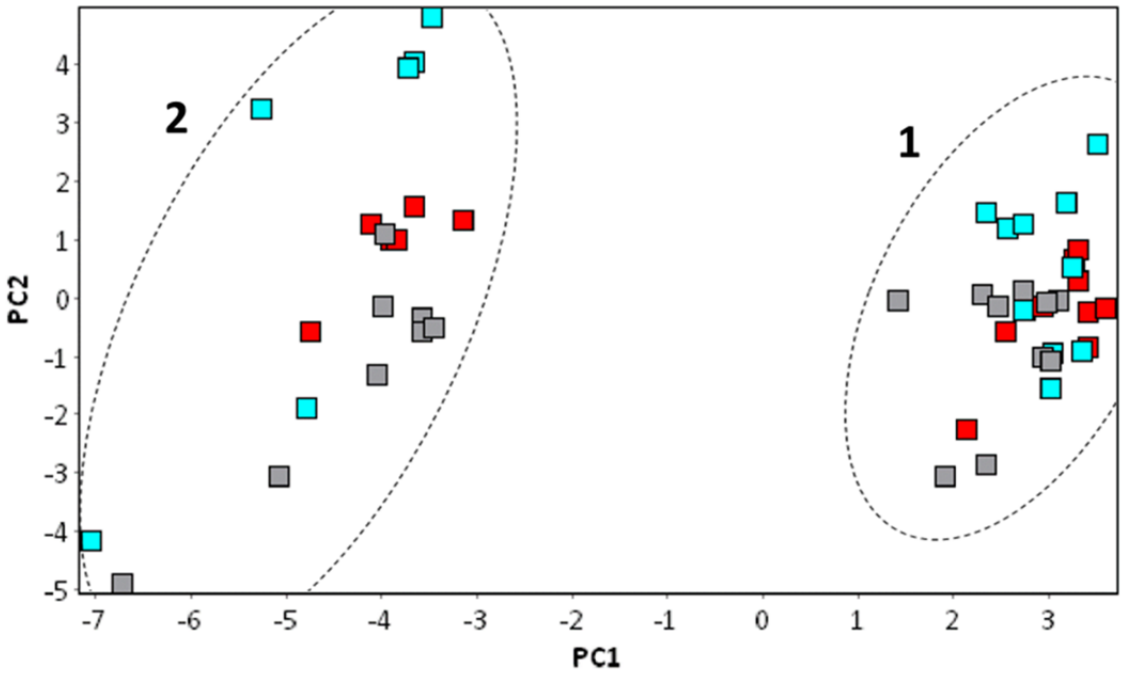

Figure 4. Hierarchical clustering of samples and miRNAs based on gene expression data.
Agglomerative hierarchical clustering was carried out on log_2 transformed expression data using the 'one minus Pearson's correlation' distance measure. Each column represents a lung tissue sample from an IAV challenged pig; each sample is named according to the pig's vaccination status (VAC/UNVAC), sampling time point (1/3/14 dpc), and a unique three digit animal ID. Each row represents expression levels of a miRNA; a relative color scheme is employed for each individual row to show the expression pattern for that miRNA across all samples. Dark red – highest relative levels of miRNA expression; dark blue – lowest relative levels of miRNA expression. Subset 1 – miRNAs which are expressed at lower levels in vaccinated pigs and at higher levels in unvaccinated pigs. Subset 2 – miRNAs which are expressed at higher levels in vaccinated pigs and at lower levels in unvaccinated pigs.

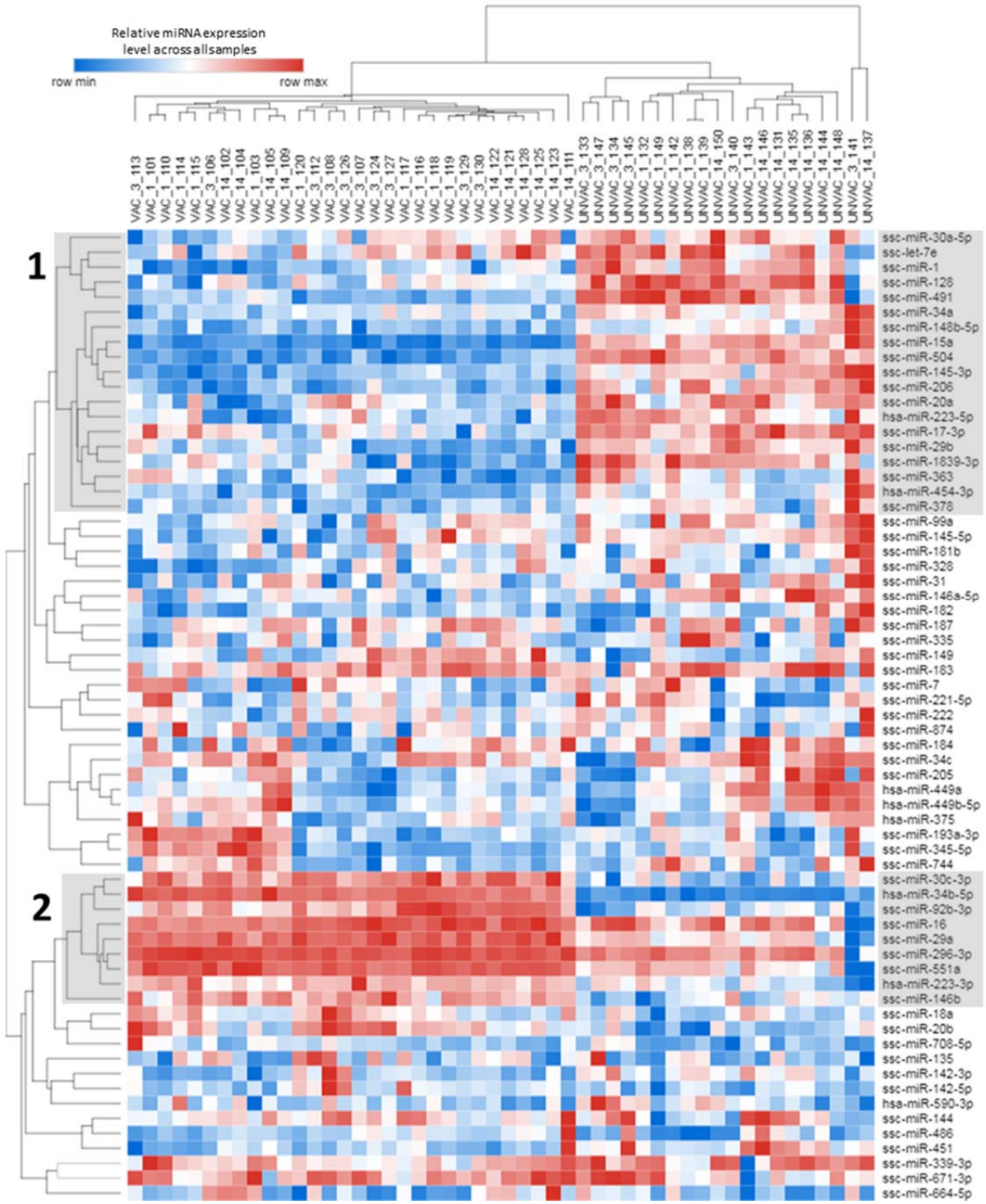
Relative miRNA expression level across all samples
row min
row max
1
2
VAC_3_113
VAC_1_101
VAC_1_110
VAC_1_114
VAC_1_115
VAC_3_106
VAC_14_102
VAC_14_104
VAC_1_103
VAC_14_105
VAC_14_109
VAC_1_120
VAC_3_112
VAC_3_108
VAC_3_126
VAC_3_107
VAC_3_124
VAC_3_127
VAC_1_117
VAC_1_116
VAC_1_118
VAC_1_119
VAC_3_129
VAC_3_130
VAC_14_122
VAC_14_121
VAC_14_128
VAC_14_125
VAC_14_123
VAC_14_111
UNVAC_3_133
UNVAC_3_147
UNVAC_3_134
UNVAC_3_145
UNVAC_1_132
UNVAC_1_149
UNVAC_1_142
UNVAC_1_138
UNVAC_1_139
UNVAC_14_150
UNVAC_3_140
UNVAC_1_143
UNVAC_14_146
UNVAC_14_131
UNVAC_14_135
UNVAC_14_136
UNVAC_14_144
UNVAC_14_148
UNVAC_3_141
UNVAC_14_137
ssc-miR-30a-5p
ssc-let-7e
ssc-miR-1
ssc-miR-128
ssc-miR-491
ssc-miR-34a
ssc-miR-148b-5p
ssc-miR-15a
ssc-miR-504
ssc-miR-145-3p
ssc-miR-206
ssc-miR-20a
hsa-miR-223-5p
ssc-miR-17-3p
ssc-miR-29b
ssc-miR-1839-3p
ssc-miR-363
hsa-miR-454-3p
ssc-miR-378
ssc-miR-99a
ssc-miR-145-5p
ssc-miR-181b
ssc-miR-328
ssc-miR-31
ssc-miR-146a-5p
ssc-miR-182
ssc-miR-187
ssc-miR-335
ssc-miR-149
ssc-miR-183
ssc-miR-7
ssc-miR-221-5p
ssc-miR-222
ssc-miR-874
ssc-miR-184
ssc-miR-34c
ssc-miR-205
hsa-miR-449a
hsa-miR-449b-5p
hsa-miR-375
ssc-miR-193a-3p
ssc-miR-345-5p
ssc-miR-744
ssc-miR-30c-3p
hsa-miR-34b-5p
ssc-miR-92b-3p
ssc-miR-16
ssc-miR-29a
ssc-miR-296-3p
ssc-miR-551a
hsa-miR-223-3p
ssc-miR-146b
ssc-miR-18a
ssc-miR-20b
ssc-miR-708-5p
ssc-miR-135
ssc-miR-142-3p
ssc-miR-142-5p
hsa-miR-590-3p
ssc-miR-144
ssc-miR-486
ssc-miR-451
ssc-miR-339-3p
ssc-miR-671-3p
ssc-miR-664-5p

Figure 5. GO Term enrichment in target gene networks of differentially expressed miRNAs. A) Top ten most significantly enriched GO Terms (Biological Process) in the protein interaction network of target genes for miRNAs found to be more highly expressed in unvaccinated pigs compared to vaccinated pigs. Bars depict the percentage of the total number of genes (n = 221) which are associated with the individual GO Terms. B) Top ten most significantly enriched GO Terms (Biological Process) in the protein interaction network of target genes for miRNAs found to be more highly expressed in vaccinated pigs compared to unvaccinated pigs. Bars depict the percentage of the total number of genes (n = 162) which are associated with the individual GO Terms.

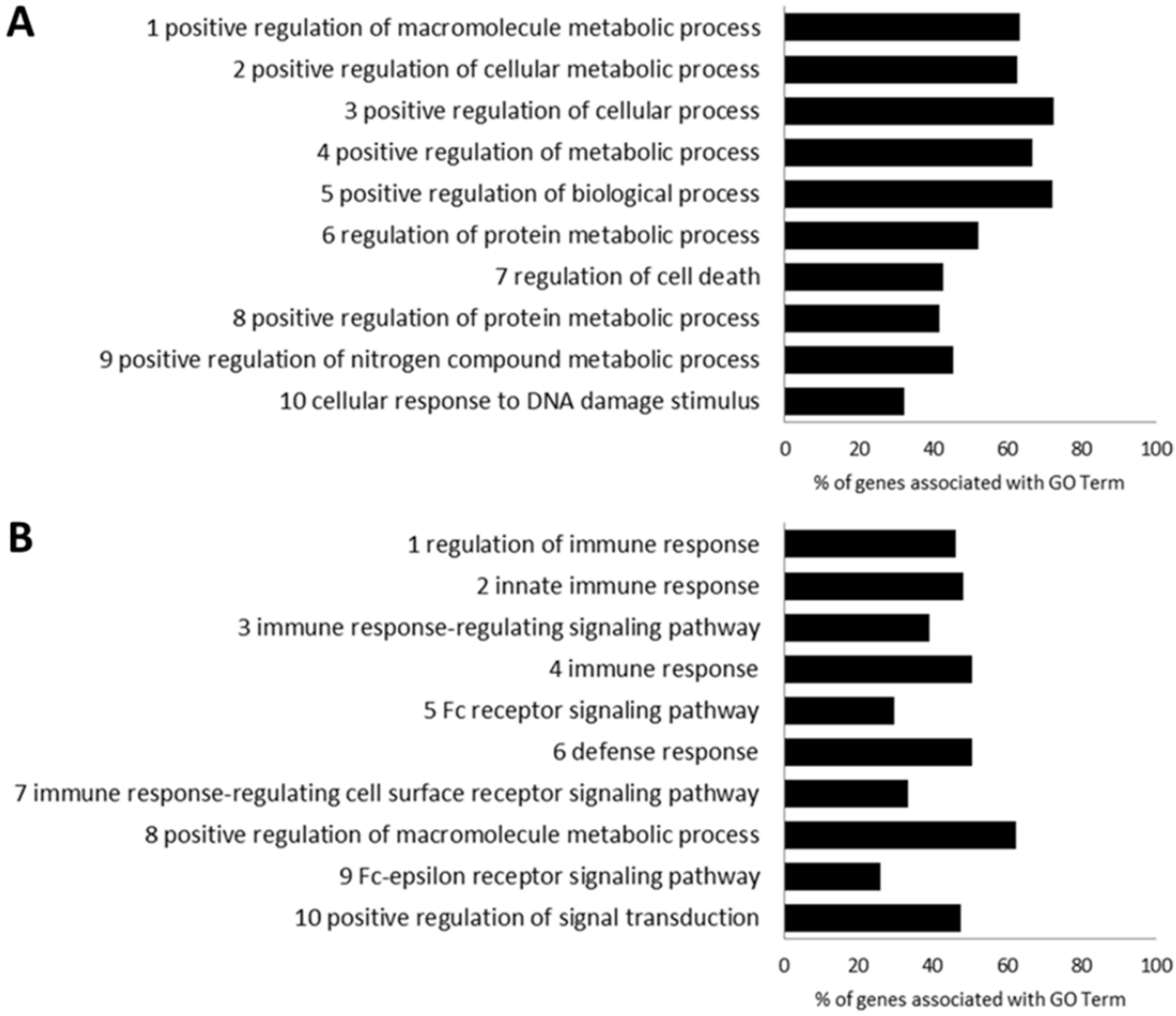

Figure 6. miRNA profiles in lungs after IAV clearance. All depicted miRNAs are expressed at significantly different levels at 14 dpc in the lungs of unvaccinated compared to vaccinated pigs (p < 0.05, Student's t-test; ≥1.5-fold higher levels). VAC – vaccinated. UNVAC – unvaccinated.

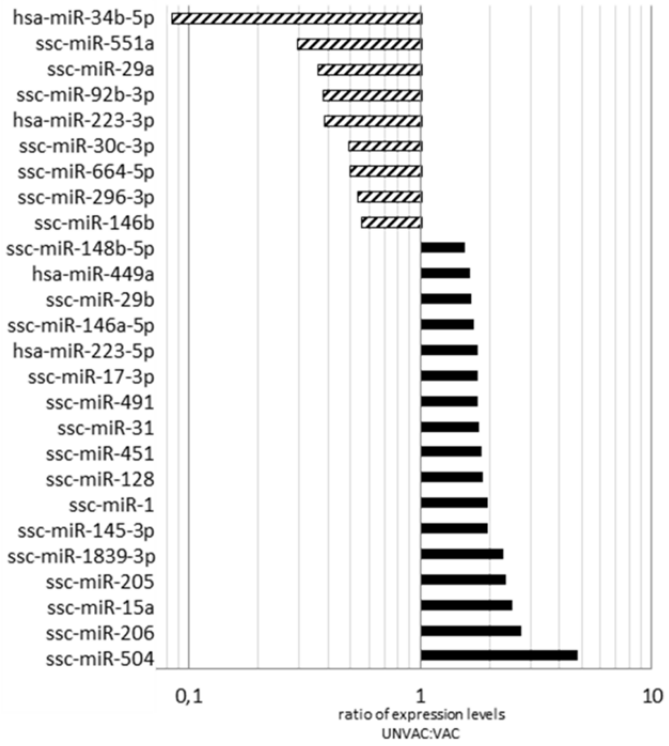

Figure 7. GO Term enrichment in target genes of miRNAs differentially expressed 14 dpc. A) Top ten most significantly enriched GO Terms (Biological Process) in the target genes for miRNAs found to be more highly expressed in unvaccinated pigs compared to vaccinated pigs at 14 dpc. Bars depict the percentage of the total number of genes (n = 141) which are associated with the individual GO Terms. B) Top ten most significantly enriched GO Terms (Biological Process) in the target genes for miRNAs found to be more highly expressed in vaccinated pigs compared to unvaccinated pigs at 14 dpc. Bars depict the percentage of the total number of genes (n = 54) which are associated with the individual GO Terms.

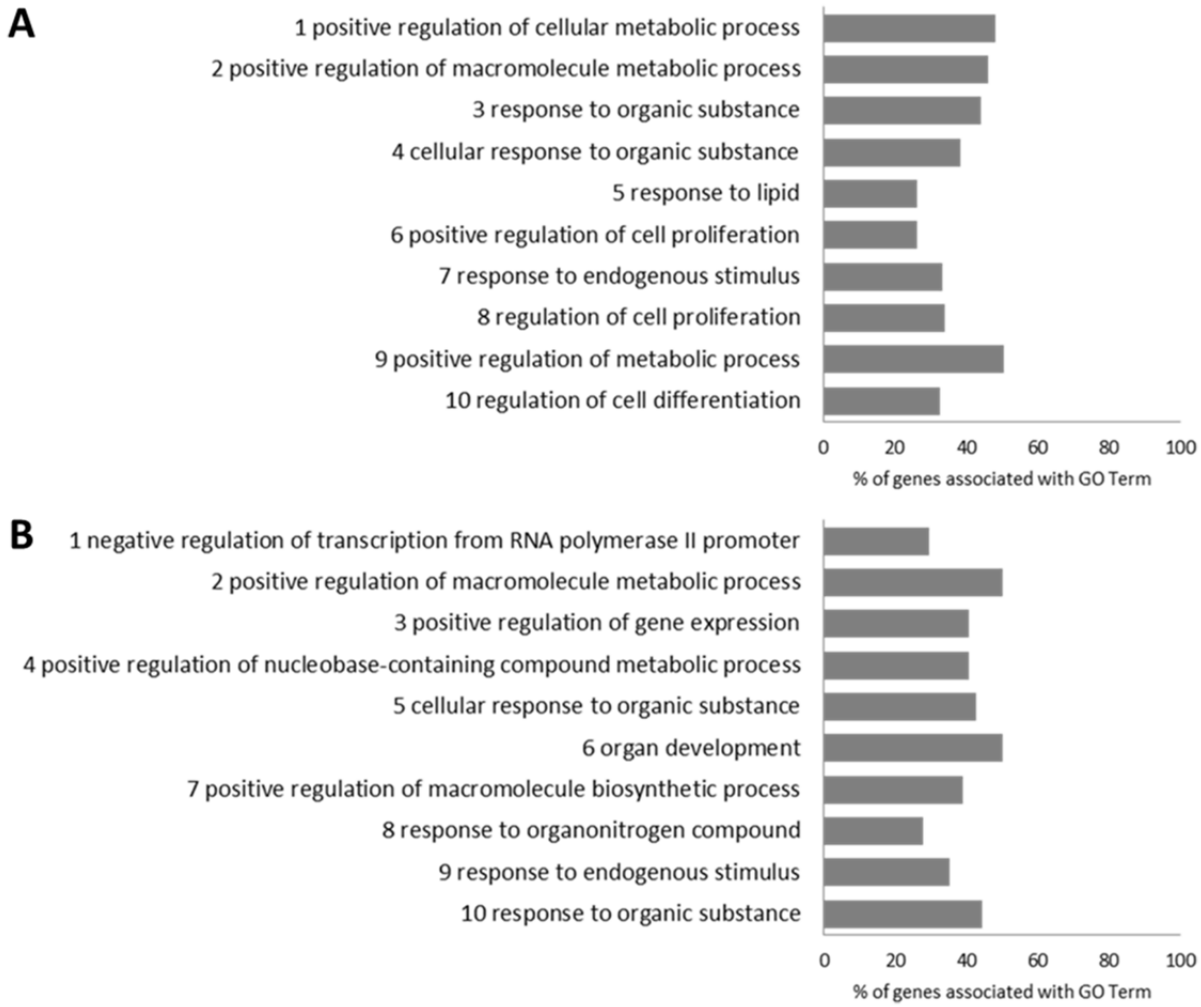

Supplementary Figure 1. Protein coding gene interaction network generated in STRING, obtained for target genes of miRNAs found to be more highly expressed in unvaccinated pigs compared to vaccinated pigs after IAV challenge based on hierarchical clustering.

Supplementary Figure 2. Protein coding gene interaction network generated in STRING, obtained for target genes of miRNAs found to be more highly expressed in vaccinated pigs compared to unvaccinated pigs after IAV challenge based on hierarchical clustering.

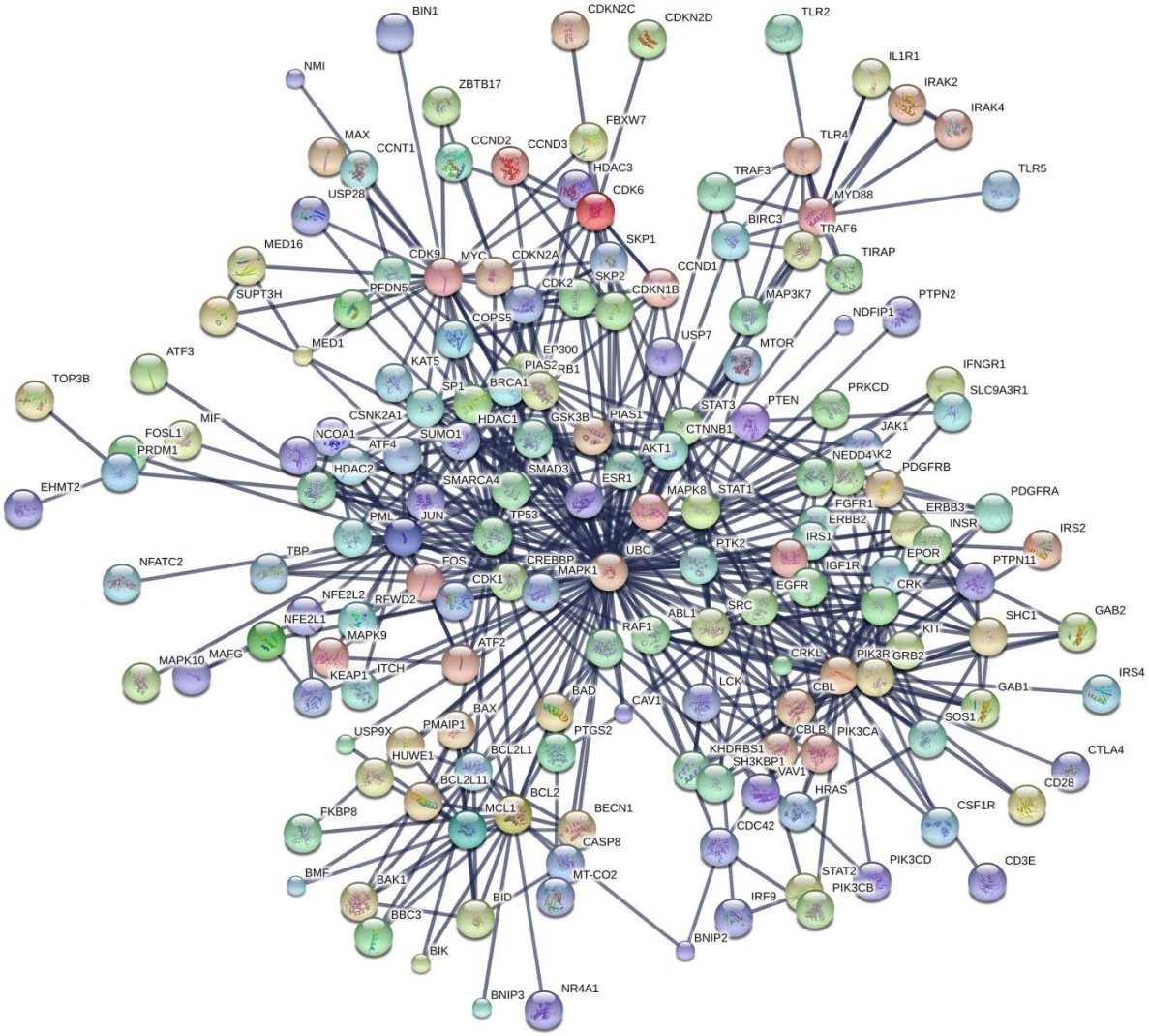

Supplementary Figure 3. Protein coding gene interaction network obtained for target genes of miRNAs found to be significantly more expressed in unvaccinated pigs compared to vaccinated pigs at 14 dpc.

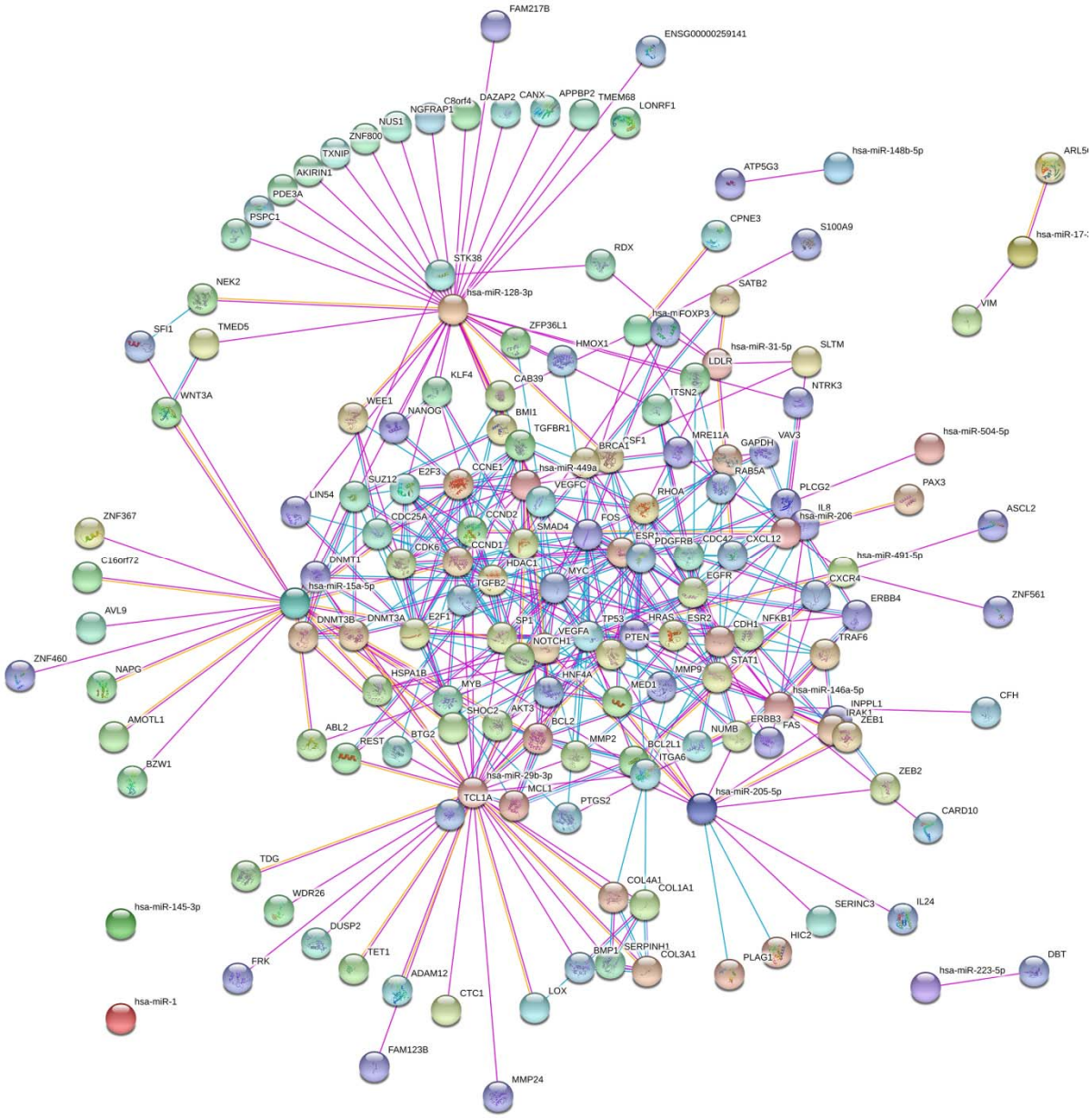

Supplementary Figure 4. Protein coding gene interaction network obtained for target genes of miRNAs found to be significantly more expressed in vaccinated pigs compared to unvaccinated pigs at 14 dpc.

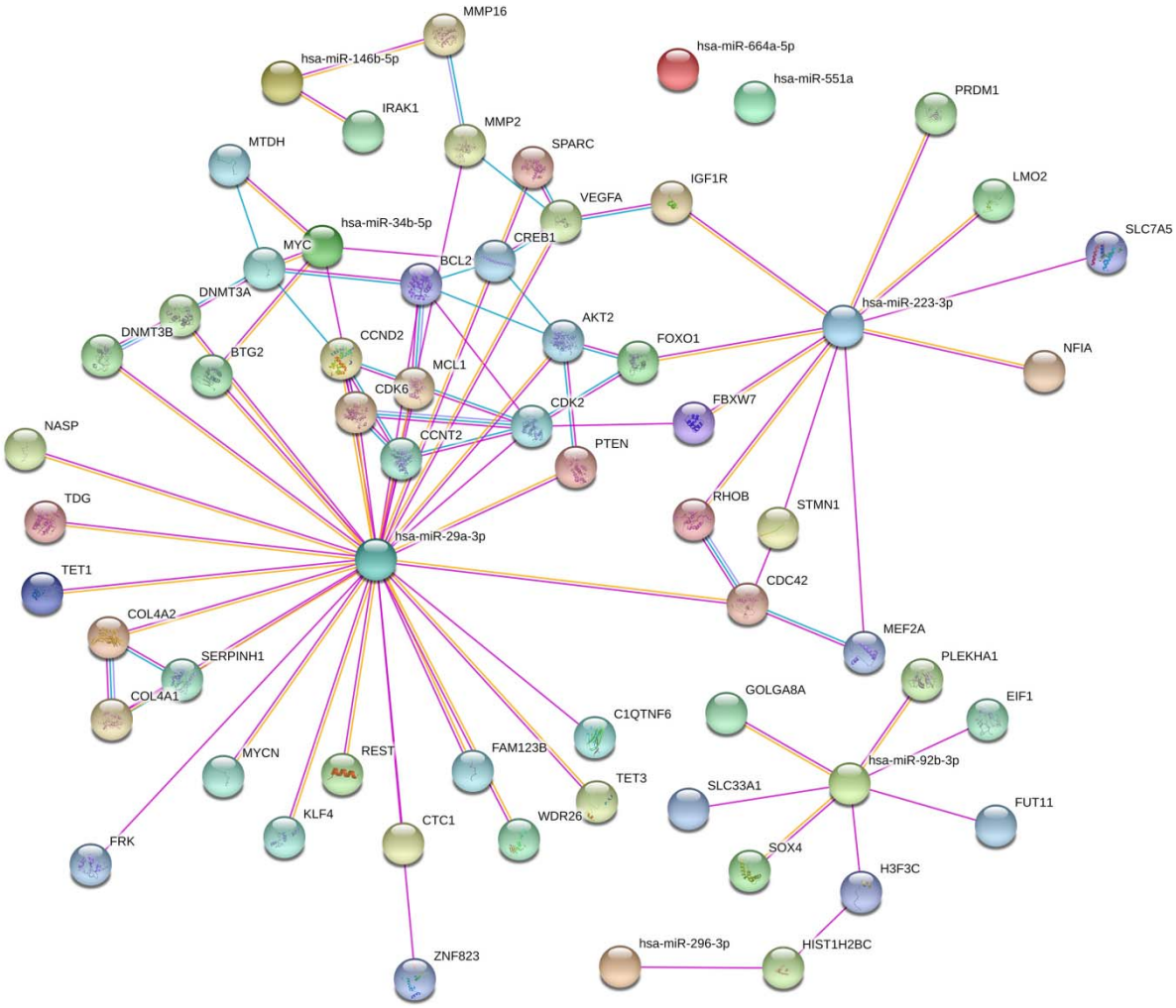

Supplementary Table 1. qPCR primer sequences and experimentally obtained qPCR efficiencies for the assayed miRNAs and protein coding genes.

Gene	Forward primer	Reverse primer	qPCR efficiency
ACTB	CTACGTCGCCCTGGACTTC	GCAGCTCGTAGCTCTTCTCC	1,01
B2M	TGAAGCACGTGACTCTCGAT	CTCTGTGATGCCGGTTAGTG	1,04
GAPDH	ACCCAGAAGACTGTGGATGG	AAGCAGGGATGATGTTCTGG	1,02
PPIA	CAAGACTGAGTGGTTGGATGG	TGTCCACAGTCAGCAATGGT	1,06
RPL13A	ATTGTGGCCAAGCAGGTACT	AATTGCCAGAAATGTTGATGC	1,06
YWHAZ	GCTGCTGGTGATGATAAGAAGG	AGTTAAGGGCCAGACCCAAT	1,04
IFNA1	TACTCAGCTGCAATGCCATC	CTCCTCATTTGTGCCAGGAG	1,01
IL1B	AGCACTGGCTGGAATGAAAC	TCCAGGATTGTCTCCAGGTC	0,96
TNF	CCCCCAGAAGGAAGAGTTTC	CGGGCTTATCTGAGGTTTGA	1,01
IL10	TACAACAGGGGCTTGCTCTT	GCCAGGAAGATCAGGCAATA	0,93
NFKB1	CTCGCACAAGGAGACATGAA	GGGTAGCCCAGTTTTTGTCA	0,95
CHUK	CCCCAACTTCAGCAGAACGT	AGAGCTTAAATGGCCAAGACAGT	1,00
IKBKB	TGGGATCACATCGGACAAACTG	CTTCACCTCGTTCTCCCGTC	1,03
JAK1	TGGGCATGGCTGTGTTGG	CTTGTAGCTGATGTCCTTGGGA	0,99
JAK2	CTCAGATATGCAAGGGTATGGAGT	CCACCAATATATTCCTTGTTGCCA	0,92
STAT1	CCTTGCAGAATAGAGAACATGATAC	CCTTTCTCTTGTTGTCAAGCATT	0,99
STAT2	TTTGCCCCATGATCTGAGACAC	ACGTTGGTGTTCTGGCTAGC	0,97
TLR3	ATTGTGCAAAAGATTCAAGGTG	TCTTCGCAAACAGAGTGCAT	0,93
TLR7	GGAAATAGCATCAGCCAAGCTC	TTCCAGGTTGCGTAGCTCTT	1,01
DDX58	ACGAAAGGGGAAGGTTGTCT	ATGCCTGCAACTTTGTACCC	1,04
IFIH1	CAGTGTGCTAGCCTGCTCTG	GCAGTGCCTTGTTTCCTCTC	0,93
IL28B	CCTGGAAGCCTCTGTCATGT	TCTCCACTGGCGACACATT	1,07
MX1	GCCGAGATCTTTCAGCACCT	CGGAGGATGAAGAACTGGATGA	1,04
ISG15	AGTTCTGGCTGACTTTCGAGG	GGTGCACATAGGCTTGAGGT	1,08
ISG20	AGATCCTGCAGCTCCTGAAA	TGCTCATGTTCTCCTTCAGC	0,98
IFITM1	CACCACGGTGATCACCATCC	GCACCAGTTCAGGAAGAGGG	1,03
IFITM3	ACCACGGTGATCAACATCCG	AGCACCAGTTCATGAAGAGGG	1,07
SOCS1	CCAGCGCATTGTGGCTAC	GCGGCCGATCATATCTGGAA	1,04
OAS1	AAGAAACCCAGGCCTGTGATTC	TAGTGCCCCTTCTACCAGCT	0,97
EIF2AK2	AGGCTGGCGTCTTAGATGTATT	AGGTCGTTTCTTGGGGTCATT	0,92
IRF7	GTGTGCTCCTGTACGGGTCT	CTGCAGCAGCTTCTCTGTGT	1,09
IL1A	TGTGCTAAATAACCTGGATGAGG	GGTTCGTCTTCGTTTTGAGC	0,98
IL6	TGGGTTCAATCAGGAGACCT	CAGCCTCGACATTTCCCTTA	1,13
IL18	CTGCTGAACCGGAAGACAAT	TCCGATTCCAGGTCTTCATC	1,02
IL8	GAAGAGAACTGAGAAGCAACAACA	TTGTGTTGGCATCTTTACTGAGA	0,97
CCL2	CTTCTGCACCCAGGTCCTT	CGCTGCATCGAGATCTTCTT	1,00
CXCL10	CCCACATGTTGAGATCATTGC	GCTTCTCTCTGTGTTCGAGGA	0,97
CSF2	CCGAGGAAACTTCCTGTGAA	GCAGTCAAAGGGGATGGTAA	0,96
BCL2	CCCTGTGGATGACTGAGTACC	AACCACACATGCACCTACCC	0,95
FAS	CACTGTAACCCTTGCACCAC	TGGAACACTTCTCTGCATTTGG	1,00
FASLG	TTCTGGTGGCCCTGGTTG	CTTTGGCTGGCAGACTCTCT	1,01
CASP3	AGCAGTTTTATTTGCGTGCTT	CAACAGGTCCATTTGTTCCA	1,04
CCNE2	AAGCCTCAGGTTTGGAATGGG	GCTTCACTGGGCTGGTACTT	0,94
CDK6	CCTGCTTCTGAAGTGCTTGAC	GGTCGTGGAAGTATGGGTGA	1,01
MCL1	GAGGCTGGGATGGGTTTGTG	TGCCAAACCAGCTCCTACTC	1,01
MYC	AGGAGACACCACCCACCAC	GCTGCCTCTTTTCCACAGAA	1,06
NFE2L1	CCTGAGGAATACCTTGGATGG	CCGGGCAGTGAAGTAATTGT	1,02
JUN	AGTGAAAACCTTGAAAGCGCAG	TGGCACCCACTGTTAACGTG	1,07
MYD88	CCAGACTAAGTTTGCACTCAGC	AGGATGCTGGGGAACTCTTT	0,91
PIK3R1	AAGTTGAACGAGTGGCTGGG	GTCTTCTCATCGTGGTGGGG	1,01
PIK3R2	TGGCTCACTCAGAAAGGTGC	TCCTCATCCTCCATCAGCGA	1,00
PTGS2	AGGCTGATACTGATAGGAGAAACG	GCAGCTCTGGGTCAAACTTC	1,06

NFKBIA	GAGGATGAGCTGCCCTATGAC	CCATGGTCTTTTAGACACTTTCC	1,03
PRDM1	GGTACACACGGGAGAGAAGC	TCTTGAGATTGCTGGTGCTG	1,10
PTEN	AGCAAATAAAGACAAGGCCAACC	GTTGAACTGCTAGCCTCTGGA	0,97
TP53	TAAGCGAGCACTGCCCAC	TCTCGGAACATCTCGAAGCG	1,04
ssc-let-7e	CAGTGAGGTAGGAGGTTGT	GGTCCAGTTTTTTTTTTTTTTTAACTATAC	1,07
ssc-miR-1	CGCAGTGGAATGTAAAGAAG	GGTCCAGTTTTTTTTTTTTTTTTACATACT	1,06
ssc-miR-7	GCAGTGGAAGACTAGTGATTTTG	GGTCCAGTTTTTTTTTTTTTTTTAACAAC	0,96
ssc-miR-15a	CAGTAGCAGCACATAATGGT	TCCAGTTTTTTTTTTTTTTTACAAACC	1,01
ssc-miR-16	GCAGTAGCAGCACGTA	CAGTTTTTTTTTTTTTTTCGCCAA	0,96
ssc-miR-17-3p	CTGCAGTGAAGGCACTT	GTCCAGTTTTTTTTTTTTTTTTCTACAAG	1,01
ssc-miR-18a	GCAGTAAGGTGCATCTAGTG	GGTCCAGTTTTTTTTTTTTTTTTATCTG	0,97
ssc-miR-20a	ACAGTAAAGTGCTTATAGTGCA	GTCCAGTTTTTTTTTTTTTTTTCTACCT	0,99
ssc-miR-20b	AGCAAAGTGCTCACAGTG	GTCCAGTTTTTTTTTTTTTTTTCTACCT	1,05
ssc-miR-29a	GCTAGCACCATCTGAAATCG	TCCAGTTTTTTTTTTTTTTTTAACCGA	0,94
ssc-miR-29b	CAGTAGCACCATTTGAAATCAG	GGTCCAGTTTTTTTTTTTTTTTTAACACT	0,96
ssc-miR-30a-5p	GCAGTGTAAACATCCTCGAC	CCAGTTTTTTTTTTTTTTTCTTCCAG	1,03
ssc-miR-30c-3p	CTGGGAGAAGGCTGTTTAC	AGGTCCAGTTTTTTTTTTTTTTTTAGAG	0,95
ssc-miR-31	GGCAAGATGCTGGCA	CCAGTTTTTTTTTTTTTTTCAGCTATG	1,01
ssc-miR-34a	GTGGCAGTGTCTTAGCTG	CCAGTTTTTTTTTTTTTTTACAACCAG	0,97
hsa-miR-34b-5p	GTAGGCAGTGTCATTAGCTG	GTCCAGTTTTTTTTTTTTTTTTCAATCAG	1,09
ssc-miR-34c	GAGGCAGTGTAGTTAGCTG	CCAGTTTTTTTTTTTTTTTGCAATCAG	1,03
ssc-miR-92b-3p	CGCAGTATTGCACTCGTC	TCCAGTTTTTTTTTTTTTTTGGAGG	1,05
ssc-miR-99a	CAGAACCCGTAGATCCGAT	GGTCCAGTTTTTTTTTTTTTTTCAC	1,03
ssc-miR-128	CACAGTGAACCGGTCTC	GGTCCAGTTTTTTTTTTTTTTTAAAGAG	1,06
ssc-miR-135	CGCAGTATGGCTTTTTATTCCT	GTCCAGTTTTTTTTTTTTTTTCACATAG	0,96
ssc-miR-142-3p	GCAGTGTAGTGTTTCCTACT	GTCCAGTTTTTTTTTTTTTTTCCAT	1,00
ssc-miR-142-5p	GCAGCATAAAGTAGAAAGCAC	GTCCAGTTTTTTTTTTTTTTTTAGTAGTG	0,97
ssc-miR-144	AGCGCAGTACAGTATAGATGA	TCCAGTTTTTTTTTTTTTTTGTACATCA	0,93
ssc-miR-145-3p	GCAGGGATTCCTGGAAATACT	TCCAGTTTTTTTTTTTTTTTAGAACAGT	0,98
ssc-miR-145-5p	GTCCAGTTTTCCCAGGAATC	GGTCCAGTTTTTTTTTTTTTTTAAGG	1,04
ssc-miR-146a-5p	GCAGTGAGAACTGAATTCCA	GGTCCAGTTTTTTTTTTTTTTTAACC	1,04
ssc-miR-146b	GCAGTGAGAACTGAATTCCA	CCAGTTTTTTTTTTTTTTTGCCTATG	0,98
ssc-miR-148b-5p	GCAGGAAGTTCTGTTATACACTC	CAGTTTTTTTTTTTTTTTGCCTGAG	0,98
ssc-miR-149	GGCTCCGTGTCTTCAC	GTCCAGTTTTTTTTTTTTTTTTGGGA	1,03
ssc-miR-181b	GAACATTCATTGCTGTCGGT	TCCAGTTTTTTTTTTTTTTTAACCCA	0,97
ssc-miR-182	AGTTTGGCAATGGTAGAACTC	GTCCAGTTTTTTTTTTTTTTTAGTGTG	1,04
ssc-miR-183	GCAGTATGGCACTGGTAGA	TCCAGTTTTTTTTTTTTTTTCAGTGA	1,05
ssc-miR-184	GTGGACGGAGAACTGATAAG	AGGTCCAGTTTTTTTTTTTTTTTACC	1,00
ssc-miR-187	TCGTGTCTTGTGTTGCAG	GTTTTTTTTTTTTTTCCGGCTG	0,98
ssc-miR-193a-3p	CAGAACTGGCCTACAAAGTC	CAGTTTTTTTTTTTTTTTACTGGGAC	1,00
ssc-miR-205	CCTTCATTCCACCGGAGT	GTCCAGTTTTTTTTTTTTTTTCAGAC	1,00
ssc-miR-206	GCAGTGGAATGTAAGGAAGTG	CCAGTTTTTTTTTTTTTTTCACACAC	0,93
ssc-miR-221-5p	AGACCTGGCATACAATGTAGA	GGTCCAGTTTTTTTTTTTTTTTTACAGA	0,99
ssc-miR-222	CTACATCTGGCTACTGGGT	GGTCCAGTTTTTTTTTTTTTTTGAGA	0,98
hsa-miR-223-3p	CGCAGTGTCAGTTTGTC	CCAGTTTTTTTTTTTTTTTGGGGTA	1,04
hsa-miR-223-5p	GCGTGTATTTGACAAGCTG	GTCCAGTTTTTTTTTTTTTTTAACTCAG	1,03
ssc-miR-296-3p	GTTGGGCGGAGGCT	GTCCAGTTTTTTTTTTTTTTTGGAAAG	0,94
ssc-miR-328	GCCCTCTCTGCCCTTC	GTCCAGTTTTTTTTTTTTTTTTACGGA	1,01
ssc-miR-335	GCAGTCAAGAGCAATAACGA	GTCCAGTTTTTTTTTTTTTTTCATTTTTC	0,98
ssc-miR-339-3p	GCTCCTCGAGGCCAG	GTTTTTTTTTTTTTTGGGCTCTG	0,96
ssc-miR-345-5p	AGGCTGACTCCTAGTCCA	CAGTTTTTTTTTTTTTTTGCACTGG	1,03
ssc-miR-363	AGAATTGCACGGTATCCATC	GGTCCAGTTTTTTTTTTTTTTTTACAGA	0,97
hsa-miR-375	CAGTTTGTTCGTTCGGCT	GGTCCAGTTTTTTTTTTTTTTTCAC	1,01
ssc-miR-378	GACTGGACTTGGAGTCAGA	CCAGTTTTTTTTTTTTTTTGCCTTCT	0,96
hsa-miR-449a	AGTGGCAGTGTATTGTTAGC	GTCCAGTTTTTTTTTTTTTTTTACCAG	1,01
hsa-miR-449b-5p	CAGAGGCAGTGTATTGTTAGC	TCCAGTTTTTTTTTTTTTTTGCCA	0,99
ssc-miR-451	CAGAAACCGTTACCATTACTGA	GGTCCAGTTTTTTTTTTTTTTTTAACTCA	1,07
hsa-miR-454-3p	GCAGTAGTGCAATATTGCTTATAG	GTCCAGTTTTTTTTTTTTTTTTACCCT	0,94

ssc-miR-486	GTCCTGTACTGAGCTGC	GGTCCAGTTTTTTTTTTTTTTCTC	0,98
ssc-miR-491	GTGGGGAACCCTTCCA	GGTCCAGTTTTTTTTTTTTTTCCT	1,08
ssc-miR-504	ACCCTGGTCTGCACTC	AGGTCCAGTTTTTTTTTTTTTTTAGATAG	1,06
ssc-miR-551a	GCGACCCACTCTTGG	CAGTTTTTTTTTTTTTTGGAAACCA	0,86
hsa-miR-590-3p	GCAGCGCAGTAATTTTATGTATAAG	TCCAGTTTTTTTTTTTTTTTACTAGCTT	0,98
ssc-miR-664-5p	AGCAGGCTAGGAGAAGTG	GTCCAGTTTTTTTTTTTTTTTATCCAATC	1,01
ssc-miR-671-3p	GCAGTCCGGTTCTCAGG	GGTCCAGTTTTTTTTTTTTTTTGGT	0,98
ssc-miR-708-5p	CGCAGAAGGAGCTTACAATC	GTCCAGTTTTTTTTTTTTTTTCCCA	1,03
ssc-miR-744	CGGGGCTAGGGCTAAC	GTCCAGTTTTTTTTTTTTTTTGCTG	1,03
ssc-miR-874	CCTGGCCCGAGGGA	CCAGTTTTTTTTTTTTTTTGTCGGT	1,04
ssc-miR-1839-3p	CGCAGAGACCTACTTTTCTAC	GGTCCAGTTTTTTTTTTTTTTTGTTG	1,02

Supplementary Table 2. Porcine miRNA sequences and their human homolog sequences applied in the retrieval of previously experimentally validated gene targets from TarBase (v. 7.0). Differences between porcine and human sequences are highlighted by bold, underlined nucleotides.

Porcine name	Porcine sequence	Human homolog name	Human homolog sequence
miRNAs which are more highly expressed in unvaccinated compared to vaccinated animals cf. Figure 4			
ssc-let-7e	ugagguaggagguuguauaguu	hsa-let-7e-5p	ugagguaggagguuguauaguu
ssc-miR-1	uggaauguaaagaaguaugua	hsa-miR-1-3p	uggaauguaaagaaguaugua**u**
ssc-miR-15a	uagcagcacauaaugguuugu	hsa-miR-15a-5p	uagcagcacauaaugguuugu**g**
ssc-miR-17-3p	acugcagugaaggcacuuguag	hsa-miR-17-3p	acugcagugaaggcacuuguag
ssc-miR-20a	uaaagugcuuauagugcaggua	hsa-miR-20a-5p	uaaagugcuuauagugcaggua**g**
ssc-miR-29b	uagcaccauuugaaaucaguguu	hsa-miR-29b-3p	uagcaccauuugaaaucaguguu
ssc-miR-30a-5p	uguaaacauccucgacuggaag	hsa-miR-30a-5p	uguaaacauccucgacuggaag
ssc-miR-34a	uggcagugucuuagcugguugu	hsa-miR-34a-5p	uggcagugucuuagcugguugu
ssc-miR-128	ucacagugaaccggucucuuu	hsa-miR-128-3p	ucacagugaaccggucucuuu
ssc-miR-145-3p	ggauuccuggaaauacuguucu	hsa-miR-145-3p	ggauuccuggaaauacuguucu
ssc-miR-148b-5p	**g**aaguucuguuauacacucaggc	hsa-miR-148b-5p	aaguucuguuauacacucaggc
ssc-miR-206	uggaauguaaggaagugugug**a**	hsa-miR-206	uggaauguaaggaagugugug**g**
Porcine sequence not annotated		hsa-miR-223-5p	cguguauuugacaagcugaguu
ssc-miR-363	aauugcacgguauccaucugua**a**	hsa-miR-363-3p	aauugcacgguauccaucugua
ssc-miR-378	acuggacuuggagucagaaggc	hsa-miR-378a-3p	acuggacuuggagucagaaggc
Porcine sequence not annotated		hsa-miR-454-3p	uagugcaauauugcuuauagggu
ssc-miR-491	agugggaacccuuccaugagg	hsa-miR-491-5p	agugggaacccuuccaugagg
ssc-miR-504	agacccuggucugcacucuauc**u**	hsa-miR-504-5p	agacccuggucugcacucuauc
ssc-miR-1839-3p	agaccuacuuuucuaccaaca	Human sequence not annotated	
miRNAs which are more highly expressed in vaccinated compared to unvaccinated animals cf. Figure 4			
ssc-miR-16	uagcagcacguaaauauuggcg	hsa-miR-16-5p	uagcagcacguaaauauuggcg
ssc-miR-29a	**c**uagcaccaucugaaaucgguua	hsa-miR-29a-3p	uagcaccaucugaaaucgguua
ssc-miR-30c-3p	cugggagaaggcuguuuacucu	hsa-miR-30c-2-3p	cugggagaaggcuguuuacucu
Porcine sequence not annotated		hsa-miR-34b-5p	uaggcagugucauuagcugauug
ssc-miR-92b-3p	uauugcacucgucccggccucc	hsa-miR-92b-3p	uauugcacucgucccggccucc
ssc-miR-146b	ugagaacugaauuccauaggc	hsa-miR-146b-5p	ugagaacugaauuccauaggc**u**
Porcine sequence not annotated		hsa-miR-223-3p	ugucaguuugucaaauacccca
ssc-miR-296-3p	aggguugggcggaggcuuucc	hsa-miR-296-3p	**g**aggguuggguggaggcucucc
ssc-miR-551a	gcgacccacucuugguuucc	hsa-miR-551a	gcgacccacucuugguuucc**a**
miRNAs which are more highly expressed in unvaccinated compared to vaccinated animals at 14 dpc cf. Figure 6			
ssc-miR-1	uggaauguaaagaaguaugua	hsa-miR-1-3p	uggaauguaaagaaguaugua**u**
ssc-miR-15a	uagcagcacauaaugguuugu	hsa-miR-15a-5p	uagcagcacauaaugguuugu**g**
ssc-miR-17-3p	acugcagugaaggcacuuguag	hsa-miR-17-3p	acugcagugaaggcacuuguag
ssc-miR-29b	uagcaccauuugaaaucaguguu	hsa-miR-29b-3p	uagcaccauuugaaaucaguguu
ssc-miR-31	aggcaagaugcuggcauagcu**g**	hsa-miR-31-5p	aggcaagaugcuggcauagcu
ssc-miR-128	ucacagugaaccggucucuuu	hsa-miR-128-3p	ucacagugaaccggucucuuu
ssc-miR-145-3p	ggauuccuggaaauacuguucu	hsa-miR-145-3p	ggauuccuggaaauacuguucu
ssc-miR-146a-5p	ugagaacugaauuccauggguu	hsa-miR-146a-5p	ugagaacugaauuccauggguu
ssc-miR-148b-5p	**g**aaguucuguuauacacucaggc	hsa-miR-148b-5p	aaguucuguuauacacucaggc
ssc-miR-205	uccuucauuccaccggagucug	hsa-miR-205-5p	uccuucauuccaccggagucug
ssc-miR-206	uggaauguaaggaagugugug**a**	hsa-miR-206	uggaauguaaggaagugugug**g**
Porcine sequence not annotated		hsa-miR-223-5p	cguguauuugacaagcugaguu
Porcine sequence not annotated		hsa-miR-449a	uggcaguguauuguuagcuggu

ssc-miR-451	aaaccguuaccauuacugaguu	hsa-miR-451a	aaaccguuaccauuacugaguu
ssc-miR-491	agugggggaacccuuccaugagg	hsa-miR-491-5p	agugggggaacccuuccaugagg
ssc-miR-504	agacccuggucugcacucuauc**u**	hsa-miR-504-5p	agacccuggucugcacucuauc
ssc-miR-1839-3p	agaccuacuuuucuaccaaca	Human sequence not annotated	
miRNAs which are more highly expressed in vaccinated compared to unvaccinated animals at 14 dpc cf. Figure 6			
ssc-miR-29a	**c**uagcaccaucugaaaucgguua	hsa-miR-29a-3p	uagcaccaucugaaaucgguua
ssc-miR-30c-3p	cugggagaaggcuguuuacucu	hsa-miR-30c-2-3p	cugggagaaggcuguuuacucu
Porcine sequence not annotated		hsa-miR-34b-5p	uaggcagugucauuagcugauug
ssc-miR-92b-3p	uauugcacucgucccggccucc	hsa-miR-92b-3p	uauugcacucgucccggccucc
ssc-miR-146b	ugagaacugaauuccauaggc	hsa-miR-146b-5p	ugagaacugaauuccauaggc**u**
Porcine sequence not annotated		hsa-miR-223-3p	ugucaguuugucaaauacccca
ssc-miR-296-3p	aggguugggcggaggcuuucc	hsa-miR-296-3p	**g**aggguugggguggaggcucucc
ssc-miR-551a	gcgacccacucuugguuucc	hsa-miR-551a	gcgacccacucuugguuucc**a**
ssc-miR-664-5p	caggcuaggagaagugauuggau	hsa-miR-664a-5p	**a**cuggcuagggaaaaugauuggau